

DO-TH 2001/17

hep-ph/0110292

October 2001

Heavy Quark Production in CC and NC DIS and The Structure of Real and Virtual Photons in NLO QCD

Dissertation

zur Erlangung des Grades eines
Doktors der Naturwissenschaften
der Abteilung Physik
der Universität Dortmund

vorgelegt von

Ingo Jan Schienbein

Juli 2001

Für meinen Vater

Granger stood looking back with Montag. "Everyone must leave something behind when he dies, my grandfather said. A child or a book or a painting or a house or a wall built or a pair of shoes made. Or a garden planted. Something your hand touched some way so your soul has somewhere to go when you die, and when people look at that tree or that flower you planted, you're there. It doesn't matter what you do, he said, so long as you change something from the way it was before you touched it into something that's like you after you take your hands away. The difference between the man who just cuts lawns and a real gardener is in the touching, he said. The lawn-cutter might just as well not have been there at all; the gardener will be there a life-time."

Ray Bradbury, Fahrenheit 451

Contents

I	Heavy Quark Production in CC and NC DIS	1
1	Introduction and Survey	2
2	Charged Current Leptoproduction of D–Mesons in the Variable Flavor Scheme	5
2.1	Introduction	5
2.2	Gluon–Fusion	6
2.3	CC Leptoproduction within ACOT	8
2.4	Numerical Results	9
2.5	Summary	10
3	Quark Masses in Deep Inelastic Structure Functions	12
3.1	Introduction	12
3.2	Heavy Quark Contributions to ACOT Structure Functions	14
3.2.1	DIS on a Massive Quark at $\mathcal{O}(\alpha_s^0)$	14
3.2.2	DIS on a Massive Quark at $\mathcal{O}(\alpha_s^1)$	17
3.2.3	Gluon Fusion Contributions at $\mathcal{O}(\alpha_s^1)$	19
3.2.4	ACOT Structure Functions at $\mathcal{O}(\alpha_s^1)$	20
3.3	Results for NC and CC Structure Functions	21
3.3.1	NC Structure Functions	21
3.3.2	CC Structure Functions	25

3.4	Conclusions	28
4	Charm Fragmentation in Deep Inelastic Scattering	29
4.1	Introduction	29
4.2	Semi-Inclusive Heavy Quark Structure Functions	31
4.2.1	Scattering on Massive Quarks	31
4.2.2	Gluon Fusion Contributions at $\mathcal{O}(\alpha_s^1)$	34
4.2.3	Subtraction Terms	34
4.2.4	SI Structure Functions at $\mathcal{O}(\alpha_s^1)$	36
4.3	The Charm Fragmentation Function in SI DIS	37
4.3.1	CC DIS	37
4.3.2	NC DIS	42
4.4	Conclusions	45
5	Summary	47
II	The Structure of Real and Virtual Photons	49
6	Introduction and Survey	50
7	Photon–Photon Scattering	54
7.1	Kinematics	55
7.1.1	The Hadronic Tensor $W^{\mu'\nu',\mu\nu}$	57
7.1.2	Derivation of the Cross Section	60
7.2	Photon Structure Functions	61
7.2.1	Structure Functions for a Spin–Averaged Photon	62
7.2.2	Longitudinal and Transverse Target Photons	63
7.3	QED–Factorization	64

8	The Doubly Virtual Box in LO	71
8.1	Unintegrated Structure Functions	72
8.2	Inclusive Structure Functions	75
8.3	Comparison with Present e^+e^- Virtual Photon Data	77
9	The Partonic Structure of Real and Virtual Photons: Theoretical Framework	82
9.1	Introduction	82
9.2	Photon Structure Functions in the QCD-Improved Parton Model	85
9.2.1	Scheme Choice	86
9.2.2	Heavy Flavor Contributions	87
9.3	Q^2 -Evolution	89
9.3.1	Evolution Equations	89
9.3.2	Analytic Solutions	92
9.3.3	Numerical Mellin-Inversion	94
9.3.4	Boundary Conditions for a Deeply Virtual Target Photon	94
9.3.5	Momentum Sum	98
9.4	Longitudinal Target Photons	100
10	Pionic Parton Densities in a Constituent Quark Model	102
11	Radiatively Generated Parton Distributions of Real and Virtual Photons	109
11.1	Introduction	109
11.2	The Parton Content of Real Photons	111
11.2.1	Boundary Conditions	111
11.2.2	Quantitative Results	113
11.3	The Photon Structure Function at Small- x	118

11.4 The Parton Content of Virtual Photons	123
11.4.1 Boundary Conditions	123
11.4.2 Quantitative Results	125
11.5 Summary and Conclusions	131
12 Has the QCD RG–Improved Parton Content of Virtual Photons been Observed?	133
12.1 Introduction	133
12.2 RG–Improved Parton Model Expectations for the Effective Structure Function F_{eff}	134
12.3 Comparison with DIS ep Data and Effective Quark Distributions	137
12.4 Possible Signatures for the QCD Parton Content of Virtual Photons	140
12.5 Summary and Conclusions	143
13 Summary	144
A Deep Inelastic Scattering on Massive Quarks at $\mathcal{O}(\alpha_s^1)$	147
A.1 Real Gluon Emission	147
A.2 Vertex Correction	149
A.2.1 Results	149
A.2.2 Calculation	151
A.3 Real and Virtual Contributions to Structure Functions	156
A.4 Comparison with E. Hoffmann and R. Moore, Z. Phys. C20 , 71 (1983)	158
B Matrix Elements for Real Gluon Emission off Massive Quarks	161
C Limits of the Doubly Virtual Box	163
C.1 General Bjorken Limit: $m^2, P^2 \ll Q^2$	165
C.2 $m^2 = 0, P^2 \ll Q^2$	165

C.3	Real Photon Limit: $P^2 = 0$	166
D	Parametrizations	168
D.1	Pion Distributions	168
D.1.1	Parametrization of LO Parton Distributions	168
D.1.2	Parametrization of NLO($\overline{\text{MS}}$) Parton Distributions	170
D.2	Photon Distributions	171
D.2.1	Parametrization of LO ‘pointlike’ Photonic Parton Distributions . .	171
D.2.2	Parametrization of NLO ‘pointlike’ Photonic Parton Distributions .	173

Preface

This thesis has been divided into two parts both being applications of perturbative Quantum Chromo Dynamics (QCD).

The first part 'Heavy Quark Production in CC and NC DIS' is a continuation of work presented in [1] and has been done in collaboration with S. Kretzer. Part I is based on the following publications [2–4]:

- S. Kretzer and I. Schienbein, *Charged-current leptonproduction of D mesons in the variable flavor scheme*, Phys. Rev. **D56**, 1804 (1997) [Chapter 2].
- S. Kretzer and I. Schienbein, *Heavy quark initiated contributions to deep inelastic structure functions*, Phys. Rev. **D58**, 094035 (1998) [Chapter 3].
- S. Kretzer and I. Schienbein, *Heavy quark fragmentation in deep inelastic scattering*, Phys. Rev. **D59**, 054004 (1999) [Chapter 4].

The second part 'The Structure of Real and Virtual Photons' has emerged from a collaboration with Prof. M. Glück and Prof. E. Reya. Part II is based on the following publications [5–8]:

- M. Glück, E. Reya, and I. Schienbein, *Pionic parton distributions revisited*, Eur. Phys. J. **C10**, 313 (1999) [Chapter 10].
- M. Glück, E. Reya, and I. Schienbein, *Radiatively generated parton distributions for real and virtual photons*, Phys. Rev. **D60**, 054019 (1999); (E) **D62** 019902 (2000) [Chapter 11].
- M. Glück, E. Reya, and I. Schienbein, *The Photon Structure Function at small- x* , Phys. Rev. **D64**, 017501 (2001) [Chapter 11].

- M. Glück, E. Reya, and I. Schienbein, *Has the QCD RG-improved parton content of virtual photons been observed?*, Phys. Rev. **D63**, 074008 (2001) [Chapter 12].

The results of Refs. [5, 6] have also been summarized in [9, 10]. The work in Section 7.3 is completely new and has been done in collaboration with C. Sieg.

Part I

Heavy Quark Production in CC and NC DIS

Chapter 1

Introduction and Survey

Part I of this thesis is devoted to heavy quark production in charged current (CC) and neutral current (NC) deep inelastic scattering (DIS) where a quark h with mass m_h is viewed as heavy if $m_h \gg \Lambda_{\text{QCD}}$ contrary to the light u, d, s quarks with $m_{u,d,s} \ll \Lambda_{\text{QCD}}$. Thus, the heavy quark mass provides a hard scale allowing for a perturbative analysis. In deep inelastic heavy quark production a second hard scale is given by the virtuality Q^2 of the probing boson (photon, Z-boson, W-boson) such that we have to deal with the theoretically interesting problem of describing a two-hard-scale process within perturbative QCD (pQCD). In the following, we will prominently deal with charm quarks being the lightest of the heavy quarks ($h = c, b, t$) in the standard model.

In addition to these general theoretical arguments, there are several important phenomenological reasons for studying heavy quark production in DIS:

- Charm contributes up to 30% to the total structure function F_2^p at small Bjorken- x as measurements at the ep collider HERA at DESY have shown [11–13]. For this reason a proper treatment of charm contributions in DIS is essential for a global analysis of structure function data and a precise extraction of the parton densities in the proton.
- NC charm production offers the possibility to extract the gluon distribution in the proton from a measurement of F_2^c [14, 15].
- CC charm production is sensitive to the nucleon’s strange sea. The momentum (z) distributions of D-mesons from the fragmentation of charm quarks produced in neutrino deep inelastic scattering have been used recently to determine the strange

quark distribution of the nucleon $s(x, Q^2)$ at leading order (LO) [16] and next-to-leading order (NLO) [17].

In the past few years considerable effort has been devoted to including heavy quark effects in DIS. If one could sum the whole perturbation series (keeping the full mass dependence) one would arrive at unique perturbative QCD predictions. However, at any finite order in perturbation theory differences arise due to distinct prescriptions (schemes) [18–25] of how to order terms in the perturbative expansion. These schemes, in turn, enter global analyses of parton distributions [26–28] and hence feed back on the resulting light parton distributions [28]. It is therefore necessary to work out the various schemes as much as possible and to compare them since a most complete possible understanding or –even better– reduction of the theoretical uncertainties is required to make concise tests of pQCD predictions against heavy flavor tagged deep inelastic data.

In this thesis we concentrate on the ACOT variable flavor number scheme (VFNS) [19, 20] which we work out to full order $\mathcal{O}(\alpha_s^1)$. Recently, this scheme has been proven by Collins [21] to work at all orders of QCD factorization theory. We will perform all required calculations with general couplings and masses in order to be able to describe both CC and NC processes in one framework.

The outline of Part I will be as follows:

- In Chapter 2 we present formulae for the momentum (z) distributions of D–mesons produced in neutrino deep inelastic scattering off strange partons. The expressions are derived within the variable flavor scheme of Aivazis et al. (ACOT scheme) [20], which is extended from its fully inclusive formulation to one–hadron inclusive lepton–production. The dependence of the results on the assumed strange quark mass m_s is investigated and the $m_s \rightarrow 0$ limit is compared to the corresponding $\overline{\text{MS}}$ results. The importance of $\mathcal{O}(\alpha_s)$ quark–initiated corrections is demonstrated for the $m_s = 0$ case.
- In Chapter 3 we perform an explicit calculation of the before missing $\mathcal{O}(\alpha_s^1)$ corrections to deep inelastic scattering amplitudes on massive quarks within the ACOT scheme using general masses and couplings thereby completing the ACOT formalism up to full $\mathcal{O}(\alpha_s)$. After identifying the correct subtraction term the convergence of these contributions towards the analogous coefficient functions for massless quarks,

obtained within the modified minimal subtraction scheme ($\overline{\text{MS}}$), is demonstrated. Furthermore, the importance of these contributions to neutral current and charged current structure functions is investigated for several choices of the mass factorization scale μ as well as the relevance of mass corrections.

- In Chapter 4 we turn to an analysis of semi-inclusive production of charm (momentum (z) distributions of D-mesons) in neutral current and charged current deep inelastic scattering at full $\mathcal{O}(\alpha_s^1)$. For this purpose we generalize the results of Chapter 3 from its fully inclusive formulation to one-hadron inclusive leptonproduction. We review the relevant massive formulae and subtraction terms and discuss their massless limits. We show how the charm fragmentation function can be measured in CC DIS and we investigate whether the charm production dynamics may be tested in NC DIS. Furthermore, we also discuss finite initial state quark mass effects in CC and NC DIS.
- Finally, we summarize our main results in Chapter 5. Some details of the calculation and lengthy formulae are relegated to the Appendices A and B.

Chapter 2

Charged Current Leptoproduction of D–Mesons in the Variable Flavor Scheme

2.1 Introduction

The momentum (z) distributions of D–mesons from the fragmentation of charm quarks produced in neutrino deep inelastic scattering (DIS) have been used recently to determine the strange quark distribution of the nucleon $s(x, Q^2)$ at leading order (LO) [16] and next-to-leading order (NLO) [17]. A proper QCD calculation of this quantity requires the convolution of a perturbative hard scattering charm production cross section with a nonperturbative $c \rightarrow D$ fragmentation function $D_c(z)$ leading at $\mathcal{O}(\alpha_s)$ to the breaking of factorization in Bjorken- x and z as is well known for light quarks [29, 30]. So far experimental analyses have assumed a factorized cross section even at NLO [17]. This shortcoming has been pointed out in [31] and the hard scattering convolution kernels needed for a correct NLO analysis have been calculated there in the $\overline{\text{MS}}$ scheme with three massless flavors (u, d, s) using dimensional regularization. In the experimental NLO analysis in [17] the variable flavor scheme (VFS) of Aivazis, Collins, Olness and Tung (ACOT) [20] for heavy flavor leptoproduction has been utilized. In this formalism one considers, in addition to the quark scattering (QS) process, e.g. $W^+s \rightarrow c$, the contribution from the gluon fusion (GF) process $W^+g \rightarrow c\bar{s}$ with its full m_s -dependence. The collinear logarithm which is already contained in the renormalized $s(x, Q^2)$ is subtracted off numerically. The quark-initiated contributions from the subprocess $W^+s \rightarrow cg$ (together

with virtual corrections) which were included in the complete NLO ($\overline{\text{MS}}$) analysis in [31] are usually neglected in the ACOT formalism. The ACOT formalism has been formulated explicitly only for fully inclusive leptonproduction [20]. It is the main purpose here to fill the gap and provide the expressions needed for a correct calculation of one–hadron (D–meson) inclusive leptonproduction also in this formalism.

2.2 Gluon–Fusion

In the following we will stick closely to the ACOT formalism as formulated in [20] except that we are not working in the helicity basis but prefer the standard tensor basis implying the usual structure functions $F_{i=1,2,3}$. We are not considering kinematical effects arising from an initial state quark mass in the $W^+s \rightarrow c$ quark scattering contribution, i.e., $s(x, Q^2)$ represents massless initial state strange quarks. This latter choice must be consistently kept in the subtraction term [20] to be identified below from the $m_s \rightarrow 0$ limit of the $W^+g \rightarrow c\bar{s}$ gluon fusion contribution. The fully massive partonic matrix elements have been calculated for the general boson–gluon fusion process $Bg \rightarrow \bar{Q}_1 Q_2$ in [32] where $B = \gamma^*, W^\pm, Z$. When they are convoluted with a nonperturbative gluon distribution $g(x, \mu^2)$ and a fragmentation function $D_{Q_2}(z)$, one obtains the GF part of the hadronic structure function $F_i(x, z, Q^2)$ describing the momentum (z) distribution of a hadron H containing the heavy quark Q_2 :

$$\begin{aligned} F_{1,3}^{GF}(x, z, Q^2) &= \int_{ax}^1 \frac{dx'}{x'} \int_{\max[z, \zeta_{\min}(x/x')] }^{\zeta_{\max}(x/x')} \frac{d\zeta}{\zeta} g(x', \mu^2) f_{1,3}\left(\frac{x}{x'}, \zeta, Q^2\right) D_{Q_2}\left(\frac{z}{\zeta}\right) \\ F_2^{GF}(x, z, Q^2) &= \int_{ax}^1 \frac{dx'}{x'} \int_{\max[z, \zeta_{\min}(x/x')] }^{\zeta_{\max}(x/x')} \frac{d\zeta}{\zeta} x' g(x', \mu^2) f_2\left(\frac{x}{x'}, \zeta, Q^2\right) D_{Q_2}\left(\frac{z}{\zeta}\right) \end{aligned} \quad (2.1)$$

with the fractional momentum variables $z = p_H \cdot p_N / q \cdot p_N$ and $\zeta = p_{Q_1} \cdot p_N / q \cdot p_N$, p_N and q being the momentum of the nucleon and the virtual boson, respectively. The structure functions $F_i(x, z, Q^2)$ generalize the usual fully inclusive structure functions $F_i(x, Q^2)$, if one considers one–hadron (H) inclusive leptonproduction. The partonic structure functions $f_i(x', \zeta, Q^2)$ are given by

$$f_{i=1,2,3}(x', \zeta, Q^2) = \frac{\alpha_s(\mu^2)}{\pi} \left[\frac{A_i}{(1-\zeta)^2} + \frac{B_i}{\zeta^2} + \frac{C_i}{1-\zeta} + \frac{D_i}{\zeta} + E_i \right] \quad (2.2)$$

with

$$\begin{aligned}
A_1(x', Q^2) &= q_+ \frac{x'^2}{4} \frac{m_1^2}{Q^2} \left(1 + \frac{\Delta m^2}{Q^2} - \frac{q_-}{q_+} \frac{2m_1 m_2}{Q^2} \right) \\
C_1(x', Q^2) &= \frac{q_+}{4} \left[\frac{1}{2} - x'(1-x') - \frac{\Delta m^2 x'}{Q^2} (1-2x') + \left(\frac{\Delta m^2 x'}{Q^2} \right)^2 \right. \\
&\quad \left. + \frac{q_-}{q_+} \frac{m_1 m_2}{Q^2} 2x' (1-x' - x' \frac{m_1^2 + m_2^2}{Q^2}) \right] \\
E_1(x', Q^2) &= \frac{q_+}{4} (-1 + 2x' - 2x'^2) \\
A_2(x', Q^2) &= q_+ x' \left[x'^2 \frac{m_1^2}{Q^2} \left(\frac{1}{2} \left(\frac{\Delta m^2}{Q^2} \right)^2 + \frac{\Delta m^2 - m_1^2}{Q^2} + \frac{1}{2} \right) \right] \\
C_2(x', Q^2) &= q_+ \frac{x'}{4} \left[1 - 2x'(1-x') + \frac{m_1^2}{Q^2} (1 + 8x' - 18x'^2) \right. \\
&\quad \left. + \frac{m_2^2}{Q^2} (1 - 4x' + 6x'^2) - \frac{m_1^4 + m_2^4}{Q^4} 2x'(1-3x') + \frac{m_1^2 m_2^2}{Q^4} 4x'(1-5x') \right. \\
&\quad \left. + \frac{\Delta m^4 \Delta m^2}{Q^6} 2x'^2 - \frac{q_-}{q_+} \frac{2m_1 m_2}{Q^2} \right] \\
E_2(x', Q^2) &= q_+ x' \left[-\frac{1}{2} + 3x'(1-x') \right] \\
A_3(x', Q^2) &= R_q m_1^2 x'^2 \frac{\Delta m^2 + Q^2}{Q^4} \\
C_3(x', Q^2) &= R_q \left[\frac{1}{2} - x'(1-x') - \frac{\Delta m^2}{Q^2} x'(1-2x') + \frac{\Delta m^4}{Q^4} x'^2 \right] \\
E_3(x', Q^2) &= 0 \\
B_{i=1,2}^{1,2}(x', Q^2) &= \pm A_i(x', Q^2) [m_1 \leftrightarrow m_2] \\
D_{i=1,2}^{1,2}(x', Q^2) &= \pm C_3(x', Q^2) [m_1 \leftrightarrow m_2]
\end{aligned}$$

where $\Delta m^n \equiv m_2^n - m_1^n$, $m_{1,2}$ being the mass of the heavy quark $Q_{1,2}$. The kinematical boundaries of phase space in the convolutions in Eq. (2.1) are

$$ax = \left[1 + \frac{(m_1 + m_2)^2}{Q^2} \right] x \quad , \quad \zeta_{min,max}(x') = \frac{1}{2} \left[1 + \frac{\Delta m^2}{Q^2} \frac{x'}{1-x'} \pm v\bar{v} \right] \quad (2.3)$$

with $v^2 = 1 - \frac{(m_1 + m_2)^2}{Q^2} \frac{x'}{1-x'}$, $\bar{v}^2 = 1 - \frac{(m_1 - m_2)^2}{Q^2} \frac{x'}{1-x'}$. The vector (V) and axialvector (A) couplings of the $\gamma_\mu(V - A\gamma_5)$ quark current enter via $q_\pm = V^2 \pm A^2$, $R_q = VA$.¹ If the partonic structure functions in Eq. (2.2) are integrated over ζ the well

¹For the γ^*Z interference term the couplings read: $q_\pm = V^\gamma V^Z \pm A^\gamma A^Z$, $R_q = 1/2(V^\gamma A^Z + V^Z A^\gamma)$.

known inclusive structure functions [33–35] for heavy flavor production are recovered:

$$\int_{\zeta_{min}(x')}^{\zeta_{max}(x')} d\zeta f_{i=1,2,3}(x', \zeta, Q^2) = \pm f_i(x', Q^2) \quad , \quad (2.4)$$

where the $f_i(x', Q^2)$ can be found in [33].

2.3 CC Leptoproduction within ACOT

In the following we will consider the special case of charged current charm production, i.e., $m_1 = m_s$, $m_2 = m_c$ ($q_{\pm} = 2, 0$; $R_q = 1$ assuming a vanishing Cabibbo angle). Of course, all formulae below can be trivially adjusted to the general case of Eqs. (2.1) and (2.2). The $m_s \rightarrow 0$ limit of the partonic structure functions in Eq. (2.2) is obtained by keeping terms up to $\mathcal{O}(m_s^2)$ in the A_i , C_i and in ζ_{max} due to the singularity of the phase space integration stemming from $\zeta \rightarrow 1$. One obtains

$$\begin{aligned} \lim_{m_s \rightarrow 0} \frac{\pi}{\alpha_s} f_i(x', \zeta, Q^2) &= c_i H_i^g\left(\frac{x'}{\lambda}, \zeta, m_s^2, \lambda\right) \\ &= c_i \delta(1 - \zeta) P_{qg}^{(0)}\left(\frac{x'}{\lambda}\right) \ln \frac{Q^2 + m_c^2}{m_s^2} + \mathcal{O}(m_s^0) \end{aligned} \quad (2.5)$$

where $P_{qg}^{(0)}(x') = \frac{1}{2}[x'^2 + (1 - x'^2)]$, $\lambda = Q^2/(Q^2 + m_c^2)$, $c_1 = 1/2$, $c_2 = x'/\lambda$, $c_3 = 1$ and the H_i^g are the dimensionally regularized $\overline{\text{MS}}$ ($m_s = 0$) gluonic coefficient functions obtained in [31]. The c_i arise from different normalizations of the f_i and the H_i^g and are such that the infrared-safe subtracted [see Sec. 2.4] convolutions in Eq. (2.1) converge towards the corresponding ones in [31] as $m_s \rightarrow 0$ if one realizes that $x'/\lambda = \xi'$, $x/\lambda = \xi \equiv x(1 + m_c^2/Q^2)$. Taking also the limit $m_c \rightarrow 0$ in Eq. (2.5) gives –besides the collinear logarithm already present in Eq. (2.5)– finite expressions which agree with the massless results of [29, 30].

In the ACOT formalism the GF convolutions in Eq. (2.1) coexist with the Born level quark scattering contributions $F_i^{QS}(x, z, Q^2) = k_i s(\xi, \mu^2) D_c(z)$, $k_{i=1,2,3} = 1$, 2ξ , 2 . The overlap between the QS and the GF contributions is removed by introducing a subtraction term (SUB) [20] which is obtained from the massless limit in Eq. (2.5)

$$F_i^{SUB} = k_i \frac{\alpha_s(\mu^2)}{2\pi} \ln \frac{\mu^2}{m_s^2} \left[\int_{\xi}^1 \frac{dx'}{x'} g(x', \mu^2) P_{qg}^{(0)}\left(\frac{\xi}{x'}\right) \right] D_c(z) \quad . \quad (2.6)$$

The complete $\mathcal{O}(\alpha_s)$ structure functions for the z distribution of charmed hadrons (i.e., dominantly D-mesons) produced in charged current DIS are then given in the ACOT formalism [20] by

$$F_i^{ACOT} = F_i^{QS} - F_i^{SUB} + F_i^{GF} \quad . \quad (2.7)$$

It is worthwhile noting that general results for polarized partonic structure functions analogous to the unpolarized ones in Eq. (2.2) have been obtained in [36] allowing for a formulation of polarized one-hadron inclusive heavy flavor leptonproduction within the ACOT scheme along the same lines.

2.4 Numerical Results

In Fig. 2.1 we show the structure function F_2^{ACOT} at experimentally relevant [16] values of x and Q^2 for several finite choices of m_s together with the asymptotic $m_s \rightarrow 0$ limit. For D_c we use a Peterson fragmentation function [37]

$$D_c(z) = N \left\{ z \left[1 - z^{-1} - \varepsilon_c / (1 - z) \right]^2 \right\}^{-1} \quad (2.8)$$

with $\varepsilon_c = 0.06$ [38–40] normalized to $\int_0^1 dz D_c(z) = 1$ and we employ the GRV94(HO) parton distributions [41] with $m_c = 1.5$ GeV. Our choice of the factorization scale is $\mu^2 = Q^2 + m_c^2$ which ensures that there is no large $\ln(Q^2 + m_c^2)/\mu^2$ present in the difference GF-SUB. As can be seen from Fig. 2.1 the effects of a finite strange mass are small and converge rapidly towards the massless $\overline{\text{MS}}$ limit provided $m_s \lesssim 200$ MeV as is usually assumed [17].

In Fig. 2.2 we show the effects of adding the quark-initiated $\mathcal{O}(\alpha_s)$ correction from the process $W^+s \rightarrow cg$ (together with virtual corrections) to the asymptotic ($m_s \rightarrow 0$) F_2^{ACOT} , employing the CTEQ4($\overline{\text{MS}}$) densities [42] with $m_c = 1.6$ GeV. The $\mathcal{O}(\alpha_s)$ quark contribution is usually neglected in the ACOT formalism since it is assumed to be effectively suppressed by one order of α_s with respect to the gluon fusion contribution due to $s(x, \mu^2)/g(x, \mu^2) \simeq \mathcal{O}(\alpha_s)$. To check this assumption for the quantity $F_2(x, z, Q^2)$ we show, besides the full result, the contributions from the distinct processes (using again $\mu^2 = Q^2 + m_c^2$). The $W^+g \rightarrow c\bar{s}$ contribution corresponds to GF-SUB in Eq. (2.7). The quark-initiated $\mathcal{O}(\alpha_s)$ contribution has been calculated in the $\overline{\text{MS}}$ scheme according to [31] which is consistent with the asymptotic gluon-initiated correction in the ACOT scheme

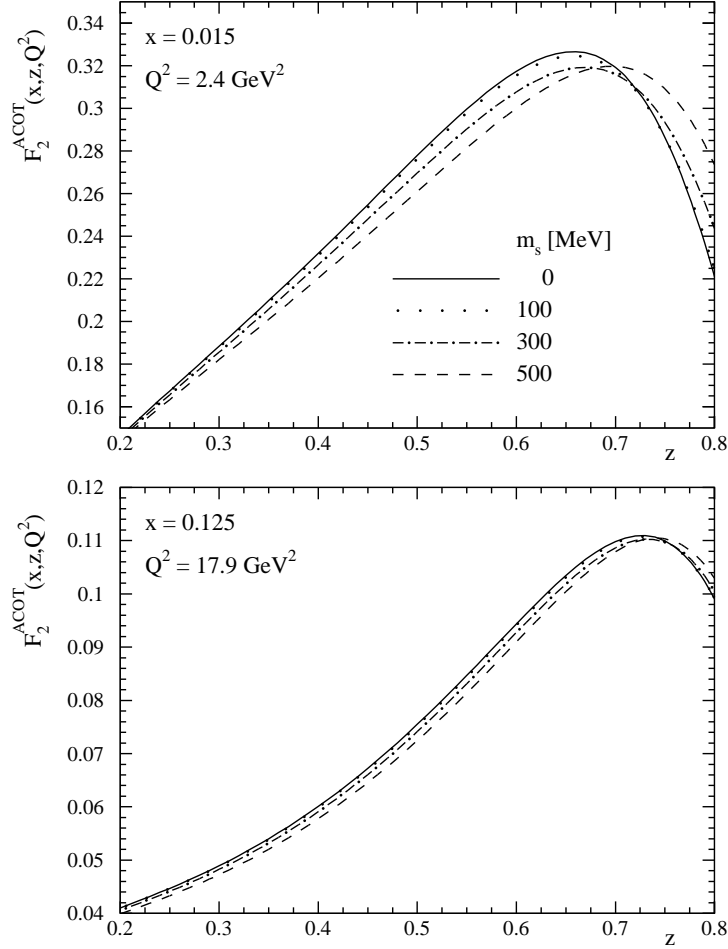


Figure 2.1: The structure function $F_2^{ACOT}(x, z, Q^2)$ as defined in Eq. (2.7) using the GRV94(HO) parton densities [41] with $m_c = 1.5$ GeV and a Peterson fragmentation function [37] with $\varepsilon_c = 0.06$. Several finite choices for m_s are shown as well as the asymptotic $m_s \rightarrow 0$ limit.

due to Eq. (2.5). It can be seen that the quark-initiated correction is comparable in size to the gluon-initiated correction around the maximum of F_2 . Since most of the experimentally measured D-mesons originate from this region the $\mathcal{O}(\alpha_s)$ quark contributions should not be neglected in a complete NLO calculation.

2.5 Summary

To summarize we have given formulae which extend the ACOT scheme [20] for the leptonproduction of heavy quarks from its fully inclusive formulation to one-hadron inclusive leptonproduction. We have applied this formulation to D-meson production in charged current DIS and studied finite m_s corrections to the asymptotic $m_s \rightarrow 0$ limit. The cor-

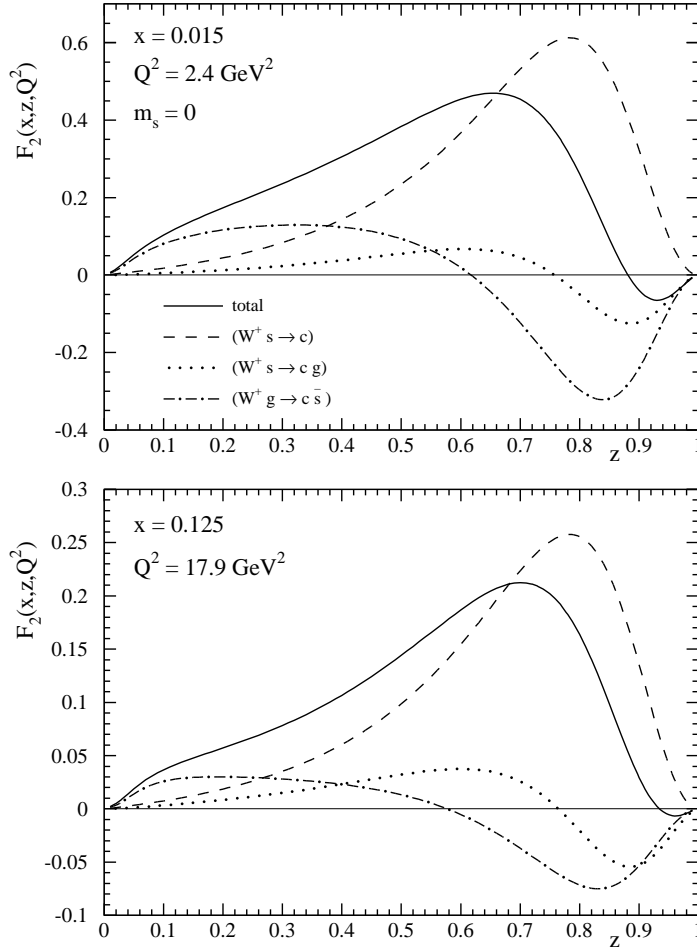


Figure 2.2: The structure function $F_2(x, z, Q^2)$ for charged current leptonproduction of D-mesons at $\mathcal{O}(\alpha_s)$ for $m_s = 0$ using the CTEQ4($\overline{\text{MS}}$) parton distributions [42] and a Peterson fragmentation function [37] with $\varepsilon_c = 0.06$. The full $\mathcal{O}(\alpha_s)$ result is shown as well as the individual contributions from the distinct quark- and gluon-initiated processes.

rections turned out to be small for reasonable choices of $m_s \lesssim 200 \text{ MeV}$ and we have shown that the $m_s \rightarrow 0$ limit reproduces the dimensionally regularized $\overline{\text{MS}}$ ($m_s = 0$) gluonic coefficient functions [31]. Furthermore we have investigated the quark-initiated $\mathcal{O}(\alpha_s)$ corrections for $m_s = 0$ using the relevant $\overline{\text{MS}}$ fermionic coefficient functions [31]. The latter corrections turned out to be numerically important at experimentally relevant values of x and Q^2 [16] and should be included in a complete NLO calculation of charged current leptonproduction of D-mesons. In the next chapter, the quark-initiated diagrams will be calculated up to $\mathcal{O}(\alpha_s)$ in the ACOT scheme allowing to study finite m_s effects stemming from these contributions as has been done in this chapter for the $\mathcal{O}(\alpha_s)$ gluon contributions.

Chapter 3

Quark Masses in Deep Inelastic Structure Functions

In this chapter we consider heavy quark contributions to inclusive deep inelastic structure functions within the ACOT variable flavor number scheme to which we contribute the calculation of the before missing Bremsstrahlung corrections (incl. virtual graphs) off initial state massive quarks. The calculation exemplifies factorization with massive quark-partons as has recently been proven to all orders in perturbation theory by Collins [21]. After identifying the correct subtraction term the convergence of these contributions towards the analogous coefficient functions for massless quarks, obtained within the modified minimal subtraction scheme ($\overline{\text{MS}}$), is demonstrated. Furthermore, the phenomenological relevance of the contributions to neutral current (NC) and charged current (CC) structure functions is investigated for several choices of the factorization scale. The results presented in this chapter are taken from Ref. [3].

3.1 Introduction

Leptoproduction of heavy quarks has become a subject of major interest in QCD phenomenology both for experimental and theoretical reasons. Heavy quark contributions are an important component of measured neutral current (NC) [11–13] and charged current (CC) [43] deep inelastic (DI) structure functions at lower values of Bjorken- x , accessible to present experiments. Charm tagging in NC and CC deep inelastic scattering (DIS) offers the possibility to pin down the nucleon’s gluon [44] and strange sea [16, 17, 45, 46] density, respectively, both of which are nearly unconstrained by global fits to inclusive DI data.

Theoretically it is challenging to understand the production mechanism of heavy quarks within perturbative QCD. The cleanest and most predictive method [18] of calculating heavy quark contributions to structure functions seems to be fixed order perturbation theory (FOPT) where heavy quarks are produced exclusively by operators built from light quarks (u,d,s) and gluons (g) and no initial state heavy quark lines show up in any Feynman diagram. Heavy quarks produced via FOPT are therefore also called ‘extrinsic’ since no contractions of heavy quark operators with the nucleon wavefunction are considered (which in turn would be characteristic for ‘intrinsic’ heavy quarks). Besides FOPT much effort has been spent on formulating variable flavor number schemes (VFNS) [19, 20, 22–24] which aim at resumming the quasi-collinear logs $[\ln(Q^2/m^2)]$; Q and m being the virtuality of the mediated gauge boson and the heavy quark mass, respectively] arising at any order in FOPT. All these schemes have in common that extrinsic FOPT induces the boundary condition [23, 47]

$$q(x, Q_0^2 = m^2) = 0 + \mathcal{O}(\alpha_s^2) \quad (3.1)$$

for an intrinsic heavy quark density, which then undergoes massless renormalization group (RG) evolution. Apart from their theoretical formulation VFNS have to be well understood phenomenologically for a comparison with FOPT and with heavy quark tagged DIS data. We will concentrate here on the scheme developed by Aivazis, Collins, Olness and Tung (ACOT) [19–21]. In the ACOT scheme full dependence on the heavy quark mass is kept in graphs containing heavy quark lines. This gives rise to the above mentioned quasi-collinear logs as well as to power suppressed terms of $\mathcal{O}[(m^2/Q^2)^k]$. While the latter give mass corrections to the massless, dimensionally regularized, standard coefficient functions (e.g. in the $\overline{\text{MS}}$ scheme), the former are removed by numerical subtraction since the collinear region of phase space is already contained in the RG evolution of the heavy quark density. Up to now explicit expressions in this scheme exist for DIS on a heavy quark at $\mathcal{O}(\alpha_s^0)$ [19] as well as for the production of heavy quarks via virtual boson gluon fusion (GF) at $\mathcal{O}(\alpha_s^1)$ [20]. In Section 3.2 we will give expressions which complete the scheme up to $\mathcal{O}(\alpha_s^1)$ and calculate DIS on a heavy quark at first order in the strong coupling, i.e. $B^*Q_1 \rightarrow Q_2g$ (incl. virtual corrections to $B^*Q_1 \rightarrow Q_2$) with general couplings of the virtual boson B^* to the heavy quarks, keeping all dependence on the masses $m_{1,2}$ of the quarks $Q_{1,2}$. It is unclear whether (heavy) quark scattering (QS) and GF at $\mathcal{O}(\alpha_s^1)$ should be considered on the same level in the perturbation series. Due to its extrinsic prehis-

tory $QS^{(1)}$ (bracketed upper indices count powers¹ of α_s) includes a collinear subgraph of $GF^{(2)}$, e.g. $\gamma^*c \rightarrow cg$ contains the part of $\gamma^*g \rightarrow c\bar{c}g$, where the gluon splits into an almost on-shell $c\bar{c}$ pair. Therefore QS at $\mathcal{O}(\alpha_s^1)$ can be considered on the level of GF at $\mathcal{O}(\alpha_s^2)$. On the other hand the standard counting for light quarks is in powers of α_s and heavy quarks should fit in. We therefore suggest that the contributions obtained in Section 3.2 should be included in complete experimental and theoretical NLO-analyses which make use of the ACOT scheme. Theoretically the inclusion is required for a complete renormalization of the heavy quark density at $\mathcal{O}(\alpha_s^1)$. However, we leave an ultimate decision on that point to numerical relevance and present numerical results in Section 3.3. Not surprisingly they will depend crucially on the exact process considered (e.g. NC or CC) and the choice of the factorization scale. Finally, in Section 3.4 we draw our conclusions. Some technical aspects and lengthy formulae are relegated to the Appendix A.

3.2 Heavy Quark Contributions to ACOT Structure Functions

In this section we will present all contributions to heavy quark structure functions up to $\mathcal{O}(\alpha_s^1)$. They are presented analytically in their fully massive form together with the relevant numerical subtraction terms which are needed to remove the collinear divergences in the high Q^2 limit. Section 3.2.1 and 3.2.3 contain no new results and are only included for completeness. In Section 3.2.2 we present our results for the massive analogue of the massless \overline{MS} coefficient functions $C_i^{q,\overline{MS}}$.

3.2.1 DIS on a Massive Quark at $\mathcal{O}(\alpha_s^0)$

The $\mathcal{O}(\alpha_s^0)$ results for $B^*Q_1 \rightarrow Q_2$, including mass effects, have been obtained in [19] within a helicity basis for the hadronic and partonic structure functions. For completeness and in order to define our normalization we repeat these results here within the standard tensor basis implying the usual structure functions $F_{i=1,2,3}$. The helicity basis seems to be advantageous since in the tensor basis partonic structure functions mix to give hadronic structure functions in the presence of masses [19]. However, the mixing matrix is diagonal [19] for the experimental relevant structure functions $F_{i=1,2,3}$ and only mixes F_4 with F_5

¹For the reasons given here we refrain in this chapter in most cases from using the standard terminology of ‘leading’ and ‘next-to-leading’ contributions and count explicit powers of α_s .

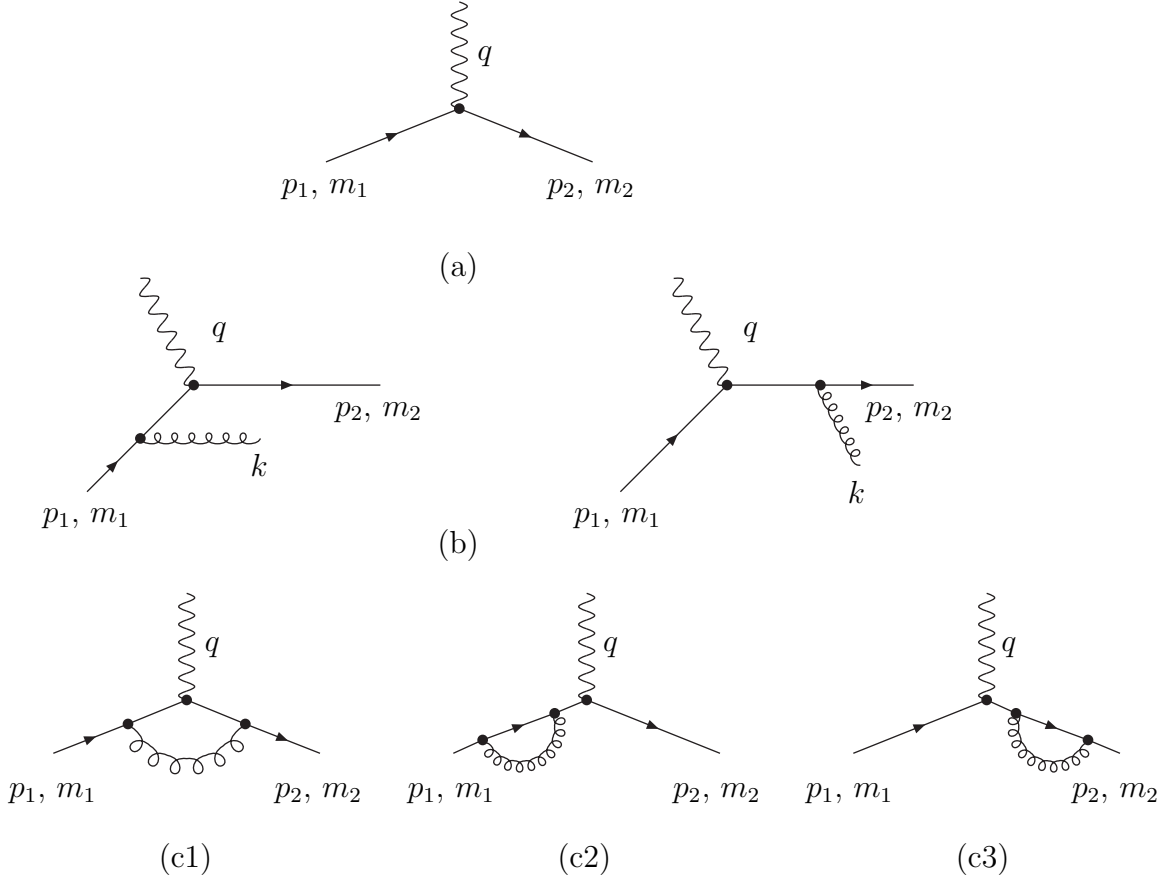


Figure 3.1: Feynman diagrams for the $QS^{(0)}$ (a) and $QS^{(1)}$ [(b), (c)] contributions to ACOT structure functions in Eqs. (3.3) and (3.9), respectively.

which are both suppressed by two powers of the lepton mass. We neglect target (nucleon) mass corrections which are important at larger values of Bjorken- x [19] where heavy quark contributions are of minor importance.

We consider DIS of the virtual Boson B^* on the quark Q_1 with mass m_1 producing the quark Q_2 with mass m_2 . At order $\mathcal{O}(\alpha_s^0)$ this proceeds through the parton model diagram in Fig. 3.1 (a).

Finite mass corrections to the massless parton model expressions are taken into account by adopting the Ansatz given in Eq. (17) of [19]

$$W^{\mu\nu} = \int \frac{d\xi}{\xi} Q_1(\xi, \mu^2) \hat{w}^{\mu\nu}|_{p_1^+ = \xi P^+} \quad . \quad (3.2)$$

$W^{\mu\nu}$ is the usual hadronic tensor and $\hat{w}^{\mu\nu}$ is its partonic analogue. Here as in the following

a hat on partonic quantities refers to unsubtracted amplitudes, i.e. expressions which still contain mass singularities in the massless limit. p_1^+ and P^+ are the light-cone momentum components of the incident quark Q_1 and the nucleon, respectively. Generally the ‘+’ light-cone component of a vector v is given by $v^+ \equiv (v^0 + v^3)/\sqrt{2}$.

Contracting the convolution in Eq. (3.2) with the projectors in Appendix A.1 gives the individual hadronic structure functions $F_{i=1,2,3}$. In leading order (LO) the latter are given by [19]

$$\begin{aligned} F_1^{QS^{(0)}}(x, Q^2) &= \frac{S_+ \Sigma_{++} - 2m_1 m_2 S_-}{2\Delta} Q_1(\chi, Q^2) \\ F_2^{QS^{(0)}}(x, Q^2) &= \frac{S_+ \Delta}{2Q^2} 2x Q_1(\chi, Q^2) \\ F_3^{QS^{(0)}}(x, Q^2) &= 2R_+ Q_1(\chi, Q^2) \end{aligned} \quad (3.3)$$

with

$$\Sigma_{\pm\pm} = Q^2 \pm m_2^2 \pm m_1^2 \quad . \quad (3.4)$$

In Eq. (3.3) we use the shorthand $\Delta \equiv \Delta[m_1^2, m_2^2, -Q^2]$, where the usual triangle function is defined by

$$\Delta[a, b, c] = \sqrt{a^2 + b^2 + c^2 - 2(ab + bc + ca)} \quad . \quad (3.5)$$

The vector (V) and axial vector (A) couplings of the $\bar{Q}_2 \gamma_\mu (V - A \gamma_5) Q_1$ quark current enter via the following combinations:

$$\begin{aligned} S_\pm &= VV' \pm AA' \\ R_\pm &= (VA' \pm V'A)/2 \end{aligned} \quad (3.6)$$

where $V, A \equiv V', A'$ in the case of pure B scattering and $V, A \neq V', A'$ in the case of B, B' interference (e.g. γ, Z^0 interference in the standard model). The scaling variable χ generalizes the usual Bjorken- x in the presence of parton masses and is given by [19]:

$$\chi = \frac{x}{2Q^2} (\Sigma_{+-} + \Delta) \quad . \quad (3.7)$$

The mass dependent structure functions in Eq. (3.3) motivate the following definitions

$$\left. \begin{aligned} \mathcal{F}_1 &= \frac{2\Delta}{S_+ \Sigma_{++} - 2m_1 m_2 S_-} F_1 \\ \mathcal{F}_2 &= \frac{2Q^2}{S_+ \Delta} \frac{1}{2x} F_2 \\ \mathcal{F}_3 &= \frac{1}{2R_+} F_3 \end{aligned} \right\} = Q_1(\chi, Q^2) + \mathcal{O}(\alpha_s^1) \quad (3.8)$$

such that $\mathcal{F}_i - \mathcal{F}_j$, $i, j = 1, 2, 3$, will be finite of $\mathcal{O}(\alpha_s)$ in the limit $m_{1,2} \rightarrow 0$.

3.2.2 DIS on a Massive Quark at $\mathcal{O}(\alpha_s^1)$

At $\mathcal{O}(\alpha_s^1)$ contributions from real gluon emission [Fig. 3.1 (b)] and virtual corrections [Fig. 3.1 (c)] have to be added to the $\mathcal{O}(\alpha_s^0)$ results of Section 3.2.1. The vertex correction with general masses and couplings [Fig. 3.1 (c)] does to our knowledge not exist in the literature and is presented in some detail in Appendix A.2. The final result (virtual+real) can be cast into the following form:

$$\begin{aligned}\hat{\mathcal{F}}_{i=1,2,3}^{QS^{(0+1)}}(x, Q^2, \mu^2) &\equiv \mathcal{F}_i^{QS^{(0)}}(x, \mu^2) + \hat{\mathcal{F}}_i^{QS^{(1)}}(x, Q^2, \mu^2) \\ &= Q_1(\chi, \mu^2) + \frac{\alpha_s(\mu^2)}{2\pi} \int_{\chi}^1 \frac{d\xi'}{\xi'} \left[Q_1\left(\frac{\chi}{\xi'}, \mu^2\right) \hat{H}_i^q(\xi', m_1, m_2) \right]\end{aligned}\quad (3.9)$$

with $\xi' \equiv \frac{\chi}{\xi}$ and

$$\hat{H}_i^q(\xi', m_1, m_2) = C_F \left[(S_i + V_i) \delta(1 - \xi') + \frac{1 - \xi'}{(1 - \xi')_+} \frac{\hat{s} - m_2^2}{8\hat{s}} N_i^{-1} \hat{f}_i^Q(\xi') \right] \quad (3.10)$$

where $\hat{s} = (p_1 + q)^2$ and the S_i , V_i , N_i and \hat{f}_i^Q are given in Appendix A.3. The factorization scale μ^2 will be taken equal to the renormalization scale throughout. The ‘+’ distribution in Eq. (3.10) is a remnant of the cancellation of the soft divergences from the real and virtual contributions. It is defined as usual:

$$\int_0^1 d\xi' f(\xi') [g(\xi')]_+ \equiv \int_0^1 d\xi' [f(\xi') - f(1)] g(\xi') \quad (3.11)$$

As indicated by the hat on \hat{H}_i^q , the full massive convolution in Eq. (3.9) still contains the mass singularity arising from quasi-collinear gluon emission from the initial state quark leg. The latter has to be removed by subtraction in such a way that in the asymptotic limit $Q^2 \rightarrow \infty$ the well known massless $\overline{\text{MS}}$ expressions are recovered. The $\overline{\text{MS}}$ limit is mandatory since all modern parton distributions –and therefore all available heavy quark densities– are defined in this particular scheme (or in the DIS scheme [48], which can be straightforwardly derived from $\overline{\text{MS}}$). The correct subtraction term can be obtained from the following limit

$$\begin{aligned}\lim_{m_1 \rightarrow 0} \int_{\chi}^1 \frac{d\xi'}{\xi'} Q_1\left(\frac{\chi}{\xi'}, \mu^2\right) \hat{H}_i^q(\xi', m_1, m_2) &= \int_{x/\lambda}^1 \frac{d\xi'}{\xi'} Q_1\left(\frac{x}{\lambda\xi'}, \mu^2\right) \left\{ H_i^{q, \overline{\text{MS}}}(\xi', \mu^2, \lambda) \right. \\ &\quad + C_F \left[\frac{1 + \xi'^2}{1 - \xi'} \left(\ln \frac{\mu^2}{m_1^2} - 1 - 2 \ln(1 - \xi') \right) \right]_+ \Big\} \\ &\quad + \mathcal{O}\left(\frac{m_1^2}{Q^2}\right)\end{aligned}\quad (3.12)$$

where $\lambda = Q^2/(Q^2 + m_2^2)$, $x/\lambda = \chi|_{m_1=0}$ and the $H_i^{q,\overline{\text{MS}}}$ can be found in [49, 50]. Obviously the $\overline{\text{MS}}$ subtraction term for a ‘heavy quark inside a heavy quark’ is given not only by the splitting function $P_{qq}^{(0)} = C_F[(1 + \xi'^2)/(1 - \xi')]_+$ times the collinear log $\ln(\mu^2/m_1^2)$ but also comprises a constant term. Herein we agree with Eq. (3.15) in [51]², where this was first pointed out in the framework of perturbative fragmentation functions for heavy quarks. We therefore define

$$\mathcal{F}_i^{SUBq}(x, Q^2, \mu^2) = \frac{\alpha_s(\mu^2)}{2\pi} C_F \int_{\chi}^1 \frac{d\xi'}{\xi'} \left[\frac{1 + \xi'^2}{1 - \xi'} \left(\ln \frac{\mu^2}{m_1^2} - 1 - 2 \ln(1 - \xi') \right) \right]_+ Q_1 \left(\frac{\chi}{\xi'}, \mu^2 \right) \quad (3.13)$$

such that

$$\lim_{m_1 \rightarrow 0} \left[\hat{\mathcal{F}}_i^{QS(1)}(x, Q^2, \mu^2) - \mathcal{F}_i^{SUBq}(x, Q^2, \mu^2) \right] = \mathcal{F}_i^{Q_1^{(1)}, \overline{\text{MS}}}(x, Q^2, \mu^2) \quad , \quad (3.14)$$

where the superscript Q_1 on $\mathcal{F}_i^{Q_1^{(1)}, \overline{\text{MS}}}$ refers to that part of the inclusive structure function \mathcal{F}_i which is initiated by the heavy quark Q_1 , i.e. which is obtained from a convolution with the heavy quark parton density. Note that the limit in Eq. (3.12) guarantees that Eq. (3.14) is also fulfilled when $m_1 = m_2 \rightarrow 0$ (e.g. NC leptonproduction of charm) since

$$\lim_{m_2 \rightarrow 0} H_i^{q, \overline{\text{MS}}}(\xi', \mu^2, \lambda) = C_i^{q, \overline{\text{MS}}}(\xi', \mu^2) + \mathcal{O}\left(\frac{m_2^2}{Q^2}\right) \quad (3.15)$$

where $C_i^{q, \overline{\text{MS}}}$ are the standard massless coefficient functions in the $\overline{\text{MS}}$ scheme, e.g. in [30, 48].

Comparison to Existing NC and CC Results

We have performed several cross checks of our results against well known calculations that exist in the literature [30, 48, 49, 52, 53]. The checks can be partly inferred from the above paragraph. Nevertheless we present here a systematic list for the reader’s convenience and to point out discrepancies of our calculation with [53].

In the charged current case $V = A = 1$ our results in Eq. (3.9) reduce in the limit $m_1 \rightarrow 0$ to the corresponding expressions in [52], or in [49, 50] if the scheme dependent term represented by Eq. (3.13) is taken into account. The latter agrees with Eq. (3.15)

²We also agree with the quark initiated coefficient functions in [52] where quark masses have been used as regulators.

in [51]. For $m_{1,2} \rightarrow 0$ we reproduce the well known $\overline{\text{MS}}$ coefficient functions, e.g., in [30, 48, 54]. The vertex correction in Appendix A.2 is implicitly tested because it contributes to any of the final results. However, as an independent cross check the well known QED textbook result can be reproduced for $m_1 = m_2$, $A = 0$.

Initial state parton mass effects in NC DIS at $\mathcal{O}(\alpha_s^1)$ have been first considered in [53] within the scenario [55] of intrinsic nonperturbative $c\bar{c}$ pairs stemming from fluctuations of the nucleon Fock space wavefunction. Although we do not consider such a scenario here we note that our results could be easily transferred to corresponding applications [56]. The main difference would be an inclusion of kinematical target mass effects which are important at larger x [19] where a possible nonperturbative charm component is expected [55] to reside. We list a detailed comparison of our calculation to the one in [53] in Appendix A.4. Since our calculation does not fully agree with [53] for reasons which we are completely able to trace back and given the amount of successful independent tests of our results we regard the disagreement with [53] as a clear evidence that the results in [53] should be updated by our calculation.

3.2.3 Gluon Fusion Contributions at $\mathcal{O}(\alpha_s^1)$

The gluon fusion contributions to heavy quark structure functions, depicted in Fig. 3.2, ($B^*g \rightarrow \bar{Q}_1 Q_2$) are known for a long time [33–35] and have been reinterpreted in [20] within the helicity basis for structure functions. Here we only briefly recall the corresponding for-

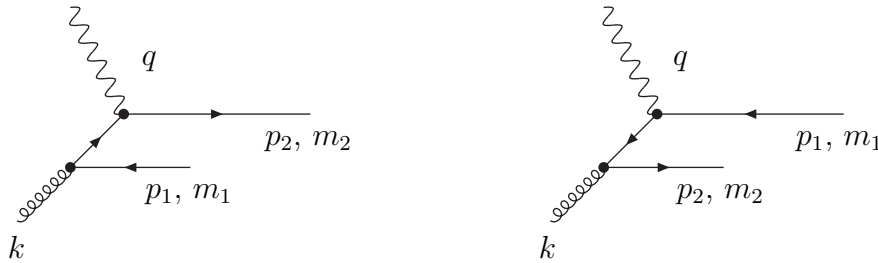


Figure 3.2: Feynman diagrams for the production of a massive quark–antiquark pair via boson–gluon fusion.

mulae in the tensor basis for completeness. The GF component of DI structure functions

is given by

$$\begin{aligned} F_{1,3}^{GF}(x, Q^2) &= \int_{ax}^1 \frac{d\xi'}{\xi'} g(\xi', \mu^2) f_{1,3}\left(\frac{x}{\xi'}, Q^2\right) \\ F_2^{GF}(x, Q^2) &= \int_{ax}^1 \frac{d\xi'}{\xi'} \xi' g(\xi', \mu^2) f_2\left(\frac{x}{\xi'}, Q^2\right) \end{aligned} \quad (3.16)$$

where $ax = [1 + (m_1 + m_2)^2/Q^2]x$ and the f_i can be found for general masses and couplings in [33]. The corresponding \mathcal{F}_i^{GF} are obtained from the F_i^{GF} by using the same normalization factors as in Eq. (3.8). Along the lines of [20] the GF contributions coexist with the QS contributions which are calculated from the heavy quark density, which is evolved via the massless RG equations in the $\overline{\text{MS}}$ scheme. As already pointed out in Section 3.2.2 the quasi-collinear log of the fully massive GF term has to be subtracted since the corresponding mass singularities are resummed to all orders in the massless RG evolution. The subtraction term for the GF contribution is given by [20]

$$\mathcal{F}_i^{SUBg}(x, Q^2, \mu^2) = \sum_k \frac{\alpha_s(\mu^2)}{2\pi} \ln \frac{\mu^2}{m_k^2} \int_\chi^1 \frac{d\xi'}{\xi'} P_{qg}^{(0)}(\xi') g\left(\frac{\chi}{\xi'}, \mu^2\right) \quad , \quad (3.17)$$

where $P_{qg}^{(0)}(\xi') = 1/2 [\xi'^2 + (1 - \xi')^2]$. Note that Eq. (3.17) as well as Eq. (3.13) are defined relative to the \mathcal{F}_i in Eq. (3.8) and not with respect to the experimental structure functions F_i . The sum in Eq. (3.17) runs over the indices of the quarks Q_k for which the quasi-collinear logs are resummed by massless evolution of a heavy quark density, i.e. $k = 1, k = 2$ or $k = 1, 2$.

3.2.4 ACOT Structure Functions at $\mathcal{O}(\alpha_s^1)$

As already mentioned in the introduction to this chapter it is not quite clear how the perturbation series should be arranged for massive quarks, i.e. whether the counting is simply in powers of α_s as for light quarks or whether an intrinsic heavy quark density carries an extra power of α_s due to its prehistory as an extrinsic particle produced by pure GF. We are here interested in the $QS^{(1)}$ component of heavy quark structure functions. Usually the latter is neglected in the ACOT formalism since it is assumed to be suppressed by one order of α_s with respect to the GF contribution as just explained above. We have, however, demonstrated in Chapter 2 within $\overline{\text{MS}}$ that this naive expectation is quantitatively not supported in the special case of semi-inclusive production of charm (dimuon events) in CC DIS. We therefore want to investigate the numerical relevance of the $QS^{(1)}$

contribution to general heavy quark structure functions. In this chapter we present results for the fully inclusive case, relevant for inclusive analyses and fits to inclusive data. We postpone experimentally more relevant semi-inclusive (z -dependent) results to Chapter 4. Our results at full $\mathcal{O}(\alpha_s^1)$ will be given by

$$F_i^{(1)} = F_i^{QS^{(0+1)}} + F_i^{GF} - F_i^{SUB_q} - F_i^{SUB_g} \quad (3.18)$$

with $F_i^{QS^{(0+1)}}$, F_i^{GF} , $F_i^{SUB_q}$ and $F_i^{SUB_g}$ given in Eqs. (3.9), (3.16), (3.13), and (3.17), respectively. Furthermore, we will also consider a perturbative expression for F_i which is constructed along the expectations of the original formulation of the ACOT scheme, i.e. $QS^{(1)}$ is neglected and therefore $F_i^{SUB_q}$ need not be introduced

$$F_i^{(0)+GF-SUB_g} = F_i^{QS^{(0)}} + F_i^{GF} - F_i^{SUB_g} \quad . \quad (3.19)$$

3.3 Results for NC and CC Structure Functions

In this section we present results which clarify the numerical relevance of $QS^{(1)}$ contributions to inclusive heavy quark structure functions in the ACOT scheme. We will restrict ourselves to NC and CC production of charm since bottom contributions are insignificant to present DI data. Our canonical parton distributions for the NC case will be CTEQ4M [42] (Figs. 3.5 and 3.6 below), which include ‘massless heavy partons’ Q_k above the scale $Q^2 = m_k^2$. Figures 3.3 and 3.4, however, have been obtained from the older GRV92 [57] distributions. The newer GRV94 [41] parametrizations do not include a resummed charm density since they are constructed exclusively along FOPT. GRV94 is employed in the CC case, Section 3.3.2. The radiative strange sea of GRV94 seems to be closest to presently available CC charm production data [31]. Furthermore, the low input scale of GRV94 allows for a wide range of variation of the factorization scale around the presently relevant experimental scales, which are lower for CC DIS than for NC DIS. Qualitatively all our results do not depend on the specific set of parton distributions chosen.

3.3.1 NC Structure Functions

For our qualitative analysis we are only considering photon exchange and we neglect the Z^0 . The relevant formulae are all given in Section 3.2 with the following identifications:

$$Q_{1,2} \rightarrow c$$

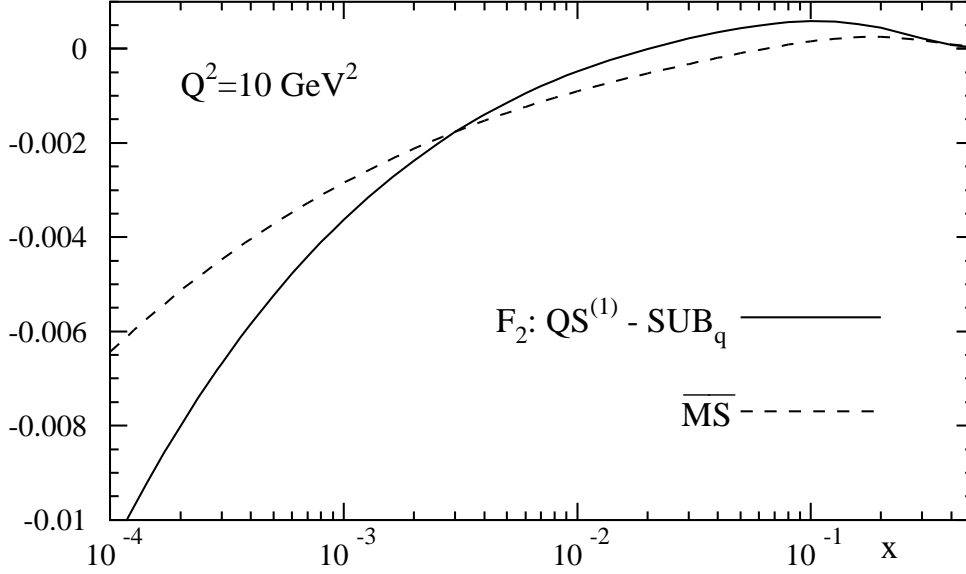


Figure 3.3: x -dependence of the subtracted $QS^{(1)}$ contribution to the NC charm structure function F_2^c (solid line). $Q^2 = \mu^2 = 10 \text{ GeV}^2$ is fixed. For comparison the $\overline{\text{MS}}$ analogue in Eq. (3.20) is shown (dashed line). The GRV92 parton distributions have been used.

$$m_{1,2} \rightarrow m_c = 1.6 \text{ (1.5) GeV for CTEQ4 (GRV92)}$$

$$V = V', A = A' \rightarrow \frac{2}{3}, 0$$

and we use $\mu^2 = Q^2$ if not otherwise noted. We consider contributions from charmed quarks and anti-quarks which are inseparably mixed by the GF contribution. This means that in Eq. (3.17) the sum runs over $k = 1, 2$ and the relevant expressions of Section 3.2.1 and 3.2.2 have to be doubled [since $c(x, \mu^2) = \bar{c}(x, \mu^2)$].

First we investigate the importance of finite mass corrections to the limit in Eq. (3.14). In Fig. 3.3 the difference $\hat{F}_2^{QS^{(1)}} - F_2^{SUB_q}$ can be compared to its $\overline{\text{MS}}$ analogue which is

$$F_2^{(c+\bar{c})^{(1)}, \overline{\text{MS}}} = \frac{4}{9} x \frac{\alpha_s(\mu^2)}{2\pi} \left[(c + \bar{c})(\mu^2) \otimes C_2^{q, \overline{\text{MS}}} \left(\frac{Q^2}{\mu^2} \right) \right] (x, Q^2) \quad (3.20)$$

where \otimes denotes the usual (massless) convolution. From Fig. 3.3 it is obvious that the relative difference between ACOT and $\overline{\text{MS}}$ depends crucially on x . It can be large and only slowly convergent to the asymptotic $\overline{\text{MS}}$ limit as can be inferred from Fig. 3.4. Note that the solid curves in Figs. 3.3, 3.4 are extremely sensitive to the precise definition of the subtraction term in Eq. (3.13), e.g. changing $\chi \rightarrow x$ —which also removes the collinear singularity in the high Q^2 limit— can change the ACOT result by about a factor of 5

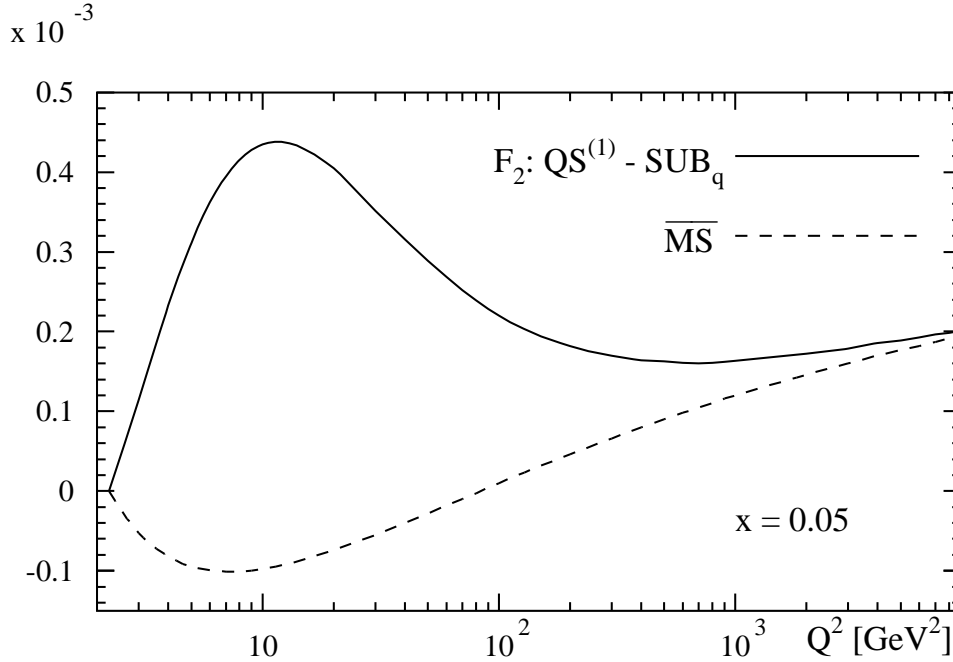


Figure 3.4: The same as Fig. 3.3 but varying $Q^2(= \mu^2)$ for fixed x .

around $Q^2 \sim 5 \text{ GeV}^2$.³ This is an example of the ambiguities in defining a variable flavor number scheme which have been formulated in a systematic manner in [22].

The relative difference between the subtracted $QS^{(1)}$ contribution calculated along ACOT and the corresponding $\overline{\text{MS}}$ contribution in Eq. (3.20) appears, however, phenomenologically irrelevant if one considers the significance of these contributions to the total charm structure function in Fig. 3.5. The complete $\mathcal{O}(\alpha_s^1)$ result (solid line) is shown over a wide range of Q^2 together with its individual contributions from Eq. (3.18). It can be clearly seen that the full massive $QS^{(1)}$ contribution is almost completely cancelled by the subtraction term SUB_q (Indeed the curves for $QS^{(1)}$ and SUB_q are hardly distinguishable on the scale of Fig. 3.5). The subtracted quark correction is numerically negligible and turns out to be indeed suppressed compared to the gluon initiated contribution, which is also shown in Fig. 3.5. Note, however, that the quark initiated corrections are not unimportant because they are intrinsically small. Rather the large massive contribution $QS^{(1)}$ is perfectly cancelled by the subtraction term SUB_q provided that $\mu^2 = Q^2$ is chosen. This is not necessarily the case for different choices of μ^2 as we will now demonstrate.

In Fig. 3.6 we show the dependence of the complete structure function and its components on the arbitrary factorization scale μ^2 . Apart from the canonical choice $\mu^2 = Q^2$

³The subtracted gluon contribution GF changes by about a factor of 2 under the same replacement.

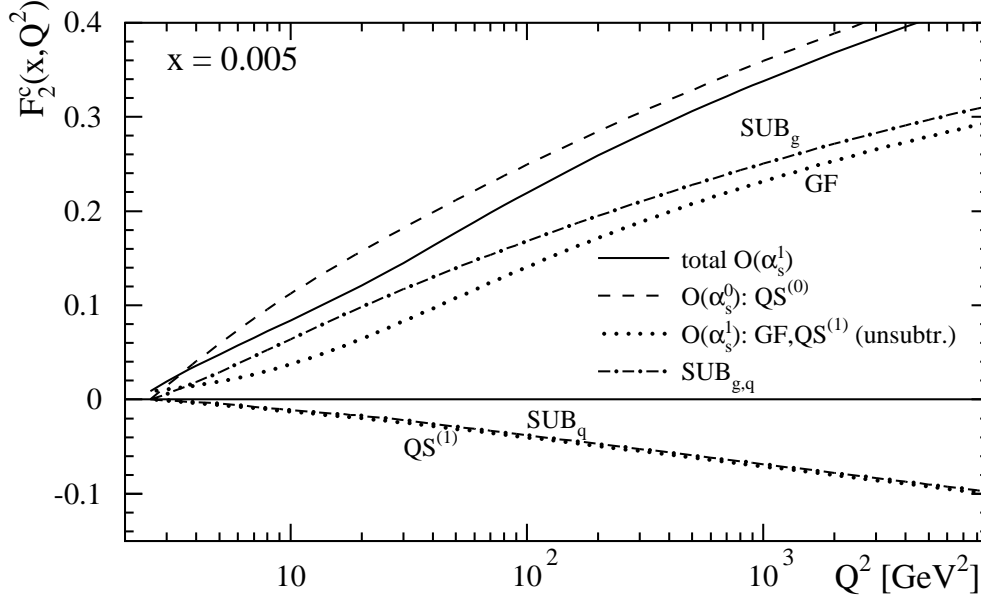


Figure 3.5: The complete $\mathcal{O}(\alpha_s^1)$ neutral current structure function F_2^c and all individual contributions over a wide range of Q^2 , calculated from the CTEQ4M distributions. Details of the distinct contributions are given in the text.

(which was used for all preceding figures) also different scales have been proposed [58, 59] like the maximum transverse momentum of the outgoing heavy quark which is approximately given by $(p_T^{max})^2 \simeq (1/x - 1) Q^2/4$. For low values of x , where heavy quark structure functions are most important, the scale $(p_T^{max})^2 \gg Q^2$. The effect of choosing a μ^2 which differs much from Q^2 can be easiest understood for the massless coefficient functions $C_i^{q,g,\overline{\text{MS}}}$ which contain an unresummed $\ln(Q^2/\mu^2)$. The latter is of course absent for $\mu^2 = Q^2$ but becomes numerically increasingly important, the more μ^2 deviates from Q^2 . This logarithmic contribution cannot be neglected since it is the unresummed part of the collinear divergence which is necessary to define the scale dependence of the charm density. This expectation is confirmed by Fig. 3.6. For larger values of μ^2 the subtracted $QS^{(1)}$ contribution is indeed still suppressed relative to the subtracted GF contribution. Nevertheless, its contribution to the total structure function becomes numerically significant and reaches the $\sim 20\%$ level around $(p_T^{max})^2$. Note that in this regime the involved formulae of Section 3.2.2 may be safely approximated by the much simpler convolution in Eq. (3.20) because they are completely dominated by the universal collinear logarithm and the finite differences $\text{ACOT} - \overline{\text{MS}}$ from Figs. 3.3 and 3.4 become immaterial. In practice it is therefore always legitimate to approximate the ACOT results of Section 3.2.2 by their $\overline{\text{MS}}$ analogues because both are either numerically insubstantial or logarithmically

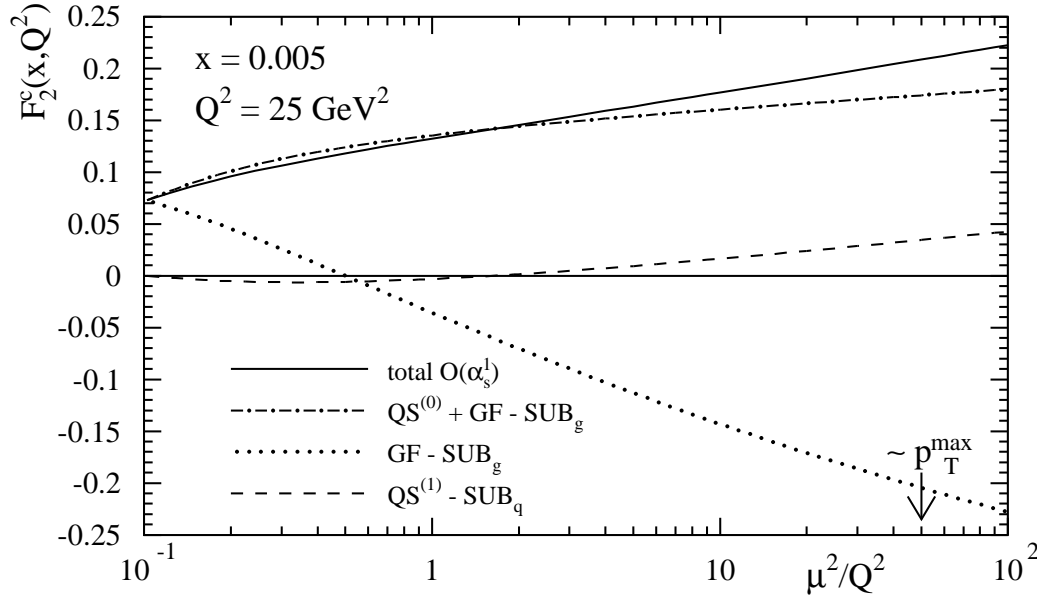


Figure 3.6: μ^2 dependence of the complete $\mathcal{O}(\alpha_s^1)$ NC structure function (CTEQ4M) in Eq. (3.18) (solid line) and of the structure function in Eq. (3.19) (dot-dashed line) where the subtracted $QS^{(1)}$ contribution is neglected. Also shown are the different subtracted $\mathcal{O}(\alpha_s^1)$ contributions GF and $QS^{(1)}$.

dominated. Finally we confirm that the scale dependence of the full $\mathcal{O}(\alpha_s^1)$ structure function $F_2^{(1)}$ in Eq. (3.18) is larger than the scale dependence of $F_i^{(0)+GF-SUB_g}$ in Eq. (3.19) which was already pointed out in [60]. Nevertheless, the subtracted $QS^{(1)}$ contribution should be respected for theoretical reasons whenever $\alpha_s \ln(Q^2/\mu^2) \not\ll 1$.

3.3.2 CC Structure Functions

Charm production in CC DIS is induced by an $s \rightarrow c$ transition at the W -Boson vertex. The strange quark is not really a heavy quark in the sense of the ACOT formalism, i.e., the production of strange quarks cannot be calculated reliably at any scale using FOPT because the strange quark mass is too small. It is nevertheless reasonable to take into account possible finite m_s effects into perturbative calculations using ACOT since the subtraction terms remove all long distance physics from the coefficient functions. Indeed the ACOT formalism has been used for an experimental analysis of CC charm production in order to extract the strange sea density of the nucleon [17]. Along the assumptions of ACOT $QS^{(1)}$ contributions have not been taken into account. This procedure is obviously questionable and has been shown not to be justified within the $\overline{\text{MS}}$ scheme in Chapter 2.

With our results in Section 3.2.2 we can investigate the importance of quark initiated $\mathcal{O}(\alpha_s^1)$ corrections within the ACOT scheme for inclusive CC DIS. As already mentioned above, results for the experimentally more important case of semi-inclusive (z -dependent) DIS will be presented in Chapter 4 of this thesis. In the following we only introduce subtraction terms for collinear divergencies correlated with the strange mass and treat all logarithms of the charm mass along FOPT. We do so for two reasons, one theoretical and one experimental: First, at present experimental scales of CC charm production $\ln(Q^2/m_c^2)$ terms can be safely treated along FOPT and no introduction of an a priori unknown charm density is necessary. Second, the introduction of a subtraction term for the mass singularity of the charm quark would simultaneously require the inclusion of the $c \rightarrow s$ QS -transition at the W -vertex with no spectator-like \bar{c} -quark as in GF . This contribution must, however, be absent when experiments tag on charm in the final state. CC DIS on massive charm quarks without final-state charm tagging has been studied in [61].

The numerics of this section can be obtained by the formulae of Section 3.2 with the following identifications:

$$\begin{aligned} Q_1 &\rightarrow s & , & & Q_2 &\rightarrow c \\ m_2 &\rightarrow m_c & = & & 1.5 \text{ GeV (GRV94)} \\ V &= V', A = A' & \rightarrow & & 1, 1 \end{aligned}$$

and the strange mass $m_1 = m_s$ will be varied in order to show its effect on the structure function F_2^c .

In Fig. 3.7 we show the structure function F_2^c and its individual contributions for two experimental values of x and Q^2 [16] under variation of the factorization scale μ^2 . Like in the NC case we show the complete $\mathcal{O}(\alpha_s^1)$ result as well as $F_2^{(0)+GF-SUB_g}$ where $QS^{(1)}$ has been neglected. The thick curves in Fig. 3.7 (a) have been obtained with a regularizing strange mass of 10 MeV. They are numerically indistinguishable from the $m_s = 0$ $\overline{\text{MS}}$ results along the lines of [49]. For the thin curves a larger strange mass of 500 MeV has been assumed as an upper limit. Finite mass effects can therefore be inferred from the difference between the thin and the thick curves. Obviously they are very small for all contributions and can be safely neglected. For the higher Q^2 value of Fig. 3.7 (b) they would be completely invisible, so we only show the $m_s = 10$ MeV results ($\equiv \overline{\text{MS}}$). Since the finite mass corrections within the ACOT scheme turn out to be negligible as compared

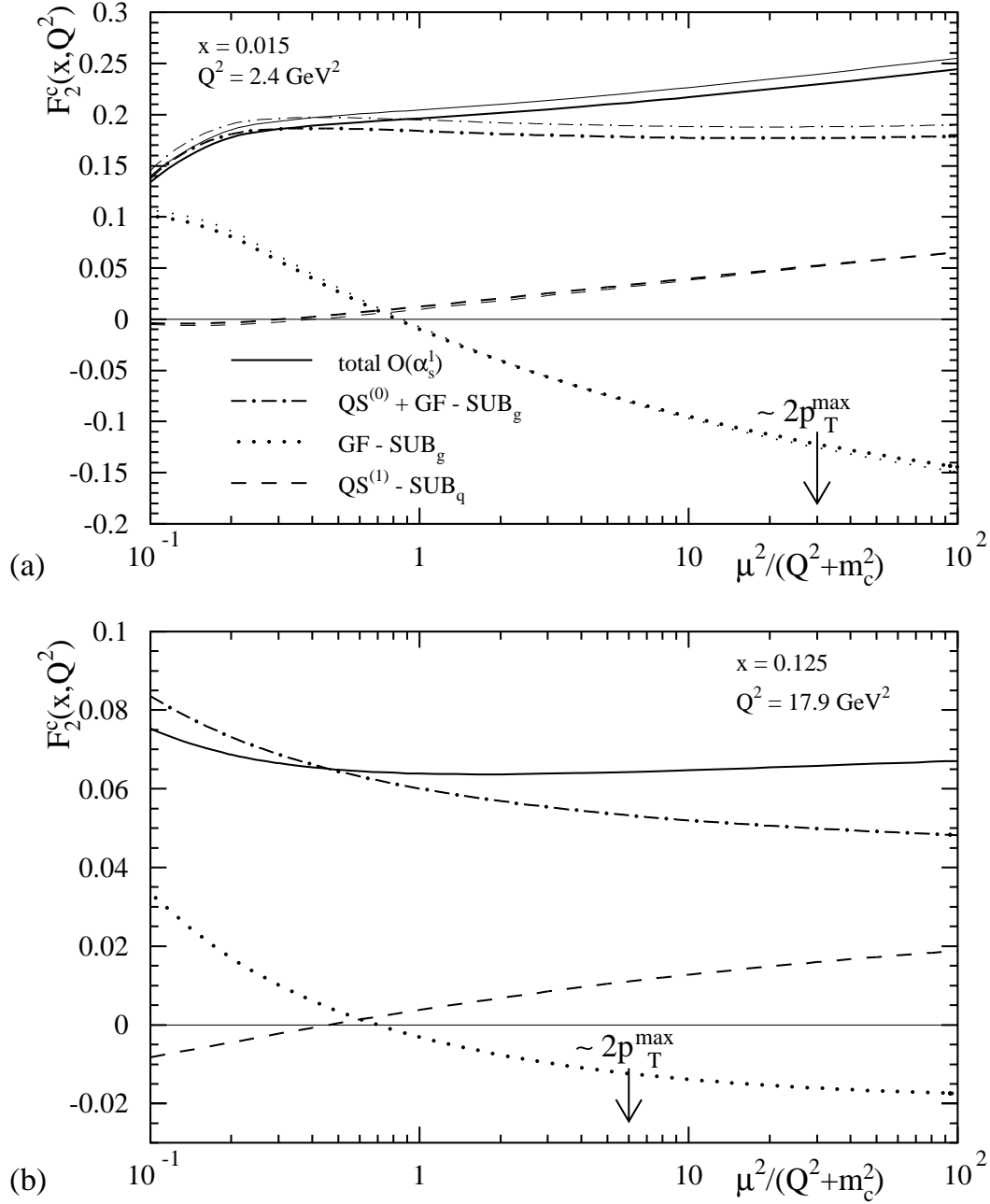


Figure 3.7: The charm production contribution to the charged current structure function F_2 for a wide range of the factorization scale μ^2 using GRV94. The curves are as for the neutral current case in Fig. 3.6. In Fig. 3.7 (a) the thicker curves have been obtained with a (purely regularizing) strange mass of 10 MeV which according to Eq. (3.14) (and to the analogous limit for the subtracted GF term [20]) numerically reproduces $\overline{\text{MS}}$. For the thinner curves a strange mass of 500 MeV has been assumed. In Fig. 3.7 (b) all curves correspond to $m_s = 10 \text{ MeV}$ ($\equiv \overline{\text{MS}}$).

to massless $\overline{\text{MS}}$ it is not surprising that we confirm the findings of Chapter 2 concerning the importance of quark initiated corrections. They are –in the case of CC production of charm– *not* suppressed with respect to gluon initiated corrections for all reasonable values of the factorization scale. Only for small choices of $\mu^2 \sim Q^2 + m_c^2$ can the quark initiated correction be neglected. In this region of μ^2 also gluon initiated corrections are moderate and Born approximation holds within $\sim 10\%$. For reasons explained in Section 3.3.1 the absolute value of both corrections –gluon and quark initiated– become very significant when large factorization scales like p_T^{max} are chosen. This can be inferred by looking at the region indicated by the arrow in Fig. 3.7 which marks the scale $\mu = 2p_T^{max}$ which was used in [17]. Analyses which use ACOT with a high factorization scale and neglect quark initiated corrections therefore undershoot the complete $\mathcal{O}(\alpha_s^1)$ result by the difference between the solid and the dot-dashed curve, which can be easily as large as $\sim 20\%$. For reasons explained in the introduction to this section we have used the radiative strange sea of GRV94. When larger strange seas like CTEQ4 are used the inclusion of the quark initiated contributions is even more important.

3.4 Conclusions

In this chapter we have calculated and analyzed DIS on massive quarks at $\mathcal{O}(\alpha_s^1)$ within the ACOT scheme for heavy quarks. For NC DIS this contribution differs significantly from its massless $\overline{\text{MS}}$ analogue for $\mu^2 = Q^2$. Both give, however, a very small contribution to the total charm structure function such that the large relative difference is phenomenologically immaterial. At higher values of the factorization scale $\mu^2 \sim (p_T^{max})^2$ the contributions become significant and their relative difference vanishes. The $QS^{(1)}$ contribution of Section 3.2.2 can therefore be safely approximated by its much simpler $\overline{\text{MS}}$ analogue at any scale. For CC DIS quark initiated corrections should always be taken into account on the same level as gluon initiated corrections. Due to the smallness of the strange quark mass ACOT gives results which are almost identical to $\overline{\text{MS}}$.

Chapter 4

Charm Fragmentation in Deep Inelastic Scattering

This chapter generalizes the theoretical considerations of Chapter 3 to the semi-inclusive deep inelastic production of heavy flavored hadrons. We apply these results to the CC and NC production of charm where we investigate the universality of charm fragmentation functions and the charm production dynamics, respectively. The work in this chapter is based on [4].

4.1 Introduction

In the preceeding chapter we have analyzed heavy quark initiated contributions to fully inclusive deep inelastic (DI) structure functions. Towards lower values of the Bjorken variable x , heavy (charm) quarks are produced in about 20% of the neutral current (NC) [11–13] and charged current (CC) [43] deep inelastic events in lepton–nucleon collisions. Therefore in this kinematical range, heavy quark events contribute an important component to the fully inclusive DI structure functions of the nucleon. However, due to acceptance losses this component can usually not be measured directly by inclusively tagging on charm events and more differential observables have to be considered like E_D [16, 17, 45], p_T or η [11–13, 15] distributions, where E_D , p_T and η are the energy, transverse momentum and pseudorapidity of the charmed hadron produced, i.e. mainly of a $D^{(*)}$ meson. In this chapter we consider E_D spectra represented by the usual scaling variable z defined below. Within DIS the charmed hadron energy spectrum is the distribution which is most sensitive to the charm fragmentation process and may give complementary information

to one hadron inclusive e^+e^- annihilation which is usually chosen to define fragmentation functions (FFs) [29, 62]. A well understanding of charm fragmentation is essential for any charm observable, e.g. the normalization of p_T and η distributions in photoproduction is substantially influenced by the hardness of the FF [63, 64]. The z distribution of charm fragments is directly measured in CC neutrino production [16, 17, 45] and may give insight into details of the charm production dynamics in NC electroproduction. It has, e.g., been shown in [11, 12] that the energy spectrum of $D^{(*)}$ -mesons produced at the ep collider HERA may be able to discriminate between intrinsic and extrinsic production of charm quarks.

Intrinsic heavy quark densities may arise due to a nonperturbative component of the nucleon wave function [55] or due to a perturbative resummation [20, 22–24] of large quasi-collinear logs $[\ln(Q^2/m^2)]$; Q and m being the virtuality of the mediated gauge boson and the heavy quark mass, respectively] arising at any order in fixed order extrinsic production (or fixed order perturbation theory: FOPT). Here we will only consider the latter possibility for inducing an intrinsic charm density $c(x, Q^2)$ which is concentrated at small x and we will ignore nonperturbative components which are expected to be located at large x [55]. Technically the resummation of large perturbative logs proceeds through calculating the boundary conditions for a transformation of the factorization scheme [23, 47, 51], which is switched from n_f to $n_f + 1$ active, massless flavors, canonically at $Q^2 = m^2$. For fully inclusive DIS the Kinoshita–Lee–Nauenberg theorem confines all quasi-collinear logs to the initial state such that they may be absorbed into $c(x, Q^2)$. For semi-inclusive DIS (SI DIS) also final state collinearities arise which are resummed in perturbative fragmentation functions $D_i^c(z, Q^2)$ (parton i decaying into charm quark c) along the lines of [51, 63]. The scale dependence of $c(x, Q^2)$ and $D_i^c(z, Q^2)$ is governed by massless renormalization group (RG) evolution.

Besides this *zero mass variable flavor number scheme*, where mass effects are only taken care of by the boundary conditions for $c(x, Q^2)$ and $D_i^c(z, Q^2)$, variable flavor number schemes have been formulated [20, 22–24], which aim at resumming the quasi-collinear logs as outlined above while also keeping power suppressed terms of $\mathcal{O}[(m^2/Q^2)^k]$ in the perturbative coefficient functions. Our reference scheme for this type of schemes will be the one developed by Aivazis, Collins, Olness and Tung (ACOT) [19–21]. In the ACOT scheme full dependence on the heavy quark mass is kept in graphs containing heavy quark lines. This gives rise to the above mentioned quasi-collinear logs and to the power

suppressed terms. While the latter are regarded as mass corrections to the massless, dimensionally regularized, standard coefficient functions (e.g. in the $\overline{\text{MS}}$ scheme), the former are removed numerically by subtraction terms, which are obtained from the small mass limit of the massive coefficient functions.

The outline of this chapter will be the following: In Section 4.2 we will shortly overview the relevant formulae for SI DIS for general masses and couplings including quark scattering (QS) and boson gluon fusion (GF) contributions up to $\mathcal{O}(\alpha_s^1)$. We will thereby present our ACOT based calculation for the $QS^{(1)1}$ component of SI structure functions. In Section 4.3 we will analyze the charm fragmentation function in CC and NC DIS. In Section 4.4 we draw our conclusions and some uncomfortably long formulae are relegated to Appendix B.

4.2 Semi-Inclusive Heavy Quark Structure Functions

This section presents the relevant formulae for one (heavy flavored) hadron inclusive DIS structure functions. The contributions from scattering events on massive quarks are given up to $\mathcal{O}(\alpha_s^1)$ in Section 4.2.1 and GF contributions are briefly recalled in Section 4.2.2. Section 4.2.3 presents all subtraction terms which render the structure functions infrared safe and includes a discussion of these terms.

4.2.1 Scattering on Massive Quarks

We consider DIS of the virtual Boson B^* with momentum q on the quark Q_1 with mass m_1 and momentum p_1 producing the quark Q_2 with mass m_2 and momentum p_2 . The latter fragments into a heavy quark flavored hadron H_{Q_2} , e.g. a $|Q_2 \bar{q}_l\rangle$ meson, q_l being any light quark. Phenomenologically most prominent are of course charm quarks fragmenting into $D^{(*)}$ -mesons which are the lightest heavy flavored hadrons.

We will strictly take over the formulae and notations of our inclusive analysis in Chapter 3 whenever possible and merely extend them for SI DIS considered here. In particular we take over the definition of the structure functions \mathcal{F}_i given in terms of the usual experimental structure functions F_i in Eq. (3.8).

¹Bracketed upper indices count powers of α_s .

Since we want to investigate the energy spectrum of charm fragments, we introduce the Lorentz-invariant $z \equiv p_{H_{Q_2}} \cdot p_N / q \cdot p_N$ which reduces to the energy $E_{H_{Q_2}}$ scaled to its maximal value $\nu = q_0$ in the target rest frame. Therefore in contrast to Eq. (A.4) we do not integrate the tensor $\hat{w}^{\mu\nu}$ over the full partonic phase space but keep it differential in the corresponding partonic variable $z' \equiv p_2 \cdot p_1 / q \cdot p_1$ or the mass corrected variable \hat{z} which is defined below. In order to obtain hadronic observables we have to extend the Ansatz of Eq. (17) in [19] such that it includes a nonperturbative hadronization function D_{Q_2} . In the limit of vanishing masses the massless parton model expressions have to be recovered. Our Ansatz will be

$$W^{\mu\nu} = \int \frac{d\xi}{\xi} \frac{d\zeta}{\zeta} Q_1(\xi, \mu^2) D_{Q_2}(\zeta, [\mu^2]) \hat{w}^{\mu\nu}|_{\{p_1^+ = \xi P^+, z = \zeta \hat{z}\}} \quad , \quad (4.1)$$

where μ is the factorization scale, $\hat{z} = z'/z'_{LO}$ with $z'_{LO} = \Sigma_{++}/\Sigma_{+-}$ and $v^+ \equiv (v^0 + v^3)/\sqrt{2}$ for a general vector v . $W^{\mu\nu}$ is the usual hadronic tensor and $\hat{w}^{\mu\nu}$ is its partonic analogue. Eq. (4.1) defines the fragmentation function D_{Q_2} to be a multiplicative factor multiplying inclusive structure functions at LO/Born accuracy, i.e.

$$\mathcal{F}_{i=1,2,3}^{QS(0)}(x, z, Q^2) = \mathcal{F}_{i=1,2,3}^{QS(0)}(x, Q^2) D_{Q_2}(z, [Q^2]) \quad , \quad (4.2)$$

where the $\mathcal{F}_{i=1,2,3}^{QS(0)}(x, Q^2)$ are defined and given in (3.8). The scale dependence of D_{Q_2} is bracketed here and in the following because it is optional; a more detailed discussion on this point will be given at the end of Section 4.2.3. We do not construct our Ansatz in Eq. (4.1) for the convolution of the fragmentation function along light front components for the outgoing particles which would only be Lorentz-invariant for boosts along a specified axis. Since the final state of DIS is spread over the entire solid angle it has no preferred axis as defined for the initial state by the beam direction of collider experiments. Note that Eq. (4.1) is in agreement with usual factorized expressions for massless initial state quanta, as considered, e.g., in Chapter 2, since there $m_1 = 0$ such that $z'_{LO} = 1$.

Up to $\mathcal{O}(\alpha_s^1)$ the hadronic structure functions for scattering on a heavy quark read

$$\begin{aligned} \hat{\mathcal{F}}_{i=1,2,3}^{QS(0+1)}(x, z, Q^2, \mu^2) &= Q_1(\chi, \mu^2) D_{Q_2}(z, [\mu^2]) + \frac{\alpha_s(\mu^2)}{2\pi} \int_{\chi}^1 \frac{d\xi'}{\xi'} \int_z^1 \frac{d\hat{z}}{\hat{z}} \\ &\times \left[Q_1\left(\frac{\chi}{\xi'}, \mu^2\right) \hat{H}_i^q(\xi', z', \mu^2) \Theta_q \right] D_{Q_2}\left(\frac{z}{\hat{z}}, [\mu^2]\right) \quad , \end{aligned} \quad (4.3)$$

with [19]

$$\chi = \frac{x}{2Q^2} (\Sigma_{+-} + \Delta) \quad . \quad (4.4)$$

As throughout this thesis we set the renormalization scale equal to the factorization scale In Eq. (4.3). The kinematical boundaries of the phase space in Eq. (4.3) are introduced by the theta function cut Θ_q . In the massless limit $\Theta_q \rightarrow 1$. The precise arguments of Θ_q are set by the kinematical requirement

$$z'_{\min} < z' < z'_{\max} \quad , \quad (4.5)$$

with

$$z'_{\min} = \frac{\pm \Delta[\hat{s}, m_1^2, -Q^2](\hat{s} - m_2^2) + (Q^2 + m_1^2 + \hat{s})(\hat{s} + m_2^2)}{2\hat{s}(\hat{s} - m_1^2 + Q^2)} \quad ,$$

where $\hat{s} = (p_1 + q)^2$. Note that Eq. (4.5) also poses an implicit constraint on ξ' via $z'_{\min} < z'_{\max}$.

The \hat{H}_i^q for nonzero masses are obtained in exactly the same way as outlined for fully inclusive structure functions in Appendix A if the partonic phase space is not fully integrated over. They are given by

$$\begin{aligned} \hat{H}_i^q(\xi', z') &= C_F \left[(S_i + V_i) \delta(1 - \xi') \delta(1 - \hat{z}) \right. \\ &\quad \left. + \frac{1 - \xi'}{(1 - \xi')_+} \frac{z'_{LO}}{8} \frac{\hat{s}_1 + \Sigma_{+-}}{\Delta'} N_i^{-1} \hat{f}_i^Q(\hat{s}_1, \hat{t}_1) \right] \quad , \end{aligned} \quad (4.6)$$

where the normalization factors N_i are given in Appendix A.3 and the Mandelstam variables read

$$\begin{aligned} \hat{s}_1(\xi') &\equiv (p_1 + q)^2 - m_2^2 \\ &= \frac{1 - \xi'}{2\xi'} [(\Delta - \Sigma_{+-})\xi' + \Delta + \Sigma_{+-}] \\ \hat{t}_1(\xi', z') &\equiv (p_1 - p_3)^2 - m_1^2 \\ &= [\hat{s}_1(\xi') + \Sigma_{+-}](z' - z'_0) \quad , \end{aligned}$$

where $z'_0 = \frac{\hat{s}_1 + \Sigma_{++}}{\hat{s}_1 + \Sigma_{+-}}$ is the would-be pole of the \hat{t} -channel propagator and we use $\Delta' \equiv \Delta[\hat{s}, m_1^2, -Q^2]$. S_i and V_i are the soft real and virtual contribution to \hat{H}_i^q , respectively. They can be found in Appendix A.3 whereas the $\hat{f}_i^Q(\hat{s}_1, \hat{t}_1)$ are listed in Appendix B. In the massless limit the \hat{H}_i^q reduce to the $\overline{\text{MS}}$ coefficient functions in [29, 30] up to some divergent subtraction terms which we will specify in Section 4.2.3.

4.2.2 Gluon Fusion Contributions at $\mathcal{O}(\alpha_s^1)$

We have already obtained the semi-inclusive coefficient functions for GF production of massive quarks for general masses and couplings in Chapter 2. They are given by

$$\begin{aligned}\hat{F}_{1,3}^{GF}(x, z, Q^2, \mu^2) &= \int_{ax}^1 \frac{dx'}{x'} \int_z^1 \frac{d\zeta}{\zeta} g(x', \mu^2) f_{1,3}\left(\frac{x}{x'}, \zeta, Q^2\right) D_{Q_2}\left(\frac{z}{\zeta}, [\mu^2]\right) \Theta_g \\ \hat{F}_2^{GF}(x, z, Q^2, \mu^2) &= \int_{ax}^1 \frac{dx'}{x'} \int_z^1 \frac{d\zeta}{\zeta} x' g(x', \mu^2) f_2\left(\frac{x}{x'}, \zeta, Q^2\right) D_{Q_2}\left(\frac{z}{\zeta}, [\mu^2]\right) \Theta_g\end{aligned}\quad (4.7)$$

with the f_i from Eq. (2.2) and $ax = [1 + (m_1 + m_2)^2/Q^2]x$. The Θ_g cut guarantees that $\zeta_{\min} < \zeta < \zeta_{\max}$ where $\zeta_{\min, \max}$ are given in Eq. (2.3). Similarly to Eq. (4.5) $\zeta_{\min} < \zeta_{\max}$ may also constrain the phase space available for the x' integration.

4.2.3 Subtraction Terms

It requires three $\overline{\text{MS}}$ subtraction terms to render the double convolutions in Eqs. (4.3), (4.7) infrared safe:

$$\begin{aligned}\mathcal{F}_i^{SUB_q}(x, z, Q^2, \mu^2) &= \frac{\alpha_s(\mu^2)}{2\pi} C_F \int_{\chi}^1 \frac{d\xi'}{\xi'} \left[\frac{1 + \xi'^2}{1 - \xi'} \left(\ln \frac{\mu^2}{m_1^2} - 1 - 2 \ln(1 - \xi') \right) \right]_+ \\ &\times Q_1\left(\frac{\chi}{\xi'}, \mu^2\right) D_{Q_2}(z, [\mu^2])\end{aligned}\quad (4.8)$$

$$\mathcal{F}_i^{SUB_g}(x, z, Q^2, \mu^2) = D_{Q_2}(z, [\mu^2]) \frac{\alpha_s(\mu^2)}{2\pi} \ln \frac{\mu^2}{m_1^2} \int_{\chi}^1 \frac{d\xi'}{\xi'} P_{qg}^{(0)}(\xi') g\left(\frac{\chi}{\xi'}, \mu^2\right) \quad (4.9)$$

$$\begin{aligned}\mathcal{F}_i^{SUB_D}(x, z, Q^2, \mu^2) &= \frac{\alpha_s(\mu^2)}{2\pi} C_F \int_z^1 \frac{dz'}{z'} \left[\frac{1 + z'^2}{1 - z'} \left(\ln \frac{\mu^2}{m_2^2} - 1 - 2 \ln(1 - z') \right) \right]_+ \\ &\times D_{Q_2}\left(\frac{z}{z'}, \mu^2\right) Q_1(\chi, \mu^2) \quad ,\end{aligned}\quad (4.10)$$

where $P_{qg}^{(0)}(\xi') = 1/2 [\xi'^2 + (1 - \xi')^2]$. Note that SUB_g in Eq. (4.9) differs slightly from Eq. (2.6) in Chapter 2 because we are allowing for a nonzero initial state parton mass m_1 here which we did not in Chapter 2.

The subtraction terms define the running of the initial state quark density (SUB_q , SUB_g) and the final state fragmentation function (SUB_D) in the massless limit. They

remove collinear logarithms and scheme defining finite terms from the convolutions in Eqs. (4.3), (4.7) and they are constructed such that the massless $\overline{\text{MS}}$ results of [29, 30] are recovered in the limit

$$\lim_{m_{1,2} \rightarrow 0} \left[\hat{\mathcal{F}}_i^{QS^{(0+1)+GF}}(x, z, Q^2, \mu^2) - \mathcal{F}_i^{SUB_q + SUB_g + SUB_D}(x, z, Q^2, \mu^2) \right] = \mathcal{F}_i^{(1), \overline{\text{MS}}}(x, z, Q^2) \quad , \quad (4.11)$$

where SUB_q and SUB_D regularize $\hat{\mathcal{F}}_i^{QS^{(0+1)}}$ whereas SUB_g regularizes $\hat{\mathcal{F}}_i^{GF}$. Contrary to the fully inclusive SUB_g term in Eq. (3.17) there is no need to include an additional $\sim \ln(\mu^2/m_2^2)$ subtraction in Eq. (4.9) because the $\zeta^{-1} \hat{u}$ -channel singularity of the massless limit of $GF^{(1)}$ is located at $\zeta = 0$ and is outside the integration volume of Eq. (4.7). If only initial state subtractions, i.e. SUB_q and SUB_g , are considered and final state subtractions, i.e. SUB_D , are not performed one reproduces, in the limit $m_1 \rightarrow 0$ the results in [31, 50] for producing a heavy quark from a light quark. Note that in this case the fragmentation function D_{Q_2} should be taken scale-independent, say of the Peterson form [37]. In the limit where also the final state quark mass m_2 approaches zero and the final state subtraction term SUB_D is subtracted from the results in [31, 50]² the massless quark results in [29, 30] are obtained and a running of D_{Q_2} is induced via a RG resummation of final state collinear logs as formulated for one hadron inclusive e^+e^- annihilation in [51, 63].

Apart from removing the long distance physics from the coefficient functions the subtraction terms set the boundary conditions for the intrinsic heavy quark density Q_1 [47] and the perturbative part of the heavy quark fragmentation function D_{Q_2} [51]:

$$Q_1(x, Q_0^2) = \frac{\alpha_s(Q_0^2)}{2\pi} \ln \frac{Q_0^2}{m_1^2} \int_x^1 \frac{d\xi}{\xi} P_{qg}^{(0)}(\xi) g\left(\frac{x}{\xi}, Q_0^2\right) \quad (4.12)$$

$$D_{Q_2}(z, \tilde{Q}_0^2) = \frac{\alpha_s(\tilde{Q}_0^2)}{2\pi} C_F \int_z^1 \frac{dz'}{z'} \left[\frac{1+z'^2}{1-z'} \left(\ln \frac{\tilde{Q}_0^2}{m_2^2} - 1 - 2 \ln(1-z') \right) \right]_+ D_{Q_2}\left(\frac{z}{z'}\right) \quad (4.13)$$

where Q_0, \tilde{Q}_0 are the transition scales at which the factorization scheme is switched from n_f to $n_f + 1, n_f + 2$ active flavors, respectively (assuming here for simplicity that $m_1 < m_2$; a generalization to $m_1 \geq m_2$ is straightforward). For general Q_0 also the gluon density and α_s undergo a scheme transformation. Canonically Q_0 is set equal to the heavy quark mass m_1 which guarantees [47] up to two loops a continuous evolution of α_s and

²See Equation (B.11) in [50].

the light parton densities across Q_0 . All available heavy quark densities are generated using $Q_0 = m_1$ and we will therefore follow this choice here although a variation of Q_0 might substantially influence the heavy quark results even far above the threshold [18] as was found in [65]. Note that at three loops a continuous evolution across Q_0 can no longer be achieved, neither for the parton distributions [23] nor for α_s [66]. Analogously to $Q_0 = m_1$ we use $\tilde{Q}_0 = m_2$ throughout. In Eq. (4.13) we have made the distinction between the scale dependent FF $D_{Q_2}(z, \tilde{Q}_0^2)$ and the scale independent FF $D_{Q_2}(z)$ explicit. Following the terminology in [51, 63] the latter corresponds to the nonperturbative part of the former and describes the hadronization process at the end of the parton shower which is described perturbatively by the massless RG evolution. Alternatively, $D_{Q_2}(z)$ corresponds to a scale-independent FF within FOPT where no collinear resummations are performed. These two points of view may induce a scheme dependence if $D_{Q_2}(z)$ is fitted to data. In principle, the massless evolution equations generate nonzero FFs also for light partons to decay into heavy flavored hadrons. These light→heavy contributions are important at LEP energies [63] but can be safely neglected at the scales considered here³ and we will assume $D_{i \neq Q_2}(z, \mu^2) = 0$ throughout.

4.2.4 SI Structure Functions at $\mathcal{O}(\alpha_s^1)$

In the next section we will consider three types of $\mathcal{O}(\alpha_s^1)$ VFNS structure functions. The first two are constructed at full $\mathcal{O}(\alpha_s^1)$

$$F_i^{QS^{(0+1)}+GF} - F_i^{SUB_q+SUB_g+[SUB_D]} \quad , \quad (4.14)$$

where the inclusion or omission of the bracketed SUB_D term corresponds to a running or scale-independent fragmentation function, respectively, as discussed in the previous section. It is somewhat unclear whether $QS^{(1)}$ contributions (and the corresponding subtractions) should be considered on the same perturbative level as $GF^{(1)}$, see the introduction to Chapter 3 for a more detailed discussion on that point. In the original formulation of the ACOT scheme [20] $QS^{(1)}$ contributions are neglected at the level we are considering here and we therefore do also consider this option via the partial $\mathcal{O}(\alpha_s^1)$ structure function

$$F_i^{QS^{(0)}+GF} - F_i^{SUB_g} \quad . \quad (4.15)$$

³We could therefore, in principle, restrict the evolution of the charm FF to the nonsinglet sector.

For obtaining the numerical results of the next section the general formulae of this section have to be adjusted by choosing masses and couplings according to the relevant NC and CC values as in Section 3.3.1 and 3.3.2. For the CC case where Q_1 should be identified with strange quarks the boundary condition in Eq. (4.12) is inadequate since $m_s^2 \sim \Lambda_{QCD}^2$ is below the perturbative regime of QCD. We will have recourse to standard strange seas from the literature [41, 42] instead.

4.3 The Charm Fragmentation Function in SI DIS

We will investigate the charm fragmentation function in CC and in NC SI DIS. In CC DIS the charm production mechanism is undebated since charm is dominantly produced by scattering on light strange quanta. Our reasoning will therefore be that D_c is directly accessible in CC DIS at relatively low spacelike momentum transfer. An extracted D_c can then be applied to NC DIS, where it might give insight into the details of the production dynamics [11]. Also a test of the universality [67] of the charm FF measured in CC DIS and e^+e^- annihilation [63] would be an important issue directly related to the factorization theorems [68] of perturbative QCD (pQCD).

All ε_c parameters discussed below refer to a Peterson type [37] functional form given in Eq. (2.8)

4.3.1 CC DIS

In CC DIS at fixed target energies one does not expect to gain much insight into the charm production process since charm is dominantly produced in scattering events on strange quarks⁴ in the nucleon, thereby permitting an experimental determination of the strange quark content of the nucleon [16, 17, 45, 46]. On the other hand the well understood production mechanism makes a direct determination of the charm fragmentation function feasible by measuring the energy spectrum of final state charm fragments. This is obvious in leading order accuracy where⁵

$$d\sigma_{LO} \propto s(\chi) D_c(z) \quad (4.16)$$

⁴We assume a vanishing Cabibbo angle. Our results remain, however, unchanged if the CKM suppressed $d \rightarrow c$ background is included.

⁵We will suppress some obvious scale-dependences in the following formulae and in their discussion.

is directly proportional to D_c . More precisely, it is not z but the closely related energy of the $c \rightarrow \mu\nu$ decay muon which can be observed in iron detectors [16, 17, 45]. The smearing effects of the decay complicates the determination of the precise shape of D_c but only weakly influences an extraction of $\langle z \rangle$ [45] which is valuable information if physically motivated one-parametric Ansätze [37, 69] for D_c are *assumed*. At NLO the production cross section is no longer of the simple factorized form of Eq. (4.16) and double convolutions (symbol \otimes below) of the form of Eqs. (4.3), (4.7) have to be considered. However, to a reasonable approximation

$$\begin{aligned}
d\sigma_{NLO} &= ([s \otimes d\hat{\sigma}_s + g \otimes d\hat{\sigma}_g] \otimes D_c)(x, z, Q^2) \\
&\equiv d\sigma_{LO} K(x, z, Q^2) \\
&\propto s(\chi) D_c(z) K(x, z, Q^2) \\
&\simeq s(\chi) \mathcal{D}_{x, Q^2}[D_c](z)
\end{aligned} \tag{4.17}$$

holds also at NLO accuracy within experimental errors and for the limited kinematical range of present data on neutrino production of charm. In Eq. (4.17) the approximate multiplicative factor \mathcal{D} absorbs the precise K -factor $K(x, z, Q^2)$ obtained from a full NLO QCD calculation. \mathcal{D} is *not* a simple universal fragmentation function but a nontrivial process-dependent functional which is, however, mainly sensitive on D_c and shows little sensitivity on the exact parton distributions considered. The occurrence of x, Q^2 and z in Eq. (4.17) as indices and as a functional argument, respectively, reflects the fact that the dependence on x and Q^2 is much weaker than is on z . Eq. (4.17) tells us that $s(\chi)$ fixes the normalization of $d\sigma$ once K is known. On the other hand K (or \mathcal{D}) can be computed from D_c with little sensitivity on $s(\chi)$, such that $s(\chi)$ and $D_c(z)$ decouple in the production dynamics and can be simultaneously extracted. This point can be clearly inferred from Fig. 4.1 where it is shown that the wide spread of CC charm production predictions which were obtained in [31] using GRV94 [41] and CTEQ4 [42] strange seas can be brought into good agreement by a mere change of the normalization given by the ratio $s_{GRV}(\chi)/s_{CTEQ4}(\chi)$. The remaining difference is not within present experimental accuracy which can be inferred from the shaded band representing a parametrization [31] of CCFR data [16]. High statistics neutrino data therefore offer an ideal scenario to measure D_c complementary to an extraction from LEP data on $e^+e^- \rightarrow DX$ [63, 70, 71]. This has been first noted in [67] where also a successful test of the universality

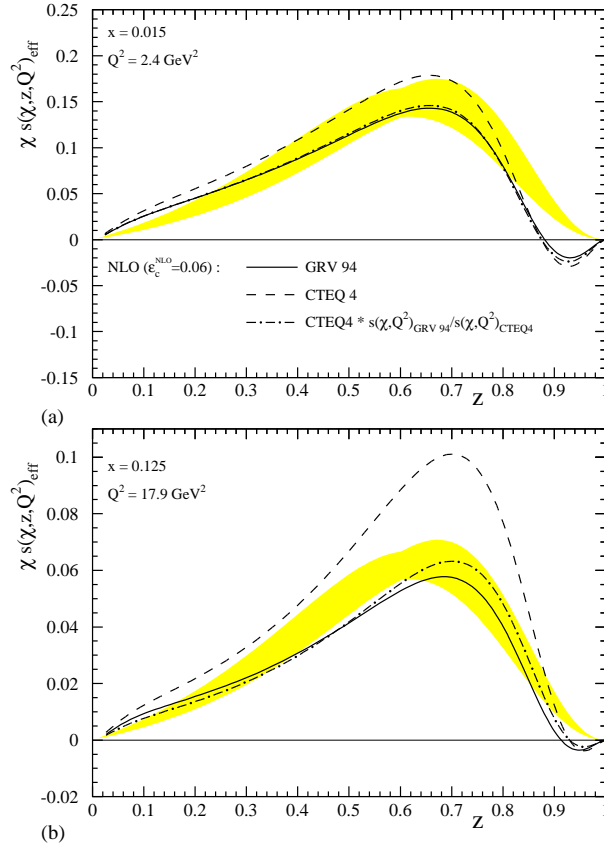


Figure 4.1: The charm production cross section obtained in [31] for two x, Q^2 points in the CCFR [16] kinematical regime. Up to a constant of normalization which was conveniently chosen in Eq. (4) of [31] s_{eff} represents the triple-differential cross section $d^3\sigma/dxdydz$ where x and y are standard and $z \equiv p_D \cdot p_N / q \cdot p_N$. Shown are the predictions using GRV94 [41] (solid) and CTEQ4 [42] (dashed) partons and a curve (dot-dashed) where the normalization of the CTEQ4 prediction is changed by multiplying with the ratio of the strange seas $s_{GRV}(\chi)/s_{CTEQ}(\chi)$. For all curves a scale-independent Peterson FF with $\varepsilon_c = 0.06$ has been used.

of the charm FF has been performed. With new data [16, 17, 45]⁶ at hand and with a sounder theoretical understanding of neutrino production of charm it would be desirable to update the analysis in [67]. Nowadays one can in principle examine the possibility of a uniform renormalization group transformation from spacelike momenta near above the charm mass ($\nu N \rightarrow DX$) to timelike momenta at the Z^0 peak ($e^+e^- \rightarrow DX$). In [63, 70, 71] charm fragmentation functions extracted from LEP data have been tested against p_T and η distributions measured in photoproduction at HERA. However, we believe that a comparison to z differential neutrino production data is worthwhile beyond,

⁶Data from NuTeV [72, 73] are to be expected in the near future; μ^\pm events observed at NOMAD await further analysis [74].

since the latter measure directly the fragmentation spectrum whereas p_T and η shapes are rather indirectly influenced by the precise hardness of the FF via their normalization [63, 64]. Unfortunately up to now no real production data are available but only strange sea extractions [16, 17, 45] resulting from an analysis of the former. We therefore strongly recommend that experiments produce real production data such that the above outlined program can be executed with rigor. Here we can only find an ε_c parameter which lies in the correct ball park and examine a few points which will become relevant for an extraction of D_c once data will become available.

An outstanding question is the possible effect of a finite strange mass on the full semi-inclusive charm production cross section including $\mathcal{O}(\alpha_s^1)$ quark scattering contributions. By comparing the thick and the thin solid curve in Fig. 4.2 (a) it is clear that the effect of a finite m_s can be neglected even at low scales and for a maximally reasonable value of $m_s = 500$ MeV. For the larger scale of Fig. 4.2 (b) the effect of choosing a finite m_s would be completely invisible. A further question which might influence the extraction of a universal FF from neutrino production is the one of the scheme dependence in handling final state quasi-collinear logarithms $\ln(Q^2/m_c^2)$. If these are subtracted from the coefficient functions as discussed in Section 4.2.3, the subtraction defines a running of the charm FF which becomes scale dependent⁷ according to Eq. (4.13). In Fig. 4.2 we examine such resummation effects for CCFR kinematics [16]. We use the same Peterson FF with $\varepsilon_c = 0.06$ once for a fixed order calculation (solid lines) and once as the nonperturbative part on the right hand side of the entire $c \rightarrow D$ FF on the left hand side of Eq. (4.13) (dashed curves). We note that towards intermediate scales around $Q^2 \sim 20 \text{ GeV}^2$ one begins to see the softening effects of the resummation which are enhanced as compared to FOPT. However, as one would expect at these scales, the resummation effects are moderate and could be compensated by only a *slight* shift of the ε_c parameter which is therefore, within experimental accuracy, insensitive to scheme transformations. We note that –as was already shown in [31]– according to Fig. 4.1 an ε_c of around 0.06 which we took from an older analysis in [38] seems to reproduce the measured spectrum quite well. For $\langle E_\nu \rangle = 80 \text{ GeV}$, $\langle Q^2 \rangle = 20 \text{ GeV}^2$ a value $\varepsilon_c \simeq 0.06$ gives an average $\langle z \rangle \simeq 0.6$ consistent with $\langle z \rangle = 0.68 \pm 0.08$ measured by CDHSW [45]. In [63]⁸ a distinctly harder

⁷Evolving the charm FF we adopt for consistency the evolution parameters $m_{c,b}$ and $\Lambda_{4,5}^{QCD}$ of the CTEQ4(M) [42] parton distribution functions and we use $\tilde{Q}_0 = m_c$.

⁸A similar ε_c has been obtained in [70] in a related scheme. The ε_c value in [71] has no connection to a massive calculation and cannot be compared to the values discussed here.

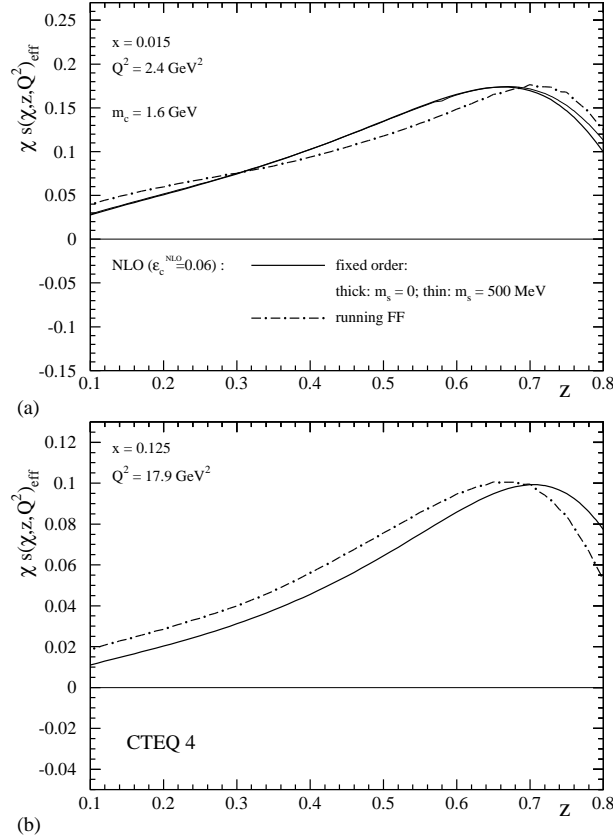


Figure 4.2: The same quantity as in Fig. 4.1. All predictions have been obtained for the CTEQ4 parton distributions. The solid curves result from a scale-independent Peterson FF with $\varepsilon_c = 0.06$. In (a) the thin solid curve has been obtained using the formulae of Section 4.2 and choosing a finite strange quark mass of $m_s = 500 \text{ MeV}$ whereas the thicker curve corresponds to the asymptotic $m_s \rightarrow 0$ limit ($\equiv \overline{\text{MS}}$). In (b) these two options would be completely indistinguishable and we only show the $\overline{\text{MS}}$ result. For the dot-dashed curves the final state quasi-collinear logarithm has been absorbed into a running of the charm FF. A Peterson FF with $\varepsilon_c = 0.06$ has been used as the nonperturbative part of the input as given in Eq. (4.13).

value of $\varepsilon_c \simeq 0.02$ was extracted from LEP data on $e^+e^- \rightarrow D^*X$. If the latter fit is evolved down to fixed target scales it is –even within the limited experimental accuracy– incompatible with the CCFR neutrino data represented in Fig. 4.1. From Fig. 4.2 it is clear that the difference cannot be attributed to a scheme dependence of the ε_c parameter which is too small to explain the discrepancy. It would of course be interesting to know how much the above mentioned smearing effect of the $c \rightarrow \mu\nu$ decay might dilute the discrepancy. In any case, charm fragmentation at LEP has been measured by tagging on D^* s whereas neutrino production experiments observe mainly D s through their semileptonic decay-channel (dimuon events). ARGUS [75] and CLEO [76] data at $\sqrt{s} \simeq 10 \text{ GeV}$ indeed

show [77] a harder energy distribution of D^* s compared to D s. It seems therefore to be possible within experimental accuracy to observe a nondegeneracy of the charm fragmentation functions into the lowest charmed pseudoscalar and vector mesons. We note that an ε_c value around 0.06 which is in agreement with neutrino data on D -production is also compatible with the D energy spectrum measured at ARGUS where the evolution may be performed either via FOPT using expressions in [62] or via a RG transformation along the lines of [51, 63]. If forthcoming experimental analyses should confirm our findings the lower decade $m_c(\sim 1 \text{ GeV}) \rightarrow \text{ARGUS}(10 \text{ GeV})$ may be added to the evolution path $\text{ARGUS}(10 \text{ GeV}) \rightarrow \text{LEP}(M_Z)$ paved in [63] for the charm FF.

4.3.2 NC DIS

The fragmentation function of charm quarks observed in NC DIS is of special interest since it allows for directly investigating [11, 12] the charm production mechanism which is a vividly discussed issue in pQCD phenomenology [18, 23, 78]. Whereas for intrinsic heavy quarks one expects to observe a Peterson-like hard spectrum attributed to the dominance of the leading order quark scattering contribution, one expects a much softer spectrum for extrinsic GF since the gluon radiates the $c\bar{c}$ pair towards lower energies (z) during the hard production process before the nonperturbative hadronization takes place. Experimental analyses have been performed in [11, 12] and the steep spectrum⁹ (best visible in Fig. 6 in [11]) of observed D -mesons together with the missing of a hard component at larger z seem to give clear evidence for the dominance of extrinsic GF over QS which was excluded at the 5% level [11]. In a complete VFNS the $QS^{(0)}$ component makes, however, just one part of the $\mathcal{O}(\alpha_s^1)$ structure functions in Eqs. (4.14), (4.15). Especially, there also exists a $GF^{(1)}$ component, albeit with the leading log part of it subtracted. Since the subtraction term in Eq. (4.9) is proportional to D_c and therefore only removes a hard component from $GF^{(1)}$ one expects the rise towards lower z to survive the subtraction. Furthermore a perturbative evolution of the charm fragmentation function $D_c(z, Q^2)$ might soften somewhat the hard QS term.

These expectations can be quantitatively confirmed in Fig. 4.3 where we show for HERA kinematics [11] the total (solid line) normalized $\mathcal{O}(\alpha_s^1)$ production cross section for transverse virtual photons ($F_L = 0$) on protons. We also show the individual compo-

⁹The variable x_D considered in [11, 12] differs slightly from z in definition. The variables are, however, identical at the 2% level [79].

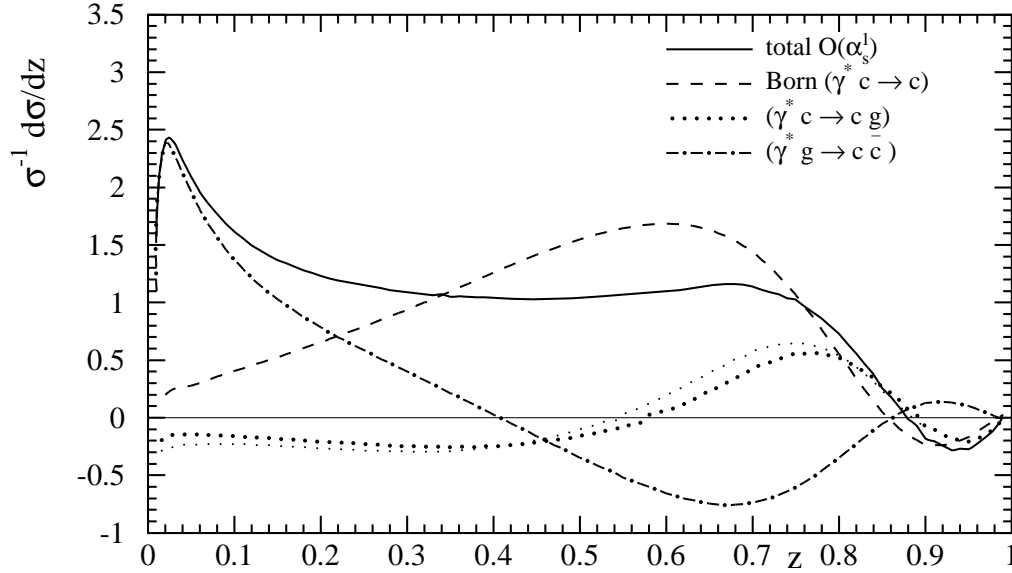


Figure 4.3: The normalized charm production cross section $d\sigma/dz$ ($z \equiv p_D \cdot p_N / q \cdot p_N$) for HERA kinematics ($\sqrt{s} = 314$ GeV). For a comparison with H1 data [11] the cross section has been integrated over $10 \text{ GeV}^2 < Q^2 < 100 \text{ GeV}^2$ and $0.01 < y < 0.7$. Following the experimental analysis [11] only contributions from transverse photons ($F_L = 0$) are considered. Shown is the total $\mathcal{O}(\alpha_s^1)$ result (solid line) and the individual contributions. Details to the calculation of the total result and the individual contributions are given in the text. The charm mass has been kept finite at the *CTEQ4* value of $m_c = 1.6$ GeV everywhere except for the thin dotted curve where the $m_c \rightarrow 0$ limit has been taken.

nents contributing to it: The processes $\gamma^* g \rightarrow c\bar{c}$ (dot-dashed) and $\gamma^* c \rightarrow cg$ (dotted; incl. virtual corrections) correspond to the $GF^{(1)} - SUB_g$ and $QS^{(1)} - SUB_q - SUB_D$ terms, respectively, subtracted at $\mu = Q$. They are *not* physically observable and only sensible if they are added to the $QS^{(0)}$ Born term (dashed) as in Eqs. (4.14), (4.15). We have perturbatively resummed all logarithms of the charm mass via massless evolution equations starting at the charm mass [$Q_0 = \tilde{Q}_0 = m_c$] and using the standard boundary conditions in Eqs. (4.12), (4.13) for $\varepsilon_c = 0.06$. Finite charm mass effects on the subtracted $QS^{(1)}$ contribution can be inferred by comparing the thick and the thin dotted curves, where the $m_c \rightarrow 0$ limit has been taken for the latter. As has been theoretically anticipated in [21] the charm mass can be safely set to zero in $QS^{(1)}$ and the involved convolutions in Eq. (4.1) may be replaced by the massless expressions in [29, 30] which simplifies the numerics essentially and which we will therefore do for the $\mu = 2m_c$ curve in Fig. 4.4 below. As also stressed in [21] it is, however, essential to keep the charm mass finite in the $GF^{(1)}$ contribution since m_c tempers the strength of the z'^{-1} \hat{u} -channel propagator singularity.

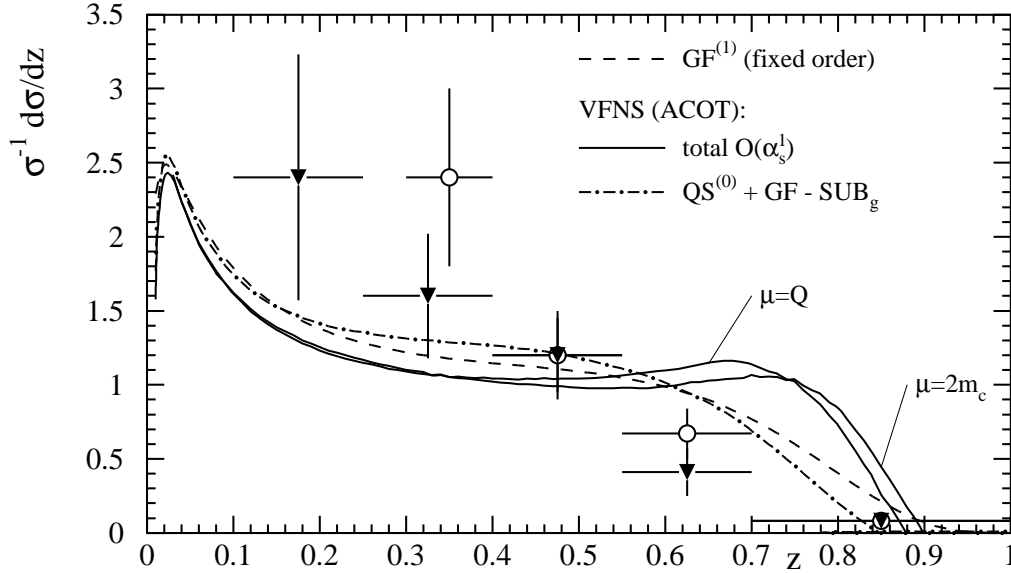


Figure 4.4: A Comparison of the total $\mathcal{O}(\alpha_s^1)$ result (solid lines) to H1 data [11] on D^0 (circles) and D^{+*} (triangles; both including charge conjugation) production. Shown are results for two choices of the factorization/renormalization scale μ . Also shown is the outcome of a fixed order $\mathcal{O}(\alpha_s^1)$ GF calculation for comparison (dashed line). The dot-dashed line follows the suggestion in [20] and neglects quark initiated contributions at $\mathcal{O}(\alpha_s^1)$, i.e. the difference between the solid ($\mu = Q$) and the dot-dashed line is given by the (thick) dotted line in Fig. 4.3. For the dot-dashed curve as well as for the fixed order calculation (dashed) only $\mu = Q$ is shown since the scale dependence is completely insignificant.

Obviously the $\mathcal{O}(\alpha_s^1)$ result of an ACOT based calculation deviates essentially from the naive Born term expectation and it seems by no means legitimate to treat $GF^{(1)}$ as a higher order correction here. Contrary to the corresponding inclusive results in Chapter 3 and to the expectations in [20] also the subtracted $QS^{(1)}$ term is numerically significant in the semi-inclusive case considered here. In the light of the huge $\mathcal{O}(\alpha_s^1)$ corrections it seems, however, undecidable as to whether include or omit $QS^{(1)}$ at $\mathcal{O}(\alpha_s^1)$ without knowing $\mathcal{O}(\alpha_s^2)$ corrections within ACOT.

In Fig. 4.4 the resummed result (VFNS: solid lines) can be compared to unsubtracted $\mathcal{O}(\alpha_s^1)^{10}$ $GF^{(1)}$ (fixed order, dashed line). We show the total $\mathcal{O}(\alpha_s^1)$ VFNS result for the choices $\mu = Q, 2m_c$. The modest scale dependence arises exclusively through the $QS^{(1)}$ term. For any of the other curves a variation of μ is completely insignificant and we therefore only show $\mu = Q$. A full VFNS calculation (solid lines) seems hardly

¹⁰An $\mathcal{O}(\alpha_s^2)$ NLO calculation [80] within FOPT gives very similar results [79].

distinguishable from fixed order perturbation theory (dashed line) within experimental accuracy. The two approaches are even closer if one follows the suggestion in [20] and does not include (dot-dashed line) the subtracted $QS^{(1)}$ term at the level of $QS^{(0)} + GF^{(1)}$. The data points in the figure correspond to H1 measurements [11] of D^0 (circles) and D^{*+} (triangles; both including charge conjugation) spectra. The measurement is restricted to $\eta_D < 1.5$. Extrapolating to the full phase space gives rise to large acceptance corrections which are, however, quite uniform [79] over the kinematical range considered and therefore have a minor effect on the *normalized* spectrum. Since FOPT and ACOT based calculations are very close it seems improbable that an experimental discrimination between the two approaches will be possible. The Born term in Fig. 4.3 is far from being the dominant contribution and an intrinsic $c(x, Q^2)$ stemming from the resummation of perturbative logs can therefore not be excluded. The tendency of the data appears somewhat softer than any of the calculations and the tendency seems to be confirmed by preliminary data in a lower z bin [81]. The resummed calculation appears to be too hard at larger z around 0.6 if the $QS^{(1)}$ component is included. As already mentioned, at the present stage of the calculations it cannot be decided whether this hints at an intrinsic problem within VFNS calculations or whether this may be cured by $\mathcal{O}(\alpha_s^2)$ corrections.

4.4 Conclusions

In this chapter we have performed an ACOT [20] based analysis of heavy quark fragmentation in DIS including a calculation of semi-inclusive scattering on massive quarks at $\mathcal{O}(\alpha_s^1)$ for general masses and couplings. As in the inclusive case of Chapter 3, effects from finite initial state quark masses can be neglected for practical applications to charm production in CC and NC DIS. The involved convolutions in Section 4.2.1 can therefore safely be replaced by their analogues in [29, 30] and in Appendix B of [50]. Neutrinoproduction is an ideal environment to extract the charm FF within DIS and a Peterson [37] type FF with $\varepsilon_c \simeq 0.06$ seems to lie in the correct ball park, where the sensitivity on the choice of scheme is small and finite m_s effects are irrelevant. The ε_c value above is compatible with e^+e^- data if a nondegeneracy of charm quarks fragmenting into D and D^* mesons is allowed for. For NC DIS it seems unlikely that a discrimination between fixed order and resummed calculations will be possible at HERA. Both approaches give similar results which show a spectrum that is somewhat harder than the tendency of the

data [11, 12, 81]. The resummed calculation is made worse if the $\mathcal{O}(\alpha_s^1)$ quark scattering contribution is included at the perturbative level considered here.

Chapter 5

Summary

In the first part of this thesis we have studied deep inelastic production of heavy quarks in neutral current and charged current processes. For this purpose we have calculated the relevant partonic subprocesses to order $\mathcal{O}(\alpha_s^1)$ (BGF, QS) for general masses and couplings taking into account massive initial state quark-partons as needed in the variable flavor number scheme of ACOT [20]. Our calculation of the vertex correction with general masses and couplings is, to our best knowledge, new.

The integrated partonic results could be used to formulate and investigate heavy quark contributions to inclusive deep inelastic structure functions within the ACOT variable flavor number scheme. By the calculation of the before missing radiative corrections to scattering amplitudes on massive quark partons (including virtual corrections) the ACOT scheme could be completed to full order $\mathcal{O}(\alpha_s^1)$. Furthermore, we utilized the unintegrated partonic structure functions to extend the original ACOT scheme [20] from its inclusive formulation to (z -differential) one-hadron-inclusive leptonproduction.

With help of these results we demonstrated in the charged current sector that the effects of a finite strange mass are small and rapidly converge towards $\overline{\text{MS}}$ in the limit $m_s \rightarrow 0$. Furthermore, it turned out that the effects of finite initial state masses can be neglected in all cases, such that the (massive) QS⁽¹⁾ contribution of Section 3.2.2 can safely be approximated by its much simpler $\overline{\text{MS}}$ analogue at any scale. Nevertheless, it should be stressed that radiative corrections to quark initiated processes are in general not negligible and should be included in complete NLO analyses employing heavy quark parton densities.

Finally, we have performed an ACOT based analysis of heavy quark fragmentation in

DIS led by the observation that semi-inclusive CC DIS is well suited to extract the charm fragmentation function. We reassured that theoretical uncertainties due to scheme choices and finite m_s effects are irrelevant and found out that a Peterson type fragmentation function with $\varepsilon_c \approx 0.06$ seems to lie in the correct ball park. The ε_c value above is compatible with e^+e^- data if a nondegeneracy of charm quarks fragmenting into D and D^* mesons is allowed for. In the case of semi-inclusive NC DIS it seems unlikely that a discrimination between fixed order and resummed calculations will be possible at HERA. Both approaches gave similar results exhibiting a spectrum that is somewhat harder than the tendency of the data [11, 12, 81]. The resummed calculation is made worse if the $\mathcal{O}(\alpha_s^1)$ quark scattering contribution is included at the perturbative level considered here.

Part II

The Structure of Real and Virtual Photons

Chapter 6

Introduction and Survey

Photon physics is an active field of research as is documented by and in a large number of reviews [82–91]. Particularly in the past few years there has been much progress due to the wealth of experimental results from the e^+e^- collider LEP and the ep collider HERA [90, 91]. Among the reactions initiated by high energy photons such processes providing a hard scale are of particular interest since they can be described (at least partly) by means of perturbative QCD. More precisely, in this thesis we are interested in processes which can be described within the well known framework of the parton model and in this case the ‘hadronic nature of the photon’ is quantitatively described by the partonic structure of the photon. The classical way of measuring the photonic parton content is deep inelastic electron–photon scattering ($\text{DIS}_{e\gamma}$) which is the main source of information. The $\text{DIS}_{e\gamma}$ data on the photon structure function $F_2^\gamma(x, Q^2)$ are mainly sensitive to the up–quark density $u^\gamma(x, Q^2)$ as can be seen from the parton model expression for F_2^γ (in LO), $F_2^\gamma \propto 4u^\gamma + d^\gamma + s^\gamma$, whereas the gluon distribution $g^\gamma(x, Q^2)$ is only indirectly constrained at small values of x due to the evolution. Complementary information has become available in the last years due to ‘resolved photon processes’ (e.g. production of (di–)jets or hadrons with large p_T (E_T), heavy quark production, isolated prompt photon production) in γp and $\gamma\gamma$ collisions at HERA and LEP, respectively, which are mainly sensitive to the gluon distribution in the photon. However, the experimental constraints on the gluon density are still weak, especially at $x < 0.1$, and one has to resort to model assumptions about the parton distributions of the photon.

It is the virtue of the phenomenologically successful radiative parton model (GRV model) [26, 41, 57, 92, 93] to predict the small– x behavior of parton distributions by pure

DGLAP–evolution of valence–like input distributions at a low input scale $\mu^2 \simeq 0.3 \text{ GeV}^2$. Recently, the parton distributions of the proton have been revised [26] due to precision measurements of the proton structure function F_2^p at HERA leading to slightly changed parameters (low input scale, α_s) and a less steep small– x increase compared to the previous GRV94 [41]. In order to test quantitatively (within the GRV approach) if protons, pions and photons show a similar small– x (i.e. high energy) behavior it is necessary to update also the parton distributions of pions and photons.

At present e^+e^- and ep collider experiments the photon beams consist of bremsstrahlung radiated off the incident lepton beam resulting in a continuous spectrum of target photons $\gamma(P^2)$ where P^2 is the photon’s virtuality. The bremsstrahlung spectrum is proportional to $1/P^2$ such that the bulk of target photons is produced at $P^2 \simeq P_{\min}^2 \simeq 0$. The parton content of such (quasi–)real photons is well established both experimentally and theoretically and it is quite natural to expect the parton distributions to decrease smoothly with increasing P^2 and not to vanish immediately. In this sense the real photon $\gamma \equiv \gamma(P^2 \simeq 0)$ is just a ‘primus inter pares’ and unified approaches to the parton content of virtual photons $\gamma(P^2)$ which comprise the real photon case in the limit $P^2 \rightarrow 0$ are highly desirable. This is also reflected by the fact that measurements of the real photon structure function F_2^γ in single–tag events integrate over the bremsstrahlung spectrum from P_{\min}^2 up to a P_{\max}^2 which depends on the experimental details. For instance, at LEP1(LEP2) P_{\max}^2 is as large as $P_{\max}^2 \simeq 1.5 \text{ GeV}^2 (4.5 \text{ GeV}^2)$, cf. Section 2.2 in [90]. Although the bulk of photons is produced at $P^2 \simeq P_{\min}^2$ the amount of ignorance of the P^2 –dependence, mainly in the range $P^2 \lesssim \Lambda^2$, feeds back on the determination of the structure function F_2^γ (parton distributions) of (quasi–)real photons.

It is the central goal of the second part of this thesis to perform LO and NLO analyses of the parton content of pions and real and virtual photons within the latest fine–tuned/improved setting of the GRV model [26].

The outline of Part II will be as follows:

- In Chapter 7 we provide the basic kinematical background for studying the structure of real and virtual photons in two–photon scattering events. Structure functions for virtual photons are defined in a general (model independent) way which will be studied in the following chapters either in fixed order perturbation theory (Chapters 8, 12) or within the framework of the QCD–improved parton model (Chapters 9,

..., 12). Furthermore, we demonstrate the factorization of the cross section for the process $ee \rightarrow eeX$ into a flux of photons times the cross section for deep inelastic scattering (DIS) on these “target” photons for arbitrary virtualities P^2 of the target photon in the Bjorken limit $P^2 \ll Q^2$. It should be noted that the factorization is essential for a theoretical description of two-photon processes in terms of structure functions of target photons $\gamma(P^2)$ which can be measured in deep inelastic electron-photon scattering.

- In Chapter 8 we calculate the photon photon cross sections σ_{ab} according to the doubly virtual box $\gamma^*(Q^2)\gamma^*(P^2) \rightarrow q\bar{q}$ in lowest order perturbation theory. The general expressions are casted in a form which easily allows to read off various important limits, e.g., the quark-parton model (QPM) results for the structure functions of real and virtual photons and the heavy quark contributions to the photon structure functions. For deeply virtual target photons the perturbative results make reliable predictions and we compare them (F_{eff}) with present e^+e^- virtual photon data. On the other hand, for quasi-real target photons these results are plagued by mass singularities which have to be subtracted and afford the introduction of parton distributions which will be done in the next chapter.
- In Chapter 9 the complete theoretical framework necessary for our phenomenological study of the parton content of real and virtual photons in Chapter 11 is provided where special emphasis is laid on a unified treatment of real and virtual photons also in NLO.
- Chapter 10 is devoted to an analysis of the parton content of the pion in LO and NLO QCD. Since only the pionic valence density $v^\pi(x, Q^2)$ is experimentally rather well known at present, we utilize a constituent quark model [94, 95] in order to unambiguously relate the pionic light sea and gluon to the much better known (recently updated) parton distributions of the proton [26] and $v^\pi(x, Q^2)$. These results will serve via vector meson dominance (VMD) as input for the hadronic component of the photon in the next chapter.
- In Chapter 11 we turn to LO and NLO analyses of the parton content of real and virtual photons within the framework of the radiative parton model. Apart from utilizing the latest refined parameters of the radiative parton model [26] there are

some novelties as compared to the original GRV_γ approach [96]. At first, the boundary conditions for the real photon are based on a coherent superposition of vector mesons which maximally enhances the up-quark contribution to the photon structure function $F_2^\gamma(x, Q^2)$ as is favored by the experimental data. As a result no extra normalization factor for the photonic boundary conditions is needed. Furthermore, in order to remove model ambiguities of the hadronic light quark sea and gluon input distributions of the photon (being related to the ones of the pion via VMD), inherent to the older GRV_γ [96] and SaS [97] parametrizations, we employ, as already mentioned, predictions for the pionic light quark sea and gluon which follow from constituent quark model constraints. The resulting predictions for the real photon structure functions $F_2^\gamma(x, Q^2)$ will be compared with all presently (January 1999) available relevant data. Most recently the OPAL collaboration [98] at the CERN-LEP collider has extended the measurements of the photon structure function $F_2^\gamma(x, Q^2)$ into the small- x region down to $x \simeq 10^{-3}$, probing lower values of x than ever before and we include a comparison with these data as well. Finally, we construct LO and NLO boundary conditions for the virtual photon which allow for a smooth transition to the real photon case and perform a careful study of the resulting predictions for the partonic content and the structure function $F_2^{\gamma(P^2)}(x, Q^2)$ of virtual photons.

- In Chapter 12 we test our model for the parton content of virtual photons in more detail and compare these QCD-resummed results with the fixed order box expressions of Chapter 8. It is demonstrated that present e^+e^- and DIS ep data on the structure of the virtual photon can be understood entirely in terms of the standard ‘naive’ quark-parton model box approach. Thus the QCD-resummed (renormalization group (RG) improved) parton distributions of virtual photons, in particular their gluonic component, have not yet been observed. The appropriate kinematical regions for their future observation are pointed out as well as suitable measurements which may demonstrate their relevance.
- Finally, in Chapter 13 we summarize our main results and discuss open questions.
- Various limits of the doubly virtual box calculation and parametrizations of our pionic and photonic parton distributions have been relegated to the Appendices C and D, respectively.

Chapter 7

Photon–Photon Scattering

In this chapter we provide the basic kinematical background for studying the structure of real and virtual photons in two–photon scattering events.

In Section 7.1 we give a short introduction into so–called two–photon processes, introduce the usual kinematical variables to describe them and derive the cross section for such events. The notation follows mainly the report of Budnev et al. [82]. Here we only present a selection of the topic needed throughout the thesis. Additional information can be found in [82] and, e.g., in the more recent reviews [85, 90].

Next, in Section 7.2 we define structure functions for virtual photons and relate them to the photon–photon scattering cross sections. These structure functions will be studied in the following chapters either in fixed order perturbation theory (Chapters 8, 12) or within the framework of the QCD–improved parton model (Chapters 9, \dots , 12).

Finally, in Section 7.3 we demonstrate the factorization of the cross section for the process $ee \rightarrow eeX$ into a flux of photons and the cross section for deep inelastic scattering (DIS) on these “target” photons. While the factorization is well known for (quasi–)real target photons with virtuality $P^2 \approx 0$ we deal with the general $P^2 \neq 0$ case in the Bjorken limit. It should be noted that the factorization is essential for a theoretical description of two–photon processes in terms of structure functions of the (real or virtual) photon.

7.1 Kinematics

The kinematics of particle production via photon–photon scattering in e^+e^- collisions

$$e^-(p_1)e^+(p_2) \rightarrow e^-(p'_1)e^+(p'_2)\gamma^*(q)\gamma^*(p) \rightarrow e^-(p'_1)e^+(p'_2)X(p_X) \quad (7.1)$$

is depicted in Fig. 7.1. The momenta of the incoming and outgoing leptons are denoted

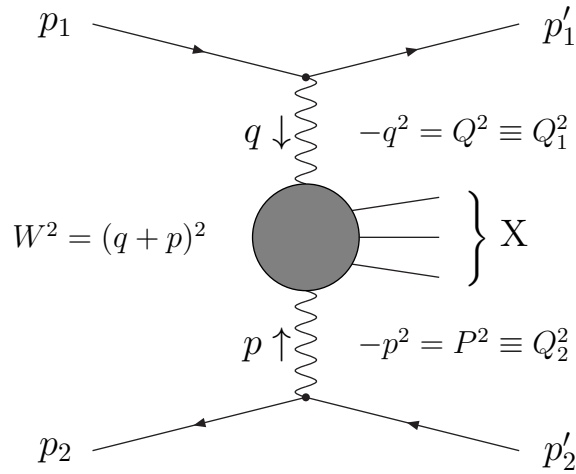


Figure 7.1: Two–photon particle production. The solid lines are the incoming and outgoing leptons and the wavy lines are virtual photons which produce a final state X consisting of hadrons (or leptons).

by $p_i \equiv (E_i, \vec{p}_i)$ and $p'_i \equiv (E'_i, \vec{p}'_i)$ ($i = 1, 2$) respectively and the momenta of the photons are given by

$$\begin{aligned} q &\equiv p_1 - p'_1, & Q^2 &= -q^2 \equiv Q_1^2, \\ p &\equiv p_2 - p'_2, & P^2 &= -p^2 \equiv Q_2^2. \end{aligned} \quad (7.2)$$

In general both photons have spacelike momenta and P^2 refers to the photon with smaller virtuality ($P^2 \leq Q^2$). X denotes the final state produced in the $\gamma^*(q) + \gamma^*(p) \rightarrow X$ subprocess. For later use, we define the following variables:

$$\begin{aligned} \nu &= p \cdot q, & x &= \frac{Q^2}{2\nu}, & \delta &= \frac{P^2}{2\nu}, & y_1 &= \frac{p \cdot q}{p \cdot p_1}, & y_2 &= \frac{p \cdot q}{q \cdot p_2}, \\ W^2 &\equiv (p + q)^2 = 2\nu(1 - x - \delta) = Q^2 \frac{1 - x}{x} - P^2. \end{aligned} \quad (7.3)$$

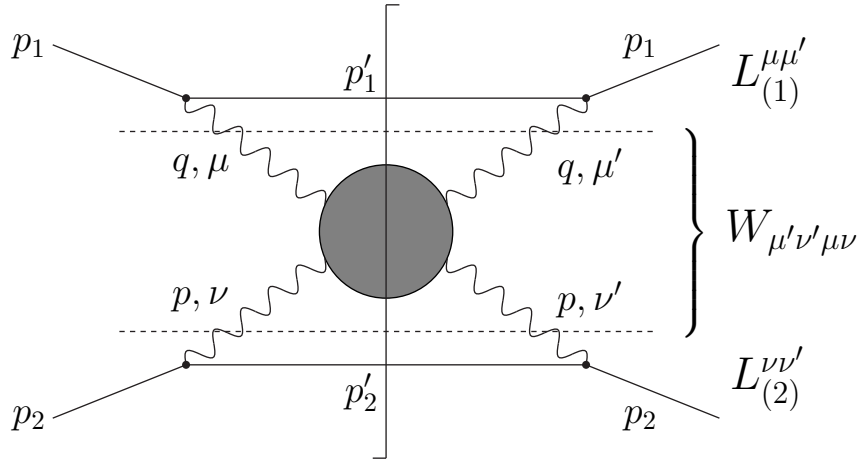


Figure 7.2: Squared matrix element of the process (7.1). Integration over the phase space of the system X is implied as indicated by the vertical cut.

The cross section for the process (7.1) is given by

$$d\sigma = \frac{1}{F_{ee}} |M|^2 dQ^{(n+2)} \quad (7.4)$$

with the invariant matrix element M , the Møller flux factor of the two incoming leptons

$$F_{ee} = 4\sqrt{(p_1 \cdot p_2)^2 - m_e^2 m_e^2}, \quad (7.5)$$

and the Lorentz-invariant $(n+2)$ -particle phase space

$$\begin{aligned} dQ^{(n+2)}(p_1 + p_2; p'_1, p'_2, k_1, \dots, k_n) &= \frac{d^3 p'_1}{(2\pi)^3 2E'_1} \frac{d^3 p'_2}{(2\pi)^3 2E'_2} dQ^{(n)}(q + p; k_1, \dots, k_n) \\ &= \frac{d^3 p'_1}{(2\pi)^3 2E'_1} \frac{d^3 p'_2}{(2\pi)^3 2E'_2} (2\pi)^4 \delta^{(4)}(q + p - p_X) d\Gamma. \end{aligned} \quad (7.6)$$

Here $p_X = \sum_i k_i$, $i \in X$ is the total momentum and $d\Gamma = \prod_i \frac{d^3 k_i}{2k_i^0 (2\pi)^3}$, $i \in X$ the phase space volume of the produced system X.

The cross section can be expressed in terms of the amplitudes $M^{\mu\nu}$ of the $\gamma^*(q) + \gamma^*(p) \rightarrow X$ subprocess as follows (see Fig. 7.2):

$$d\sigma = \frac{d^3 p'_1 d^3 p'_2}{2E'_1 2E'_2 (2\pi)^6} \frac{(4\pi\alpha)^2}{Q^4 P^4} \frac{1}{F_{ee}} L^{\mu\mu'}_{(1)} L^{\nu\nu'}_{(2)} W_{\mu'\nu',\mu\nu} \quad (7.7)$$

with

$$W^{\mu'\nu',\mu\nu} = \frac{1}{2} \int M^{\star\mu'\nu'} M^{\mu\nu} (2\pi)^4 \delta^{(4)}(q + p - p_X) d\Gamma . \quad (7.8)$$

For unpolarized leptons the (leptonic) tensors $L_{(1)}$ and $L_{(2)}$ (see Fig. 7.2) are given by

$$L_{(i)}^{\alpha\beta} = \frac{1}{2} \text{Tr}[(\not{p}_i + m_e) \gamma^\alpha (\not{p}'_i + m_e) \gamma^\beta] . \quad (7.9)$$

The factor 1/2 is due to a spin average over the incoming leptons. In addition, we introduce the dimensionless quantities [82]

$$\rho_i^{\alpha\beta} = \frac{1}{Q_i^2} L_{(i)}^{\alpha\beta} = - \left(g^{\alpha\beta} - \frac{q_i^\alpha q_i^\beta}{q_i^2} \right) - \frac{(2p_i - q_i)^\alpha (2p_i - q_i)^\beta}{q_i^2} \quad (7.10)$$

which have the interpretation of (unnormalized) density matrices for the corresponding virtual photons.

7.1.1 The Hadronic Tensor $W^{\mu'\nu',\mu\nu}$

According to the optical theorem $W^{\mu'\nu',\mu\nu}$ is the absorptive part of the virtual $\gamma\gamma$ forward amplitude shown in Fig. 7.3.

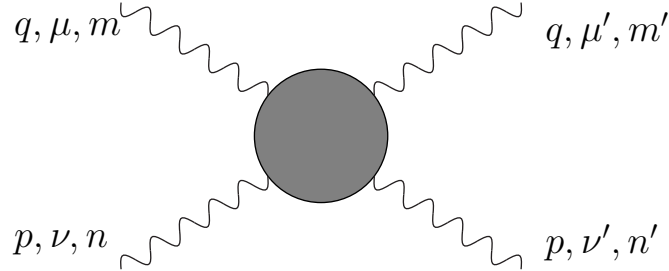


Figure 7.3: The photon–photon forward scattering amplitude $T^{\mu'\nu',\mu\nu}$; m , n , m' , and n' are helicity indices. The tensor $W^{\mu'\nu',\mu\nu}$ defined in (7.8) is the absorptive part of the $\gamma\gamma$ forward amplitude: $W^{\mu'\nu',\mu\nu} = \frac{1}{\pi} \text{Im} T^{\mu'\nu',\mu\nu}$.

Taking into account P– and T–invariance (symmetry $\mu'\nu' \leftrightarrow \mu\nu$) and gauge invariance, i.e.

$$q_\mu W^{\mu'\nu',\mu\nu} = q_{\mu'} W^{\mu'\nu',\mu\nu} = p_\nu W^{\mu'\nu',\mu\nu} = p_{\nu'} W^{\mu'\nu',\mu\nu} = 0 ,$$

the Lorentz-tensor $W^{\mu'\nu',\mu\nu}$ can be expanded in terms of a basis of 8 independent tensors constructed from the vectors q, p and the metric tensor g . The choice of the tensor basis in which the expansion is carried out is clearly arbitrary and different forms are discussed in the literature [82, 99, 100]. In the following we will stick to the expansion given in [82]:

$$\begin{aligned}
W^{\mu'\nu',\mu\nu} = & R^{\mu'\mu} R^{\nu'\nu} W_{\text{TT}} + R^{\mu'\mu} Q_2^\nu Q_2^{\nu'} W_{\text{TL}} + Q_1^{\mu'} Q_1^\mu R^{\nu'\nu} W_{\text{LT}} + Q_1^{\mu'} Q_1^\mu Q_2^{\nu'} Q_2^\nu W_{\text{LL}} \\
& + \frac{1}{2} (R^{\mu'\nu'} R^{\mu\nu} + R^{\nu'\nu} R^{\mu'\mu} - R^{\mu'\mu} R^{\nu'\nu}) W_{\text{TT}}^\tau \\
& - (R^{\mu\nu} Q_1^{\mu'} Q_2^{\nu'} + R^{\nu'\mu} Q_1^{\mu'} Q_2^\nu + R^{\mu'\nu'} Q_1^\mu Q_2^\nu + R^{\mu'\nu} Q_2^{\nu'} Q_1^\mu) W_{\text{TL}}^\tau \\
& + (R^{\mu'\nu'} R^{\mu\nu} - R^{\nu'\mu} R^{\mu'\nu}) W_{\text{TT}}^a \\
& - (R^{\mu\nu} Q_1^{\mu'} Q_2^{\nu'} - R^{\nu'\mu} Q_1^{\mu'} Q_2^\nu + R^{\mu'\nu'} Q_1^\mu Q_2^\nu - R^{\mu'\nu} Q_2^{\nu'} Q_1^\mu) W_{\text{TL}}^a .
\end{aligned} \tag{7.11}$$

The tensor structures used in (7.11) are connected to the photon polarization vectors, see App. B and C in [82]:

$$\begin{aligned}
\epsilon_0^\alpha(q) &= iQ_1^\alpha , & \epsilon_0^\alpha(p) &= -iQ_2^\alpha , \\
\epsilon_\pm^{\star\alpha}(q)\epsilon_\pm^\beta(q) &= \frac{1}{2} \left[R^{\alpha\beta} \pm i \frac{1}{\nu\beta} \varepsilon^{\alpha\beta\rho\sigma} q_\rho p_\sigma \right] , & \epsilon_\pm^{\star\alpha}(p)\epsilon_\pm^\beta(p) &= \epsilon_\mp^{\star\alpha}(q)\epsilon_\mp^\beta(q)
\end{aligned} \tag{7.12}$$

with $\bar{\beta}^2 \equiv 1 - 4x\delta$ and

$$\begin{aligned}
R^{\alpha\beta} &= -g^{\alpha\beta} + \frac{\nu(p^\alpha q^\beta + q^\alpha p^\beta) - p^2 q^\alpha q^\beta - q^2 p^\alpha p^\beta}{\nu^2 \bar{\beta}^2} , \\
Q_1^\alpha &= \frac{\sqrt{-q^2}}{\nu\bar{\beta}} \left(p^\alpha - \frac{\nu}{q^2} q^\alpha \right) , & Q_2^\alpha &= \frac{\sqrt{-p^2}}{\nu\bar{\beta}} \left(q^\alpha - \frac{\nu}{p^2} p^\alpha \right) .
\end{aligned} \tag{7.13}$$

The photon momenta q, p , the unit vectors Q_1, Q_2 , and the symmetric tensor $R^{\alpha\beta}$ satisfy the following (orthogonality) relations:

$$\begin{aligned}
q \cdot Q_1 &= p \cdot Q_2 = 0 , & Q_{1,2}^2 &= 1 , \\
q^\alpha R_{\alpha\beta} &= p^\alpha R_{\alpha\beta} = Q_{1,2}^\alpha R_{\alpha\beta} = 0 , & R_{\alpha\beta} R^{\alpha\beta} &= 2 , & R_\beta^\alpha R^{\beta\gamma} &= -R^{\alpha\gamma} .
\end{aligned} \tag{7.14}$$

With help of these relations it is easy to see that the various tensors in front of the invariant functions W_{ab} in Eq. (7.11) are mutually orthogonal and therefore can be used to project out the invariant functions. With obvious notation ($P_{W_{\text{TT}}}^{\mu'\nu',\mu\nu} W_{\mu'\nu',\mu\nu} = W_{\text{TT}}$

etc.) the projectors read:

$$\begin{aligned}
P_{\text{W}_{\text{TT}}}^{\mu'\nu',\mu\nu} &= \frac{1}{4} R^{\mu'\mu} R^{\nu'\nu} , \\
P_{\text{W}_{\text{TL}}}^{\mu'\nu',\mu\nu} &= \frac{1}{2} R^{\mu'\mu} Q_2^\nu Q_2^{\nu'} , \\
P_{\text{W}_{\text{LT}}}^{\mu'\nu',\mu\nu} &= \frac{1}{2} Q_1^{\mu'} Q_1^\mu R^{\nu'\nu} , \\
P_{\text{W}_{\text{LL}}}^{\mu'\nu',\mu\nu} &= Q_1^{\mu'} Q_1^\mu Q_2^{\nu'} Q_2^\nu , \\
P_{\text{W}_{\text{TT}}}^{\mu'\nu',\mu\nu} &= \frac{1}{4} (R^{\mu'\nu'} R^{\mu\nu} + R^{\mu'\nu} R^{\nu'\mu} - R^{\mu'\mu} R^{\nu'\nu}) , \\
P_{\text{W}_{\text{TL}}}^{\mu'\nu',\mu\nu} &= \frac{-1}{8} (R^{\mu\nu} Q_1^{\mu'} Q_2^{\nu'} + R^{\nu'\mu} Q_1^{\mu'} Q_2^\nu + R^{\mu'\nu'} Q_1^\mu Q_2^\nu + R^{\mu'\nu} Q_2^{\nu'} Q_1^\mu) , \\
P_{\text{W}_{\text{TT}}}^{\text{a}\mu'\nu',\mu\nu} &= \frac{1}{4} (R^{\mu'\nu'} R^{\mu\nu} - R^{\nu'\mu} R^{\mu'\nu}) , \\
P_{\text{W}_{\text{TL}}}^{\text{a}\mu'\nu',\mu\nu} &= \frac{-1}{8} (R^{\mu\nu} Q_1^{\mu'} Q_2^{\nu'} - R^{\nu'\mu} Q_1^{\mu'} Q_2^\nu + R^{\mu'\nu'} Q_1^\mu Q_2^\nu - R^{\mu'\nu} Q_2^{\nu'} Q_1^\mu) . \tag{7.15}
\end{aligned}$$

The dimensionless invariant functions W_{ab} depend only on the invariants W^2 , Q^2 and P^2 and are related to the $\gamma\gamma$ -helicity amplitudes¹ $W_{m'n',mn}$ in the $\gamma\gamma$ -CMS via [82]

$$\begin{aligned}
W_{\text{TT}} &= \frac{1}{2} (W_{++,++} + W_{+,-,+}) , & W_{\text{TL}} &= W_{+0,+0} , \\
W_{\text{LT}} &= W_{0+,0+} , & W_{\text{LL}} &= W_{00,00} , \\
W_{\text{TT}}^\tau &= W_{+,-,-} , & W_{\text{TL}}^\tau &= \frac{1}{2} (W_{++,00} + W_{0+,-0}) , \\
W_{\text{TT}}^{\text{a}} &= \frac{1}{2} (W_{++,++} - W_{+,-,+}) , & W_{\text{TL}}^{\text{a}} &= \frac{1}{2} (W_{++,00} - W_{0+,-0}) . \tag{7.16}
\end{aligned}$$

The amplitudes W_{TT}^τ , W_{TL}^τ , and W_{TL}^{a} correspond to transitions with spin flip for each of the photons (with total helicity conservation). As we will see in the next section only 6 of these amplitudes (W_{TT} , W_{TL} , W_{LT} , W_{LL} , W_{TT}^τ , W_{TL}^τ) enter the cross section for unpolarized lepton beams because the tensors in (7.10) are symmetric whereas the tensor structures multiplying W_{TT}^{a} and W_{TL}^{a} in (7.11) are anti-symmetric such that these terms do not contribute when the leptonic and the hadronic tensors are contracted. Only if the initial leptons are polarized, can the amplitudes W_{TT}^{a} and W_{TL}^{a} be measured as well [82].

¹The photon helicities can adopt the values $m', n', m, n = +1, -1, 0$. Total helicity conservation for forward $\gamma\gamma$ -scattering implies $m' - n' = m - n$ and due to P- and T-invariance ($W_{m'n',mn} \stackrel{P}{=} (-1)^{m'-n'+m-n} W_{-m'-n',-m-n} = W_{-m'-n',-m-n} \stackrel{T}{=} W_{mn,m'n'}$) there exist 8 independent helicity amplitudes. See App. C in Ref. [82] and Ref. [100] for further details.

7.1.2 Derivation of the Cross Section

Using Eqs. (7.9), (7.10) and (7.11) one obtains by a straightforward (but tedious) calculation

$$L_{(1)}^{\mu\mu'} L_{(2)}^{\nu\nu'} W_{\mu'\nu',\mu\nu} = Q^2 P^2 \left[4\rho_1^{++} \rho_2^{++} W_{\text{TT}} + 2|\rho_1^{+-} \rho_2^{+-}| W_{\text{TT}}^\tau \cos 2\bar{\phi} + 2\rho_1^{++} \rho_2^{00} W_{\text{TL}} \right. \\ \left. + 2\rho_1^{00} \rho_2^{++} W_{\text{LT}} + \rho_1^{00} \rho_2^{00} W_{\text{LL}} - 8|\rho_1^{+0} \rho_2^{+0}| W_{\text{TL}}^\tau \cos \bar{\phi} \right] \quad (7.17)$$

where $\bar{\phi}$ is the angle between the scattering planes of the e^- and the e^+ in the center-of-mass system (CMS) of the colliding photons and the ρ_i 's are elements of the photon density matrix:

$$\begin{aligned} 2\rho_1^{++} &= 2\rho_1^{--} = \rho_1^{\alpha\beta} R_{\alpha\beta} = \frac{(2p_1 \cdot p - p \cdot q)^2}{(p \cdot q)^2 - Q^2 P^2} + 1 - 4\frac{m_e^2}{Q^2}, \\ 2\rho_2^{++} &= 2\rho_2^{--} = \rho_2^{\alpha\beta} R_{\alpha\beta} = \frac{(2p_2 \cdot q - p \cdot q)^2}{(p \cdot q)^2 - Q^2 P^2} + 1 - 4\frac{m_e^2}{P^2}, \\ \rho_1^{00} &= \rho_1^{\alpha\beta} Q_{1\alpha} Q_{1\beta} = 2\rho_1^{++} - 2 + 4\frac{m_e^2}{Q^2}, \\ \rho_2^{00} &= \rho_2^{\alpha\beta} Q_{2\alpha} Q_{2\beta} = 2\rho_2^{++} - 2 + 4\frac{m_e^2}{P^2}, \\ 2|\rho_1^{+-} \rho_2^{+-}| \cos 2\bar{\phi} &= \frac{C^2}{Q^2 P^2} - 2(\rho_1^{++} - 1)(\rho_2^{++} - 1), \\ 8|\rho_1^{+0} \rho_2^{+0}| \cos \bar{\phi} &= \frac{4C}{\sqrt{Q^2 P^2}} \frac{(2p_1 \cdot p - p \cdot q)(2p_2 \cdot q - p \cdot q)}{(p \cdot q)^2 - Q^2 P^2} \\ \text{with } C &= (2p_1 - q)^\alpha (2p_2 - p)^\beta R_{\alpha\beta} = -(2p_1 - q) \cdot (2p_2 - p) \\ &\quad + \frac{p \cdot q}{(p \cdot q)^2 - Q^2 P^2} (2p_1 \cdot p - p \cdot q)(2p_2 \cdot q - p \cdot q), \\ |\rho_i^{+-}| &= \rho_i^{++} - 1, \\ |\rho_i^{+0}| &= \sqrt{(\rho_i^{00} + 1)|\rho_i^{+-}|}. \end{aligned} \quad (7.18)$$

Note that all these quantities are expressed in terms of the measurable momenta p_1, p_2 and p'_1, p'_2 (respectively q, p) only and therefore are entirely known.

With help of Eqs. (7.7) and (7.17) we easily find the fully general final result for the

$ee \rightarrow eeX$ cross section [82, 85, 90]:

$$d^6\sigma(ee \rightarrow eeX) = \frac{d^3p'_1 d^3p'_2}{E'_1 E'_2} \frac{\alpha^2}{16\pi^4 Q^2 P^2} \frac{F_{\gamma\gamma}}{F_{ee}} \left[4\rho_1^{++}\rho_2^{++}\sigma_{\text{TT}} + 2\rho_1^{00}\rho_2^{++}\sigma_{\text{LT}} + 2\rho_1^{++}\rho_2^{00}\sigma_{\text{TL}} \right. \\ \left. + \rho_1^{00}\rho_2^{00}\sigma_{\text{LL}} + 2|\rho_1^{+-}\rho_2^{+-}|\tau_{\text{TT}}\cos 2\bar{\phi} - 8|\rho_1^{+0}\rho_2^{+0}|\tau_{\text{TL}}\cos \bar{\phi} \right] \\ \text{with} \\ \frac{F_{\gamma\gamma}}{F_{ee}} = \left[\frac{(p \cdot q)^2 - Q^2 P^2}{(p_1 \cdot p_2)^2 - m_e^2 m_e^2} \right]^{1/2}. \quad (7.19)$$

Here the cross sections σ_{ab} (used as a shorthand for σ_{TT} , σ_{TL} , σ_{LT} , σ_{LL} , τ_{TT} , τ_{TL} , τ_{TT}^a , τ_{TL}^a) are identical to the corresponding structure functions W_{ab} up to a division by the appropriate flux factor of the two incoming photons², i.e.

$$\sigma_{ab} = \frac{1}{2\sqrt{(p \cdot q)^2 - Q^2 P^2}} W_{ab} = \frac{1}{2\nu\beta} W_{ab}. \quad (7.20)$$

The cross section in (7.19) considerably simplifies in certain kinematical regions [82, 85, 90]. For instance, if both photons are highly virtual Eq. (7.19) can be evaluated in the limit $Q^2, P^2 \gg m_e^2$ [90] in which some relations between the elements of the photon density matrix exist. Of special interest in this thesis is the case where one of the lepton scattering angles becomes small leading to a small virtuality $P^2 \approx 0$ of the corresponding photon while the other photon provides a hard scale $Q^2 \gtrsim 1 \text{ GeV}^2$. In this limit the cross section factorizes into a product of a flux of quasi-real target photons times the cross section for deep inelastic electron-photon scattering, see for example [90]. This process is the classical way of measuring the structure of (quasi-real) photons. The findings in the latter limit can be generalized to the case of photons with non-zero virtuality $P^2 \neq 0$ as we will see in Section 7.3. This allows to study the structure of virtual photons in deep inelastic $e\gamma(P^2)$ scattering processes in a continuous range of the scale P^2 .

7.2 Photon Structure Functions

It is the aim of this section to relate the structure functions of a (virtual) *target* photon to the invariant functions W_{ab} . The defining relations are generally valid for arbitrary P^2 . However, they only have a meaningful interpretation as structure functions of a target

²Note that a factor $\frac{1}{2}$ has already been absorbed into the definition of $W^{\mu'\nu',\mu\nu}$ in Eq. (7.8).

photon probed by a deeply virtual photon $\gamma(Q^2)$ in the limit $P^2 \ll Q^2$. The following expressions are simplified if one introduces the transverse components of a four-vector x_μ and of $g_{\mu\nu}$

$$x_\mu^T = x_\mu - \frac{q \cdot x}{q^2} q_\mu, \quad g_{\mu\nu}^T = g_{\mu\nu} - \frac{1}{q^2} q_\mu q_\nu, \quad (7.21)$$

where 'transverse' refers to q : $q \cdot x^T = 0$, $q^\mu g_{\mu\nu}^T = q^\nu g_{\mu\nu}^T = 0$.

7.2.1 Structure Functions for a Spin-Averaged Photon

Usually one introduces structure functions for a *spin-averaged* target photon. The corresponding structure tensor can be obtained by contracting $W_{\mu'\nu',\mu\nu}$ given in Eq. (7.11) with the metric tensor $g^{\nu\nu'}$. With the help of Eqs. (7.13) and (7.14) one obtains³:

$$\begin{aligned} W_{\mu'\mu}^{<\gamma>} &\equiv \frac{-g^{\nu\nu'}}{2} W_{\mu'\nu',\mu\nu} \\ &= R_{\mu'\mu} \left[W_{\text{TT}} - \frac{1}{2} W_{\text{TL}} \right] + Q_{1\mu'} Q_{1\mu} \left[W_{\text{LT}} - \frac{1}{2} W_{\text{LL}} \right] \\ &= -g_{\mu'\mu}^T \left[W_{\text{TT}} - \frac{1}{2} W_{\text{TL}} \right] + p_{\mu'}^T p_\mu^T \frac{Q^2}{\nu^2 \bar{\beta}^2} \left[W_{2\text{T}} - \frac{1}{2} W_{2\text{L}} \right] \end{aligned} \quad (7.22)$$

where $W_{2\text{T}} \equiv W_{\text{TT}} + W_{\text{LT}}$ and $W_{2\text{L}} \equiv W_{\text{TL}} + W_{\text{LL}}$.

Alternatively the spin-averaged tensor can be expressed in standard form in terms of the structure functions $F_1 \equiv W_1$ and $F_2 \equiv \nu W_2$:

$$\frac{1}{8\pi^2\alpha} W_{\mu'\mu}^{<\gamma>} = -g_{\mu'\mu}^T F_1^{<\gamma>} + p_{\mu'}^T p_\mu^T \frac{1}{\nu} F_2^{<\gamma>}. \quad (7.23)$$

Comparing Eqs. (7.22) and (7.23) we find

$$\begin{aligned} 2xF_1^{<\gamma>} &= \frac{1}{8\pi^2\alpha} \frac{Q^2}{\nu} \left[W_{\text{TT}} - \frac{1}{2} W_{\text{TL}} \right] \\ F_2^{<\gamma>} &= \frac{1}{8\pi^2\alpha} \frac{Q^2}{\nu} \frac{1}{\bar{\beta}^2} \left[W_{2\text{T}} - \frac{1}{2} W_{2\text{L}} \right]. \end{aligned} \quad (7.24)$$

These relations can be re-expressed in terms of the photon-photon cross sections $\sigma_{ab} = W_{ab}/(2\nu\bar{\beta})$ ($a, b = 2, \text{L}, \text{T}$) [82, 85, 90]

$$\begin{aligned} 2xF_1^{<\gamma>} &= \frac{Q^2}{4\pi^2\alpha} \bar{\beta} \left[\sigma_{\text{TT}} - \frac{1}{2} \sigma_{\text{TL}} \right] \\ F_2^{<\gamma>} &= \frac{Q^2}{4\pi^2\alpha} \frac{1}{\bar{\beta}} \left[\sigma_{2\text{T}} - \frac{1}{2} \sigma_{2\text{L}} \right]. \end{aligned} \quad (7.25)$$

³Of course the virtual photon has three (+, −, 0) degrees of freedom. The factor 1/2 guarantees the *conventional* normalization in the real photon limit with only two (+, −) transverse degrees of freedom.

Finally, F_L satisfies the usual relation

$$F_L^{<\gamma>} = \bar{\beta}^2 F_2^{<\gamma>} - 2x F_1^{<\gamma>} . \quad (7.26)$$

This can be seen by contracting $W_{\mu'\mu}^{<\gamma>}$ with the polarization vectors of longitudinal *probe* photons given in Eq. (7.12) thereby employing again the orthogonality relations in Eq. (7.14)

$$\begin{aligned} W_L^{<\gamma>} &\equiv \epsilon_0^{\star\mu'}(q) \epsilon_0^\mu(q) W_{\mu'\mu}^{<\gamma>} = Q_1^{\mu'} Q_1^\mu W_{\mu'\mu}^{<\gamma>} = W_{LT} - \frac{1}{2} W_{LL} \\ &= 8\pi^2 \alpha \left[-F_1^{<\gamma>} + \frac{\bar{\beta}^2}{2x} F_2^{<\gamma>} \right] \end{aligned}$$

followed by the appropriate normalization:

$$F_L^{<\gamma>} = \frac{1}{8\pi^2 \alpha} 2x W_L^{<\gamma>} .$$

7.2.2 Longitudinal and Transverse Target Photons

Since the fluxes of transverse and longitudinal virtual photons will turn out to be *different* (see Eq. (7.37) below) it is most convenient to introduce structure functions of transverse respectively longitudinal target photons (instead of spin-averaged target photons). The procedure is completely analogous to the one in the previous section using Eqs. (7.12)–(7.14) and for this reason the description will be brief.

I. Transverse Photons

With the help of Eq. (7.12) we can construct the structure tensor for a transverse photon target which can be cast again into different forms

$$\begin{aligned} W_{\mu'\mu}^{\gamma_T} &\equiv \frac{1}{2} [\epsilon_+^{\star\nu'}(p) \epsilon_+^\nu(p) + \epsilon_-^{\star\nu'}(p) \epsilon_-^\nu(p)] W_{\mu'\nu',\mu\nu} = \frac{1}{2} R^{\nu'\nu} W_{\mu'\nu',\mu\nu} \\ &= R_{\mu'\mu} W_{TT} + Q_{1\mu'} Q_{1\mu} W_{LT} = -g_{\mu'\mu}^T W_{TT} + p_{\mu'}^T p_\mu^T \frac{Q^2}{\nu^2 \bar{\beta}^2} W_{2T} \\ &\stackrel{!}{=} 8\pi^2 \alpha \left[-g_{\mu'\mu}^T F_1^{\gamma_T} + p_{\mu'}^T p_\mu^T \frac{1}{\nu} F_2^{\gamma_T} \right] \end{aligned} \quad (7.27)$$

and we can directly read off the structure functions:

$$\begin{aligned} 2x F_1^{\gamma_T} &= \frac{1}{8\pi^2 \alpha} \frac{Q^2}{\nu} W_{TT} = \frac{Q^2}{4\pi^2 \alpha} \bar{\beta} \sigma_{TT} \\ F_2^{\gamma_T} &= \frac{1}{8\pi^2 \alpha} \frac{Q^2}{\nu} \frac{1}{\bar{\beta}^2} W_{2T} = \frac{Q^2}{4\pi^2 \alpha} \frac{1}{\bar{\beta}} \sigma_{2T} . \end{aligned} \quad (7.28)$$

Repeating the steps in Sec. 7.2.1 to determine $F_L^{<\gamma>}$, we obtain $W_L^{\gamma_T} = W_{LT}$ implying

$$F_L^{\gamma_T} = \frac{1}{8\pi^2\alpha} 2x W_L^{\gamma_T} = \bar{\beta}^2 F_2^{\gamma_T} - 2x F_1^{\gamma_T} . \quad (7.29)$$

II. Longitudinal Photons

The structure tensor for a longitudinal photon target is given by (using again Eq. (7.12))

$$\begin{aligned} W_{\mu'\mu}^{\gamma_L} &\equiv \epsilon_0^{\star\nu'}(p) \epsilon_0^\nu(p) W_{\mu'\nu',\mu\nu} = Q_2^{\nu'} Q_2^\nu W_{\mu'\nu',\mu\nu} \\ &= R_{\mu'\mu} W_{TL} + Q_{1\mu'} Q_{1\mu} W_{LL} = -g_{\mu'\mu}^T W_{TL} + p_{\mu'}^T p_\mu^T \frac{Q^2}{\nu^2 \bar{\beta}^2} W_{2L} \\ &\stackrel{!}{=} 8\pi^2\alpha \left[-g_{\mu'\mu}^T F_1^{\gamma_L} + p_{\mu'}^T p_\mu^T \frac{1}{\nu} F_2^{\gamma_L} \right] \end{aligned} \quad (7.30)$$

and we find the following result for a longitudinal target photon:

$$\begin{aligned} 2x F_1^{\gamma_L} &= \frac{1}{8\pi^2\alpha} \frac{Q^2}{\nu} W_{TL} = \frac{Q^2}{4\pi^2\alpha} \bar{\beta} \sigma_{TL} \\ F_2^{\gamma_L} &= \frac{1}{8\pi^2\alpha} \frac{Q^2}{\nu} \frac{1}{\bar{\beta}^2} W_{2L} = \frac{Q^2}{4\pi^2\alpha} \frac{1}{\bar{\beta}} \sigma_{2L} . \end{aligned} \quad (7.31)$$

Finally, we have (as could be expected)

$$W_L^{\gamma_L} = W_{LL} \quad \Rightarrow \quad F_L^{\gamma_L} = \frac{1}{8\pi^2\alpha} 2x W_L^{\gamma_L} = \bar{\beta}^2 F_2^{\gamma_L} - 2x F_1^{\gamma_L} . \quad (7.32)$$

Further inspection of Eqs. (7.22)–(7.32) reveals a relation [$<\gamma> = \gamma_T - \frac{1}{2}\gamma_L$] between the spin-averaged, transverse and longitudinal target photons

$$\begin{aligned} W_{\mu'\mu}^{<\gamma>} &= W_{\mu'\mu}^{\gamma_T} - \frac{1}{2} W_{\mu'\mu}^{\gamma_L} \\ F_i^{<\gamma>} &= F_i^{\gamma_T} - \frac{1}{2} F_i^{\gamma_L} \quad (i = 1, 2, L) \end{aligned} \quad (7.33)$$

which is a consequence of the completeness relation for *spacelike* photons (cf. [82], Eq. (B.1)):

$$\underbrace{\epsilon_+^{\star\mu}(p) \epsilon_+^\nu(p) + \epsilon_-^{\star\mu}(p) \epsilon_-^\nu(p)}_{2\gamma_T} - \underbrace{\epsilon_0^{\star\mu}(p) \epsilon_0^\nu(p)}_{\gamma_L} = \underbrace{-g^{\mu\nu} + \frac{p^\mu p^\nu}{p^2}}_{2<\gamma>} . \quad (7.34)$$

7.3 QED–Factorization

It is well known that for $P^2 \approx 0$ the general cross section for the process $ee \rightarrow ee\gamma\gamma \rightarrow eeX$ factorizes into a product of a flux of target photons (radiated off the electron) with the

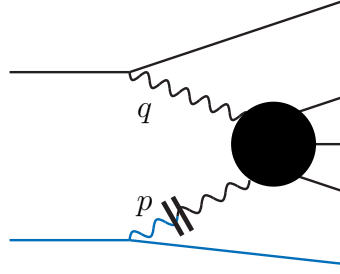


Figure 7.4: Factorization of the $ee \rightarrow ee\gamma\gamma \rightarrow eeX$ cross section into a flux of “target” photons radiated off the lower lepton line times the cross section for deep inelastic electron–photon scattering (black part). The cut in the photon line indicates a time order between the two subprocesses (photon emission *followed* by deep inelastic $e\gamma$ scattering) and implies also that these two factors are independent of each other.

deep inelastic electron–photon scattering cross section [85, 90], see Fig. 7.4 for a graphical representation:

$$\frac{d\sigma(ee \rightarrow eeX)}{dx dQ^2 dz dP^2} = f_{\gamma T/e}(z, P^2) \frac{d\sigma(e\gamma \rightarrow eX)}{dx dQ^2} \quad (P^2 \approx 0) \quad (7.35)$$

where $z = E_\gamma/E \approx y_2$ is the fraction of the lepton energy carried by the photon (in the e^+e^- -CMS). The cross section for deep inelastic electron–photon scattering in Eq. (7.35) reads

$$\begin{aligned} \frac{d\sigma(e\gamma \rightarrow eX)}{dx dQ^2} &= \frac{4\pi^2\alpha y}{xQ^2} \frac{\alpha}{2\pi} \left[\frac{1 + (1-y)^2}{y} \frac{1}{Q^2} \right] \left[2xF_1^\gamma + \frac{2(1-y)}{1 + (1-y)^2} F_L^\gamma \right] \\ &= \frac{2\pi\alpha^2}{xQ^4} [(1 + (1-y)^2)2xF_1^\gamma + 2(1-y)F_L^\gamma] \end{aligned} \quad (7.36)$$

with the usual variable $y = \frac{p \cdot q}{p \cdot p_1} = y_1$. Furthermore, $f_{\gamma T/e}$ denotes the flux factor of *transversely* (or circularly) polarized photons with virtuality P^2 . For use below we also provide the flux factor $f_{\gamma L/e}$ of longitudinally polarized photons:

$$\begin{aligned} f_{\gamma T/e}(z, P^2) &= \frac{\alpha}{2\pi} \left[\frac{1 + (1-z)^2}{z} \frac{1}{P^2} - \frac{2m_e^2 z}{P^4} \right] \\ f_{\gamma L/e}(z, P^2) &= \frac{\alpha}{2\pi} \left[\frac{2(1-z)}{z} \frac{1}{P^2} \right]. \end{aligned} \quad (7.37)$$

The factorization in (7.35) is *essential* for relating the concept of the structure of a (real) photon to experimental measurements of two-photon processes. For this reason we

want to generalize Eq. (7.35) for photons with virtuality $P^2 \neq 0$ and show that, in the Bjorken limit, factorization holds for virtual “target” photons as well. For definiteness, as the Bjorken limit we consider

$$Q^2 \equiv Q_1^2 \rightarrow \infty, \quad \nu \rightarrow \infty, \quad x = Q^2/2\nu = \text{fixed}. \quad (7.38)$$

Practically, this means $P^2 \equiv Q_2^2 \ll Q^2, \nu$ such that $\delta \equiv P^2/2\nu = xP^2/Q^2$ is a small quantity which can be neglected.

The starting point is the general cross section in Eq. (7.19). Employing Eqs. (7.28), (7.29), (7.31), and (7.32) and rearranging the terms inside the square brackets it can be written as

$$d^6\sigma = \frac{d^3p'_1 d^3p'_2}{E'_1 E'_2} \frac{\alpha^2}{16\pi^4 Q^2 P^2} \frac{F_{\gamma\gamma}}{F_{ee}} \left[\frac{4\pi^2 \alpha}{Q^2 \bar{\beta}} \left(2\rho_2^{++} 2\rho_1^{++} [2xF_1^{\gamma_T} + \varepsilon F_L^{\gamma_T}] \right. \right. \\ \left. \left. + \rho_2^{00} 2\rho_1^{++} [2xF_1^{\gamma_L} + \varepsilon F_L^{\gamma_L}] \right) + 2|\rho_1^{+-} \rho_2^{+-}| \tau_{TT} \cos 2\bar{\phi} - 8|\rho_1^{+0} \rho_2^{+0}| \tau_{TL} \cos \bar{\phi} \right] \quad (7.39)$$

with $\varepsilon = \frac{\rho_1^{00}}{2\rho_1^{++}}.$

The general strategy will be to demonstrate that ρ_2^{++} and ρ_2^{00} are proportional to the flux factors of transverse and longitudinal photons, respectively, radiated off an electron and that the interference terms disappear after having performed an appropriate angular integration.

In the Bjorken limit it is useful to perform a “light cone decomposition” of the 4-momenta of the two photons [82]:

$$q = \xi_q^+ p_1 + \xi_q^- p_2 + q_\perp \quad p = \xi_p^+ p_1 + \xi_p^- p_2 + p_\perp$$

with

$$p_i^2 = 0, \quad p_i \cdot q_\perp = p_i \cdot p_\perp = 0, \quad p_1 \cdot p_2 = S/2 \quad (7.40)$$

where S is the square of the ee -CMS energy. The momentum fractions ξ_q^+ , ξ_q^- , ξ_p^+ and

ξ_p^- and the transverse momenta can be easily calculated:

$$\begin{aligned}
2p_1 \cdot q &= S\xi_q^- = -Q^2 &\Rightarrow &\xi_q^- = -Q^2/S \\
2p_2 \cdot q &= S\xi_q^+ &\Rightarrow &\xi_q^+ = 2p_2 \cdot q/S (\approx y_1) \\
2p_1 \cdot p &= S\xi_p^- &\Rightarrow &\xi_p^- = 2p_1 \cdot p/S (\approx y_2) \\
2p_2 \cdot p &= S\xi_p^+ = -P^2 &\Rightarrow &\xi_p^+ = -P^2/S \\
Q^2 &= -S\xi_q^+\xi_q^- - q_\perp^2 &\Rightarrow &q_\perp^2 = -Q^2(1 - \xi_q^+) \\
P^2 &= -S\xi_p^+\xi_p^- - p_\perp^2 &\Rightarrow &p_\perp^2 = -P^2(1 - \xi_p^-) \\
q_\perp \cdot p_\perp &\equiv -\sqrt{q_\perp^2 p_\perp^2} \cos \phi = -\sqrt{Q^2 P^2 (1 - \xi_q^+)(1 - \xi_p^-)} \cos \phi .
\end{aligned} \tag{7.41}$$

Here ϕ is the angle between the scattering planes of the e^- and e^+ in the e^+e^- -CMS. Obviously ξ_p^+ is negligibly small such that we can use⁴

$$p = \xi_p^- p_2 + p_\perp . \tag{7.42}$$

(On the other hand ξ_q^- *cannot* be neglected in the Bjorken limit.) In the e^+e^- -CMS the 4-momenta of the incoming leptons can be written as $p_1 = (E, 0, 0, E)$ and $p_2 = (E, 0, 0, -E)$ where $E = \frac{\sqrt{S}}{2}$ (neglecting terms of the order $\mathcal{O}(\frac{m_e^2}{S})$). Since the transverse 4-vector is given by $p_\perp = (0, p_{\perp x}, p_{\perp y}, 0)$ we can infer from Eq. (7.42) that $E_\gamma = \xi_p^- E$, i.e., in the e^+e^- -CMS ξ_p^- is the energy fraction of the lepton energy transferred to the photon. For a *real* ($P^2 = 0$) photon we recover the familiar relation $p = \xi_p^- p_2$ between the 4-momenta p and p_2 of the collinearly radiated photon and its (massless) “parent” lepton, respectively.

Before turning to the photon density matrix elements in the Bjorken limit it is helpful to relate the variable $\nu \equiv p \cdot q$ to ξ_q^+ , ξ_p^- and the transverse momenta:

$$2\nu = S\xi_p^-\xi_q^+(1 + \rho) \quad \text{with} \quad \rho \equiv \frac{2p_\perp \cdot q_\perp}{S\xi_p^-\xi_q^+} \approx -2\sqrt{x\delta(1 - \xi_q^+)(1 - \xi_p^-)} \cos \phi , \tag{7.43}$$

where $\rho \propto \sqrt{\delta}$ is small in the Bjorken limit. Employing Eq. (7.43) we find in addition

$$y_1 \equiv \frac{\nu}{p \cdot p_1} = \xi_q^+(1 + \rho) , \quad y_2 \equiv \frac{\nu}{q \cdot p_2} = \xi_p^-(1 + \rho) . \tag{7.44}$$

Introducing the variables $\omega_1 \equiv q \cdot (p_1 + p_2)/\sqrt{S} = \frac{\sqrt{S}}{2}(\xi_q^- + \xi_q^+)$ and $\omega_2 \equiv p \cdot (p_1 + p_2)/\sqrt{S} = \frac{\sqrt{S}}{2}(\xi_p^- + \xi_p^+)$ the phase space can be written as [82] [Eq.(5.15b)] (up to terms

⁴Of course, in the calculation of quantities which are themselves small of the order P^2 (e.g. p_\perp^2 in the e^+e^- -CMS or $p_{2\perp}^2$ in the $\gamma\gamma$ -CMS) ξ_p^+ must be taken into account.

of the order $\mathcal{O}(\frac{m_e^2}{S})$

$$\begin{aligned} \frac{d^3 p'_1}{E'_1} \frac{d^3 p'_2}{E'_2} &= \frac{2\pi}{S} dQ^2 dP^2 d\omega_1 d\omega_2 d\phi = \frac{\pi}{2} dQ^2 d\xi_q^+ dP^2 d\xi_p^- d\phi \\ &= \frac{\pi}{2} dQ^2 dy_1 dP^2 d\xi_p^- d\phi (1 + \mathcal{O}(\rho)) \end{aligned} \quad (7.45)$$

where the third equality can be understood with the help of Eq. (7.44).

In the Bjorken limit the photon density matrix elements in Eq. (7.18) can be cast in a very compact form using the symmetric notation $Q_1^2 = Q^2$ and $Q_2^2 = P^2$:

$$\begin{aligned} 2\rho_1^{++} &= \frac{2}{y_i} Q_i^2 \left[\frac{1 + (1 - y_i)^2}{y_i} \frac{1}{Q_i^2} - \frac{2m_e^2 y_i}{Q_i^4} \right] + \mathcal{O}(\delta) \\ \rho_i^{00} &= \frac{2}{y_i} Q_i^2 \left[\frac{2(1 - y_i)}{y_i} \frac{1}{Q_i^2} \right] + \mathcal{O}(\delta) \\ |\rho_i^{+-}| &= \frac{1}{y_i} Q_i^2 \left[\frac{2(1 - y_i)}{y_i} \frac{1}{Q_i^2} - \frac{2m_e^2 y_i}{Q_i^4} \right] + \mathcal{O}(\delta) . \end{aligned} \quad (7.46)$$

These results have to be expressed by the independent integration variables Q^2 , y_1 , P^2 , and ξ_p^- . Furthermore, from here on we identify $y_1 \equiv y$.

Obviously ρ_2^{++} and ρ_2^{00} are proportional to the flux factors of transverse respectively longitudinal photons in Eq. (7.37)

$$\begin{aligned} 2\rho_2^{++} &= \frac{2}{\xi_p^-} P^2 \frac{2\pi}{\alpha} f_{\gamma_T/e}(\xi_p^-, P^2) + \mathcal{O}(\rho) \\ \rho_2^{00} &= \frac{2}{\xi_p^-} P^2 \frac{2\pi}{\alpha} f_{\gamma_L/e}(\xi_p^-, P^2) + \mathcal{O}(\rho) \end{aligned} \quad (7.47)$$

and similarly we can write

$$\begin{aligned} 2\rho_1^{++} &= \frac{2}{y} Q^2 \left[\frac{1 + (1 - y)^2}{y} \frac{1}{Q^2} \right] , \quad \rho_1^{00} = \frac{2}{y} Q^2 \left[\frac{2(1 - y)}{y} \frac{1}{Q^2} \right] \\ \varepsilon &= \frac{\rho_1^{00}}{2\rho_1^{++}} = \frac{2(1 - y)}{1 + (1 - y)^2} \end{aligned} \quad (7.48)$$

where we have discarded the mass terms due to $Q^2 \gg m_e^2$.

Inserting Eqs. (7.47), (7.46), and (7.45) into Eq. (7.39) one straightforwardly obtains (using $\frac{F_{\gamma\gamma}}{F_{ee}} = 2\nu\bar{\beta}/S = \xi_p^- y\bar{\beta}$)

$$\begin{aligned} d\sigma &= dQ^2 dy dP^2 d\xi_p^- \frac{d\phi}{2\pi} \left\{ f_{\gamma_T/e}(\xi_p^-, P^2) \frac{d\sigma(e\gamma_T \rightarrow eX)}{dy dQ^2} \Big|_{\hat{S}=\xi_p^- S} + [\gamma_T \rightarrow \gamma_L] \right. \\ &\quad \left. + \mathcal{O}(\rho) + \text{interference-terms} \right\} \end{aligned} \quad (7.49)$$

with the cross sections for deep inelastic electron-photon scattering given by [cf. Eq. (7.36)]

$$\frac{d\sigma(e\gamma_{T,L} \rightarrow eX)}{dydQ^2} \Big|_{\hat{s}=\xi_p^- s} = \frac{4\pi^2\alpha}{Q^2} \frac{\alpha}{2\pi} \left[\frac{1+(1-y)^2}{y} \frac{1}{Q^2} \right] [2xF_1^{\gamma_{T,L}}(x, Q^2) + \varepsilon F_L^{\gamma_{T,L}}(x, Q^2)] \quad (7.50)$$

where ε can be found in Eq. (7.48). Note that only two of the variables x , y , and Q^2 are independent since they are related via $Q^2 = \hat{S}xy$. The terms proportional to ρ vanish after ϕ -integration like terms of the order $\mathcal{O}(\delta)$.

Unfortunately, the interference terms are proportional to $\cos \bar{\phi}$ and $\cos 2\bar{\phi}$ where $\bar{\phi}$ is the angle of the electron scattering planes in the $\gamma\gamma$ -CMS while ϕ is the angle of the electron scattering planes in the e^+e^- -CMS (\equiv laboratory system). However, we show below that

$$\cos \bar{\phi} = \cos \phi (1 + \mathcal{O}(\rho)) . \quad (7.51)$$

Therefore, we can also get rid of the interference terms (proportional to $\cos \bar{\phi} \approx \cos \phi$) by integrating over ϕ , leaving a remainder of the order $\mathcal{O}(\sqrt{\delta})$. The latter becomes obvious if we remember that the variable ρ defined in (7.43) is proportional to $\sqrt{\delta} \cos \phi$ such that terms $\rho \cos \phi$ occurring for example in Eq. (7.51) are proportional to $\sqrt{\delta} \cos^2 \phi$ which do *not* vanish by integrating over ϕ .

Before calculating $\cos \bar{\phi}$ let us state the final factorization formula:

$$\begin{aligned} \frac{d\sigma(ee \rightarrow eeX)}{dydQ^2 d\xi_p^- dP^2} = & f_{\gamma_{T/e}}(\xi_p^-, P^2) \frac{d\sigma(e\gamma_T \rightarrow eX)}{dydQ^2} \Big|_{\hat{s}=\xi_p^- s} + \mathcal{O}(\delta) \\ & + f_{\gamma_{L/e}}(\xi_p^-, P^2) \frac{d\sigma(e\gamma_L \rightarrow eX)}{dydQ^2} \Big|_{\hat{s}=\xi_p^- s} + \mathcal{O}(\delta) \\ & + \mathcal{O}(\sqrt{\delta}) . \end{aligned} \quad (7.52)$$

A few comments are in order:

- In the limit $P^2 \rightarrow 0$ the contributions from longitudinal target photons have to vanish since a real photon has only two transverse physical degrees of freedom and we recover Eq. (7.35).⁵

⁵More precisely, assuming that the structure functions of a longitudinal target photon vanish like P^2/Λ^2 where Λ is a typical hadronic scale, say $\Lambda = m_\rho$, we obtain a *non-zero* result because $f_{\gamma_{L/e}} \propto 1/P^2$ which is, however, negligible compared to the contribution from transverse target photons.

- The factorized result in Eq. (7.52) is valid up to terms $\mathcal{O}(\sqrt{\delta})$ which formally go to zero in the Bjorken limit. However, for practical purposes it is not clear when $\delta = xP^2/Q^2$ is small enough for Eq. (7.52) to be a good approximation of the exact cross section in Eq. (7.19). Here, a numerical comparison of the factorization formula with the exact cross section would be interesting.

To complete our derivation we still have to show that $\cos \bar{\phi} = \cos \phi + \mathcal{O}(\rho)$ where $\cos \bar{\phi}$ is given by Eq. (A.4) in [82]

$$\cos \bar{\phi} \equiv \frac{-p_{1\perp} \cdot p_{2\perp}}{\sqrt{p_{1\perp}^2 p_{2\perp}^2}} \quad \text{with} \quad p_{i\perp}^\mu = -p_{i\nu} R^{\mu\nu}(q, p) \quad (7.53)$$

and where $R^{\mu\nu}(q, p)$ has been defined in Eq. (7.13). Using the decomposition in Eq. (7.40) it is straightforward to obtain

$$\begin{aligned} p_{1\perp} \cdot p_{2\perp} &= \frac{p_\perp \cdot q_\perp}{\xi_p^- \xi_q^+} \\ p_{1\perp}^2 &= -\frac{Q^2}{\xi_q^{+2}} (1 - \xi_q^+) + \mathcal{O}(\rho) \\ p_{2\perp}^2 &= -\frac{P^2}{\xi_p^{-2}} (1 - \xi_p^-) + \mathcal{O}(\rho) . \end{aligned} \quad (7.54)$$

Inserting these relations into Eq. (7.53) and comparing with the definition of $\cos \phi$ in Eq. (7.41) we find the above stated result

$$\cos \bar{\phi} = \frac{-p_\perp \cdot q_\perp}{\sqrt{p_\perp^2 q_\perp^2}} + \mathcal{O}(\rho) = \cos \phi + \mathcal{O}(\rho) . \quad (7.55)$$

Chapter 8

The Doubly Virtual Box in LO

In this chapter we calculate the invariant amplitudes W_{ab} (or the cross sections σ_{ab}) in lowest order perturbation theory and compare them with present e^+e^- virtual photon data. These expressions are usually referred to as box results due to the diagram representing the tensor $W^{\mu'\nu',\mu\nu}$, where the photons are attached to a fermion box, see Fig. 8.1.

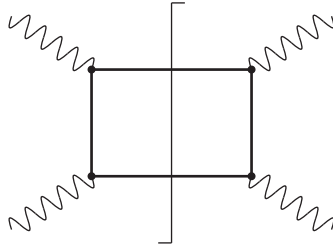


Figure 8.1: Box-diagram for $\gamma^*(q, \mu)\gamma^*(p, \nu) \rightarrow \gamma^*(q, \mu')\gamma^*(p, \nu')$. There are 4 possibilities to attach the photons to the vertices. (2 for the initial state times 2 for the final state.)

The calculation is a straightforward application of Feynman rules and will only be shortly outlined here. In order to obtain $W^{\mu'\nu',\mu\nu}$ according to Eq. (7.8) one has to build up the amplitude $M^{\mu\nu}$ of the process $\gamma^*(q, \mu)\gamma^*(p, \nu) \rightarrow f(k_1)\bar{f}(k_2)$ shown in Fig. 8.2 where f is either a lepton or a quark of mass m . The kinematics can be described with the help of the 4-momentum conservation relation $q + p = k_1 + k_2$ and the usual Mandelstam variables

$$s = (q + p)^2, \quad t = (q - k_1)^2 = (p - k_2)^2, \quad u = (p - k_1)^2 = (q - k_2)^2,$$

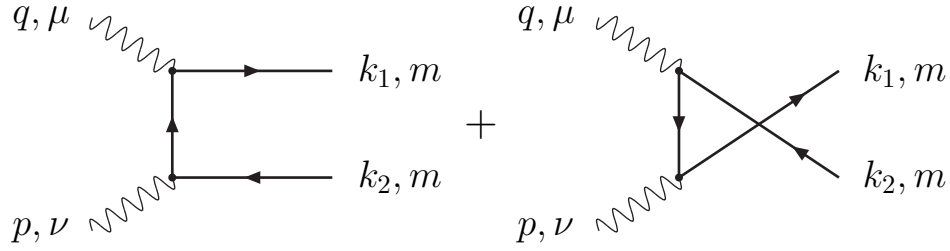


Figure 8.2: Amplitude $M^{\mu\nu}$ for the process $\gamma^*(q, \mu)\gamma^*(p, \nu) \rightarrow f(k_1)\bar{f}(k_2)$ where f is a fermion of mass m .

$$s_1 \equiv 2q \cdot p = s + Q^2 + P^2, \quad t_1 \equiv t - m^2, \quad u_1 \equiv u - m^2 \quad (8.1)$$

satisfying $s_1 + t_1 + u_1 = 0$.

The external fermion lines are on-shell, i.e. $k_1^2 = k_2^2 = m^2$, whereas the two photons are virtual (space-like): $q^2 = -Q^2 < 0$, $p^2 = -P^2 < 0$. The Dirac traces occurring in $W^{\mu'\nu',\mu\nu}$ (due to the closed fermion loop) have been evaluated with the help of the **Mathematica** [101] package **Tracer** [102]. Finally, the individual structure functions W_{ab} have been projected out using the projection operators given in Eq. (7.15).

8.1 Unintegrated Structure Functions

The general structure of the boson-boson fusion cross section (in lowest order) is given by¹

$$\frac{dW_{ab}}{dz_1} = 16\pi^2\alpha^2 e_q^4 N_c \left[\frac{A_{W_{ab}}}{(1-z_1)^2} + \frac{B_{W_{ab}}}{z_1^2} + \frac{C_{W_{ab}}}{1-z_1} + \frac{D_{W_{ab}}}{z_1} + E_{W_{ab}} \right] \quad (8.2)$$

where $z_1 = 1 + t_1/s_1$, $N_c = 3$ is the number of colors and e_q is the quark charge. The QED case can be obtained from Eq. (8.2) by setting $N_c e_q \rightarrow 1$. Note that z_1 is very similar to the fractional momentum variables used in Part I of this thesis to describe energy spectra of heavy quarks (mesons):

$$z_1 = \frac{k_1 \cdot p}{q \cdot p} - \frac{p^2}{2q \cdot p}.$$

¹The t -channel amplitude has a propagator $1/t_1$ and therefore has the form $(a + bt_1)/t_1$. The u -channel is obtained by $t_1 \leftrightarrow u_1 = -(s_1 + t_1)$ and thus reads $(a + bu_1)/u_1 = (c + dt_1)/(s_1 + t_1)$. Squaring the amplitudes generates the structure in Eq. (8.2).

On the other hand, $z_1 = -u_1/s_1$ (or $1 - z_1 = -t_1/s_1$) can be viewed as a natural dimensionless combination of the Mandelstam variables of the problem. Furthermore, it is convenient to use the dimensionless variables

$$x = \frac{Q^2}{s_1} = \frac{Q^2}{2\nu}, \quad \delta = \frac{P^2}{s_1} = \frac{P^2}{2\nu}, \quad \lambda = \frac{4m^2}{s} \quad (8.3)$$

in order to write the coefficients in a form which is manifestly symmetric under $x \leftrightarrow \delta$ and which easily allows to read off the important “massless limits” $P^2 \rightarrow 0$ or $m^2 \rightarrow 0$ to be discussed in Appendix C.

With $\bar{\beta} = \sqrt{1 - 4x\delta}$ the coefficients read:

$$\begin{aligned} A_{W_{\text{TT}}} &= \frac{-1}{32\pi\bar{\beta}^5} \left[2x\bar{\beta}^2 - (1 - x - \delta)(4x\delta + \lambda\bar{\beta}^2) \right] \left[2\delta\bar{\beta}^2 - (1 - x - \delta)(4x\delta + \lambda\bar{\beta}^2) \right] \\ C_{W_{\text{TT}}} &= \frac{-1}{16\pi\bar{\beta}^5} \left[\lambda^2\bar{\beta}^4(1 - x - \delta)^2 - 2\lambda\bar{\beta}^2(1 - x - \delta)^2 - 2 \left(1 - 2x(1 - x) - 2\delta(1 - \delta) \right. \right. \\ &\quad \left. \left. - 4x\delta(x^2 + \delta^2) + 8x^2\delta^2 [1 + (1 - x - \delta)^2] \right) \right] \\ E_{W_{\text{TT}}} &= \frac{-1}{4\pi\bar{\beta}^5} \left[1 - 2x(1 - x) - 2\delta(1 - \delta) + 4x\delta(1 - 2x)(1 - 2\delta) \right] \\ A_{W_{\text{TL}}} &= \frac{\delta(1 - x - \delta)}{4\pi\bar{\beta}^5} x \left[2x\bar{\beta}^2 - (1 - x - \delta)(4x\delta + \lambda\bar{\beta}^2) \right] \\ C_{W_{\text{TL}}} &= \frac{\delta(1 - x - \delta)}{-4\pi\bar{\beta}^5} \left[\lambda\bar{\beta}^2 \left(1 + 2x(-1 + x - \delta) \right) + 4x \left(-1 + 2x + 2\delta - 2x\delta(1 + x + \delta) \right) \right] \\ E_{W_{\text{TL}}} &= \frac{\delta(1 - x - \delta)}{\pi\bar{\beta}^5} (1 - 2x)^2 \\ A_{W_{\text{LL}}} &= -\frac{2x^2\delta^2(1 - x - \delta)^2}{\pi\bar{\beta}^5} \\ C_{W_{\text{LL}}} &= \frac{2x\delta(1 - x - \delta)^2}{\pi\bar{\beta}^5} (1 + 2x\delta) \\ E_{W_{\text{LL}}} &= -\frac{8x\delta(1 - x - \delta)^2}{\pi\bar{\beta}^5} \\ A_{W_{\text{T}\bar{\text{T}}}} &= \frac{-1}{32\pi\bar{\beta}^5} (1 - x - \delta)^2 [4x\delta + \lambda\bar{\beta}^2]^2 \end{aligned}$$

²Note however that neither W_{TL} nor W_{LT} but only the *sum* $W_{\text{TL}} + W_{\text{LT}}$ is invariant under exchanging x and δ .

$$C_{W_{\text{TT}}^\tau} = \frac{-1}{16\pi\bar{\beta}^5} \left[\lambda^2 \bar{\beta}^4 (1-x-\delta)^2 - 4\lambda\bar{\beta}^2 (1-x-\delta) \left(-x-\delta + 2x\delta(1+x+\delta) \right) \right. \\ \left. - x\delta \left(1-2x(1-x) - 2\delta(1-\delta) + 2x\delta(1-2x-2\delta-x^2-\delta^2+6x\delta) \right) \right] \\ E_{W_{\text{TT}}^\tau} = \frac{-1}{2\pi\bar{\beta}^5} (x+\delta-4x\delta)^2$$

$$A_{W_{\text{TL}}^\tau} = \frac{\sqrt{x\delta}(1-x-\delta)}{16\pi\bar{\beta}^5} (1-2x)(1-2\delta)(4x\delta+\lambda\bar{\beta}^2) \\ C_{W_{\text{TL}}^\tau} = \frac{\sqrt{x\delta}(1-x-\delta)}{4\pi\bar{\beta}^5} \left[4x\delta(-3+x+\delta) + 2x+2\delta - \lambda\bar{\beta}^2(1-x-\delta) \right] \\ E_{W_{\text{TL}}^\tau} = \frac{\sqrt{x\delta}(1-x-\delta)}{2\pi\bar{\beta}^5} (1-4x-4\delta+12x\delta)$$

$$A_{W_{\text{TT}}^a} = \frac{1}{16\pi\bar{\beta}^3} \left[-2x\delta\bar{\beta}^2 + (1-x-\delta)(4x\delta+\lambda\bar{\beta}^2) \right] \\ C_{W_{\text{TT}}^a} = -\frac{(1-2x)(1-2\delta)}{8\pi\bar{\beta}^3} \\ E_{W_{\text{TT}}^a} = \frac{(1-2x)(1-2\delta)}{4\pi\bar{\beta}^3}$$

$$A_{W_{\text{TL}}^a} = \frac{\sqrt{x\delta}(1-x-\delta)}{16\pi\bar{\beta}^3} (-4x\delta+\lambda\bar{\beta}^2) \\ C_{W_{\text{TL}}^a} = \frac{\sqrt{x\delta}(1-x-\delta)}{\pi\bar{\beta}^3} x\delta \\ E_{W_{\text{TL}}^a} = -\frac{\sqrt{x\delta}(1-x-\delta)}{2\pi\bar{\beta}^3}$$

$$B_{W_{ab}} = A_{W_{ab}}, \quad D_{W_{ab}} = C_{W_{ab}}. \quad (8.4)$$

The coefficients of W_{LT} can be obtained from the corresponding ones of W_{TL} by exchanging $x \leftrightarrow \delta$: $A_{W_{\text{LT}}} = A_{W_{\text{TL}}}[x \leftrightarrow \delta]$, $C_{W_{\text{LT}}} = C_{W_{\text{TL}}}[x \leftrightarrow \delta]$, and $E_{W_{\text{LT}}} = E_{W_{\text{TL}}}[x \leftrightarrow \delta]$.

It is noteworthy that our results in Eq. (8.2) generalize the z -differential expressions for the (QED) structure functions F_2^γ , F_L^γ , and F_T^γ of real photons given in [103] to the $P^2 \neq 0$ case.

8.2 Inclusive Structure Functions

The desired inclusive structure functions are obtained by integrating over the kinematically allowed range in z_1 . The boundaries for the z_1 -integration are given by

$$z_{1,\pm} = (1 \pm \beta\bar{\beta})/2 \quad (8.5)$$

with $\beta^2 = 1 - 4m^2/s = 1 - \lambda$ and $\bar{\beta}^2 = 1 - 4x^2P^2/Q^2 = 1 - 4x\delta$.

Noticing that

$$\begin{aligned} z_{1,+} - z_{1,-} &= \beta\bar{\beta}, & 1 - z_{1,+} &= z_{1,-}, & 1 - z_{1,-} &= z_{1,+}, \\ z_{1,+}z_{1,-} &= (1 - z_{1,+})(1 - z_{1,-}) = \frac{4x\delta + \lambda\bar{\beta}^2}{4} \end{aligned} \quad (8.6)$$

the required integrals can be immediately obtained

$$\begin{aligned} \int_{z_{1,-}}^{z_{1,+}} \frac{dz_1}{(1 - z_1)^2} &= \int_{z_{1,-}}^{z_{1,+}} \frac{dz_1}{z_1^2} = \frac{\beta\bar{\beta}}{z_{1,+}z_{1,-}} = \frac{4\beta\bar{\beta}}{4x\delta + \lambda\bar{\beta}^2} \\ \int_{z_{1,-}}^{z_{1,+}} \frac{dz_1}{(1 - z_1)} &= \int_{z_{1,-}}^{z_{1,+}} \frac{dz_1}{z_1} = \ln \frac{z_{1,+}}{z_{1,-}} = \ln \frac{1 + \beta\bar{\beta}}{1 - \beta\bar{\beta}} \\ \int_{z_{1,-}}^{z_{1,+}} dz_1 &= \beta\bar{\beta}. \end{aligned} \quad (8.7)$$

Now Eq. (8.2) can be integrated using Eq. (8.7) and we arrive at the following result for the inclusive structure functions expressed by the coefficients given in the previous Section 8.1:

$$W_{ab} = 16\pi^2\alpha^2e_q^4N_c\Theta(\beta^2) \left\{ 2C_{W_{ab}}L + \beta\bar{\beta} \left(2A_{W_{ab}}\frac{4}{4x\delta + \lambda\bar{\beta}^2} + E_{W_{ab}} \right) \right\} \quad (8.8)$$

with

$$L = \ln \frac{1 + \beta\bar{\beta}}{1 - \beta\bar{\beta}}. \quad (8.9)$$

The Θ -function guarantees that the physical threshold condition $s \geq 4m^2$ is satisfied.³

Recalling the relation $\sigma_{ab} = \frac{1}{2\nu\bar{\beta}}W_{ab}$ we can rewrite Eq. (8.8) for the photon-photon cross sections

$$\sigma_{ab} = N \left\{ 2C_{W_{ab}}L + \beta\bar{\beta} \left(2A_{W_{ab}}\frac{4}{4x\delta + \lambda\bar{\beta}^2} + E_{W_{ab}} \right) \right\}, \quad N \equiv \frac{16\pi^2\alpha^2N_ce_q^4}{2\nu\bar{\beta}}\Theta(\beta^2). \quad (8.10)$$

³It is easy to see that $\beta^2 \geq 0$ also implies $\bar{\beta}^2 \geq 0$.

Inserting the coefficients given in Eq. (8.4) into Eq. (8.10) one obtains the final result for the doubly virtual box $\gamma^*(Q^2)\gamma^*(P^2) \rightarrow q\bar{q}$ in leading order:

$$\begin{aligned} \sigma_{\text{TT}} = \frac{N}{4\pi} \frac{1}{\bar{\beta}^5} & \left\{ \left[1 - 2x(1-x) - 2\delta(1-\delta) - 4x\delta(x^2 + \delta^2) + 8x^2\delta^2 [1 + (1-x-\delta)^2] \right. \right. \\ & + \lambda\bar{\beta}^2(1-x-\delta)^2 - \frac{1}{2}\lambda^2\bar{\beta}^4(1-x-\delta)^2 \Big] L + \beta\bar{\beta} \left[4x(1-x) - 1 \right. \\ & \left. \left. + 4\delta(1-\delta) - 8x\delta(1-x^2-\delta^2) - (4x\delta + \lambda\bar{\beta}^2)(1-x-\delta)^2 - \frac{4x\delta\bar{\beta}^4}{4x\delta + \lambda\bar{\beta}^2} \right] \right\} \end{aligned}$$

$$\begin{aligned} \sigma_{\text{LT}} = \frac{N}{4\pi} \frac{4}{\bar{\beta}^5} (1-x-\delta) & \left\{ x \left[-\frac{1}{2}\lambda\bar{\beta}^2(1-2\delta(1+x-\delta)) - 2\delta(-1+2x+2\delta \right. \right. \\ & \left. \left. - 2x\delta(1+x+\delta)) \right] L + \beta\bar{\beta} \left[x(1-6\delta+6\delta^2+2x\delta) + \delta\bar{\beta}^2 \frac{4x\delta}{4x\delta + \lambda\bar{\beta}^2} \right] \right\} \end{aligned}$$

$$\sigma_{\text{TL}} = \sigma_{\text{LT}}[x \leftrightarrow \delta]$$

$$\sigma_{\text{LL}} = \frac{N}{4\pi} \frac{16}{\bar{\beta}^5} x\delta(1-x-\delta)^2 \left\{ (1+2x\delta)L - 2\beta\bar{\beta} \frac{6x\delta + \lambda\bar{\beta}^2}{4x\delta + \lambda\bar{\beta}^2} \right\}$$

$$\begin{aligned} \tau_{\text{TT}} = \frac{N}{4\pi} \frac{1}{\bar{\beta}^5} & \left\{ \left[\frac{1}{2}x\delta(1-2x(1-x) - 2\delta(1-\delta) + 2x\delta(1-2x-2\delta-x^2-\delta^2+6x\delta)) \right. \right. \\ & - 2\lambda\bar{\beta}^2(1-x-\delta)(x+\delta-2x\delta(1+x+\delta)) - \frac{1}{2}\lambda^2\bar{\beta}^4(1-x-\delta)^2 \Big] L \\ & \left. - \beta\bar{\beta} \left[(1-x-\delta)^2(4x\delta + \lambda\bar{\beta}^2) + 2(x+\delta-4x\delta)^2 \right] \right\} \end{aligned}$$

$$\begin{aligned} \tau_{\text{TL}} = \frac{N}{4\pi} \frac{2}{\bar{\beta}^5} \sqrt{x\delta}(1-x-\delta) & \left\{ \left[2x+2\delta-4x\delta(3-x-\delta) - \lambda\bar{\beta}^2(1-x-\delta) \right] L \right. \\ & \left. + \beta\bar{\beta}(1-3x-3\delta+8x\delta) \right\} \end{aligned}$$

$$\begin{aligned}\tau_{\text{TT}}^{\text{a}} &= \frac{N}{4\pi} \frac{1}{\bar{\beta}^3} \left\{ (2x-1)(1-2\delta)L + \beta\bar{\beta} \left[\frac{-4x\delta\bar{\beta}^2}{4x\delta + \lambda\bar{\beta}^2} + 3 - 4x - 4\delta + 4x\delta \right] \right\} \\ \tau_{\text{TL}}^{\text{a}} &= \frac{N}{4\pi} \frac{4}{\bar{\beta}^3} \sqrt{x\delta}(1-x-\delta) \left\{ 2x\delta L - \beta\bar{\beta} \frac{4x\delta}{4x\delta + \lambda\bar{\beta}^2} \right\}\end{aligned}\quad (8.11)$$

This recalculation is in agreement with the results of Ref. [82] (with $N_c e_q^4 \rightarrow 1$) with exception of a relative sign between the part containing the logarithm L and the part proportional to $\beta\bar{\beta}$ in $\tau_{\text{TL}}^{\text{a}}$ ⁴.

A derivation of various important limits of the doubly virtual box expressions in (8.11) can be found in App. C.

8.3 Comparison with Present e^+e^- Virtual Photon Data

We will now compare our LO-box expressions with present e^+e^- virtual photon data. The physically measured effective structure function in the Bjorken limit is [82, 85, 90]

$$F_{\text{eff}}(x; Q^2, y_1; P^2, y_2) = \frac{Q^2}{4\pi^2\alpha} \frac{1}{\beta} \left[\sigma_{\text{TT}} + \varepsilon(y_1)\sigma_{\text{LT}} + \varepsilon(y_2)\sigma_{\text{TL}} + \varepsilon(y_1)\varepsilon(y_2)\sigma_{\text{LL}} \right] \quad (8.12)$$

where the kinematical variables have been given in Eqs. (7.2) and (7.1) and where $\varepsilon(y_i)$ are the ratios of longitudinal to transverse photon fluxes,

$$\varepsilon(y_i) = 2(1-y_i)/[1+(1-y_i)^2]. \quad (8.13)$$

Furthermore, the photon-photon cross sections $\sigma_{ab} = \sigma_{ab}(x, Q^2, P^2)$ with $a = (\text{L}, \text{T})$, $b = (\text{L}, \text{T})$ have been defined in (7.20). In the following we shall consider the kinematical region $y_i \ll 1$ relevant for double-tag experiments [105, 106] performed thus far where Eq. (8.12) reduces to

$$F_{\text{eff}}(x, Q^2, P^2) \simeq \frac{Q^2}{4\pi^2\alpha} \frac{1}{\beta} \left[\sigma_{\text{TT}} + \sigma_{\text{LT}} + \sigma_{\text{TL}} + \sigma_{\text{LL}} \right]. \quad (8.14)$$

⁴This relative sign has also been noted in [104] where in addition the overall sign in τ_{TL} is different. Concerning the latter, we agree with the results of [82].

Recalling the general definitions of the structure functions of spin-averaged, transverse and longitudinal target photons in Sec. 7.2 we can finally write

$$\begin{aligned} F_{\text{eff}}(x, Q^2, P^2) &\simeq F_2^{\gamma_T(P^2)}(x, Q^2) + F_2^{\gamma_L(P^2)}(x, Q^2) \\ &= F_2^{<\gamma(P^2)>}(x, Q^2) + \frac{3}{2} F_2^{\gamma_L(P^2)}(x, Q^2) . \end{aligned} \quad (8.15)$$

So far, our results are entirely general.

We shall furthermore introduce the decomposition

$$\sigma_{ab} = \sigma_{ab}^\ell + \sigma_{ab}^h \quad (8.16)$$

with $\sigma_{ab}^{\ell(h)}$ denoting the light (heavy) quark $q = u, d, s$ ($h = c, b, t$) contributions. The light u, d, s contributions to σ_{ab}^ℓ are obtained from Eq. (8.11) by setting $m \equiv m_q = 0$ ($\lambda = 0$) and summing over $q = u, d, s$. (Note that the box expressions involving a real photon, $\gamma^*(Q^2) \gamma(P^2 = 0) \rightarrow q\bar{q}$, require on the contrary a finite regulator mass $m \equiv m_q \neq 0$; here one usually chooses m_q to be, somewhat inconsistently, a constant, i.e. Q^2 -independent effective constituent mass, $m_q \simeq 0.3$ GeV.) For each heavy quark flavor $h = c, b, t$ the heavy contribution σ_{ab}^h in (8.16) is obtained from Eq. (8.11) with $e_q \equiv e_h$ and $m \equiv m_h$. Only charm gives a non-negligible contribution for which we choose $m_c = 1.4$ GeV throughout.

Finally, it is instructive to recall the asymptotic results of our virtual ($P^2 \neq 0$) box expressions for the light $q = u, d, s$ quarks derived from (8.11) in the Bjorken limit $P^2/Q^2 \ll 1$, see App. C.2:

$$\begin{aligned} \sigma_{\text{TT}}^\ell &\simeq N_c(\Sigma e_q^4) \frac{4\pi\alpha^2}{Q^2} x \left\{ [x^2 + (1-x)^2] \ln \frac{Q^2}{P^2 x^2} + 4x(1-x) - 2 \right\} \\ \sigma_{\text{TL}}^\ell &\simeq \sigma_{\text{LT}}^\ell \simeq N_c(\Sigma e_q^4) \frac{4\pi\alpha^2}{Q^2} x [4x(1-x)] \\ \sigma_{\text{LL}}^\ell &\simeq 0 . \end{aligned} \quad (8.17)$$

We now turn to a comparison of the effective structure function F_{eff} obtained in lowest order perturbation theory with all presently available e^+e^- data of PLUTO [106] and the recent one of LEP-L3 [105]. In addition to the full LO-box calculation of F_{eff} (solid line) we show the 'asymptotic box' results (dotted line) where the light quark contributions have been calculated according to (8.17). As can be seen the 'full' and the 'asymptotic' curves are very similar and coincide in Fig. 8.4 over the entire x -range. Furthermore,

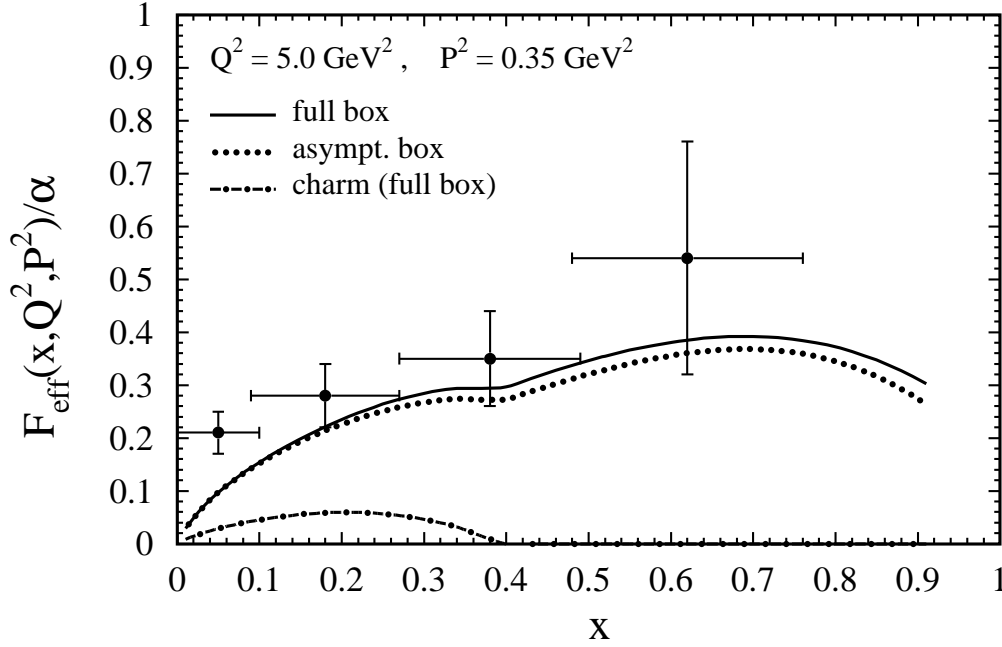


Figure 8.3: Predictions for F_{eff} as defined in (8.14). The light (u, d, s) and heavy (charm) contributions in (8.16) of the ‘full box’ expressions in (8.11) are calculated as explained in the text below Eq. (8.16). The ‘asymptotic box’ results refer to the light quark contributions being given by (8.17). The PLUTO data are taken from [106].

the charm contribution (dash-dotted line) is shown separately to demonstrate its relative importance due to the charge factor e_q^4 in Eq. (8.11) suppressing contributions from down-type quarks by a factor of 16 relative to the up-type quarks. Of course, in Fig. 8.3 the charm contribution is restricted by the available phase space for producing a $c\bar{c}$ pair. Generally, the LO-box predictions for F_{eff} in (8.14) shown in Figs. 8.3 and 8.4 are in agreement with the present low statistics data.⁵ This is not unexpected in the case of the L3 data shown in Fig. 8.4 since the target photon is deeply virtual, $P^2 = 3.7 \text{ GeV}^2$, such that perturbation theory is applicable. On the other hand the PLUTO data (Fig. 8.3) with $P^2 = 0.35 \text{ GeV}^2$ are just in the transition region from deeply virtual ($P^2 \gg \Lambda^2$) to real ($P^2 = 0$) photons where non-perturbative effects are expected to become increasingly important, especially in the small- x region. Clearly, more precise data for F_{eff} in this ‘transition region’ with intermediate target virtualities are highly desirable.

Two questions naturally arise:

⁵Note also, that the rightmost data point in Fig. 8.4 is already close to the boundary of the phase space $x_{\text{max}} = (1 + P^2/Q^2)^{-1}$.

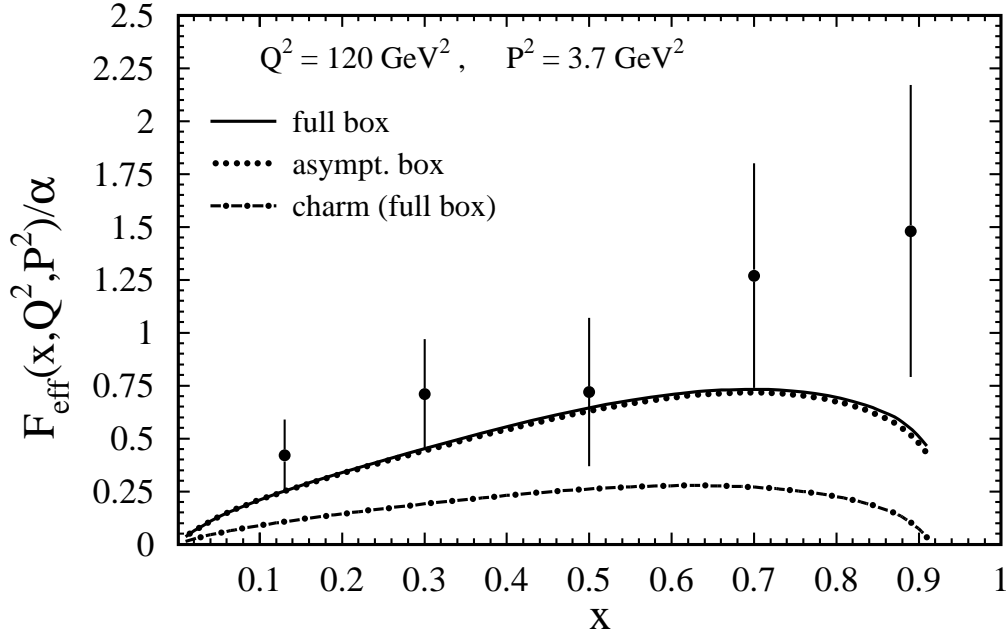


Figure 8.4: As in Fig. 8.3, but for $Q^2 = 120 \text{ GeV}^2$ and $P^2 = 3.7 \text{ GeV}^2$ appropriate for the LEP-L3 data [105].

- (i) Firstly, it would be interesting to see if NLO corrections to the doubly virtual box [107, 108] can further improve the description of the data.
- (ii) The other interesting question is whether for $Q^2 \gg P^2 \gg \Lambda^2$ it is necessary to resum 'large' collinear logarithms $\ln Q^2/P^2$ occurring in Eq. (8.17)⁶ to all orders in perturbation theory via renormalization group (RG) techniques. This issue will be addressed in Chapter 12 where we compare RG-resummed parton model expectations for F_{eff} with the fixed order box results presented here.

It should be emphasized that, at $Q^2 \gg P^2 \gg \Lambda^2$, the $\ln Q^2/P^2$ terms in (8.17) are *finite* which therefore need not necessarily be resummed but only if a resummation is phenomenologically relevant. This is in contrast to the situation for the real photon ($P^2 = 0$) with its well known mass singularities $\ln Q^2/m_q^2$, see Eq. (C.14), which *afford* the introduction of scale dependent (RG-improved) parton distributions which are a priori unknown unless one resorts to some model assumptions about their shape at some low

⁶It has, however, already been noted in [104] that the term containing $\ln Q^2/P^2$ dominates only if (Q^2/P^2) is very large.

resolution scale (see, e.g., [6] and the recent reviews [89, 90]).

In the next chapter we present the necessary theoretical background for describing (virtual) photon structure functions within the QCD-improved (RG-improved) parton model.

Chapter 9

The Partonic Structure of Real and Virtual Photons: Theoretical Framework

The following chapters are mainly devoted to an analysis of the structure of the (real and virtual) photon within the framework of the renormalization group (RG) improved parton model. It is the main purpose here to provide the necessary theoretical background for these phenomenological studies where special emphasis is laid on a unified treatment of both real ($P^2 = 0$) and virtual ($P^2 \neq 0$) photons.

After motivating our unified approach in Sec. 9.1 we turn to a detailed description of the unpolarized photon structure functions within the QCD improved parton model in Sec. 9.2. This section provides the complete technical framework for our analysis of the parton content of real and virtual photons in Chapter 11. In Sec. 9.3 we deal with the RG-based evolution equations for photonic parton distributions and their solutions. For completeness, we discuss boundary conditions for a deeply virtual target photon and from the evolution equations we derive leading and next-to-leading order expressions for the momentum sum carried by the photon's quark and gluon densities. Finally, in Sec. 9.4 we briefly discuss how to include contributions from longitudinal target photons.

9.1 Introduction

We have seen in Chapter 7 that the cross section for the process $ee \rightarrow eeX$ factorizes in the Bjorken limit into fluxes of transversely (longitudinally) polarized photons and the cross

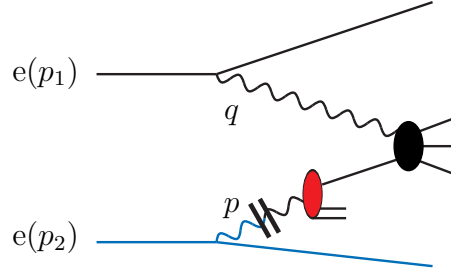


Figure 9.1: Deep inelastic electron–photon scattering (cf. Fig. 7.4) in the parton model where the target photon is produced by the bremsstrahlung process. According to the factorization theorems [68, 109] the $e\gamma$ cross section factorizes into ‘long distance’ (non–perturbative) parton distributions (grey oval) describing the internal structure of the photon and ‘short distance’ (perturbatively calculable) electron–parton subprocesses (black oval).

sections for deep inelastic scattering on these transverse (longitudinal) target photons. The deep inelastic scattering cross sections can in turn be expressed in terms of two independent structure functions, e.g. $F_2^{\gamma T(P^2)}(x, Q^2)$ and $F_L^{\gamma T(P^2)}(x, Q^2)$ ($F_2^{\gamma L(P^2)}(x, Q^2)$, $F_L^{\gamma L(P^2)}(x, Q^2)$).

Furthermore, in Chapter 8 we have obtained these structure functions (or the effective structure function F_{eff}) according to a perturbative calculation of the doubly virtual box $\gamma^*(Q^2)\gamma^*(P^2) \rightarrow q\bar{q}$ in lowest order perturbation theory. As has been discussed there in the deeply virtual case $P^2 \gg \Lambda^2$ (where Λ is a hadronic scale) perturbation theory is expected to be reliable and we have compared these fixed order ‘box results’ $F_{\text{eff}}^{\text{box}}$ with presently available e^+e^- data leaving the open question if resummations of the collinear logarithms $\ln Q^2/P^2$ might further improve the situation. On the other hand, for $P^2 \lesssim \Lambda^2$ the perturbatively calculated structure functions (cross sections) are invalidated by non–perturbative (long–distance) mass singularities which have to be subtracted. This problem can be consistently solved by turning to a parton model description (see Fig. 9.1): Since we are considering the Bjorken limit, the structure functions can be described in terms of photonic parton distributions, quite similar to the hadronic case where factorization theorems [68, 109] state that the structure functions are given by convolutions of parton distributions with Wilson coefficient functions. The parton distributions contain the long–distance part of the cross section and therefore can (in general) *not* be calculated perturbatively and have to be fixed by experimental information or model assumptions. On the other hand the coefficient functions involve only short–distance physics and are

calculable in perturbation theory. The main value of this approach lies in the fact that the parton distribution functions (PDFs) are *universal*, i.e. do *not* depend on the particular hard scattering subprocess. Once fixed by experimental information from, e.g., deep inelastic electron–photon scattering the PDF’s can be used to make predictions for other processes, for example photo–and electroproduction of jets or heavy quarks.

Due to QED gauge invariance the contributions (structure functions, cross sections) from longitudinal target photons have to vanish in the real photon limit ($P^2 \rightarrow 0$). More specifically, they are suppressed by a factor P^2 divided by a typical hadronic scale, say P^2/m_ρ^2 [82], for not too large virtualities P^2 of the target photon. Therefore, we will mainly focus on the structure functions of *transverse* target photons. The contributions from longitudinal photon targets will be considered at the end of this chapter. In the following we can therefore drop the index T and use instead $\gamma(P^2)$ to denote transverse target photons. Our main interest will lie on $F_2^{\gamma(P^2)}(x, Q^2)$ since up to now the cross section has been measured only for small values of y where the contribution of $F_L(\propto y^2)$ is negligible.

The following parton content can be assigned to a *transverse* photon target: $q^{\gamma(P^2)}(x, Q^2)$, $g^{\gamma(P^2)}(x, Q^2)$, and $\Gamma^{\gamma(P^2)}(x, Q^2)$ where q and g are the photonic analogues of the usual quark and gluon parton distributions inside hadrons. In addition the target photon also contains an elementary photon–parton $\Gamma^{\gamma(P^2)}$ reflecting the fact that the photon is a genuinely elementary particle which can directly enter a partonic subprocess. As usual in a massless parton model approach (justified by the factorization theorems [68, 109]) the partonic subprocesses are calculated with *on-shell* partons partly due to the P^2/Q^2 power suppression of effects invoked by the off-shellness of the partons (which is of the order $\mathcal{O}(P^2)$). While this is quite familiar for the quarks and gluons the latter rule also refers to the photon–parton $\Gamma^{\gamma(P^2)}(x, Q^2)$ in the target photon, i.e., the ‘direct’ subprocesses, e.g., $\gamma^*(Q^2)\Gamma^{\gamma(P^2)} \rightarrow q\bar{q}$ have to be calculated with $P^2 = 0$ (cf. rule (ii) in [6]). Consequently we can use the *same* (massless) short distance coefficient functions in our calculations *irrespective* of P^2 . All effects due to a non-zero target virtuality are entirely taken care of by the P^2 –dependence of the parton distributions $f^{\gamma(P^2)}$ (and by the Weizsäcker–Williams flux factors) which of course have to be given in the same factorization scheme as the coefficient functions in order to obtain a physically meaningful, i.e. factorization scheme independent, result. By construction a physically smooth behavior in P^2 (including a smooth transition to the real photon case $P^2 = 0$) of the observable

structure functions can be automatically achieved by demanding a smooth behavior of the boundary conditions for the parton distributions.

The heavy quark contributions deserve special care due to the additional scale m_h provided by the heavy quark mass. In this case terms P^2/m_h^2 are possibly not negligible and have to be kept in the heavy quark coefficient functions. We will come back to this point in Sec. 9.2.2.

9.2 Photon Structure Functions in the QCD-Improved Parton Model

We shall introduce the decomposition

$$F_i^{\gamma(P^2)}(x, Q^2) = F_{i,\ell}^{\gamma(P^2)}(x, Q^2) + F_{i,h}^{\gamma(P^2)}(x, Q^2) \quad (9.1)$$

with $F_{i,\ell}^{\gamma(P^2)}$ denoting contributions with light quarks $q = u, d, s$ (heavy quarks $h = c, b, t$) in the final state. In NLO($\overline{\text{MS}}$) $F_{2,\ell}^{\gamma(P^2)}(x, Q^2)$ and $F_{1,\ell}^{\gamma(P^2)}(x, Q^2)$ are given by the following expressions:

$$\begin{aligned} \frac{1}{x} F_{2,\ell}^{\gamma(P^2)}(x, Q^2) &= \sum_{q=u,d,s} e_q^2 \left\{ q^{\gamma(P^2)}(x, Q^2) + \bar{q}^{\gamma(P^2)}(x, Q^2) + \frac{\alpha_s(Q^2)}{2\pi} \right. \\ &\quad \times \left[C_{q,2} \otimes (q + \bar{q})^{\gamma(P^2)} + 2 C_{g,2} \otimes g^{\gamma(P^2)} \right] + \frac{\alpha}{\pi} e_q^2 C_{\gamma,2}(x) \left. \right\} \quad (9.2) \end{aligned}$$

$$\begin{aligned} F_{1,\ell}^{\gamma(P^2)}(x, Q^2) &= \frac{1}{2} \sum_{q=u,d,s} e_q^2 \left\{ q^{\gamma(P^2)}(x, Q^2) + \bar{q}^{\gamma(P^2)}(x, Q^2) + \frac{\alpha_s(Q^2)}{2\pi} \right. \\ &\quad \times \left[C_{q,1} \otimes (q + \bar{q})^{\gamma(P^2)} + 2 C_{g,1} \otimes g^{\gamma(P^2)} \right] + \frac{\alpha}{\pi} e_q^2 C_{\gamma,1}(x) \left. \right\} \quad (9.3) \end{aligned}$$

where \otimes denotes the usual convolution integral of two functions f and g defined on the interval $[0, 1]$:

$$(f \otimes g)(x) = \int_0^1 dx_1 \int_0^1 dx_2 f(x_1) g(x_2) \delta(x - x_1 x_2) = \int_x^1 \frac{dz}{z} f(z) g(x/z) . \quad (9.4)$$

Here $\bar{q}^{\gamma(P^2)}(x, Q^2) = q^{\gamma(P^2)}(x, Q^2)$ and $g^{\gamma(P^2)}(x, Q^2)$ provide the so-called ‘resolved’ contributions of $\gamma(P^2)$ to $F_i^{\gamma(P^2)}$ with the $\overline{\text{MS}}$ coefficient functions [30, 48, 54]

$$\begin{aligned} C_{q,2}(x) &= C_{q,1}(x) + \frac{4}{3} 2x \\ &= \frac{4}{3} \left[\frac{1+x^2}{1-x} \left(\ln \frac{1-x}{x} - \frac{3}{4} \right) + \frac{1}{4} (9+5x) \right]_+ \end{aligned}$$

$$\begin{aligned}
C_{g,2}(x) &= C_{g,1}(x) + \frac{1}{2} 4x(1-x) \\
&= \frac{1}{2} \left[(x^2 + (1-x)^2) \ln \frac{1-x}{x} + 8x(1-x) - 1 \right], \tag{9.5}
\end{aligned}$$

while $C_{\gamma,2,1}$ in (9.2) provides the ‘direct’ contribution as calculated according to the ‘box’ diagram $\gamma^*(Q^2)\gamma \rightarrow q\bar{q}$ [110]:

$$C_{\gamma,i}(x) = \frac{3}{(1/2)} C_{g,i}(x) \tag{9.6}$$

with $i = 1, 2$. The convolution with the $[\]_+$ distribution can be evaluated using, for example, Eq. (A.21) in Ref. [57]:

$$f_+ \otimes g = \int_x^1 \frac{dy}{y} f\left(\frac{x}{y}\right) \left[g(y) - \frac{x}{y} g(x) \right] - g(x) \int_0^x dy f(y). \tag{9.7}$$

The coefficient functions $C_{q,L}$ and $C_{g,L}$ for the longitudinal structure function $F_L^{\gamma(P^2)} = F_2^{\gamma(P^2)} - 2xF_1^{\gamma(P^2)}$ may be deduced from Eqs. (9.5) and (9.6) and are given by [111]:

$$C_{q,L}(x) = \frac{4}{3} 2x, \quad C_{g,L}(x) = \frac{1}{2} 4x(1-x), \quad C_{\gamma,L}(x) = \frac{3}{(1/2)} C_{g,L}(x). \tag{9.8}$$

9.2.1 Scheme Choice

In order to avoid the usual instabilities encountered in $\text{NLO}(\overline{\text{MS}})$ in the large- x region due to the $\ln(1-x)$ term in $C_{\gamma,2}(x)$ in Eq. (9.6), we follow Ref. [96, 112] and absorb such terms into the photonic $\overline{\text{MS}}$ quark distributions in Eq. (9.2): this results in the so-called DIS_γ factorization scheme which originally has been introduced for real photons by absorbing the entire ‘direct’ $C_{\gamma,2}$ term appearing in Eq. (9.2) into the $\text{NLO}(\overline{\text{MS}})$ quark densities $q^{\gamma(P^2)}(x, Q^2) = \bar{q}^{\gamma(P^2)}(x, Q^2)$, i.e.

$$\begin{aligned}
(q + \bar{q})_{\text{DIS}_\gamma}^{\gamma(P^2)} &= (q + \bar{q})_{\overline{\text{MS}}}^{\gamma(P^2)} + e_q^2 \frac{\alpha}{\pi} C_{\gamma,2}(x) \\
g_{\text{DIS}_\gamma}^{\gamma(P^2)} &= g_{\overline{\text{MS}}}^{\gamma(P^2)}
\end{aligned} \tag{9.9}$$

with $C_{\gamma,2}(x)$ given by Eq. (9.6). How much of the ‘finite’ terms in Eq. (9.6) is absorbed into the $\overline{\text{MS}}$ distributions in Eq. (9.9), is of course arbitrary and a matter of convention [113]. Since such different conventions [113, 114] differ by terms of higher order and turn out to be of minor importance for our quantitative results to be discussed in Chap. 11, we prefer to stick to the original DIS_γ scheme [96, 112] as defined in Eq. (9.9). Furthermore,

the redefinition of the parton densities in Eq. (9.9) implies that the NLO($\overline{\text{MS}}$) splitting functions $k_{q,g}^{(1)}(x)$ of the photon into quarks and gluons, appearing in the inhomogeneous NLO RG evolution equations for $f^{\gamma(P^2)}(x, Q^2)$, have to be transformed according to [96, 112, 115]

$$\begin{aligned} k_q^{(1)}|_{\text{DIS}_\gamma} &= k_q^{(1)} - e_q^2 P_{qq}^{(0)} \otimes C_{\gamma,2} \\ k_g^{(1)}|_{\text{DIS}_\gamma} &= k_g^{(1)} - 2 \sum_q e_q^2 P_{gq}^{(0)} \otimes C_{\gamma,2} \end{aligned} \quad (9.10)$$

where

$$\begin{aligned} k_q^{(1)}(x) &= \frac{1}{2} 3e_q^2 \frac{4}{3} \left\{ -(1-2x) \ln^2 x - (1-4x) \ln x + 4 \ln(1-x) - 9x + 4 \right. \\ &\quad \left. + [x^2 + (1-x)^2] \left[2 \ln^2 x + 2 \ln^2(1-x) + 4 \ln x - 4 \ln x \ln(1-x) \right. \right. \\ &\quad \left. \left. - 4 \ln(1-x) + 10 - \frac{2}{3} \pi^2 \right] \right\} \\ k_g^{(1)}(x) &= 3 \sum_q e_q^2 \frac{4}{3} \left\{ -2(1+x) \ln^2 x - (6+10x) \ln x + \frac{4}{3x} + \frac{20}{3} x^2 + 8x - 16 \right\} \end{aligned} \quad (9.11)$$

with $k_q^{(1)}$ referring to each single (anti)quark flavor. The LO splitting functions are given by $P_{qq}^{(0)} = \frac{4}{3} \left(\frac{1+x^2}{1-x} \right)_+$ and $P_{gq}^{(0)} = \frac{4}{3} [1 + (1-x)^2] / x$.

In NLO the expression for $F_2^{\gamma(P^2)}$ in the above DIS_γ factorization scheme is given by retaining the $C_{q,2}, C_{g,2}$ terms while dropping the destabilizing $C_{\gamma,2}$ term in Eq. (9.2), which has already been absorbed into the quark densities according to Eq. (9.9). Similarly, $C_{q,1}$ and $C_{g,1}$ remain unchanged while $C_{\gamma,1}$ has to be modified according to $C_{\gamma,1}^{\text{DIS}_\gamma} = C_{\gamma,1}^{\overline{\text{MS}}} - C_{\gamma,2}^{\overline{\text{MS}}} = -12x(1-x)$.

The LO expression for $F_i^{\gamma(P^2)}$ ($i = 1, 2$) are obviously entailed in Eq. (9.2) by simply dropping all NLO terms proportional to $C_{q,i}, C_{g,i}$ as well as $C_{\gamma,i}$.

9.2.2 Heavy Flavor Contributions

The photonic quark distributions discussed thus far and which appear in Eq. (9.2) are adequate for the $f = 3$ light u, d, s flavors. Since heavy quarks $h = c, b, t$ will not be considered as ‘light’ partons in the photon (as in the case of the proton [26] and the pion [5, 116]), their contributions to $F_i^{\gamma(P^2)}$ ($i = 1, 2, L$) have to be calculated in fixed order

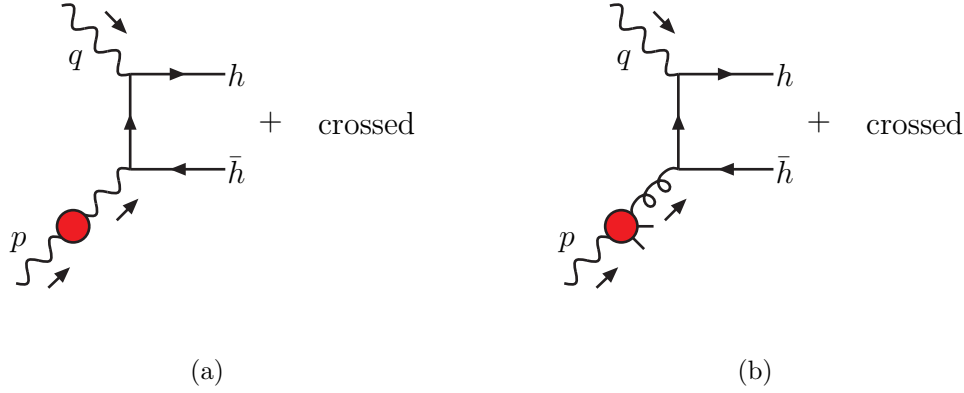


Figure 9.2: *Direct (a) and resolved (b) contribution of a heavy quark h in deep inelastic $e\gamma(P^2)$ scattering.*

perturbation theory. The heavy quark contribution consist of two parts, a 'direct' one and a 'resolved' one as depicted in Fig. 9.2:

$$F_{i,h}^{\gamma(P^2)} = F_{i,h}^{\gamma(P^2),\text{dir}} + F_{i,h}^{\gamma(P^2),\text{res}}. \quad (9.12)$$

The 'direct' contribution derives from the box-diagram $\gamma^*(Q^2) \gamma \rightarrow h\bar{h}$ expression, i.e. the usual Bethe-Heitler cross section [117]

$$\begin{aligned} \frac{1}{x} F_{2,h}^{\gamma(P^2),\text{dir}}(x, Q^2) &= 3e_h^4 \frac{\alpha}{\pi} \theta(\beta^2) \left\{ \beta \left[8x(1-x) - 1 - x(1-x) \frac{4m_h^2}{Q^2} \right] \right. \\ &\quad \left. + \left[x^2 + (1-x)^2 + x(1-3x) \frac{4m_h^2}{Q^2} - x^2 \frac{8m_h^4}{Q^4} \right] \ln \frac{1+\beta}{1-\beta} \right\} \\ 2F_{1,h}^{\gamma(P^2),\text{dir}}(x, Q^2) &= 3e_h^4 \frac{\alpha}{\pi} \theta(\beta^2) \left\{ \beta \left[4x(1-x) - 1 - x(1-x) \frac{4m_h^2}{Q^2} \right] \right. \\ &\quad \left. + \left[x^2 + (1-x)^2 + x(1-x) \frac{4m_h^2}{Q^2} - x^2 \frac{8m_h^4}{Q^4} \right] \ln \frac{1+\beta}{1-\beta} \right\} \end{aligned} \quad (9.13)$$

where $\beta^2 \equiv 1 - 4m_h^2/W^2 = 1 - 4m_h^2x/(1-x)Q^2$. A similar expression holds for the longitudinal structure function [111] $F_L \equiv F_2 - 2xF_1$. The 'resolved' heavy quark contribution to $F_i^{\gamma(P^2)}$ has to be calculated via $\gamma^*(Q^2)g \rightarrow h\bar{h}$ and is given by [111]

$$\begin{aligned} F_{2,h}^{\gamma(P^2),\text{res}}(x, Q^2) &= \int_{z_{\min}}^1 \frac{dz}{z} z g^{\gamma(P^2)}(z, \mu_F^2) \hat{f}_2^{\gamma^*(Q^2)g \rightarrow h\bar{h}}\left(\frac{x}{z}, Q^2\right) \\ F_{1,h}^{\gamma(P^2),\text{res}}(x, Q^2) &= \int_{z_{\min}}^1 \frac{dz}{z} g^{\gamma(P^2)}(z, \mu_F^2) \hat{f}_1^{\gamma^*(Q^2)g \rightarrow h\bar{h}}\left(\frac{x}{z}, Q^2\right) \end{aligned} \quad (9.14)$$

where $\frac{1}{x} \hat{f}_2^{\gamma^*(Q^2)g \rightarrow h\bar{h}}(x, Q^2)$ and $2\hat{f}_1^{\gamma^*(Q^2)g \rightarrow h\bar{h}}(x, Q^2)$ are given by Eq. (9.13) with $e_h^4 \alpha \rightarrow e_h^2 \alpha_s(\mu_F^2)/6$, $z_{\min} = x(1 + 4m_h^2/Q^2)$ and $\mu_F^2 \simeq 4m_h^2$ [18]¹. To ease the calculations we shall keep these LO expressions in Eqs. (9.13) and (9.14) also in NLO, since the full NLO expressions for heavy quark production [119] turn out to be a small correction to the already not too sizeable (at most about 20%) contribution in LO. Notice that such small corrections are not larger than ambiguities due to different choices for m_h and for the factorization scale μ_F . For our purposes it is sufficient to include only the charm contributions which will be calculated using $m_c = 1.4$ GeV.

As already mentioned in the introduction the heavy quark contributions deserve special care due to the additional scale m_h provided by the heavy quark mass. For general $P^2 (\ll Q^2)$ terms P^2/m_h^2 are not always power-suppressed and have to be kept in the heavy quark coefficient functions. The corresponding 'direct' and 'resolved' heavy quark contributions can be found in Eqs. (18) and (19) of Ref. [111].

9.3 Q^2 –Evolution

9.3.1 Evolution Equations

As motivated in Sec. 9.1 a *transverse* hadronic photon can be described by its partonic quark, gluon and photon content denoted by $q_i^{\gamma(P^2)}(x, Q^2)$ ($i = 1, \dots, f$) with $q_1 = u$, $q_2 = d$, $q_3 = s$ and so on², $g^{\gamma(P^2)}(x, Q^2)$, and $\Gamma^{\gamma(P^2)}(x, Q^2)$. The general evolution equations for these parton densities are given by (suppressing the x - and Q^2 -dependence)

$$\begin{aligned} \frac{dq_i^{\gamma(P^2)}}{d \ln Q^2} &= \bar{P}_{q_i \gamma} \otimes \Gamma^{\gamma(P^2)} + 2 \sum_{k=1}^f \bar{P}_{q_i q_k} \otimes q_k^{\gamma(P^2)} + \bar{P}_{q_i g} \otimes g^{\gamma(P^2)} \\ \frac{dg^{\gamma(P^2)}}{d \ln Q^2} &= \bar{P}_{g \gamma} \otimes \Gamma^{\gamma(P^2)} + 2 \sum_{k=1}^f \bar{P}_{g q_k} \otimes q_k^{\gamma(P^2)} + \bar{P}_{g g} \otimes g^{\gamma(P^2)} \\ \frac{d\Gamma^{\gamma(P^2)}}{d \ln Q^2} &= \bar{P}_{\gamma \gamma} \otimes \Gamma^{\gamma(P^2)} + 2 \sum_{k=1}^f \bar{P}_{\gamma q_k} \otimes q_k^{\gamma(P^2)} + \bar{P}_{\gamma g} \otimes g^{\gamma(P^2)} \end{aligned} \quad (9.15)$$

¹An alternative choice would be $\mu_F^2 = Q^2 + 4m_h^2$ [118] which satisfies the requirement $\mu_F^2 \gg P^2$ also for large P^2 .

²Note that due to charge conjugation invariance $\bar{q}_i^{\gamma(P^2)}(x, Q^2) = q_i^{\gamma(P^2)}(x, Q^2)$.

where f denotes the number of active (massless) quark flavors. The evolution kernels \bar{P}_{ij} are generalized splitting functions

$$\bar{P}_{ij}(x, \alpha, \alpha_s) = \sum_{l,m=0} \frac{\alpha^l \alpha_s^m}{(2\pi)^{l+m}} \bar{P}_{ij}^{(l,m)}(x), \quad (9.16)$$

with $\bar{P}_{q_i q_k}$ being the average of the quark–quark and antiquark–quark splitting functions. Note that terms due to photon radiation from the quark line are taken into account in Eq. (9.15) as it must be in order to guarantee momentum conservation (see the erratum to [120]).

Since the electromagnetic coupling constant $\alpha \ll 1$ we can safely neglect terms of order $\mathcal{O}(\alpha^2)$ in Eq. (9.15)³. Noticing that $q^{\gamma(P^2)}$ and $g^{\gamma(P^2)}$ are already of order $\mathcal{O}(\alpha)$ we can take $l = 0$ in all generalized splitting functions in (9.16) which are multiplied by $q^{\gamma(P^2)}$ or $g^{\gamma(P^2)}$ such that the functions \bar{P}_{ij} reduce in this case to the conventional QCD splitting functions $P_{ij}(x, \alpha_s)$. On the other hand in $\bar{P}_{q_i \gamma}$, $\bar{P}_{g \gamma}$ and $\bar{P}_{\gamma \gamma}$ the contributions with $l = 0$ obviously vanish such that the only contribution to order $\mathcal{O}(\alpha)$ comes from setting $l = 1$ in Eq. (9.16) in this case. Furthermore, the terms proportional to $P_{\gamma q_k}$ and $P_{\gamma g}$ are of the order $\mathcal{O}(\alpha^2)$ and can be dropped such that the evolution equation for the photon distribution decouples and can be solved separately as will be discussed in Sec. 9.3.5. Here it suffices to know the photon density at order α^0 only in order to obtain the quark and gluon densities in Eq. (9.15) and the structure functions in Eq. (9.2) consistently to order $\mathcal{O}(\alpha)$. At 0th order, however, no splitting is possible and the photon carries its full momentum with probability one: $\Gamma^{\gamma(P^2)}(x, Q^2) = \delta(1 - x) + \mathcal{O}(\alpha)$.

Therefore, Eq. (9.15) can be reduced to the following inhomogeneous evolution equations for the quark and gluon content of the photon [120]:

$$\begin{aligned} \frac{dq_i^{\gamma(P^2)}}{d \ln Q^2} &= k_{q_i} + 2 \sum_{k=1}^f P_{q_i q_k} \otimes q_k^{\gamma(P^2)} + P_{q_i g} \otimes g^{\gamma(P^2)} \\ \frac{dg^{\gamma(P^2)}}{d \ln Q^2} &= k_g + 2 \sum_{k=1}^f P_{g q_k} \otimes q_k^{\gamma(P^2)} + P_{g g} \otimes g^{\gamma(P^2)} \end{aligned} \quad (9.17)$$

where we have utilized the standard notation $k_{q_i} \equiv P_{q_i \gamma}$, $k_g \equiv P_{g \gamma}$ for the photon–quark and photon–gluon splitting functions. The splitting functions $P_{ij}(x, \alpha_s)$ are presently known to next-to-leading order in α_s and can be found in [112, 121, 122].

³For this reason we can also neglect the running of $\alpha(Q^2)$ and use $\alpha \simeq 1/137$.

The Q^2 -evolution is most conveniently treated in the Mellin moment space where the convolutions turn into ordinary products: $(a \otimes b)(x) \rightarrow (a \otimes b)^n = a^n b^n$ where the n -th Mellin moment of a function $f(x, Q^2)$ is defined by

$$f^n(Q^2) = \int_0^1 dx x^{n-1} f(x, Q^2) . \quad (9.18)$$

Hence the evolution of n -moments is governed by a set of ordinary coupled differential equations which can be solved analytically [112].

In order to decouple the evolution equations as far as possible we introduce flavor non-singlet (NS) quark combinations:

$$q_{\text{NS},\ell}^{\gamma(P^2)} = 2 \left[\sum_{i=1}^j q_i^{\gamma(P^2)} - j q_j^{\gamma(P^2)} \right] \quad (9.19)$$

with $i, j = 1, \dots, f$ and the group theoretical index $\ell = j^2 - 1$. Thus, for three active flavors (u, d, s) we have two non-vanishing NS combinations $q_{\text{NS},3} = 2(u - d)$ and $q_{\text{NS},8} = 2(u + d - 2s)$. Furthermore, we define a singlet (S) vector which helps to write the singlet evolution equations and their solutions in a compact matrix form:

$$\vec{q}_{\text{S}}^{\gamma(P^2)} = \begin{pmatrix} \Sigma^{\gamma(P^2)} \\ g^{\gamma(P^2)} \end{pmatrix} , \quad \Sigma^{\gamma(P^2)} = 2 \sum_{i=1}^f q_i^{\gamma(P^2)} . \quad (9.20)$$

We wish to make an expansion of the solutions of the evolution equations and eventually of the structure functions in terms of α_s . For this reason the evolution equations will be rewritten as differential equations in α_s with help of the renormalization group equation for the strong coupling constant:

$$\frac{d\alpha_s}{d \ln Q^2} = -\frac{\beta_0}{4\pi} \alpha_s^2(Q^2) - \frac{\beta_1}{(4\pi)^2} \alpha_s^3(Q^2) + \mathcal{O}(\alpha_s^4) \quad (9.21)$$

with $\beta_0 = 11 - (2/3)f$ and $\beta_1 = 102 - (38/3)f$. Expanding the splitting functions in α_s in a form which can be generically written as $P = \frac{\alpha_s}{2\pi}(P^{(0)} + \frac{\alpha_s}{2\pi}P^{(1)} + \dots)$ and $k = \frac{\alpha}{2\pi}(k^{(0)} + \frac{\alpha_s}{2\pi}k^{(1)} + \dots)$, respectively, and neglecting terms of the order $\mathcal{O}(\alpha_s^2)$ the inhomogeneous evolution equations can be brought into the following form:

$$\begin{aligned} \frac{d}{d\alpha_s} q_{\text{NS},\ell}^{\gamma(P^2),n} = & -\frac{\alpha}{\alpha_s^2} \frac{2}{\beta_0} k_{\ell}^{(0)n} - \frac{\alpha}{\alpha_s} \frac{1}{\pi \beta_0} \left(k_{\ell}^{(1)n} - \frac{\beta_1}{2\beta_0} k_{\ell}^{(0)n} \right) \\ & - \left[\frac{1}{\alpha_s} \frac{2}{\beta_0} P_{qq}^{(0)n} + \frac{1}{\pi \beta_0} \left(P_+^{(1)n} - \frac{\beta_1}{2\beta_0} P_{qq}^{(0)n} \right) \right] q_{\text{NS},\ell}^{\gamma(P^2),n} \end{aligned}$$

$$\begin{aligned} \frac{d}{d\alpha_s} \vec{q}_S^{\gamma(P^2),n} = & -\frac{\alpha}{\alpha_s^2} \frac{2}{\beta_0} \vec{k}^{(0)n} - \frac{\alpha}{\alpha_s} \frac{1}{\pi\beta_0} \left(\vec{k}^{(1)n} - \frac{\beta_1}{2\beta_0} \vec{k}^{(0)n} \right) \\ & - \left[\frac{1}{\alpha_s} \frac{2}{\beta_0} \hat{P}^{(0)n} + \frac{1}{\pi\beta_0} \left(\hat{P}^{(1)n} - \frac{\beta_1}{2\beta_0} \hat{P}^{(0)n} \right) \right] \vec{q}_S^{\gamma(P^2),n} . \end{aligned} \quad (9.22)$$

Here $\vec{k}^{(0)n}$ and $\vec{k}^{(1)n}$ denote the LO and NLO photon-to-parton splitting functions in the singlet sector: $\vec{k}^n = (k_\Sigma^n, k_g^n)^T$ with $k_\Sigma^n = 2 \sum_{i=1}^f k_{q_i}^n$ while $k_\ell^{(0)n}$ and $k_\ell^{(1)n}$ are the LO and NLO parts of the non-singlet combination $k_\ell^n = 2 \left[\sum_{i=1}^j k_{q_i}^n - j k_{q_j}^n \right]$. Furthermore, $\hat{P}^{(0)n}$ and $\hat{P}^{(1)n}$ refer to LO and NLO 2×2 matrices of one- and two-loop splitting functions whereas $P_+^{(1)n}$ and $P_{qq}^{(0)n}$ occurring in the NS equation are scalar functions. The complete set of LO and NLO (non-)singlet splitting functions can be found, e.g., in [112, 123].

9.3.2 Analytic Solutions

The general solutions of the inhomogeneous evolution equations (9.22) are formally identical to the ones of a real photon [112] and can be written, as usual, as a sum of a ('pointlike') particular solution q_{pl} of the inhomogeneous problem and a general solution q_{had} of the homogeneous ('hadronic') equations :

$$q = q_{\text{pl}} + q_{\text{had}} , \quad q = q_{\text{NS},\ell}^{\gamma(P^2),n}, \vec{q}_S^{\gamma(P^2),n}, q^{\gamma(P^2),n}, \dots . \quad (9.23)$$

The particular solution is not unique and we fix it by the condition $q_{\text{pl}}(Q_0^2) \equiv 0$ at the reference scale Q_0^2 .

The NLO 'pointlike' (inhomogeneous) flavor-singlet solution is given by [111, 112]

$$\begin{aligned} \vec{q}_{\text{S,pl}}^{\gamma(P^2),n}(Q^2) = & \frac{2\pi}{\alpha_s(Q^2)} \left(1 + \frac{\alpha_s(Q^2)}{2\pi} \hat{U}^n \right) \left[1 - L^{1+\hat{d}_n} \right] \frac{1}{1+\hat{d}_n} \frac{\alpha}{\pi\beta_0} \vec{k}^{(0)n} \\ & + \left[1 - L^{\hat{d}_n} \right] \frac{1}{\hat{d}_n} \frac{\alpha}{\pi\beta_0} \left(\vec{k}^{(1)n} - \frac{\beta_1}{2\beta_0} \vec{k}^{(0)n} - \hat{U}^n \vec{k}^{(0)n} \right) \end{aligned} \quad (9.24)$$

where $\hat{d}_n \equiv -(2/\beta_0) \hat{P}^{(0)n}$, $L \equiv \alpha_s(Q^2)/\alpha_s(Q_0^2)$ and the 2×2 NLO evolution matrix \hat{U} is fixed through the commutation relation $[\hat{U}^n, \hat{P}^{(0)n}] = \frac{\beta_0}{2} \hat{U}^n + \hat{P}^{(1)n} - \frac{\beta_1}{2\beta_0} \hat{P}^{(0)n}$ [30, 112, 123]. The NLO 'hadronic' (homogeneous) solution depending on input distributions $\vec{q}_{\text{S,had}}^{\gamma(P^2),n}(Q_0^2) = \vec{q}_S^{\gamma(P^2),n}(Q_0^2)$ which will be specified in Chapter 11 is given by [111, 112]

$$\vec{q}_{\text{S,had}}^{\gamma(P^2),n}(Q^2) = \left[L^{\hat{d}_n} + \frac{\alpha_s(Q^2)}{2\pi} \hat{U}^n L^{\hat{d}_n} - \frac{\alpha_s(Q_0^2)}{2\pi} L^{\hat{d}_n} \hat{U}^n \right] \vec{q}_{\text{S,had}}^{\gamma(P^2),n}(Q_0^2) . \quad (9.25)$$

The LO results are obviously entailed in these expressions by simply dropping all higher order terms $(\beta_1, \vec{k}^{(1)n}, \hat{U})$. The non-singlet solutions can be easily obtained from Eqs. (9.24) and (9.25) by the obvious replacements $\hat{P}^{(0)} \rightarrow P_{qq}^{(0)}$, $\hat{P}^{(1)} \rightarrow P_+^{(1)}$, $\vec{k} \rightarrow k_\ell$ together with $\hat{U} \rightarrow U_{+, \ell} = -\frac{2}{\beta_0} \left(P_+^{(1)} - \frac{\beta_1}{2\beta_0} P_{qq}^{(0)} \right)$ [112, 123].

Note that the solutions (9.24) and (9.25) are valid for a *fixed number* f of active flavors. Evolving beyond an $\overline{\text{MS}}$ 'threshold', set by the heavy quark masses m_c , m_b and m_t , the number of active flavors has to be increased by one, i.e., $f \rightarrow f + 1$ in the calculation of α_s . The evolution of $\alpha_s^{(f)}(Q^2)$, corresponding to a number of f active flavors, is obtained by exactly solving in NLO($\overline{\text{MS}}$)

$$\frac{d\alpha_s^{(f)}(Q^2)}{d \ln Q^2} = -\frac{\beta_0^{(f)}}{4\pi} [\alpha_s^{(f)}(Q^2)]^2 - \frac{\beta_1^{(f)}}{16\pi^2} [\alpha_s^{(f)}(Q^2)]^3 \quad (9.26)$$

numerically [26] using $\alpha_s^{(5)}(M_Z^2) = 0.114$, rather than using the more conventional approximate solution

$$\frac{\alpha_s^{(f)}(Q^2)}{4\pi} \simeq \frac{1}{\beta_0^{(f)} \ln(Q^2/\Lambda^2)} - \frac{\beta_1^{(f)}}{(\beta_0^{(f)})^3} \frac{\ln \ln(Q^2/\Lambda^2)}{[\ln(Q^2/\Lambda^2)]^2} \quad (9.27)$$

which becomes sufficiently accurate only for $Q^2 \gtrsim m_c^2 \simeq 2 \text{ GeV}^2$ with [26] $\Lambda_{\overline{\text{MS}}}^{(f=4,5,6)} = 257, 173.4, 68.1 \text{ MeV}$, whereas in LO ($\beta_1 \equiv 0$) $\Lambda_{\text{LO}}^{(4,5,6)} = 175, 132, 66.5 \text{ MeV}$. Furthermore, $\beta_0^{(f)} = 11 - 2f/3$ and $\beta_1^{(f)} = 102 - 38f/3$. For matching α_s at the $\overline{\text{MS}}$ 'thresholds' $Q \equiv Q_f = m_f$, i.e. $\alpha_s^{(f+1)}(m_{f+1}^2) = \alpha_s^{(f)}(m_{f+1}^2)$, we have used [26] $m_c = 1.4 \text{ GeV}$, $m_b = 4.5 \text{ GeV}$ and $m_t = 175 \text{ GeV}$. On the other hand, we fix $f = 3$ in the splitting functions $P_{ij}^{(0,1)}$ in Eqs. (9.24) and (9.25) for consistency since we treat the heavy quark sector (c, b, \dots) by the perturbatively stable full production cross sections in fixed-order perturbation theory, i.e. $\gamma^*(Q^2)\Gamma^{\gamma(P^2)} \rightarrow c\bar{c}$ and $\gamma^*(Q^2)g^{\gamma(P^2)} \rightarrow c\bar{c}$, etc., keeping $m_c \neq 0$.

Thus the full solutions can be obtained iteratively by the following procedure written out in detail in [124]: Between thresholds we can use Eqs. (9.24) and (9.25) for the corresponding value of f . Crossing a threshold $Q^2 = m_h^2$ we have to replace f by $f + 1$ in the following expressions occurring in Eqs. (9.24) and (9.25):

$$\begin{aligned} \alpha_s^{(f)}(Q^2 = m_h^2) &\rightarrow \alpha_s^{(f+1)}(Q^2 = m_h^2) \\ \hat{d}_n^{(f)} &= -(2/\beta_0^{(f)})\hat{P}^{(0)n} \rightarrow \hat{d}_n^{(f+1)} \end{aligned}$$

and the *full* solution at the threshold evolved with f active flavors so far then serves as input at the new 'input' scale $Q_0^2 = m_h^2$ which subsequently has to be evolved using Eqs. (9.24) and (9.25) with $f + 1$ active flavors.

9.3.3 Numerical Mellin–Inversion

The solutions in x -space are then obtained by numerically inverting the Mellin transformation in Eq. (9.18) according to

$$f(x, Q^2) = \frac{1}{2\pi i} \int_c dn \, x^{-n} f^n(Q^2) \quad (9.28)$$

where the integration contour c has to enclose all poles in the complex n -plane. This can be realized, e.g., if the contour ranges from negatively to positively infinite imaginary values and lies to the right of all singularities of f^n . In the case of parton distributions and structure functions all singularities are located on the real axis and hence we can parameterize the contour as follows:

$$c(z) = c_0 + e^{i\phi} z, \quad c_0 \in \mathbf{R}. \quad (9.29)$$

For such contours the transformation (9.28) can be written as [112]

$$f(x, Q^2) = \frac{1}{\pi} \int_0^\infty dz \, \text{Im} \{ e^{i\phi} x^{-c(z)} f^{n=c(z)}(Q^2) \}. \quad (9.30)$$

Employing $\phi > \frac{\pi}{2}$ the factor $x^{-z \exp(i\phi)}$ dampens the integrand for increasing values of z allowing for a smaller upper limit z_{\max} in the numerical calculation of (9.30) as compared to the standard integration contour with $\phi = \frac{\pi}{2}$. We choose the following parameters in all practical applications of Eq. (9.30) [112, 123]⁴:

$$\phi = \frac{3}{4}\pi, \quad z_{\max} = 5 + \frac{10}{\ln(1/x)}, \quad c_0 = \begin{cases} 0.8 & \text{for non-singlet inversions} \\ 1.8 & \text{for singlet inversions} \end{cases}$$

where the difference between non-singlet and singlet inversions is due to the different singularity structures of the corresponding splitting functions the rightmost pole lying at $n = 0$ and $n = 1$, respectively.

9.3.4 Boundary Conditions for a Deeply Virtual Target Photon

For a deeply virtual target photon $\gamma(P^2)$ with $\Lambda^2 \ll P^2 \ll Q^2$ the photon structure functions are perturbatively calculable according to the doubly virtual box $\gamma^*(Q^2)\gamma^*(P^2) \rightarrow q\bar{q}$

⁴The upper limit of integration z_{\max} refers to the photon case only. For inversions of pionic parton densities in Chap. 10 we have used $z_{\max}(x \leq 0.001) = 24$, $z_{\max}(0.001 < x \leq 0.05) = 40$, $z_{\max}(0.05 < x \leq 0.2) = 56$, $z_{\max}(0.2 < x \leq 0.4) = 72$, $z_{\max}(0.4 < x \leq 0.7) = 88$ and $z_{\max}(0.7 < x < 1) = 136$.

(and higher order corrections) either within fixed order perturbation theory (FOPT) or by resumming large collinear logarithms $\ln Q^2/P^2$ occurring in the fixed order calculation with help of renormalization group (RG) techniques to leading order [125] and next-to-leading order [126, 127] accuracy.

More specifically, in Ref. [126] the framework of the RG-improved operator product expansion (OPE) has been adopted in order to calculate predictions for the unpolarized (twist-2) structure functions $F_{2,L}^{<\gamma(P^2)>}(x, Q^2)$ of a spin-averaged target photon. These (OPE) results can be translated by a one-to-one correspondence into the framework of the RG-improved parton model (PM) by utilizing 'technical' boundary conditions given at the input scale $Q^2 = P^2 \gg \Lambda^2$ such that the condition

$$F_2^{\text{OPE}}(x, P^2, Q^2) \stackrel{!}{=} F_2^{<\gamma(P^2)>, \text{PM}}(x, Q^2) \quad (9.31)$$

is fulfilled for $Q^2 \gg P^2$. The appropriate boundary conditions are given by [111, 126, 127]

$$f_{\text{LO}}^{<\gamma(P^2)>}(x, Q^2 = P^2) = 0 \quad (9.32)$$

in LO and by

$$\begin{aligned} q_{\text{DIS}_\gamma}^{<\gamma(P^2)>}(x, Q^2 = P^2) &= \bar{q}_{\text{DIS}_\gamma}^{<\gamma(P^2)>}(x, Q^2 = P^2) \\ &= N_c e_q^2 \frac{\alpha}{2\pi} \left\{ [x^2 + (1-x)^2] \ln \frac{1}{x^2} + 6x(1-x) - 2 \right\} \\ g_{\text{DIS}_\gamma}^{<\gamma(P^2)>}(x, Q^2 = P^2) &= 0. \end{aligned} \quad (9.33)$$

in the NLO(DIS_γ) factorization scheme. It should be noted, that these 'technical' boundary conditions have no direct physical interpretation at $Q^2 = P^2$ since the virtual target photon $\gamma(P^2)$ is not resolved by the scale $Q^2 = P^2$. Furthermore, at $Q^2 = P^2$, the x -range is kinematically restrained to $x \leq 1/2$ due to $0 \leq x \leq (1 + P^2/Q^2)^{-1}$. However, the boundary conditions (9.32) and (9.33) generate the correct parton content at $Q^2 \gg P^2$ needed to reproduce the purely perturbative results of [126] in the Bjorken limit over the whole x -range $0 \leq x \lesssim 1$.⁵

It is instructive to derive Eqs. (9.32) and (9.33) from our fixed order calculation of the doubly virtual box $\gamma^*(Q^2)\gamma^*(P^2) \rightarrow q\bar{q}$ in Chapter 8. The universal asymptotic ($Q^2 \gg P^2$)

⁵To be precise, Eq. (9.2) supplemented with the boundary conditions in (9.33) reproduces the OPE result of [126] up to spurious terms of the order $\mathcal{O}(\alpha\alpha_s)$ which are of next-to-next-to-leading order (NNLO) in a perturbative expansion of the photon structure function $F_2^{<\gamma(P^2)>}$ in powers of α_s .

leading log (LL) part of the box to the structure function $F_{2,\text{box}}^{<\gamma(P^2)>}(x, Q^2)$ in Eq. (C.10) (or Eq. (C.8)) may be used to define light (anti-)quark distributions in the virtual photon target

$$\begin{aligned} F_{2,\text{box}}^{<\gamma(P^2)>}(x, Q^2)|_{\text{univ}} &= N_c \sum e_q^4 \frac{\alpha}{\pi} x [x^2 + (1-x)^2] \ln \frac{Q^2}{P^2} \\ &\equiv \sum_{q=u,d,s} x e_q^2 \left[q_{\text{box}}^{<\gamma(P^2)>}(x, Q^2) + \bar{q}_{\text{box}}^{<\gamma(P^2)>}(x, Q^2) \right] \end{aligned} \quad (9.34)$$

with

$$q_{\text{box}}^{<\gamma(P^2)>}(x, Q^2) = \bar{q}_{\text{box}}^{<\gamma(P^2)>}(x, Q^2) = N_c e_q^2 \frac{\alpha}{2\pi} [x^2 + (1-x)^2] \ln \frac{Q^2}{P^2}. \quad (9.35)$$

Note that these fixed order box expressions do imply to this order a vanishing gluon component in the virtual photon, $g_{\text{box}}^{<\gamma(P^2)>}(x, Q^2) = 0$.

Higher powers of the finite but asymptotically large logarithm $\ln Q^2/P^2$ occurring in (9.35) may be resummed to all orders in perturbation theory with help of the renormalization group by imposing leading order boundary conditions⁶

$$f_{\text{LO}}^{<\gamma(P^2)>}(x, Q^2 = P^2) = f_{\text{box}}^{<\gamma(P^2)>}(x, Q^2 = P^2) = 0, \quad (f = q, g). \quad (9.36)$$

In order to derive the NLO input distributions in (9.33) we have to take into account the full asymptotic box structure function $F_{2,\text{box}}^{<\gamma(P^2)>}(x, Q^2)$ in Eq. (C.10) following from Eq. (8.11) in the limit $P^2 \ll Q^2$ for the light quarks ($m \equiv 0$) which can be used to define scheme-dependent light (anti-)quark distributions in the virtual photon target in NLO

$$F_{2,\text{box}}^{<\gamma(P^2)>}(x, Q^2) \equiv F_2^{<\gamma>, \text{dir}, \text{DIS}_\gamma}(x, Q^2) + 2 \sum e_q^2 x q_{\text{box}, \text{DIS}_\gamma}^{<\gamma(P^2)>}(x, Q^2) \quad (9.37)$$

where the 'direct' term $F_2^{<\gamma>, \text{dir}}(x, Q^2)$ vanishes in the DIS_γ scheme implying

$$\begin{aligned} q_{\text{box}, \text{DIS}_\gamma}^{<\gamma(P^2)>}(x, Q^2) &= \bar{q}_{\text{box}, \text{DIS}_\gamma}^{<\gamma(P^2)>}(x, Q^2) = N_c e_q^2 \frac{\alpha}{2\pi} \left\{ [x^2 + (1-x)^2] \ln \frac{Q^2}{P^2} \right. \\ &\quad \left. + [x^2 + (1-x)^2] \ln \frac{1}{x^2} + 6x(1-x) - 2 \right\}. \end{aligned} \quad (9.38)$$

The fixed order box' distributions in the DIS_γ scheme can again be resummed employing the NLO(DIS_γ) evolution equations with the input distributions

$$\begin{aligned} q_{\text{DIS}_\gamma}^{<\gamma(P^2)>}(x, Q^2 = P^2) &= q_{\text{box}, \text{DIS}_\gamma}^{<\gamma(P^2)>}(x, Q^2 = P^2) \\ &= N_c e_q^2 \frac{\alpha}{2\pi} \left\{ [x^2 + (1-x)^2] \ln \frac{1}{x^2} + 6x(1-x) - 2 \right\} \end{aligned}$$

⁶This is quite similar to the case of heavy quark production studied in Part I of this thesis where logarithms $\ln Q^2/m_h^2$ of the heavy quark mass m_h may be resummed to all orders using perturbatively calculable boundary conditions for the heavy quark distribution function in a hadron.

$$g_{\text{DIS}_\gamma}^{<\gamma(P^2)>}(x, Q^2 = P^2) = g_{\text{box,DIS}_\gamma}^{<\gamma(P^2)>}(x, Q^2 = P^2) = 0 \quad (9.39)$$

which coincide with the results in Eq. (9.33).

So far, the discussion has been for a spin-averaged target photon. However, the boundary conditions for a transverse target photon can be obtained for free from $F_{2,\text{box}}^{\gamma_T(P^2)}(x, Q^2)$ given in Eq. (C.8) by changing $6x(1-x)$ to $8x(1-x)$ in (9.39):

$$\begin{aligned} q_{\text{DIS}_\gamma}^{\gamma_T(P^2)}(x, Q^2 = P^2) &= \bar{q}_{\text{DIS}_\gamma}^{\gamma_T(P^2)}(x, Q^2 = P^2) \\ &= N_c e_q^2 \frac{\alpha}{2\pi} \left\{ [x^2 + (1-x)^2] \ln \frac{1}{x^2} + 8x(1-x) - 2 \right\} \\ g_{\text{DIS}_\gamma}^{\gamma_T(P^2)}(x, Q^2 = P^2) &= 0. \end{aligned} \quad (9.40)$$

The corresponding results in the $\overline{\text{MS}}$ scheme can either be obtained by the factorization scheme transformation in (9.9) or by repeating the above described steps in the $\overline{\text{MS}}$ scheme with the 'direct' term

$$F_2^{<\gamma>, \text{dir}, \overline{\text{MS}}}(x, Q^2) = N_c \sum e_q^4 \frac{\alpha}{\pi} x \left\{ [x^2 + (1-x)^2] \ln \frac{1-x}{x} + 8x(1-x) - 1 \right\}. \quad (9.41)$$

Finally, let us stress that the *finite* collinear logarithm $\ln Q^2/P^2$ a priori needs *not* to be resummed. This issue has to be decided by phenomenological relevance. In addition, the predictive power of observables obtained from perturbatively calculated boundary conditions generally appears to be weakened by the freedom in choosing the input scale Q_0^2 [65] (at least at low orders in perturbation theory). Albeit $Q_0^2 = P^2$ is a 'natural' choice for the input scale due to the vanishing of the collinear logarithm $\ln Q^2/P^2$ it is by no means compelling and a different input scale $Q_0^2 \neq P^2$ would result in equally well justified boundary conditions

$$\begin{aligned} q_{\text{LO}}^{\gamma_T(P^2)}(x, Q_0^2) &= N_c e_q^2 \frac{\alpha}{2\pi} [x^2 + (1-x)^2] \ln \frac{Q_0^2}{P^2} \\ q_{\text{DIS}_\gamma}^{\gamma_T(P^2)}(x, Q_0^2) &= N_c e_q^2 \frac{\alpha}{2\pi} \left\{ [x^2 + (1-x)^2] \ln \frac{Q_0^2}{P^2} \right. \\ &\quad \left. + [x^2 + (1-x)^2] \ln \frac{1}{x^2} + 8x(1-x) - 2 \right\} \\ g_{\text{LO,DIS}_\gamma}^{\gamma_T(P^2)}(x, Q_0^2) &= 0 \end{aligned} \quad (9.42)$$

as long as $\ln Q_0^2/P^2$ is not large. Writing $\ln Q^2/P^2 = \ln Q_0^2/P^2 + \ln Q^2/Q_0^2$ we see in this case that a part of the collinear logarithm is kept in fixed order ($\ln Q_0^2/P^2$) while the other part ($\ln Q^2/Q_0^2$) is resummed to all orders.

9.3.5 Momentum Sum

Due to energy–momentum conservation the momentum fractions carried by the individual partons must add up to one⁷:

$$\int_0^1 dx \, x \left[\sum_{f=q,\bar{q},g} f^{\gamma(P^2)}(x, Q^2) + \Gamma^{\gamma(P^2)}(x, Q^2) \right] = 1 . \quad (9.43)$$

However, as we have seen before $\Gamma^{\gamma(P^2)}(x, Q^2)$ drops out of the general evolution equations in (9.15) leaving inhomogeneous evolution equations, see (9.17) and (9.22), for the (resolved) partonic content of the photon and their solutions require boundary conditions at some reference scale (input scale) Q_0^2 . A sum rule for the total momentum of the quarks and gluons in the photon

$$M_2^{\gamma(P^2)}(Q^2) \equiv \sum_{f=q,\bar{q},g} \int_0^1 dx \, x f^{\gamma(P^2)}(x, Q^2) \quad (9.44)$$

would provide useful information for constraining the input distributions. Eqs. (9.43) and (9.44) can be rewritten in terms of Mellin moments (suppressing the obvious Q^2 - and P^2 -dependence)

$$\Sigma^{n=2} + g^{n=2} + \Gamma^{n=2} = 1, \quad M_2 \equiv \Sigma^{n=2} + g^{n=2} = 1 - \Gamma^{n=2} . \quad (9.45)$$

To order α the evolution equation for $\Gamma^{\gamma(P^2)}$ reduces to

$$\frac{d\Gamma^{\gamma(P^2)}}{d \ln Q^2} = P_{\gamma\gamma} \otimes \Gamma^{\gamma(P^2)} \quad (9.46)$$

where the photon–photon splitting function $P_{\gamma\gamma}$ can be constructed from the second moments of $k_\Sigma \equiv 2 \sum k_q$ and k_g as follows: Using the evolution equations (9.17) for the quark and gluon densities and (9.46) for the photon and exploiting in addition the conservation of the hadronic energy–momentum tensor one can write

$$0 = \frac{d}{d \ln Q^2} (\Sigma^{n=2} + g^{n=2} + \Gamma^{n=2}) = (k_\Sigma^{n=2} + k_g^{n=2} + P_{\gamma\gamma}^{n=2}) \Gamma^{n=2} . \quad (9.47)$$

Furthermore, $P_{\gamma\gamma} \propto \delta(1-x)$ to all orders in α_s because in order $\mathcal{O}(\alpha)$ only virtual diagrams contribute to photon–photon splittings while radiation of real photons starts at order $\mathcal{O}(\alpha^2)$ and we can write

$$P_{\gamma\gamma} = \delta(1-x) P_{\gamma\gamma}^{n=2} = -\delta(1-x) (k_\Sigma^{n=2} + k_g^{n=2}) . \quad (9.48)$$

⁷This is certainly true for a transversely polarized target photon considered here whereas the longitudinal degrees of freedom deserve possibly some attention.

The n -moments of the photon-gluon and photon-quark splitting functions can be found, e.g., in [112, 123]. The second ($n = 2$) moments then read

$$k_{\Sigma}^{(0)n=2} + k_g^{(0)n=2} = k_{\Sigma}^{(0)n=2} = 2 \sum_q e_q^2, \quad k_{\Sigma}^{(1)n=2} + k_g^{(1)n=2} = 4 \sum_q e_q^2 \quad (9.49)$$

where the latter equation is valid both in the $\overline{\text{MS}}$ and the DIS_{γ} scheme as follows from Eq. (9.10) with $P_{qq}^{(0)n=2} + P_{gq}^{(0)n=2} = 0$.

Recalling the expansion $k = \frac{\alpha}{2\pi}(k^{(0)} + \frac{\alpha_s}{2\pi}k^{(1)} + \dots)$ we arrive at the following expression for the photon-photon splitting function (to order α)⁸:

$$P_{\gamma\gamma} = -\delta(1-x) \frac{\alpha}{\pi} \sum_q e_q^2 \left[1 + \frac{\alpha_s}{\pi} + \mathcal{O}(\alpha_s^2) \right]. \quad (9.50)$$

Eq. (9.46) can be solved analytically either in n -moment space or directly in x -space since the convolution becomes trivial due to the $\delta(1-x)$ in (9.50) and one easily finds

$$\begin{aligned} \Gamma(x, Q^2) &= \Gamma(x, Q_0^2) \exp \left(-\frac{\alpha}{\pi} \sum_q e_q^2 \left(\ln \frac{Q^2}{Q_0^2} + 4I_1 \right) \right) \\ &= \delta(1-x) \left[1 - \frac{\alpha}{\pi} \left(\sum_q e_q^2 \ln \frac{Q^2}{Q_0^2} + c_1(Q_0^2, P^2) + 4 \sum_q e_q^2 I_1 \right) \right] + \mathcal{O}(\alpha^2) \end{aligned} \quad (9.51)$$

with c_1 being a constant (depending on Q_0^2 and P^2) which automatically enters the description due to the boundary condition $\Gamma(x, Q_0^2) = \delta(1-x)[1 + \mathcal{O}(\alpha)]$ and $I_1 = \int \frac{\alpha_s(Q^2)}{4\pi} d \ln Q^2$. Employing the renormalization group equation for the strong coupling in (9.21) I_1 can be trivially integrated and one obtains

$$I_1 = \frac{1}{\beta_0} \ln \frac{\alpha_s(Q_0^2)}{\alpha_s(Q^2)} + \frac{1}{\beta_0} \ln \frac{4\pi\beta_0 + \beta_1\alpha_s(Q^2)}{4\pi\beta_0 + \beta_1\alpha_s(Q_0^2)}. \quad (9.52)$$

where the first logarithm in (9.52) dominates over the second one which is approximately $\frac{\beta_1}{4\pi\beta_0}(\alpha_s(Q^2) - \alpha_s(Q_0^2))$ and hence parametrically of NNLO. Note that contributions proportional to $\alpha_s(Q^2) - \alpha_s(Q_0^2)$ are generated also from terms of the order $\mathcal{O}(\alpha_s^2)$ in (9.50).

Eq. (9.43) holds order by order in α , so that (9.51) implies for the total momentum carried by the (resolved) photonic partons in LO-QCD [114]

$$M_2^{\gamma(P^2)}(Q^2) = \frac{\alpha}{\pi} \left(\sum_q e_q^2 \ln \frac{Q^2}{Q_0^2} + c_1(Q_0^2, P^2) \right) \quad (9.53)$$

⁸Alternatively, $P_{\gamma\gamma}$ can be inferred from the Abelian ($C_A = 0$), diagonal (independent of n) part of P_{gg} with the appropriate replacement $T_R \equiv \frac{f}{2} \rightarrow N_c \sum_q e_q^2$.

and in NLO(DIS_γ)

$$M_2^{\gamma(P^2)}(Q^2) = \frac{\alpha}{\pi} \left(\sum_q e_q^2 \ln \frac{Q^2}{Q_0^2} + c_1(Q_0^2, P^2) + \frac{4}{\beta_0} \sum_q e_q^2 \ln \frac{\alpha_s(Q_0^2)}{\alpha_s(Q^2)} \right. \\ \left. + \frac{4}{\beta_0} \sum_q e_q^2 \ln \frac{4\pi\beta_0 + \beta_1\alpha_s(Q^2)}{4\pi\beta_0 + \beta_1\alpha_s(Q_0^2)} \right) \quad (9.54)$$

where the sum $\sum_q e_q^2$ always extends over the 'light' u , d , and s quarks in the scheme adopted here (with $f = 3$ fixed in the splitting functions) whereas β_0 , β_1 and α_s depend on the number of active flavors (and therefore the heavy quark thresholds have to be taken into account by an iterative procedure as described in Sec. 9.3.2).

The constant c_1 is tightly related to the momentum sum of the hadronic input distributions at $Q^2 = Q_0^2$: $M_2(Q^2 = Q_0^2)/\alpha = c_1/\pi$. While c_1 is perturbatively calculable for large $P^2 \gg \Lambda^2$ from the boundary conditions in (9.32), (9.33) or (9.40) this is generally *not* the case for $P^2 \lesssim \Lambda^2$, especially not for real $P^2 = 0$ photons and an important constraint on the parton densities seems to be missing.

In the past few years some attempts were undertaken [97, 128, 129] to infer c_1 from elsewhere by relating Eq. (9.51) to the hadronic part of the photon vacuum polarization which in turn can be determined via a dispersion relation from the well measured cross section $\sigma_h \equiv \sigma(e^+e^- \rightarrow \text{hadrons})$. However, it turns out that the usefulness of such an approach is spoiled by higher-twist contributions present in the experimental quantity [129]. We will return to this issue when we discuss boundary conditions for the real photon in Chapter 11.

9.4 Longitudinal Target Photons

Before turning to our analysis of the parton content of pions within a constituent quark model needed as basic ingredient for our analysis of the parton content of real and transversely polarized virtual photons within the framework of the radiative parton model in Chapter 11 let us discuss for completeness also the case of longitudinally polarized virtual target photons. While these contributions vanish like, say, P^2/m_ρ^2 in the real photon limit due to gauge invariance they yield a *finite* contribution if $P^2 \gg \Lambda^2$ and should be taken into account in Eq. (7.52).

As already mentioned in Sec. 9.3.4, the structure functions of (transverse or longitudinal) deeply virtual target photons $\gamma(P^2)$ with $\Lambda^2 \ll P^2 \ll Q^2$ are reliably calculable in fixed order according to the doubly virtual box $\gamma^*(Q^2)\gamma^*(P^2) \rightarrow q\bar{q}$. Nevertheless, it has been demonstrated recently [130, 131] that a partonic treatment of $\gamma_L(P^2)$ is phenomenologically useful and relevant. The quark and gluon distribution functions $q^{\gamma_L(P^2)}(x, Q^2)$ and $g^{\gamma_L(P^2)}(x, Q^2)$ of a *longitudinal* target photon satisfy *homogeneous* evolution equations [132] in line with the expectation that (to order $\mathcal{O}(\alpha)$) there is no (on-shell and therefore) transverse photon-parton inside the longitudinal target photon, $\Gamma^{\gamma_L(P^2)}(x, Q^2) = 0$. In any case, the complete theoretical framework for the longitudinal photon target γ_L is obtainable from Sec. 9.2 and 9.3 by formally setting $\Gamma^{\gamma_L} = 0$, i.e by dropping all 'direct' contributions ($k_q \otimes \Gamma^{\gamma_L} = 0, \Gamma^{\gamma_L} \otimes C_\gamma = 0$ etc) and by using the perturbatively calculable boundary conditions at $P^2 \gg \Lambda^2$ [132]

$$\begin{aligned} q^{\gamma_L(P^2)}(x, Q^2 = P^2) &= \bar{q}^{\gamma_L(P^2)}(x, Q^2 = P^2) = N_c e_q^2 \frac{\alpha}{2\pi} 4x(1-x) \\ g^{\gamma_L(P^2)}(x, Q^2 = P^2) &= 0, \end{aligned} \tag{9.55}$$

which follow directly from the asymptotic box expression in Eq. (C.9).

Chapter 10

Pionic Parton Densities in a Constituent Quark Model

Before specifying our boundary conditions for the parton distributions of real and virtual photons we derive pionic parton distributions from constituent quark model constraints. Being, of course, also interesting in their own rights, they will serve in the next chapter as input for the hadronic component of the photon. The analysis presented in this chapter is almost identical to Ref. [5].

The parton content of the pion is poorly known at present. The main experimental source about these distributions is mainly due to data of Drell–Yan dilepton production in π^- -tungsten reactions [133–137], which determine the shape of the pionic valence density $v^\pi(x, Q^2)$ rather well, and due to measurements of direct photon production in $\pi^\pm p \rightarrow \gamma X$ [133, 138–140] which constrain the pionic gluon distribution $g^\pi(x, Q^2)$ only in the large- x region [141]. In general, however, present data are not sufficient for fixing g^π uniquely, in particular the pionic sea density $\bar{q}^\pi(x, Q^2)$ remains entirely unconstrained experimentally. Therefore in [116] a constituent quark model [142] has been utilized to relate \bar{q}^π and g^π to the much better known radiatively generated parton distributions $f^p(x, Q^2)$ of the proton [41]. Therefore, previously [116] a constituent quark model [142] has been utilized to relate \bar{q}^π and g^π to the much better known radiatively generated parton distributions $f^p(x, Q^2)$ of the proton [41]. These relations arise as follows: describing the constituent quark structure of the proton $p = UUD$ and the pion, say $\pi^+ = U\bar{D}$, by the scale (Q^2) independent distributions $U^{p,\pi^+}(x)$, $D^p(x)$ and $\bar{D}^{\pi^+}(x)$, and their universal (i.e. hadron independent) partonic content by $v_c(x, Q^2)$, $g_c(x, Q^2)$ and $\bar{q}_c(x, Q^2)$, the usual parton

content of the proton and the pion is then given by

$$f^p(x, Q^2) = \int_x^1 \frac{dy}{y} [U^p(y) + D^p(y)] f_c\left(\frac{x}{y}, Q^2\right) \quad (10.1)$$

$$f^\pi(x, Q^2) = \int_x^1 \frac{dy}{y} [U^{\pi^+}(y) + \bar{D}^{\pi^+}(y)] f_c\left(\frac{x}{y}, Q^2\right) \quad (10.2)$$

where $f = v, \bar{q}, g$ with $v^p = u_v^p + d_v^p$, $\bar{q}^p = (\bar{u}^p + \bar{d}^p)/2$, $v^\pi = u_v^{\pi^+} + \bar{d}_v^{\pi^+}$, $\bar{q}^\pi = (\bar{u}^{\pi^+} + d^{\pi^+})/2$ and $\bar{u}^{\pi^+} = d^{\pi^+}$ due to ignoring minor $SU(2)_{\text{flavor}}$ breaking effects in the pion ‘sea’ distributions. Assuming these relations to apply at the low resolution scale $Q^2 = \mu^2$ ($\mu_{\text{LO}}^2 = 0.23 \text{ GeV}^2$, $\mu_{\text{NLO}}^2 = 0.34 \text{ GeV}^2$) of [41] where the strange quark content was considered to be negligible,

$$s^p(x, \mu^2) = \bar{s}^p(x, \mu^2) = s^\pi(x, \mu^2) = \bar{s}^\pi(x, \mu^2) = 0, \quad (10.3)$$

one obtains from (10.1) and (10.2) the constituent quark independent relations [116]

$$\frac{v^\pi(n, \mu^2)}{v^p(n, \mu^2)} = \frac{\bar{q}^\pi(n, \mu^2)}{\bar{q}^p(n, \mu^2)} = \frac{g^\pi(n, \mu^2)}{g^p(n, \mu^2)} \quad (10.4)$$

where for convenience we have taken the Mellin n -moments of Eqs. (10.1) and (10.2), i.e. $f(n, Q^2) \equiv \int_0^1 x^{n-1} f(x, Q^2) dx$. Thus, as soon as $v^\pi(x, \mu^2)$ is reasonably well determined from experiment, our basic relations (10.4) uniquely fix the gluon and sea densities of the pion in terms of the rather well known parton distributions of the proton:

$$g^\pi(n, \mu^2) = \frac{v^\pi(n, \mu^2)}{v^p(n, \mu^2)} g^p(n, \mu^2), \quad \bar{q}^\pi(n, \mu^2) = \frac{v^\pi(n, \mu^2)}{v^p(n, \mu^2)} \bar{q}^p(n, \mu^2). \quad (10.5)$$

Furthermore, the sum rules [116]

$$\int_0^1 v^\pi(x, Q^2) dx = 2 \quad (10.6)$$

$$\int_0^1 x v^\pi(x, Q^2) dx = \int_0^1 x v^p(x, Q^2) dx \quad (10.7)$$

impose strong constraints on $v^\pi(x, \mu^2)$ which are very useful for its almost unambiguous determination from the πN Drell–Yan data. Notice that Eq. (10.7), together with (10.4), implies the energy–momentum sum rule for f^π to be manifestly satisfied. In addition, Eq. (10.7) implies that the valence quarks in the proton and the pion carry similar total fractional momentum as suggested by independent analyses within the framework of the radiative parton model [41, 141].

The relations in Eq. (10.5) imply that any updating of $f^p(x, \mu^2)$ yields a corresponding updating of $f^\pi(x, \mu^2)$. Recently an updating of $f^p(x, \mu^2)$ within the framework of the radiative (dynamical) parton model was undertaken [26] utilizing additional improved data on $F_2^p(x, Q^2)$ from HERA [143–148] and a somewhat increased $\alpha_s(M_Z^2) = 0.114$ resulting in a slight increase in μ^2 ($\mu_{\text{LO}}^2 = 0.26 \text{ GeV}^2$, $\mu_{\text{NLO}}^2 = 0.40 \text{ GeV}^2$). An improved treatment of the running $\alpha_s(Q^2)$ at low Q^2 was furthermore implemented by solving in NLO($\overline{\text{MS}}$) Eq. (9.26) numerically [26] rather than using the approximate NLO solution in Eq. (9.27) as done in [41, 116, 141], which is sufficiently accurate only for $Q^2 \gtrsim m_c^2 \simeq 2 \text{ GeV}^2$ [26]. The LO and NLO evolutions of $f^\pi(n, Q^2)$ to $Q^2 > \mu^2$ are performed in Mellin n -moment space, followed by a straightforward numerical Mellin-inversion [92] to Bjorken- x space as described in Chapter 9. It should be noted that the evolutions are always performed in the fixed (light) $f = 3$ flavor factorization scheme [18, 26, 41, 116], i.e. we refrain from generating radiatively massless ‘heavy’ quark densities $h^\pi(x, Q^2)$ where $h = c, b$, etc., in contrast to [141]. Hence heavy quark contributions have to be calculated in fixed order perturbation theory via, e.g., $g^\pi g^p \rightarrow h\bar{h}$, $\bar{u}^\pi u^p \rightarrow h\bar{h}$, etc. (Nevertheless, rough estimates of ‘heavy’ quark effects, valid to within a factor of 2, say, can be easier obtained with the help of the massless densities $c^\pi(x, Q^2)$ and $b^\pi(x, Q^2)$ given in [141].)

Using all these modified ingredients together with the new updated [26] $f^p(x, \mu^2)$ in our basic predictions in Eq. (10.5), the present reanalysis of the available Drell–Yan data [134–136], closely following the procedure described in [116], yields

$$v_{\text{LO}}^\pi(x, \mu_{\text{LO}}^2) = 1.129x^{-0.496}(1-x)^{0.349}(1+0.153\sqrt{x}) \quad (10.8)$$

$$v_{\text{NLO}}^\pi(x, \mu_{\text{NLO}}^2) = 1.391x^{-0.447}(1-x)^{0.426} \quad (10.9)$$

where [26] $\mu_{\text{LO}}^2 = 0.26 \text{ GeV}^2$ and $\mu_{\text{NLO}}^2 = 0.40 \text{ GeV}^2$. These updated input valence densities correspond to total momentum fractions

$$\int_0^1 x v_{\text{LO}}^\pi(x, \mu_{\text{LO}}^2) dx = 0.563 \quad (10.10)$$

$$\int_0^1 x v_{\text{NLO}}^\pi(x, \mu_{\text{NLO}}^2) dx = 0.559 \quad (10.11)$$

as dictated by the valence densities of the proton [26] via Eq. (10.7).

Our new updated input distributions in Eqs. (10.8), (10.9) and (10.5) are rather different than the original GRV $_\pi$ input [141] in Fig. 10.1 which is mainly due to the vanishing sea input of GRV $_\pi$ in contrast to the present one in Eq. (10.5). On the other hand, our

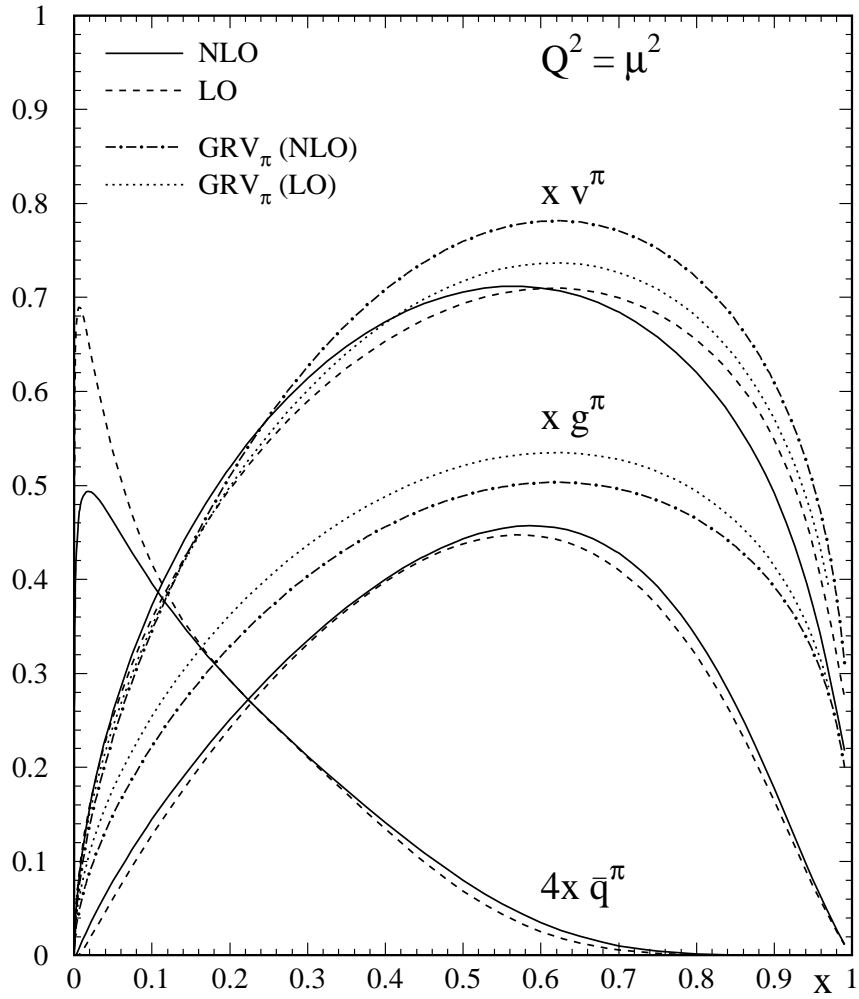


Figure 10.1: The valence and valence-like input distributions $xf^\pi(x, Q^2 = \mu^2)$ with $f = v, \bar{q}, g$ as compared to those of GRV_π [141]. Notice that GRV_π employs a vanishing $\text{SU}(3)_{\text{flavor}}$ symmetric \bar{q}^π input at $\mu_{\text{LO}}^2 = 0.25 \text{ GeV}^2$ and $\mu_{\text{NLO}}^2 = 0.3 \text{ GeV}^2$ [141]. Our present $\text{SU}(3)_{\text{flavor}}$ broken sea densities refer to a vanishing s^π input in (10.3), as for GRV_π [141].

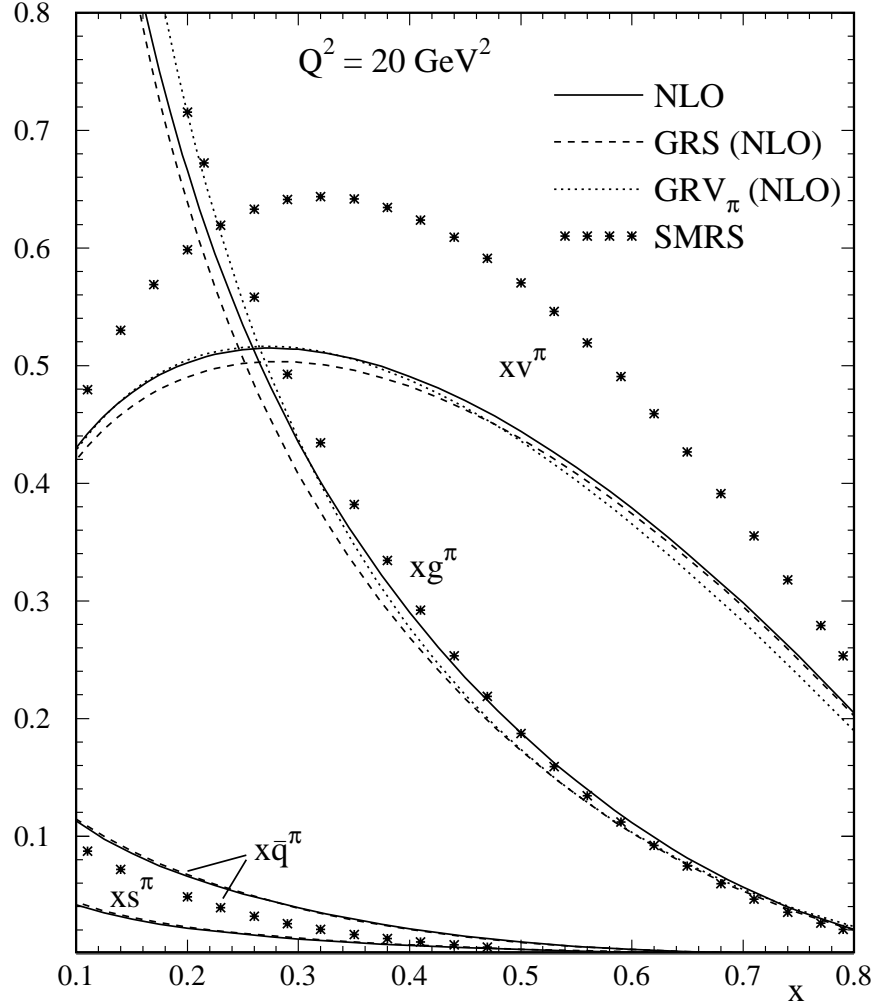


Figure 10.2: Comparison of our NLO valence distribution at $Q^2 = 20 \text{ GeV}^2$ with the one of GRV_π [141] and GRS [116]. This density plays the dominant role for describing presently available πN Drell–Yan dimuon production data. For illustration, the gluon and sea densities are shown as well. The $\text{SU}(3)_{\text{flavor}}$ symmetric GRV_π sea $\bar{q}^\pi = s^\pi$ is not shown, since it is similar to s^π of our present analysis and of GRS which are all generated from a vanishing input at $Q^2 = \mu^2$, cf. Eq. (10.3). The SMRS [137] results refer also to a $\text{SU}(3)_{\text{flavor}}$ symmetric sea $\bar{q}^\pi \equiv \bar{u}^{\pi^+} = d^{\pi^+} = s^\pi = \bar{s}^\pi$.

updated input in Fig. 10.1 is, as expected, rather similar to the one of [116]. In both cases, however, the valence and gluon distributions become practically indistinguishable from our present updated ones at scales relevant for present Drell–Yan dimuon and direct- γ production data, $Q^2 \equiv M_{\mu^+\mu^-}^2 \simeq 20 \text{ GeV}^2$, as illustrated in Fig. 10.2. Therefore our present updated pionic distributions give an equally good description of all available πN Drell–Yan data as the ones shown in [116]. Notice that the different gluon distributions presented in Fig. 10.2 can *not* be discriminated by present direct-photon production data [138–140] due to the uncertainty of the theoretically calculated cross section arising from variations of the chosen factorization scale and from possible intrinsic k_T contributions, cf. for example L. Apanasevich et al. [138–140].

For completeness let us mention that our basic predictions (10.5) for the valence-like gluon and sea densities at $Q^2 = \mu^2$, as shown in Fig. 10.1, can be simply parametrized in Bjorken- x space : in LO at $Q^2 = \mu_{\text{LO}}^2 = 0.26 \text{ GeV}^2$

$$\begin{aligned} x g^\pi(x, \mu_{\text{LO}}^2) &= 7.326 x^{1.433} (1 - 1.919 \sqrt{x} + 1.524 x)(1 - x)^{1.326} \\ x \bar{q}^\pi(x, \mu_{\text{LO}}^2) &= 0.522 x^{0.160} (1 - 3.243 \sqrt{x} + 5.206 x)(1 - x)^{5.20}, \end{aligned} \quad (10.12)$$

whereas in NLO at $Q^2 = \mu_{\text{NLO}}^2 = 0.40 \text{ GeV}^2$ we get

$$\begin{aligned} x g^\pi(x, \mu_{\text{NLO}}^2) &= 5.90 x^{1.270} (1 - 2.074 \sqrt{x} + 1.824 x)(1 - x)^{1.290} \\ x \bar{q}^\pi(x, \mu_{\text{NLO}}^2) &= 0.417 x^{0.207} (1 - 2.466 \sqrt{x} + 3.855 x)(1 - x)^{4.454}. \end{aligned} \quad (10.13)$$

Finally, Fig. 10.3 shows our resulting predictions for $x g^\pi(x, Q^2)$ and $x \bar{q}^\pi(x, Q^2)$ as compared to the former GRV_π results [141]. The GRV_π results for $x \bar{q}^\pi$ are significantly steeper and softer for $x \gtrsim 0.01$ due to the vanishing $\text{SU}(3)_{\text{flavor}}$ symmetric (light) sea input $x \bar{q}^\pi(x, \mu^2) = 0$, in contrast to our present approach [116] based on a more realistic finite light sea input in Eq. (10.5). The valence-like gluon and sea inputs at $Q^2 = \mu^2$, which become (vanishingly) small at $x < 10^{-2}$, are also shown in Fig. 10.3. This illustrates again the purely dynamical origin of the small- x structure of gluon and sea quark densities at $Q^2 > \mu^2$. Our predictions for $s^\pi = \bar{s}^\pi$, as evolved from the vanishing input in Eq. (10.3), are not shown in the figure since they practically coincide with $\bar{q}^\pi(x, Q^2)$ of GRV_π shown in Fig. 10.3 which also results from a vanishing input [141]. Simple analytic parametrizations of our LO and NLO predictions for $f^\pi(x, Q^2)$ are given in Appendix D.

To conclude let us recall that an improvement of $f^\pi(x, Q^2)$ is particularly important in view of its central role in the construction of the photon structure function and the

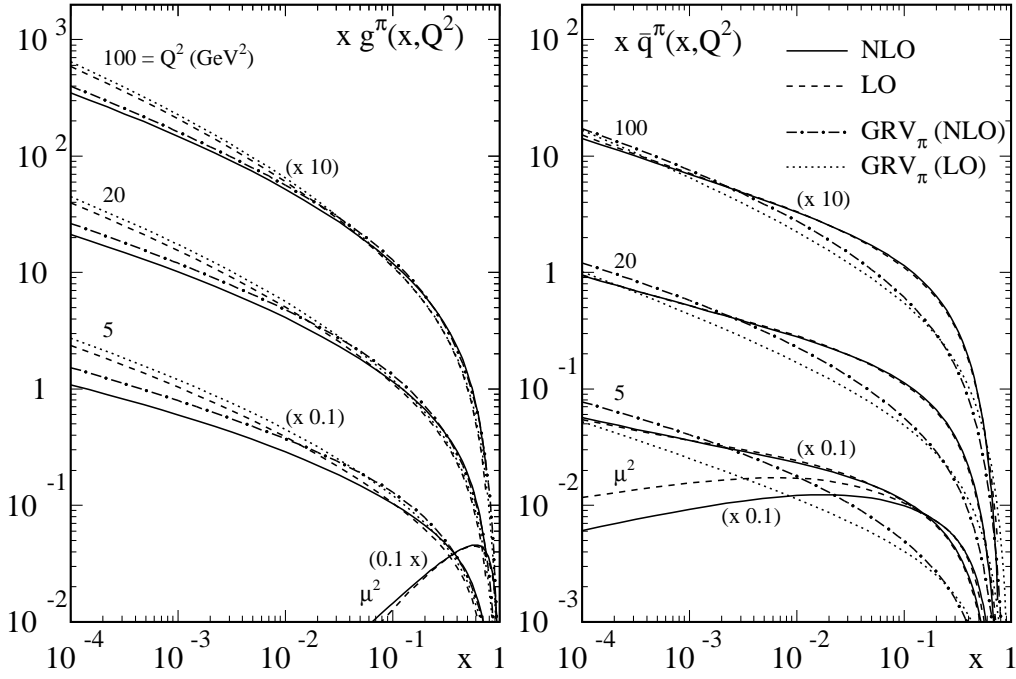


Figure 10.3: The small- x predictions of our radiatively generated pionic gluon and sea-quark distributions in LO and NLO at various fixed values of Q^2 as compared to those of GRV_π [141]. The valence-like inputs, according to Eq. (10.5) as presented in Fig. 10.1, are shown for illustration by the lowest curves referring to μ^2 . The predictions for the strange sea density $s^\pi = \bar{s}^\pi$ are similar to the GRV_π results for \bar{q}^π . The results are multiplied by the numbers indicated in brackets.

photonic parton distributions [96, 97, 112–114, 149]. Furthermore, recent (large rapidity gap) measurements of leading proton and neutron production in deep inelastic scattering at HERA [150] allow, under certain (diffractive) model assumptions, to constrain and test the pion structure functions for the first time at far smaller values of x (down to about 10^{-3}) than those attained from fixed target πN experiments.

Chapter 11

Radiatively Generated Parton Distributions of Real and Virtual Photons

Having presented the general theoretical framework in Chapter 9 we now turn to an analysis of the partonic content of (virtual) photons within the phenomenologically successful framework of the radiative parton model [26, 41, 57, 92, 93]. This analysis follows Ref. [6]. The results in Sec. 11.3 have been taken from [7].

11.1 Introduction

Modern theoretical QCD studies [96, 112, 113, 149, 151] of the parton distributions of *real*, i.e. on-shell, photons $f^\gamma(x, Q^2)$, $f = q, \bar{q}, g$, agree surprisingly well with measurements of the (anti-)quark and gluon contents of the resolved real photons as obtained from e^+e^- and ep reactions at collider energies (for recent reviews, see [89, 114, 152]). For clarity let us denote the resolved real target photon with virtuality $P^2 \equiv -p^2 \simeq 0$ by $\gamma \equiv \gamma(P^2 \simeq 0)$ which is probed by the virtual probe photon $\gamma^*(Q^2)$, $Q^2 \equiv -q^2$, via the subprocess $\gamma^*(Q^2)\gamma \rightarrow X$ as in $e^+e^- \rightarrow e^+e^-X$. Here, p denotes the four-momentum of the photon emitted from, say, an electron in an e^+e^- or ep collider. In the latter case it is common to use Q^2 instead of P^2 for denoting the photon's virtuality, but we prefer P^2 for the subprocess $\gamma(P^2)p \rightarrow X$ according to the original notation used in e^+e^- annihilations. (Thus the factorization scale in $f^{\gamma(P^2)}(x, Q^2)$ refers now to some properly chosen scale of the produced hadronic system X , e.g. $Q \sim p_T^{\text{jet}}$ in high- p_T jet events, etc.).

In general one expects [97, 104, 111, 125–127, 153–155] also a *virtual* photon $\gamma(P^2 \neq 0)$ to possess a parton content $f^{\gamma(P^2)}(x, Q^2)$. It is a major problem to formulate a consistent set of boundary conditions which allow for a calculation of $f^{\gamma(P^2)}(x, Q^2)$ also in the next-to-leading order (NLO) of QCD *as well as* for a smooth transition to $P^2 = 0$, i.e. to the parton distributions of a real photon (see Refs. [97, 111, 156] for a detailed discussion). Indeed, experimental studies of the transition of the deep inelastic (di-)jet cross section from the real photon to the virtual photon region at HERA point to the existence of a nonvanishing, though suppressed, parton content for virtual photons [157–161]. These measurements have triggered various analyses of the dependence of the ep jet production cross section on the virtuality of the exchanged photon [162, 163] and experimental tests of such predictions will elucidate the so far unanswered question as to when a deep inelastic scattering (DIS) ep process is eventually dominated by the usual ‘direct’ $\gamma^* \equiv \gamma(P^2)$ induced cross sections, *not* contaminated by the so far poorly known *resolved* virtual photon contributions. More recently, NLO calculations of the (di-)jet rate in ep (and $e\gamma$) scattering, which properly include the contributions of resolved virtual photons, have become available [164] and the resolved virtual photon contributions have already been included in a Monte Carlo event generator [165] as well.

It is the main purpose of the present chapter to formulate a consistent set of boundary conditions, utilizing valence-like input parton distributions at the universal target-mass independent [41, 57, 93, 96, 112, 141] low resolution scale $Q_0^2 = \mu^2 \simeq 0.3 \text{ GeV}^2$, which allow for a calculation of $f^{\gamma(P^2)}(x, Q^2)$ also in NLO-QCD as well as for a smooth transition to the parton distributions of a real photon, $P^2 = 0$. We shall furthermore employ the pionic parton distributions of Chapter 10, $f^\pi(x, Q^2)$, which are required for describing, via vector meson dominance (VMD), the hadronic components of the photon. It should be recalled that the pionic gluon and sea densities, $g^\pi(x, Q^2)$ and $\bar{q}^\pi(x, Q^2)$, have been uniquely derived from the experimentally rather well known pionic valence density $v^\pi(x, Q^2)$ and the (recently updated [26] dynamical) parton distributions $f(x, Q^2)$ of the proton. Thus we arrive at essentially parameter-*free* predictions for $f^{\gamma(P^2)}(x, Q^2)$ which are furthermore in good agreement with all present measurements of the structure function of real photons, $F_2^\gamma(x, Q^2)$.

Sec. 11.2 is devoted to an analysis of the parton distributions and structure functions of real photons and the resulting predictions are compared with recent experiments. In Sec. 11.3 we compare our unique small- x predictions –characteristic for the radiative

parton model– with very recent small- x measurements of the photon structure function $F_2^\gamma(x, Q^2)$ by the LEP–OPAL collaboration. Sec. 11.4 contains the formulation of our model for the parton distributions of virtual photons, together with some quantitative predictions for structure functions as well as a comparison with very recent data extracted from DIS dijet events. Our conclusions are drawn in Sec. 11.5. In App. D we present simple analytic parametrizations of our LO and NLO predictions for the parton distributions of real and virtual photons.

11.2 The Parton Content of Real Photons

11.2.1 Boundary Conditions

The pionic parton distributions presented in the previous chapter will now be utilized to construct LO and NLO input distributions for the real photon via a vector meson dominance ansatz at the low resolution scale $Q_0^2 = \mu^2 \simeq 0.3 \text{ GeV}^2$.

In NLO the nonperturbative hadronic VMD input $f^\gamma(x, Q_0^2)$ refers to the partons in the DIS_γ scheme which guarantees the perturbative stability of the resulting $F_2^\gamma(x, Q^2)$ provided this input is given by the NLO $f^\pi(x, Q_0^2)$ of Chap. 10, while the corresponding input in LO is given via VMD by the LO $f^\pi(x, Q_0^2)$ of Chap. 10. We shall assume that the input resolution scale $Q_0^2 = \mu^2 \simeq 0.3 \text{ GeV}^2$ for the valence-like parton structure is universal, i.e. independent of the mass of the considered targets p, π, γ , etc. [41, 57, 93, 96, 112, 116, 141].

The hadronic VMD ansatz for $f^\gamma(x, \mu^2)$ is based on a coherent superposition of vector mesons [97]

$$|\gamma\rangle_{\mu^2, \text{had}} \simeq \frac{e}{f_\rho} |\rho\rangle_{\mu^2} + \frac{e}{f_\omega} |\omega\rangle_{\mu^2} \quad (11.1)$$

where the ϕ -meson contribution is considered to be strongly suppressed at $\mu^2 \ll m_\phi^2$. As usual, we identify the parton distribution functions in the parton model with matrix elements of local twist-2 operators within the operator product expansion (OPE) formalism and we obtain using (11.1)

$$\begin{aligned} f^\gamma(\mu^2) &= f_{\text{had}}^\gamma(\mu^2) = \langle \gamma | O_f | \gamma \rangle_{\mu^2, \text{had}} \\ &= \frac{e^2}{f_\rho^2} \langle \rho | O_f | \rho \rangle_{\mu^2} + \frac{e^2}{f_\rho f_\omega} (\langle \rho | O_f | \omega \rangle_{\mu^2} + \langle \omega | O_f | \rho \rangle_{\mu^2}) + \frac{e^2}{f_\omega^2} \langle \omega | O_f | \omega \rangle_{\mu^2} \end{aligned}$$

with $f = u, d, s, g$. Assuming, within the OPE,

$$\begin{aligned}\langle \rho | O_q | \rho \rangle_{\mu^2} &= \langle \omega | O_q | \omega \rangle_{\mu^2} = \langle \pi^0 | O_q | \pi^0 \rangle_{\mu^2}, & \langle \rho | O_q | \omega \rangle_{\mu^2} &= 2 I_{3q} e^{-i\theta} \langle \pi^0 | O_q | \pi^0 \rangle_{\mu^2} \\ \langle \rho | O_g | \rho \rangle_{\mu^2} &= \langle \omega | O_g | \omega \rangle_{\mu^2} = \langle \pi^0 | O_g | \pi^0 \rangle_{\mu^2}, & \langle \rho | O_g | \omega \rangle &= 0\end{aligned}$$

where the last equation holds due to isospin conservation, one obtains

$$\begin{aligned}(u + \bar{u})^\gamma(x, \mu^2) &= \alpha(g_\rho^2 + g_\omega^2 + 2g_\rho g_\omega \cos \theta)(u + \bar{u})^{\pi^0}(x, \mu^2) \\ (d + \bar{d})^\gamma(x, \mu^2) &= \alpha(g_\rho^2 + g_\omega^2 - 2g_\rho g_\omega \cos \theta)(d + \bar{d})^{\pi^0}(x, \mu^2) \\ (s + \bar{s})^\gamma(x, \mu^2) &= \alpha(g_\rho^2 + g_\omega^2)(s + \bar{s})^{\pi^0}(x, \mu^2) = 0 \\ g^\gamma(x, \mu^2) &= \alpha(g_\rho^2 + g_\omega^2)g^{\pi^0}(x, \mu^2).\end{aligned}\tag{11.2}$$

Here $O_{q,g}$ refer to the leading twist-2 quark and gluon operators and $g_V^2 \equiv 4\pi/f_V^2$ with

$$g_\rho^2 = 0.50, \quad g_\omega^2 = 0.043, \tag{11.3}$$

i.e. $f_\rho^2/4\pi = 2.0$ and $f_\omega^2/4\pi = 23.26$, as obtained from a zero-width calculation of the relevant leptonic widths $\Gamma(V \rightarrow \ell^+ \ell^-) = \alpha^2 m_V g_V^2/3$ presented in [166]. The omission of a finite-width correction for g_ρ^2 is due to the central role [166] of the precise results in [167] which do not require such a correction in contrast to the situation for the less precise resonance analysis at e^+e^- colliders [85, 168, 169].

For the a priori unknown coherence factor (fit parameter) $\cos \theta$ in Eq. (11.2) we take $\cos \theta = 1$, i.e. we favor a superposition of u and d quarks which maximally enhances the contributions of the up-quarks to F_2^γ in Eq. (9.1). This favored value for $\cos \theta$ is also supported by fitting $\cos \theta$ in (11.2) to all presently available data on $F_2^\gamma(x, Q^2)$, to be discussed below, which always resulted in $\cos \theta \simeq 1$ in LO as well as NLO. This is also in agreement with the LO results obtained in Ref. [97]. The LO and NLO input distributions $f^\pi(x, \mu^2)$ of the pion in (11.2) are taken from the analysis in the previous chapter which correspond to $[5, 26] \mu_{\text{LO}}^2 = 0.26 \text{ GeV}^2$ and $\mu_{\text{NLO}}^2 = 0.40 \text{ GeV}^2$ in LO and NLO, respectively. Since by now all free input quantities have been fixed in Eq. (11.2), we arrive at rather unique parameter-free predictions for $f^\gamma(x, Q^2)$ and $F_2^\gamma(x, Q^2)$.

The calculation of $f^\gamma(x, Q^2)$ at $Q^2 > \mu^2$ follows from the well known inhomogeneous renormalization group (RG) evolution equations in LO and NLO which we solve, as usual, analytically for the n -th Mellin moment of $f^\gamma(x, Q^2)$, followed by a straightforward Mellin-inversion to Bjorken- x space as described in detail in Chapter 9. The general

structure of these solutions is

$$f^\gamma(x, Q^2) = f_{\text{pl}}^\gamma(x, Q^2) + f_{\text{had}}^\gamma(x, Q^2). \quad (11.4)$$

Here f_{pl}^γ denotes the perturbative ‘pointlike’ solution which vanishes at $Q^2 = \mu^2$ and is driven by the pointlike photon splitting functions $k_{q,g}^{(0,1)}(x)$ appearing in the inhomogeneous evolution equations, while f_{had}^γ depends on the hadronic input $f^\gamma(x, \mu^2)$ in Eq. (11.2) and evolves according to the standard homogeneous evolution equations.

The prescription for the VMD ansatz in Eq. (11.2) at the input scale μ^2 , together with $\cos \theta = 1$ as discussed above, yields a simple expression for the general Q^2 -dependence of $f^\gamma(x, Q^2)$:

$$f^\gamma(x, Q^2) = f_{\text{pl}}^\gamma(x, Q^2) + \alpha \left[G_f^2 f^\pi(x, Q^2) + \delta_f \frac{1}{2} (G_u^2 - G_d^2) s^\pi(x, Q^2) \right] \quad (11.5)$$

with $\delta_u = -1$, $\delta_d = +1$ and $\delta_s = \delta_g = 0$, and where the index π obviously refers to π^0 and

$$\begin{aligned} G_u^2 &= (g_\rho + g_\omega)^2 \simeq 0.836 \\ G_d^2 &= (g_\rho - g_\omega)^2 \simeq 0.250 \\ G_s^2 &= G_g^2 = g_\rho^2 + g_\omega^2 = 0.543. \end{aligned} \quad (11.6)$$

Simple analytic LO and NLO(DIS $_\gamma$) parametrizations for the pointlike piece $f_{\text{pl}}^\gamma(x, Q^2)$ are given in App. D.2, whereas the ones for $f^\pi(x, Q^2)$ can be found in App. D.1.

11.2.2 Quantitative Results

Having outlined the theoretical basis for our photonic parton distributions, we now turn to the quantitative results. First we apply our parameter-free predictions for $f^\gamma(x, Q^2)$ to the structure function of real photons which, according to Eq. (9.1), is finally given by

$$\begin{aligned} \frac{1}{x} F_2^\gamma(x, Q^2) &= 2 \sum_{q=u,d,s} e_q^2 \left\{ q^\gamma(x, Q^2) + \frac{\alpha_s(Q^2)}{2\pi} [C_{q,2} \otimes q^\gamma + C_{g,2} \otimes g^\gamma] \right\} \\ &+ \frac{1}{x} F_{2,c}^\gamma(x, Q^2) + \frac{1}{x} F_{2,c}^{g^\gamma}(x, Q^2) \end{aligned} \quad (11.7)$$

where $f^\gamma(x, Q^2)$ refers to the DIS $_\gamma$ factorization scheme defined in (9.9) and the charm contributions $F_{2,c}^\gamma$ and $F_{2,c}^{g^\gamma}$ are given by Eqs. (9.13) and (9.14), respectively.

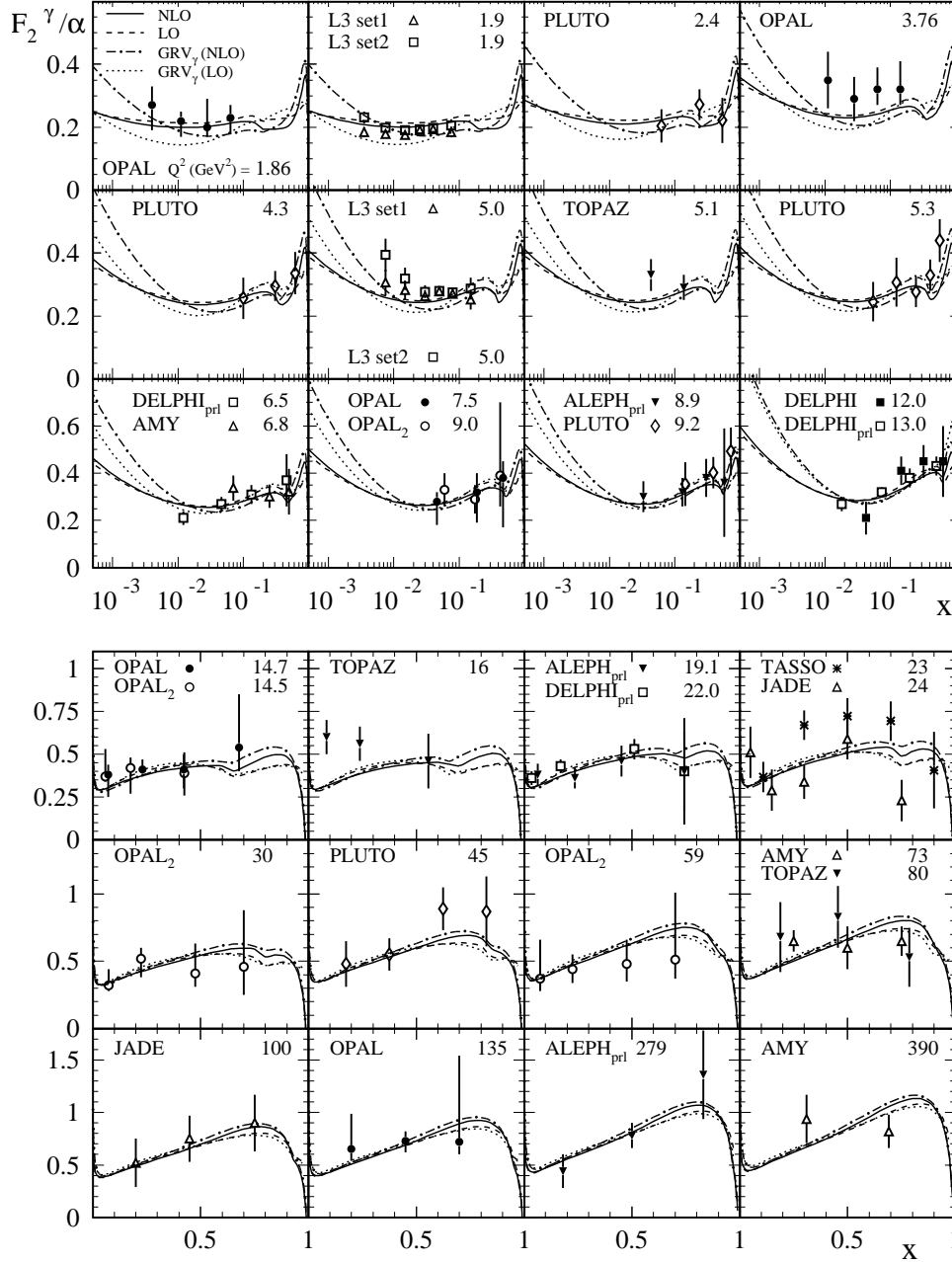


Figure 11.1: Comparison of our radiatively generated LO and NLO(DIS $_\gamma$) predictions for $F_2^\gamma(x, Q^2)$, based on the valence-like parameter-free VMD input in Eq. (11.2), with the data of Ref. [170–179]. For our comparison the GRV $_\gamma$ [96, 112] results are shown as well. In both cases, the charm contribution has been added, in the relevant kinematic region $W \geq 2m_c$, according to Eqs. (9.13) and (9.14).

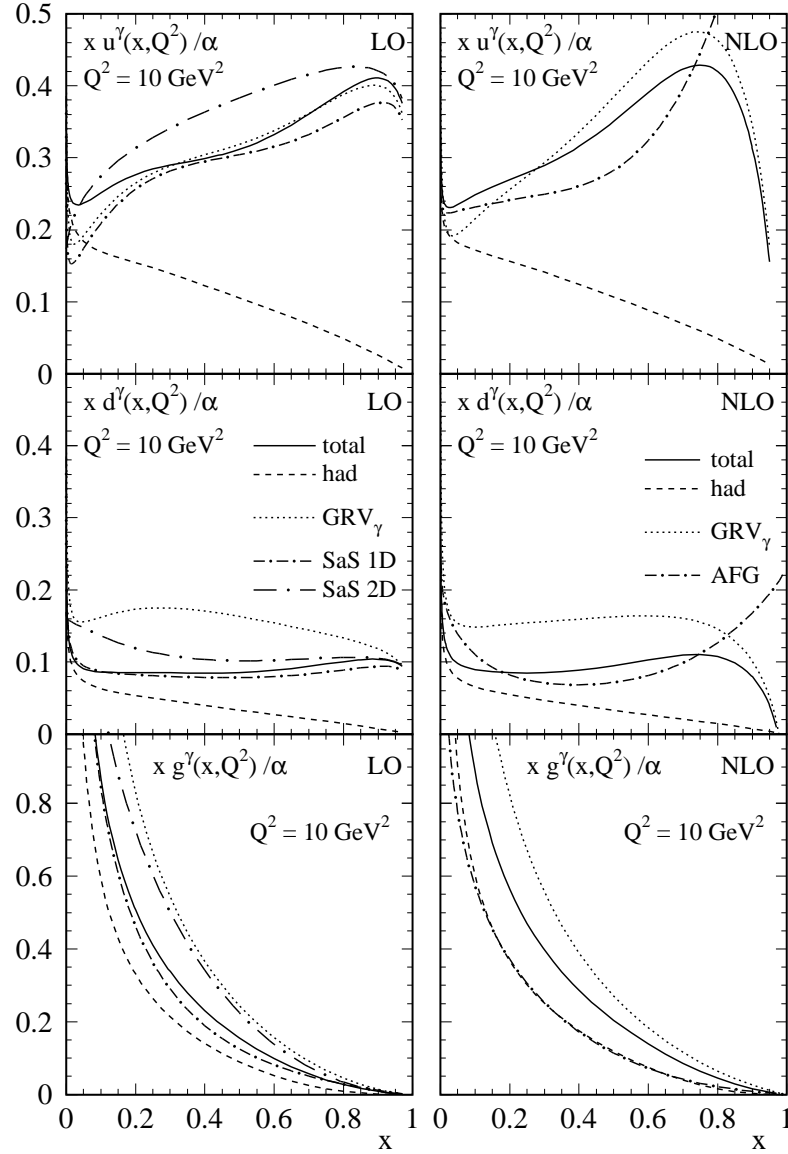


Figure 11.2: Comparison of our predicted LO and NLO(DIS $_\gamma$) distributions $u^\gamma = \bar{u}^\gamma$, $d^\gamma = \bar{d}^\gamma$ and g^γ at $Q^2 = 10 \text{ GeV}^2$ with the LO/NLO GRV $_\gamma$ densities [96, 112], the LO SaS 1D and 2D [97] and the NLO AFG [113] distributions. The 'hadronic' (pionic) components of our total LO and NLO results in Eq. (11.4) are displayed by the dashed curves.

In Fig. 11.1 we compare our LO and NLO predictions with all available¹ relevant data [170–179] for F_2^γ of the real photon. Our present new NLO results are rather similar to the ones of AFG [113], but differ from the previous (GRV $_\gamma$) predictions [96, 112] which are steeper in the small- x region, as shown in Fig. 11.1, because the dominant hadronic (pionic) sea density $\bar{q}^\pi(x, Q^2)$ is steeper since it has been generated purely dynamically from a vanishing input at $Q^2 = \mu^2$ [96, 112, 141]. Similarly the SaS 1D [97] expectations, for example, fall systematically below the data in the small to medium Q^2 region around $Q^2 \simeq 5 \text{ GeV}^2$, partly due to a somewhat different treatment of the hadronic coherent VMD input as compared to our results in Eqs. (11.2), (11.5), and (11.6).

The relevant LO and NLO photonic parton densities are compared in Fig. 11.2 at $Q^2 = 10 \text{ GeV}^2$. For illustration we also show the purely ‘hadronic’ component (homogeneous solution) in (11.4) of f^γ which demonstrates the dominance of the ‘pointlike’ component (inhomogeneous solution) in (11.4) for u^γ and d^γ in the large- x region, $x > 0.1$.

In Fig. 11.3 we show our predictions for $xu^\gamma(x, Q^2)$ and $xg^\gamma(x, Q^2)$. The parton distributions of the photon behave, in contrast to the ones of a hadron, very differently in the limits of large and small x . In the former case, the purely perturbative pointlike part in (11.4) dominates for $x \gtrsim 0.1$, especially for the quark distributions. On the other hand, this uniquely calculable contribution amounts at most to about 20% at very small x where the hadronic VMD component in (11.4) dominates, giving rise to a very similar increase for $x \rightarrow 0$ as observed in the proton case. In Fig. 11.3 we also show our valence-like inputs at $Q^2 = \mu_{\text{LO,NLO}}^2$ which become (vanishingly) small at $x < 10^{-2}$. This illustrates the purely dynamical origin of the small- x increase at $Q^2 > \mu^2$. Also noteworthy is the perturbative LO/NLO stability of $u^\gamma(x, Q^2)$ which is almost as good as the one required for a physical quantity like $F_2^\gamma(x, Q^2)$ in Fig. 11.1. The situation is, as usual [26, 41, 57, 93, 96, 112], different for $g^\gamma(x, Q^2)$. Nevertheless, despite the sizable difference between the LO and NLO gluon distributions in Fig. 11.3 in the small- x region, the directly measurable F_2^γ and the gluon-dominated heavy quark contribution in Eq. (9.14) shows a remarkable perturbative stability [26].

Next, we compare in Fig. 11.4 our predictions for $xg^\gamma(x, Q^2)$ at $Q^2 \equiv (p_T^{\text{jet}})^2 = 75 \text{ GeV}^2$ with recent HERA (H1) measurements [180, 181]. Our somewhat flatter results for xg^γ in the small- x region, as compared to the older GRV $_\gamma$ expectations [96, 112], is caused by the recently favored flatter gluon distribution in the proton [26] which determines g^γ via

¹January 1999

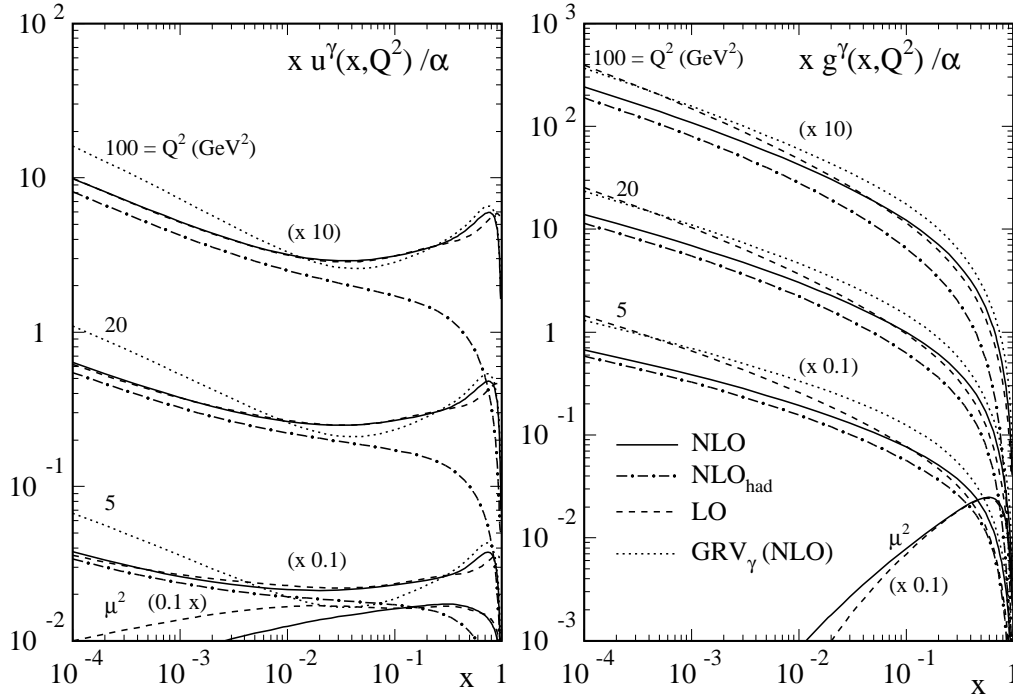


Figure 11.3: Detailed small- x (as well as large- x) behavior and predictions of our radiatively generated $u^\gamma = \bar{u}^\gamma$ and g^γ distributions in LO and NLO(DIS $_\gamma$) at fixed values of Q^2 . The dashed-dotted curves show the hadronic NLO contribution f_{had}^γ to $f^\gamma = f_{\text{pl}}^\gamma + f_{\text{had}}^\gamma$ in Eq. (11.4). The valence-like inputs at $Q^2 = \mu_{\text{LO,NLO}}^2$, according to Eq. (11.2), are shown by the lowest curves referring to μ^2 . For comparison we show the steeper NLO GRV $_\gamma$ [96, 112] expectations as well. The results have been multiplied by the number indicated in brackets.

g^π [5], cf. Eq. (11.2), at small x .

Finally it is interesting to consider the total momenta carried by the photonic partons,

$$M_2^\gamma(Q^2) \equiv \sum_{f=q,\bar{q},g} \int_0^1 x f^\gamma(x, Q^2) dx. \quad (11.8)$$

Inspired by the ideas and suggestions put forward in Refs. [97, 128], it has been conjectured recently [129] that this leading twist-2 quantity M_2^γ should satisfy, in LO-QCD,

$$M_2^\gamma(Q^2) \simeq \Pi_h(Q^2) \quad (11.9)$$

where the well known dispersion relation relates the hadronic part of the photon's vacuum polarization

$$\Pi_h(Q^2) = \frac{Q^2}{4\pi^2\alpha} \int_{4m_\pi^2}^\infty \frac{\sigma_h(s)}{s + Q^2} ds \quad (11.10)$$

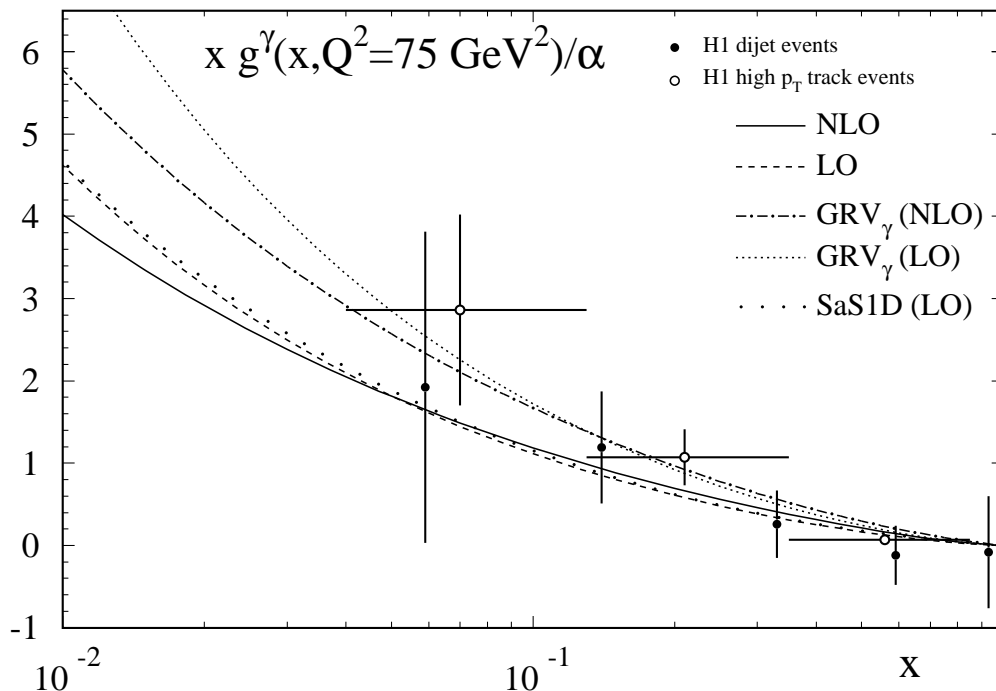


Figure 11.4: Comparison of our LO and NLO predictions for xg^γ at $Q^2 \equiv \langle (p_T^{\text{jet}})^2 \rangle = 75 \text{ GeV}^2$ with HERA(H1) measurements [180, 181]. The GRV_γ and SaS expectations are taken from Refs. [96, 112] and [97], respectively.

to $\sigma_h \equiv \sigma(e^+e^- \rightarrow \text{hadrons})$. It should be noted that $\Pi_h(Q^2)$, being an experimental quantity, includes, besides the usual twist-2 term, all possible nonperturbative higher-twist contributions. The ‘consistency’ relation (11.9) is, however, expected to hold already at $Q^2 \gtrsim 2$ to 4 GeV^2 to within, say, 20 to 30% where the twist-2 component in $\Pi_h(Q^2)$ may become dominant, as possibly indicated by DIS ep processes. Indeed, our LO results imply $M_2^\gamma(2 \text{ GeV}^2)/\alpha \simeq 0.976$ and $M_2^\gamma(4 \text{ GeV}^2)/\alpha \simeq 1.123$ which compares favorably with [182] $\Pi_h(2 \text{ GeV}^2)/\alpha = 0.694 \pm 0.028$ and $\Pi_h(4 \text{ GeV}^2)/\alpha = 0.894 \pm 0.036$, respectively.

11.3 The Photon Structure Function at Small- x

Recently the OPAL collaboration [98] at the CERN-LEP collider has extended the measurements of the photon structure function $F_2^\gamma(x, Q^2)$ into the small- x region down to $x \simeq 10^{-3}$, probing lower values of x than ever before. The observed rise of F_2^γ towards low values of x , $x < 0.1$, is in agreement with general QCD renormalization group improved expectations. It has, however, been noted that the rising small- x data at lower

scales $Q^2 \simeq 2 - 4 \text{ GeV}^2$ lie above the original QCD expectations anticipated almost a decade ago [96, 97].

In the following we will demonstrate that our updated parameter-free QCD predictions for $F_2^\gamma(x, Q^2)$ [6], discussed in Sec. 11.2, are in general also consistent with the OPAL small- x measurements at all presently accessible values of Q^2 .

Before presenting our results it is instructive to recapitulate briefly the main differences between the original GRV_γ [96] approach to the photonic parton distributions and our parameter-free predictions of Sec. 11.2. In the latter approach a coherent superposition of vector mesons has been employed, which maximally enhances the u -quark contributions to F_2^γ , for determining the hadronic parton input $f_{\text{had}}^\gamma(x, Q_0^2)$ at a GRV-like [26] input scale $Q_0^2 \equiv \mu_{\text{LO}}^2 = 0.26 \text{ GeV}^2$ and $Q_0^2 \equiv \mu_{\text{NLO}}^2 = 0.40 \text{ GeV}^2$ for calculating the (anti)quark and gluon distributions $f^\gamma(x, Q^2)$ of a real photon in leading order (LO) and next-to-LO (NLO) of QCD. Furthermore, in order to remove the ambiguity of the hadronic light quark sea and gluon input distributions of the photon (being related to the ones of the pion, $f^\pi(x, Q_0^2)$, via vector meson dominance), inherent to the older GRV_γ [96] and SaS [97] parametrizations, predictions [5, 116] for $\bar{q}^\pi(x, Q^2)$ and $g^\pi(x, Q^2)$, cf. Chapter 10, have been used in our present approach which follow from constituent quark model constraints [94, 95]. These latter constraints allow to express \bar{q}^π and g^π entirely in terms of the experimentally known pionic valence density and the rather well known quark-sea and gluon distributions of the nucleon, using most recent updated valence-like input parton densities of the nucleon. Since more recent DIS small- x measurements at HERA imply somewhat less steep sea and gluon distributions of the proton [26], the structure functions of the photon will therefore also rise less steeply in x than the previous GRV_γ [96] ones as was already discussed in the previous section and as will be seen in the figures shown below. In this way one arrives at truly parameter-free predictions for the structure functions and parton distributions of the photon.

In Figs. 11.5 and 11.6 we compare our predictions of Section 11.2, denoted by GRSc [6] and the older GRV_γ results [96] with the recent small- x OPAL measurements [98] and, for completeness, some relevant L3 data [179] are shown as well. Our parameter-free LO and NLO expectations are confirmed by the small- x OPAL data² at *all* (small and large) experimentally accessible scales Q^2 . This is in contrast to the GRV_γ and SaS results

²Note that the new OPAL data [98] at $Q^2 = 1.9$ and 3.7 GeV^2 supersede the older OPAL data shown in Fig. 11.1 at $Q^2 = 1.86$ and 3.76 GeV^2 , see [98].

which at LO are somewhat below the data at small Q^2 in Fig. 11.5 and seem to increase too strongly at small x in NLO, in particular at larger values of Q^2 as shown in Fig. 11.6. The main reason for this latter stronger and steeper x -dependence in LO and NLO derives from the assumed vanishing (pionic) quark-sea input at $Q_0^2 = \mu_{\text{LO,NLO}}^2$ for the anti(quark) distributions of the photon as well as from relating the hadronic gluon input of the photon directly to its (pionic) valence distribution [96, 141]. This is in contrast to the more realistic (input) boundary conditions employed here.

Clearly these small- x measurements imply that the photon must contain [98] a dominant hadron-like component at low x , since the simple direct ‘box’ cross section (based on the subprocess $\gamma^*(Q^2)\gamma \rightarrow q\bar{q}$) yields $F_{2,\text{box}}^\gamma \rightarrow 0$ as $x \rightarrow 0$, in contrast to the data for $x < 0.1$ in Figs. 11.5 and 11.6. The QCD RG-improved parton distributions of the photon are thus essential for understanding the data on $F_2^\gamma(x, Q^2)$, with its dominant contributions deriving from $q^\gamma(x, Q^2) = \bar{q}^\gamma(x, Q^2)$. It would be also interesting and important to extend present measurements [89, 90, 180, 181] of the gluon distribution of the photon, $g^\gamma(x, Q^2)$, *below* the presently measured region $0.1 \lesssim x < 1$ where similarly $g^\gamma(x < 0.1, Q^2)$ is expected to be also somewhat flatter, see Fig. 11.4, in the small- x region than previously anticipated [96].

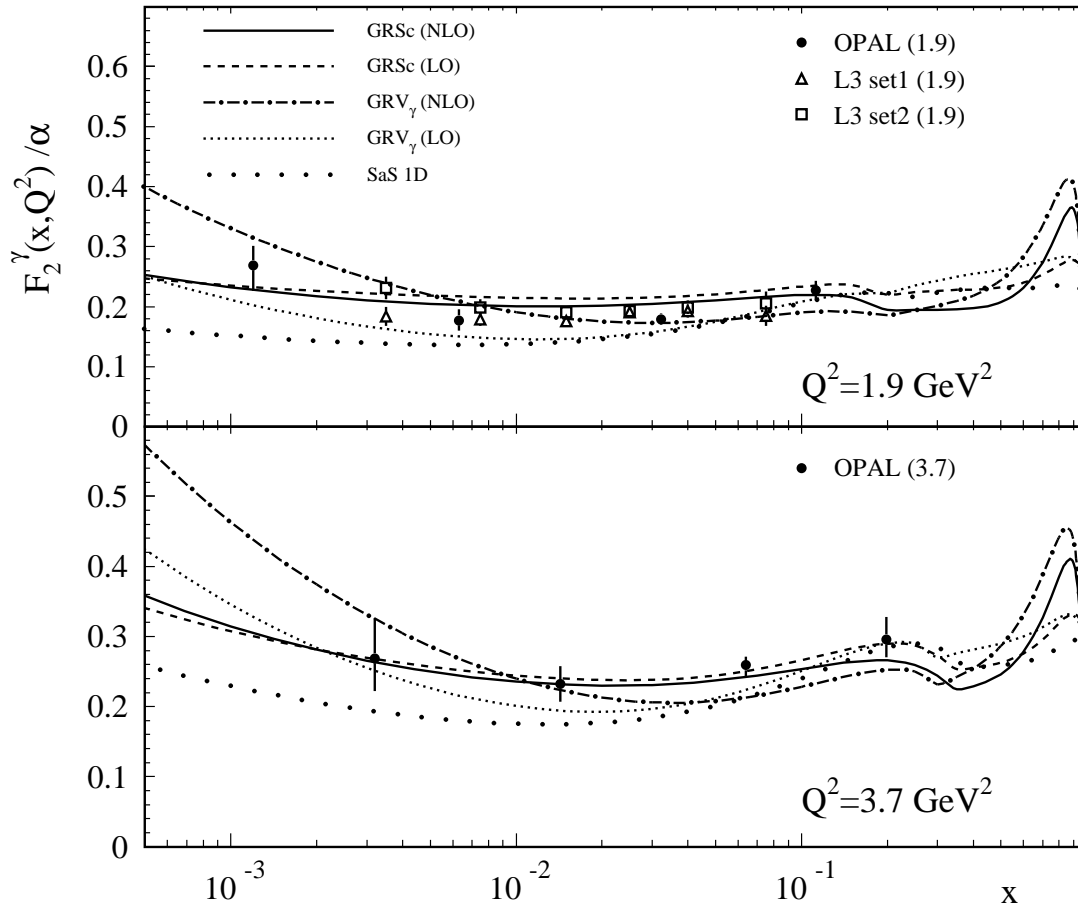


Figure 11.5: Comparison of our parameter-free predictions from Sec. 11.2 denoted by GRSc [6], the previous GRV $_\gamma$ [96] and SaS [97] results for $F_2^\gamma(x, Q^2)$ with the recent OPAL (1.9 GeV 2) small- x measurements [98] at two fixed lower scales Q^2 . Some relevant L3 data [179] are displayed as well.

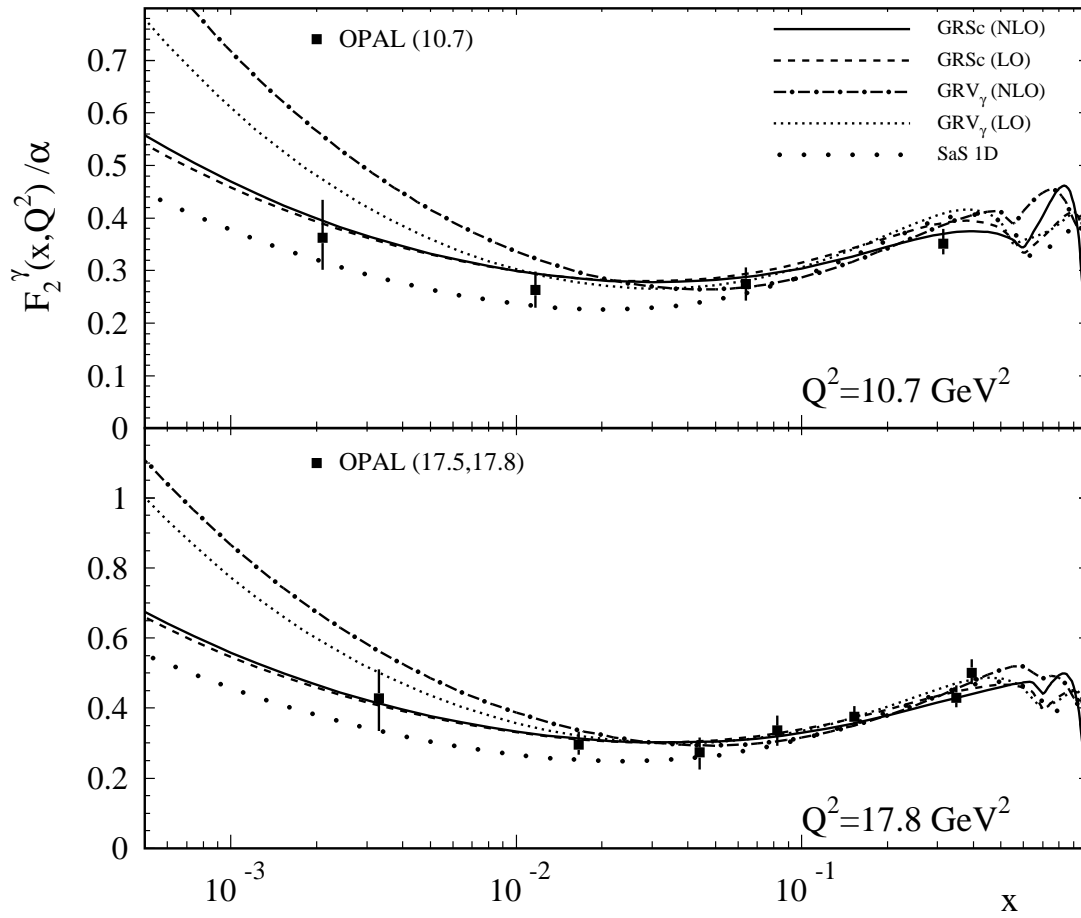


Figure 11.6: As in Fig. 11.5 but at two fixed scales Q^2 . The recent OPAL small- x data are taken from Ref. [98].

11.4 The Parton Content of Virtual Photons

Next we turn to the somewhat more speculative concept and models of ‘resolved’ virtual photons ($P^2 \neq 0$). As motivated in Chap. 9 the dependence on the target virtuality P^2 will be entirely taken care of by the boundary conditions whereas the partons will be treated as if they were on-shell. Of course, this is quite familiar for the quarks and gluons, however, the latter rule also refers to the photon-parton $\Gamma^{\gamma(P^2)}(x, Q^2)$ in the target photon, i.e., the ‘direct’ subprocesses, e.g., $\gamma^*(Q^2)\Gamma^{\gamma(P^2)} \rightarrow q\bar{q}$ have to be calculated with $P^2 = 0$ (cf. rule (ii) in [6]). Thus we can implement the same DIS_γ factorization scheme as for real photons in Eq. (9.9), and the structure function $F_2^{\gamma(P^2)}(x, Q^2)$ of a transverse virtual target photon becomes formally very similar to Eq. (11.7):

$$\begin{aligned} \frac{1}{x} F_2^{\gamma(P^2)}(x, Q^2) &= 2 \sum_{q=u,d,s} e_q^2 \left\{ q^{\gamma(P^2)}(x, Q^2) + \frac{\alpha_s(Q^2)}{2\pi} \left[C_{q,2} \otimes q^{\gamma(P^2)} + C_{g,2} \otimes g^{\gamma(P^2)} \right] \right\} \\ &\quad + \frac{1}{x} F_{2,c}^\gamma(x, Q^2) + \frac{1}{x} F_{2,c}^{g^{\gamma(P^2)}}(x, Q^2) \end{aligned} \quad (11.11)$$

with $C_{q,2}(x), C_{g,2}(x)$ given in (9.5). The ‘direct’ heavy (charm) quark contribution is given by Eq. (9.13) as for real photons and the ‘resolved’ charm contribution $F_{2,c}^{g^{\gamma(P^2)}}$ is as in Eq. (9.14) with the gluon distribution $g^\gamma(z, \mu_F^2) \rightarrow g^{\gamma(P^2)}(z, \mu_F^2)$.

It is physically compelling to expect a smooth behavior of the observable structure function in Eq. (11.11) with respect to P^2 . Especially, in the real photon limit Eq. (11.7) has to be recovered imposing the condition $f^{\gamma(P^2)}(x, Q^2) \rightarrow f^\gamma(x, Q^2)$ as $P^2 \rightarrow 0$ for the parton distributions. Note that this requirement is automatically satisfied as soon as it has been implemented at the input scale Q_0^2 since the PDFs are governed by the *same* evolution equations which is a consequence of our unified approach.

11.4.1 Boundary Conditions

The above smoothness requirements are fulfilled by the following boundary conditions for $f^{\gamma(P^2)}$, cf. Eq. (11.5),

$$f^{\gamma(P^2)}(x, Q^2 = \tilde{P}^2) = f_{\text{had}}^{\gamma(P^2)}(x, \tilde{P}^2) = \eta(P^2) f_{\text{had}}^\gamma(x, \tilde{P}^2) \quad (11.12)$$

in LO *as well as* in NLO. Here $\tilde{P}^2 = \max(P^2, \mu^2)$ as dictated by continuity in P^2 [111] and $\eta(P^2) = (1 + P^2/m_\rho^2)^{-2}$ is a dipole suppression factor with $m_\rho = 0.59 \text{ GeV}$. The scale \tilde{P}^2

is dictated not only by the above mentioned continuity requirement, but also by the fact that the hadronic component of $f^{\gamma(P^2)}(x, Q^2)$ is probed at the scale $Q^2 = \tilde{P}^2$ [97, 111, 154] where the pointlike component vanishes by definition. The boundary condition in Eq. (11.12) guarantees, as should be evident, a far better perturbative stability as compared to the situation in [111] where the NLO input differed drastically from its LO counterpart (cf. Eq. (8) in Ref. [111]).

The evolution to $Q^2 > \tilde{P}^2$ is now analogous to the case of real photons in the previous section and the general solution for the resulting parton distributions is similar to the one in Eq. (11.4) and Eq. (11.5),

$$\begin{aligned} f^{\gamma(P^2)}(x, Q^2) &= f_{\text{pl}}^{\gamma(P^2)}(x, Q^2) + f_{\text{had}}^{\gamma(P^2)}(x, Q^2) \\ &= f_{\text{pl}}^{\gamma(P^2)}(x, Q^2) + \eta(P^2) \alpha \left[G_f^2 f^\pi(x, Q^2) + \delta_f \frac{1}{2} (G_u^2 - G_d^2) s^\pi(x, Q^2) \right] \end{aligned} \quad (11.13)$$

with δ_f as in Eq. (11.5) and where $f_{\text{had}}^{\gamma(P^2)}$ refers again to the solution of the homogeneous RG evolution equations, being driven by the hadronic input in (11.12), which is explicitly given by Eq. (9.25). Its parametrization is fixed by the available parametrization for $f^\pi(x, Q^2)$ in App. D.1. The inhomogeneous ‘pointlike’ solution in (11.13) is explicitly given by Eq. (9.24) where $L = \alpha_s(Q^2)/\alpha_s(\tilde{P}^2)$. A parametrization of $f_{\text{pl}}^{\gamma(P^2)}(x, Q^2)$ in LO is thus easily obtained from the one for the real photon $f_{\text{pl}}^\gamma(x, Q^2)$ in (11.5) in terms of $\ln L^{-1} = \ln [\alpha_s(\mu^2)/\alpha_s(Q^2)]$, where now $\alpha_s(\mu^2)$ has simply to be replaced by $\alpha_s(\tilde{P}^2)$ as described in detail in App. D.2. Furthermore, since our NLO predictions for $f^{\gamma(P^2)}(x, Q^2)$ turn out to be rather similar to the LO ones, as will be shown below, the simple analytic LO parametrizations for $f^{\gamma(P^2)}(x, Q^2)$ can be used for NLO calculations as well. This is certainly sufficiently accurate and reliable in view of additional model ambiguities inherent in the parton distributions of virtual photons.

It should be emphasized that the RG resummed results in (11.13) are relevant whenever $P^2 \ll Q^2$, typically [111, 162] $P^2 \simeq \frac{1}{10} Q^2$, so as to suppress power-like (possibly higher twist) terms $(P^2/Q^2)^n$ which would spoil the dominance of the resummed logarithmic contributions. For P^2 approaching Q^2 , the $e^+e^- \rightarrow e^+e^-X$ reaction, for example, should be simply described by the full fixed order box $\gamma^*(Q^2)\gamma^*(P^2) \rightarrow q\bar{q}$ keeping all $(P^2/Q^2)^n$ terms (cf. Chap. 8). A calculation of the full perturbative $\mathcal{O}(\alpha_s)$ corrections to this virtual box [108] will offer the possibility to determine reliably at what values of P^2 (and possibly x) this $\mathcal{O}(\alpha_s)$ corrected virtual box becomes the more appropriate and correct description. Similar remarks hold for a DIS process $ep \rightarrow eX$, i.e. $\gamma(P^2)p \rightarrow X$,

where $\mathcal{O}(\alpha_s)$ corrections to pointlike virtual $\gamma(P^2)$ -parton subprocesses have to be analyzed in detail in order to decide at what P^2 these pointlike expressions become the more appropriate description and the virtual photonic parton distributions (i.e., resummations) become irrelevant.

Our unified approach implies that the ‘direct’ photon contribution to any process whatsoever should always be calculated as if this photon is real apart from the fact that its flux should be evaluated according to Eq. (7.37) with $P^2 \neq 0$ [155, 162, 163]. This differs from the somewhat inconsistent procedure adopted by the HERA–H1 collaboration [157–161] where exact $eq \rightarrow eqg$ and $eg \rightarrow eq\bar{q}$ matrix elements were used for the direct photon contribution to the dijet cross section. As long as $P^2 \lesssim \frac{1}{10} Q^2$, the exact treatment of matrix elements, however, should not differ too much [164] from the more appropriate treatment described above. To conclude let us stress that our unified approach, as illustrated by the foregoing examples, is not a free option but a *necessary consistency condition* for introducing the concept of the resolved parton content of the virtual photon as an *alternative* to a non-resummed fixed order perturbative analysis at $P^2 \neq 0$. This consistency requirement is related to the fact that all the resolved contributions due to $f^{\gamma(P^2)}(x, Q^2)$ are calculated (evolved) as if these partons are massless [7 – 11] (i.e. employing photon splitting functions for real photons, etc.) in spite of the fact that their actual virtuality is given by $P^2 \neq 0$. Thus the direct photon contribution should obviously be also treated accordingly.

11.4.2 Quantitative Results

Now we turn to our quantitative predictions and we first present in Fig. 11.7 detailed predictions for $F_2^{\gamma(P^2)}(x, Q^2)$ for various virtualities P^2 and scales Q^2 . Since the ‘pointlike’ component in (11.13) is uniquely calculable perturbatively, a detailed measurement of the x and P^2 dependence at various fixed values of Q^2 , as shown in Fig. 11.7, would shed light on the theoretically more speculative and far less understood nonperturbative ‘hadronic’ contribution in Eq. (11.13) and eventually establish the absolute perturbative predictions. Our LO and NLO predictions in Fig. 11.7 show a remarkable perturbative stability throughout the whole x -region shown, except perhaps for $P^2 \gg 1 \text{ GeV}^2$ where the perturbatively very stable [5, 116] ‘hadronic’ component in (11.13) becomes strongly suppressed with respect to the ‘pointlike’ solution which is less stable in the small x region, $x < 10^{-2}$, as is evident from the right hand side of Fig. 11.7.

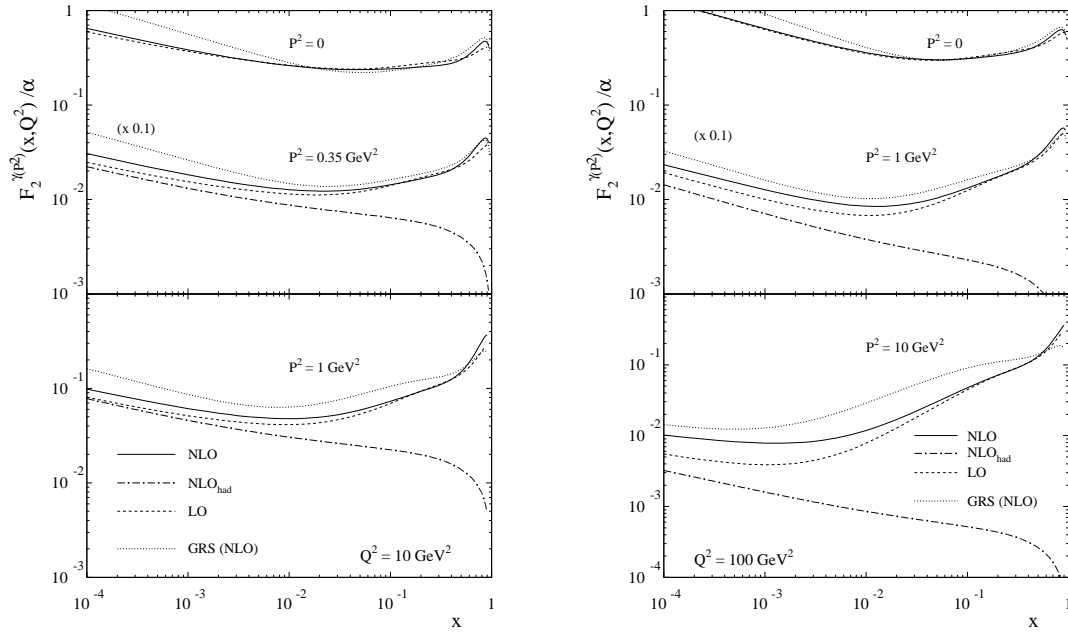


Figure 11.7: LO and NLO predictions for the x dependence of the virtual photon structure function $F_2^{\gamma(P^2)}$ at $Q^2 = 10$ and 100 GeV^2 and various fixed values of $P^2 \ll Q^2$, neglecting any heavy quark contribution. For comparison we also show the NLO Glück–Reya–Stratmann (GRS) [111] results as well as the predictions for a real ($P^2 = 0$) photon. Notice that the dotted curve for $P^2 = 0$ referred to as GRS obviously coincides with the GRV_γ result [96, 112]. The results have been multiplied by the number indicated in brackets.

The individual LO and NLO parton distributions of the virtual photon at $Q^2 = 10 \text{ GeV}^2$ are shown in Fig. 11.8 where they are compared with the ones of Glück, Reya and Stratmann (GRS) [111]. The LO SaS expectations [97] are compared with our LO predictions in Fig. 11.9.

In Fig. 11.10 we show our predictions for $xu^{\gamma(P^2)}(x, Q^2)$ and $xg^{\gamma(P^2)}(x, Q^2)$ with particular emphasis on the very small x region. For comparison we also show the results for a real ($P^2 = 0$) photon. Plotting the ‘hadronic’ component in (11.13) separately in the upper two panels of Fig. 11.10 demonstrates that the perturbative ‘pointlike’ component in (11.13) dominates for $x > 10^{-2}$. In the lower two panels of Fig. 11.10, at $P^2 = 5, 10 \text{ GeV}^2$, the hadronic part is nearly vanishing even at small x [$\eta(P^2(\text{GeV}^2) = 5, 10) = 0.01, 0.003$]. Furthermore the expected perturbative stability of our present LO and NLO predictions is fulfilled. This is in contrast to the GRS results which are unstable [111] throughout the whole x -region for $P^2 \gtrsim 1 \text{ GeV}^2$, as illustrated in the lower half of Fig. 11.10 at

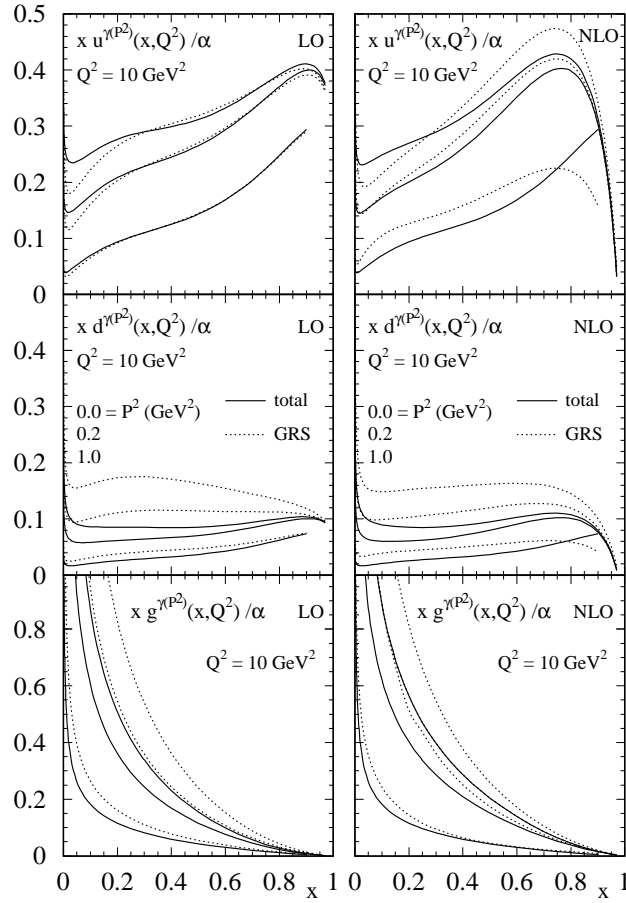


Figure 11.8: Comparison of our predicted LO and NLO(DIS_γ) distributions of the virtual photon at $Q^2 = 10 \text{ GeV}^2$ and various fixed values of $P^2 \ll Q^2$ with the GRS densities [111]. The curves refer from top to bottom to $P^2 = 0, 0.2$ and 1 GeV^2 , respectively. The results for the real photon ($P^2 = 0$) are very similar to the ones in Fig. 11.2 where the GRV_γ curves practically coincide with GRS.

$Q^2 = 100 \text{ GeV}^2$, due to the very different perturbative (box) input in LO and NLO [111]. In general, however, as soon as the perturbatively very stable ‘hadronic’ component in (11.13) becomes suppressed for $P^2 \gg 1 \text{ GeV}^2$, the remaining perturbatively less stable ‘pointlike’ component destabilizes the total results for $q^{\gamma(P^2)}(x, Q^2)$ in the very small x region, $x \lesssim 10^{-3}$, as can be seen in Fig. 11.10 for $u^{\gamma(P^2)}$ at $Q^2 = 100 \text{ GeV}^2$ (cf. Fig. 11.7).

Finally in Fig. 11.11 we confront our LO predictions for $f^{\gamma(P^2)}(x, Q^2)$ with the effective parton density

$$\tilde{f}^{\gamma(P^2)}(x, Q^2) = \sum_{q=u,d,s} \left(q^{\gamma(P^2)} + \bar{q}^{\gamma(P^2)} \right) + \frac{9}{4} g^{\gamma(P^2)} \quad (11.14)$$

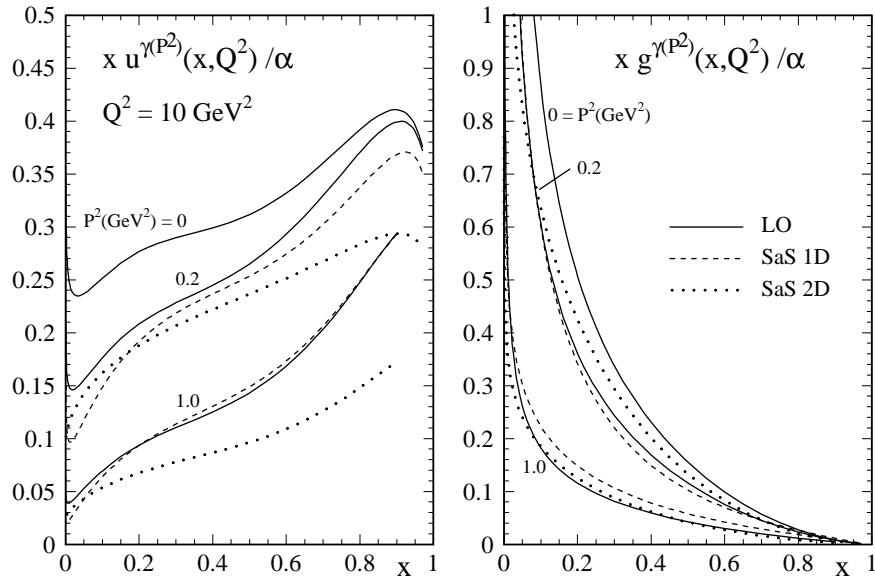


Figure 11.9: Our LO distributions as in Fig. 11.8 compared with the ones of SaS [97].

extracted in LO from DIS dijet data by the HERA–H1 collaboration [157–161] very recently. The predicted dependence on the photon’s virtuality P^2 at the scale $Q^2 \equiv (p_T^{\text{jett}})^2 = 85 \text{ GeV}^2$ agrees reasonably well with the measurements in the relevant kinematic region $P^2 \ll Q^2$. This is also the case at other scales $Q^2 \equiv (p_T^{\text{jett}})^2$ and fixed values of x [157–161] not shown in Fig. 11.11. As discussed above, it should be kept in mind, however, that for larger values of P^2 approaching Q^2 , which refer to the dashed curves in Fig. 11.11, the whole concept of RG resummed parton distributions of virtual photons is *not* appropriate anymore. Since the resolved contributions of a virtual photon with virtuality as large as $P^2 = 10 - 15 \text{ GeV}^2$ are by a factor of about 10 smaller than the ones of a real ($P^2 = 0$) photon, it is reasonable to conclude from Fig. 11.11 that for $P^2 \gtrsim 10 \text{ GeV}^2$ the DIS $ep \rightarrow eX$ process considered is dominated by the usual direct $\gamma^* \equiv \gamma(P^2)$ exchange cross sections and *not* ‘contaminated’ anymore by resolved contributions.

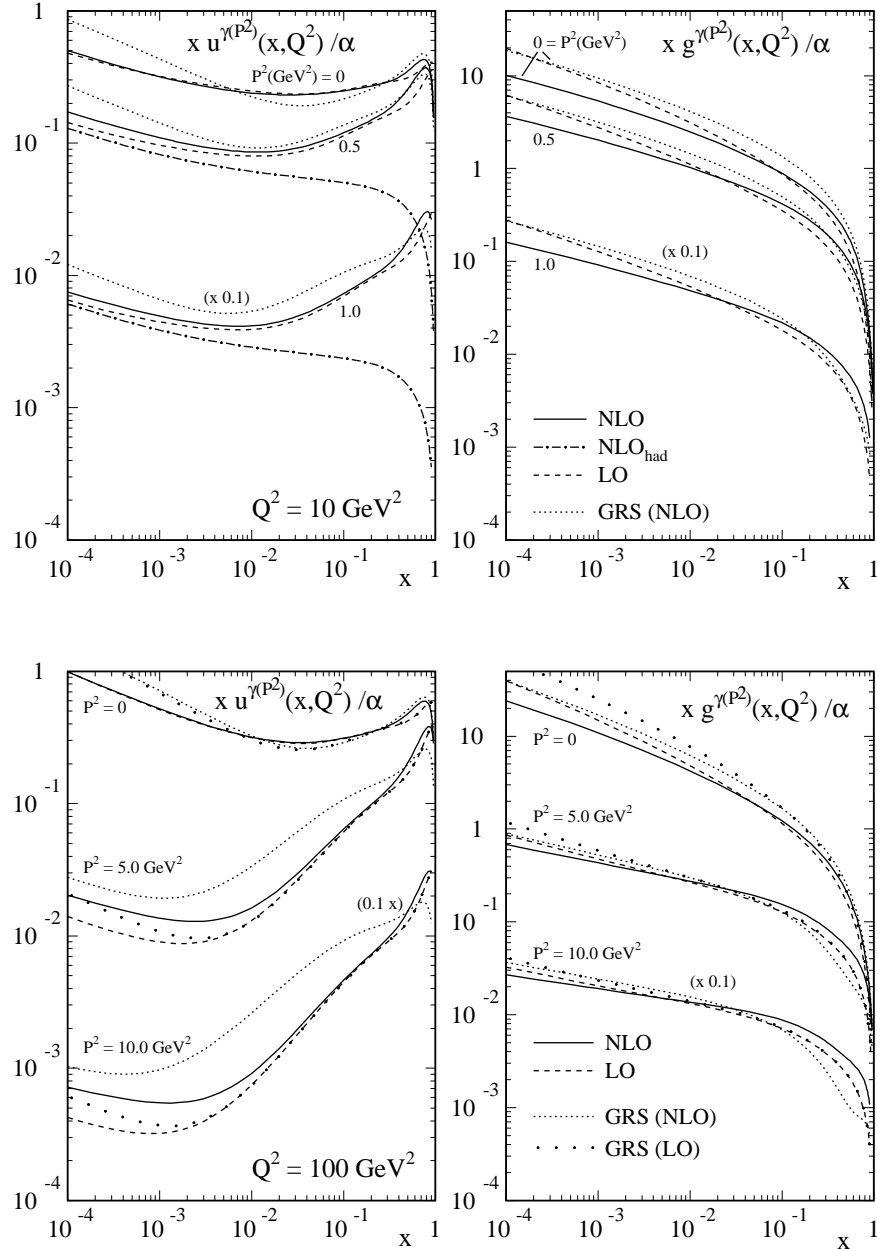


Figure 11.10: LO and NLO predictions for the up-quark and gluon distributions of a virtual photon $\gamma(P^2)$ at $Q^2 = 10$ and 100 GeV^2 . For comparison the results for the real photon ($P^2 = 0$) are shown as well. In the upper half the NLO ‘hadronic’ contribution in (11.13) is also shown separately. The GRS expectations are taken from Ref. [111]. The DIS_γ results for $u^{\gamma(P^2)}$ can be easily converted to the $\overline{\text{MS}}$ scheme with the help of Eq. (9.9), whereas $g^{\gamma(P^2)}$ remains the same in both schemes. The results have been multiplied by the numbers indicated in brackets.

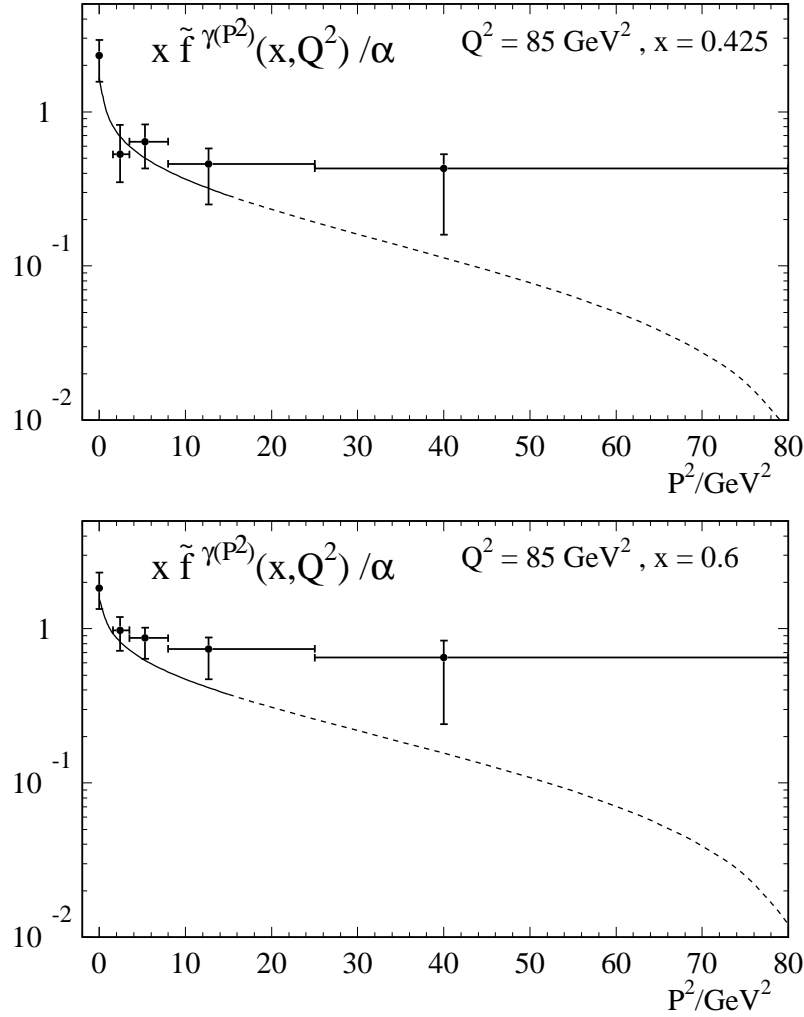


Figure 11.11: Predictions for the LO effective parton density $x \tilde{f}^{\gamma(P^2)}(x, Q^2)$, defined in Eq. (11.14), at the scale $Q^2 \equiv (p_T^{\text{jet}})^2 = 85 \text{ GeV}^2$ and at two fixed values of x . The H1 data [157–161] have been extracted from DIS ep dijet production. The solid curves refer to our predictions in the theoretically legitimate region $P^2 \ll Q^2 \equiv (p_T^{\text{jet}})^2$, whereas the dashed curves extend into the kinematic region of larger P^2 approaching Q^2 where the concept of parton distributions of virtual photons is not valid anymore (see text).

11.5 Summary and Conclusions

The main purpose of the present chapter was to formulate a consistent set of boundary conditions which allow for a perturbatively stable LO and NLO calculation of the photonic parton distributions $f^{\gamma(P^2)}(x, Q^2)$ as well as for a smooth transition to the parton densities of a real ($P^2 = 0$) photon. Employing the pionic distributions $f^\pi(x, Q^2)$ of Chapter 10, required for describing, via VMD, the nonpointlike hadronic components of a photon, we arrive at essentially parameter-free predictions for $f^{\gamma(P^2)}(x, Q^2)$ which are furthermore in good agreement with all present measurements of the structure function $F_2^\gamma(x, Q^2)$ of real photons $\gamma \equiv \gamma(P^2 = 0)$. It should be noted that the experimentally almost unconstrained pionic gluon and sea distributions, $g^\pi(x, Q^2)$ and $\bar{q}^\pi(x, Q^2)$, have been uniquely derived from the experimentally rather well known pionic valence density $v^\pi(x, Q^2)$ and the (recently updated [26] dynamical) parton distributions of the proton. We have furthermore implemented these hadronic components by using a VMD ansatz for a coherent superposition of vector mesons which maximally enhances the contributions of the up-quarks to F_2^γ as favored by all present data. Since these hadronic contributions are generated from the valence-like input parton distributions at the universal target-mass independent low resolution scale $Q_0^2 = \mu^2 \simeq 0.3 \text{ GeV}^2$, we arrive, at least for real ($P^2 = 0$) photons, at unique small- x predictions for $x \lesssim 10^{-2}$ at $Q^2 > \mu^2$ which are of purely dynamical origin, as in the case of hadrons. As has been demonstrated in Sec. 11.3 these small- x predictions are in perfect agreement with recent small- x measurements of the photon structure function $F_2^\gamma(x, Q^2)$ [98] at all presently accessible values of Q^2 . Furthermore, since our universal input scale μ^2 fixes also uniquely the perturbative pointlike part of the photonic parton distributions, which dominates for $x \gtrsim 0.1$, the large- x behavior of photonic structure functions is unambiguously predicted as well.

Our expectations for the parton content of virtual ($P^2 \neq 0$) photons are clearly more speculative, depending on how one models the hadronic component (input) of a virtual photon. The latter is usually assumed to be similar to the VMD input for a real photon, times a dipole suppression factor which derives from an effective vector-meson P^2 -propagator, cf. Eq. (11.12). Whenever a virtual photon is probed at a scale $Q^2 \gg P^2$, with its virtuality being entirely taken care of by the (transverse) equivalent photon flux factor and the boundary conditions for the photonic parton distributions, all cross sections of partonic subprocesses (resolved *and* direct) should be calculated as if $P^2 = 0$. In

other words, the treatment and expressions for $f^{\gamma(P^2)}(x, Q^2)$ as *on-shell* transverse partons obeying the usual RG Q^2 -evolution equations (with the usual splitting functions of *real* photons, etc.) dictate an identification of the relevant sub-cross-sections $f^{\gamma(P^2)}X \rightarrow X'$ with that of the *real* photon, $\hat{\sigma}(f^{\gamma(P^2)}X \rightarrow X') = \hat{\sigma}(f^\gamma X \rightarrow X')$. In particular, the calculation of $F_2^{\gamma(P^2)}(x, Q^2)$ requires the *same* photonic Wilson coefficient $C_\gamma(x)$ as for $P^2 = 0$. This allows to formulate similar boundary conditions in LO and NLO which give rise to perturbatively stable parton distributions, cross sections (i.e. also structure functions) of virtual photons $\gamma(P^2)$ as long as they are probed at scales $Q^2 \gg P^2$ where $Q^2 \equiv 4m_c^2, \left(p_T^{\text{jet}}\right)^2$, etc., and typically $P^2 \lesssim \frac{1}{10} Q^2$. It should be emphasized that only in this latter kinematic range $P^2 \ll Q^2$ is the whole concept of RG resummed parton distributions of (resolved) virtual photons appropriate and relevant. Parton distributions of virtual photons extracted recently from DIS ep dijet data are in good agreement with our (parameter-free) predictions.

Finally, we present simple analytic parametrizations of our predicted LO and NLO(DIS $_\gamma$) parton distributions of real photons. From these LO parametrizations one can easily obtain also the ones for a virtual photon which, within sufficient accuracy, may also be used in NLO. Our NLO(DIS $_\gamma$) parametrizations of the parton densities of the real photon can be easily transformed to the $\overline{\text{MS}}$ scheme according to Eq. (9.9) which might be relevant for future NLO analyses of resolved photon contributions to hard processes where most NLO subprocesses have so far been calculated in the $\overline{\text{MS}}$ scheme.

A FORTRAN package containing our most recent parametrizations can be obtained by electronic mail on request.

Chapter 12

Has the QCD RG–Improved Parton Content of Virtual Photons been Observed?

It is demonstrated that present e^+e^- and DIS ep data on the structure of the virtual photon can be understood entirely in terms of the standard ‘naive’ quark–parton model box approach. Thus the QCD renormalization group (RG) improved parton distributions of virtual photons, in particular their gluonic component, have not yet been observed. The appropriate kinematical regions for their future observation are pointed out as well as suitable measurements which may demonstrate their relevance. The results presented in this chapter are taken from [8].

12.1 Introduction

Recent measurements and experimental studies of dijet events in deep inelastic ep [161] and of double-tagged e^+e^- [105] reactions have indicated a necessity for assigning a (QCD resummed) parton content of virtual photons $\gamma(P^2)$ as suggested and predicted theoretically [6, 97, 104, 111, 125–127, 153–155]. In particular the DIS dijet production data [161] appear to imply a sizeable gluon component $g^{\gamma(P^2)}(x, Q^2)$ in the derived effective parton density of the virtual photon, where Q^2 refers to the hadronic scale of the process, $Q \sim p_T^{\text{jet}}$, or to the virtuality of the probe photon $\gamma^*(Q^2)$ which probes the virtual target photon $\gamma(P^2)$ in $e^+e^- \rightarrow e^+e^-X$. It is the main purpose of this chapter to demonstrate that this is *not* the case and that all present data on virtual photons can be explained entirely in

terms of the conventional QED doubly virtual box contribution $\gamma^*(Q^2)\gamma^*(P^2) \rightarrow q\bar{q}$ in fixed order perturbation theory –sometimes also referred to as the quark–parton model (QPM).

This is of course in contrast to the well known case of a real photon $\gamma \equiv \gamma(P^2 \equiv 0)$ whose (anti–)quark and gluon content has been already experimentally established (for recent reviews see [89, 90]) which result mainly from resummations (inhomogeneous evolutions) of the pointlike mass singularities proportional to $\ln Q^2/m_q^2$ occurring in the box diagram of $\gamma^*(Q^2)\gamma \rightarrow q\bar{q}$ for the light $q = u, d, s$ quarks. This is in contrast to a virtual photon target where $\gamma^*(Q^2)\gamma^*(P^2) \rightarrow q\bar{q}$ does *not* give rise to collinear (mass) singularities but instead just to finite contributions proportional to $\ln Q^2/P^2$ which a priori need not be resummed to all orders in QCD.

This chapter is organized as follows:

In Sec. 12.2 we compare fixed order box and QCD resummed expectations for the effective structure function F_{eff} with present e^+e^- data, while Sec. 12.3 contains a comparison of an effective leading order parton density for the virtual photon with DIS ep data. Suggestions of experimental signatures which can probe the QCD parton content, in particular the gluon content of virtual photons are presented in Sec. 12.4 and our conclusions are finally drawn in Section 12.5.

12.2 RG–Improved Parton Model Expectations for the Effective Structure Function F_{eff}

As promised in Chap. 8 we shall now turn to a quantitative study of the various QED–box and QCD Q^2 –evoluted structure function expectations for a virtual photon target and confront them with all presently available e^+e^- data of PLUTO [106] and the recent one of LEP–L3 [105]. The ‘asymptotic’ and ‘full’ box results for F_{eff} have already been presented in Chap. 8 and details of their calculation can be found there. The QCD resummed expectations for F_{eff} according to our model in the previous chapter are given by

$$F_{\text{eff}}(x, Q^2, P^2) = F_2^{\gamma(P^2)}(x, Q^2) \quad (12.1)$$

since we neglect any effects due to longitudinal target photons in our approach [6].

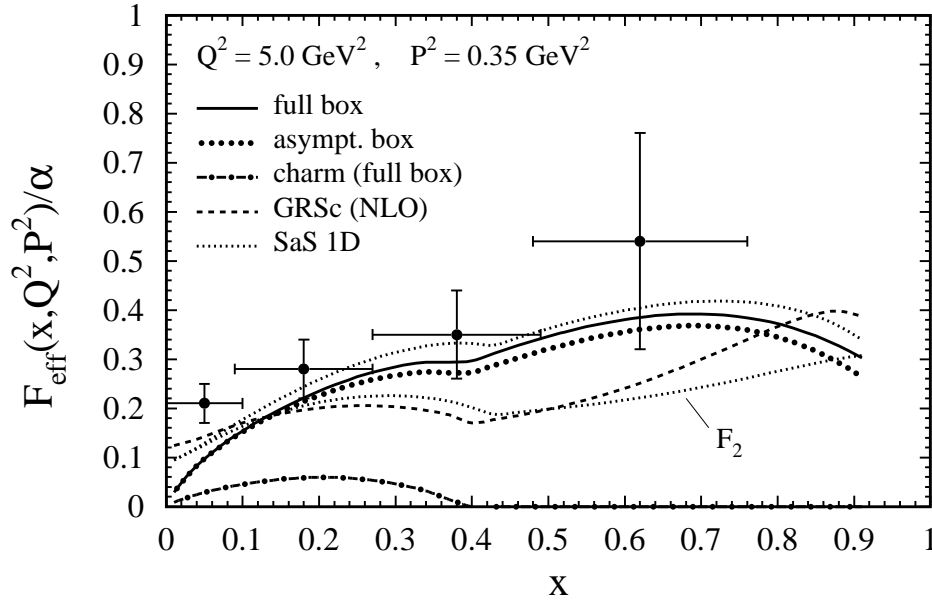


Figure 12.1: Predictions for F_{eff} as defined in (8.14). The box results are as in Fig. 8.3. The QCD resummed NLO expectations of GRSc [6] for F_2 in (12.1) turn out to be similar to the LO ones [6]. Also shown are the LO-resummed results of SaS 1D [97] for F_2 and $F_{\text{eff}} = F_2 + \frac{3}{2} F_{\text{LT}}$ (see text). The total charm contribution to the latter two QCD results involves also a ‘resolved’ component $F_{2,h}^{\gamma(P^2),\text{res}}(x, Q^2)$ according to Eq. (9.14) which turns out to be small as compared to the box contribution shown which dominates in the kinematic region considered. The PLUTO data are taken from [106].

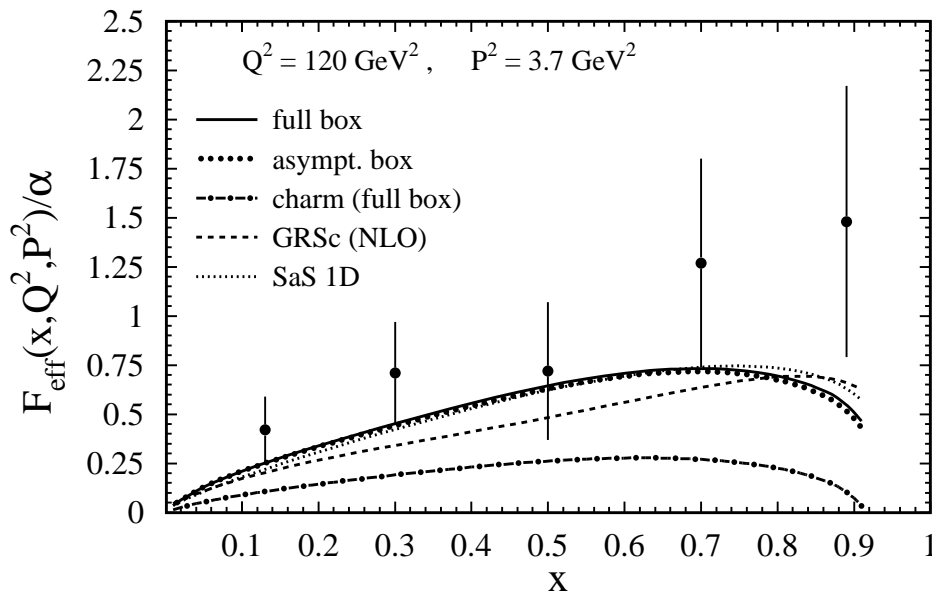


Figure 12.2: As in Fig. 12.1, but for $Q^2 = 120 \text{ GeV}^2$ and $P^2 = 3.7 \text{ GeV}^2$ appropriate for the LEP-L3 data [105].

A different approach has been suggested by Schuler and Sjöstrand [97]. Apart from using somewhat different input scales Q_0 and parton densities, the perturbatively exactly calculable box expressions for $\Lambda^2 \ll P^2 \ll Q^2$ (cf. App. C.2) are, together with their LO-QCD Q^2 -evolutions, extrapolated to the case of real photons $P^2 = 0$ by employing some dispersion-integral-like relations. These link perturbative and non-perturbative contributions and allow a smooth limit $P^2 \rightarrow 0$. (Note, however, that the LO Q^2 -evolutions are performed by using again the splitting functions of real photons and on-shell partons.) Since one works here explicitly with virtual ($P^2 \neq 0$) expressions, the longitudinal contributions of the virtual photon target should be also taken into account when calculating $F_{\text{eff}} = F_2 + \frac{3}{2}xF_{\text{LT}}$ with $F_{ab} \equiv Q^2/(4\pi^2\alpha)(x\bar{\beta})^{-1}\sigma_{ab}$ ($a = (\text{L}, \text{T})$, $b = (\text{L}, \text{T})$) and where σ_{ab} is given in Eq. (8.11), as described for example in [111], which is in contrast to our approach in (12.1).¹

¹In an alternative approach [130, 132] one may consider the longitudinal component of the virtual photon target $\gamma_{\text{L}}(P^2)$ to possess, like the transverse component, a universal process independent hadronic content obtained radiatively via the standard homogeneous (Altarelli-Parisi) Q^2 -evolution equations with the boundary conditions for the pointlike component at $Q^2 = P^2$ given in Eq. (9.55). We have checked that the predictions for $F_{\text{eff}}(x, Q^2, P^2)$ obtained in this approach differ only slightly (typically about 10% or less) from those of the standard fixed order perturbative approach at presently relevant kinematical regions ($P^2 \lesssim \frac{1}{10}Q^2$, $x \gtrsim 0.05$) due to the smallness of F_{TL}^ℓ relative to F_{TT}^ℓ deriving from σ_{TL}^ℓ and σ_{TT}^ℓ , respectively, in (8.17).

Despite the limited statistics of present data the box predictions for F_{eff} in (8.14) shown in Figs. 12.1 and 12.2 appear to be in even better agreement with present measurements than the QCD resummed expectations of SaS [97] and GRSc [6]. Typical QCD effects like the increase in the small- x region in Fig. 12.1, being partly caused by the presence of a finite gluon content $g^{\gamma(P^2)}(x, Q^2)$, cannot be delineated with the present poor statistics data.

These results clearly demonstrate that the naive QPM predictions derived from the doubly virtual box $\gamma^*(Q^2)\gamma^*(P^2) \rightarrow q\bar{q}$ fully reproduce all e^+e^- data on the structure of virtual photons $\gamma(P^2)$. In other words, there is *no* sign of a QCD resummed parton content in virtual photons in present data, in particular of a finite gluon content $g^{\gamma(P^2)}(x, Q^2)$ which is absent in the ‘naive’ box (QPM) approach.

Characteristic possible signatures for QCD effects which are caused by the presence of a finite and dominant gluon component $g^{\gamma(P^2)}$ will be discussed in Sec. 12.4.

12.3 Comparison of Theoretical Expectations with DIS ep Data and Effective Quark Distributions of Virtual Photons

In order to extract the parton densities of virtual photons from DIS ep dijet data, the H1 collaboration [161] has adopted the ‘single effective subprocess approximation’ [183] which exploits the fact that the dominant contributions to the cross section in LO-QCD comes from the $2 \rightarrow 2$ parton-parton hard scattering subprocesses that have similar shapes and thus differ mainly by their associated color factors. Therefore the sum over the partonic subprocesses can be replaced by a single effective subprocess cross section and effective parton densities for the virtual photon given by

$$\tilde{f}^{\gamma(P^2)}(x, Q^2) = \sum_{q=u, d, s} \left[q^{\gamma(P^2)}(x, Q^2) + \bar{q}^{\gamma(P^2)}(x, Q^2) \right] + \frac{9}{4} g^{\gamma(P^2)}(x, Q^2) \quad (12.2)$$

with a similar relation for the proton $\tilde{f}^p(x, Q^2)$ which is assumed to be known. It should be emphasized that such an effective procedure does not hold in NLO where all additional (very different) $2 \rightarrow 3$ subprocesses contribute [164]. This NLO analysis affords therefore a confrontation with more detailed data on the triple-differential dijet cross section as compared to presently available data [161] which are not yet sufficient for examining the

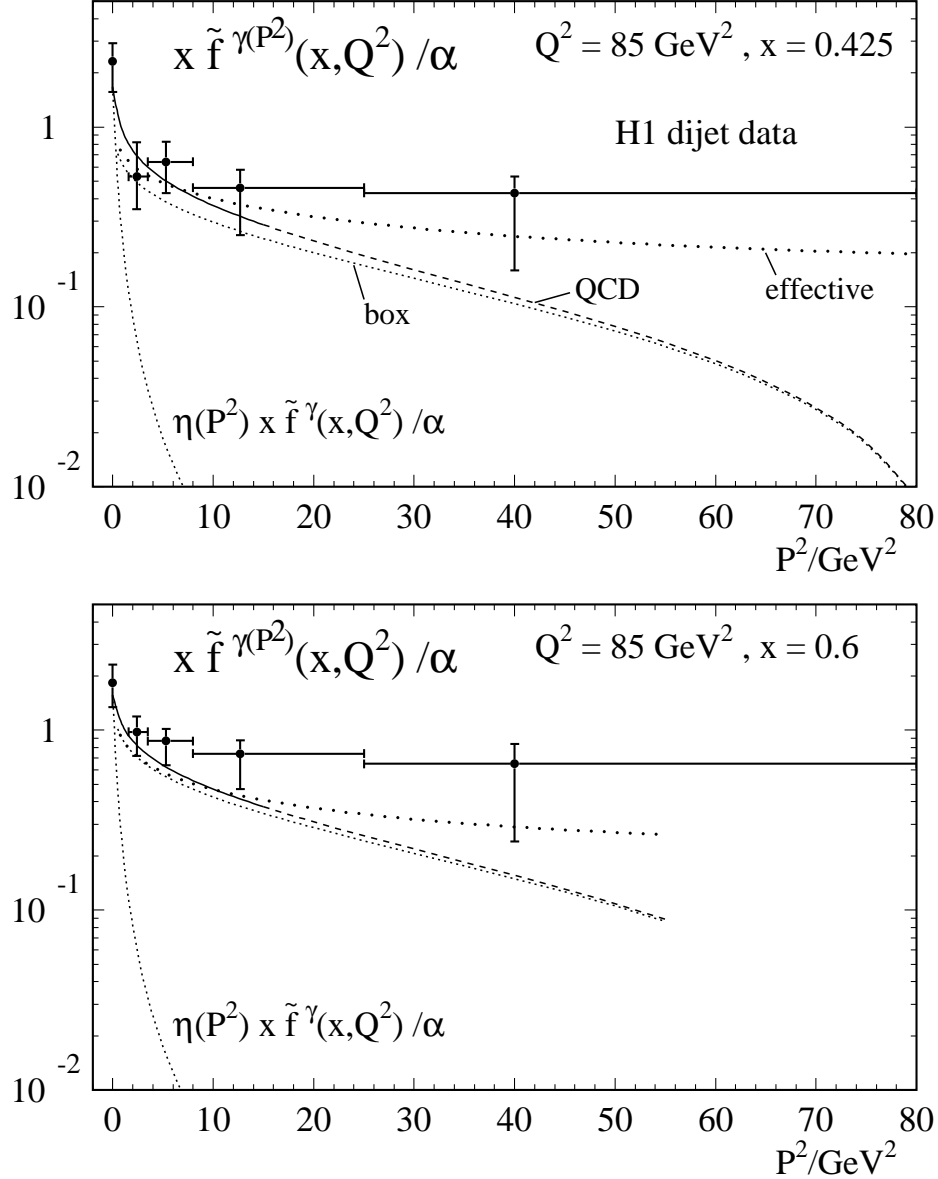


Figure 12.3: Predictions for the effective parton density defined in Eq. (12.2). The ‘box’ results refer to the universal $q_{\text{box}}^{\gamma(P^2)}$ in (12.3), and the ‘effective’ ones to $q_{\text{eff}}^{\gamma(P^2)}$ as defined in (12.4) as derived from the full box expressions (8.11) including all $\mathcal{O}(P^2/Q^2)$ contributions. The LO–QCD predictions of GRSc [6] are shown by the solid curves which refer to the predictions in the theoretically legitimate region $P^2 \ll Q^2$, whereas the dashed curves extend into the kinematic region of larger P^2 approaching Q^2 where the concept of QCD–resummed parton distributions of virtual photons is not valid anymore. (Note that the results for $x = 0.6$ terminate at $P^2 \simeq 54 \text{ GeV}^2$ due to the kinematic constraint $W^2 > 0$, with W^2 being defined in (7.1), i.e. $x < (1 + P^2/Q^2)^{-1}$.) For illustration we also show the effective LO–QCD parton density \tilde{f}^{γ} of a real photon $\gamma \equiv \gamma(P^2 = 0)$ of GRSc [6] multiplied by the simple ρ –pole suppression factor $\eta(P^2)$ in (11.12) which clearly underestimates the H1–data [161].

relative contributions of $q^{\gamma(P^2)}(x, Q^2)$ and $g^{\gamma(P^2)}(x, Q^2)$. In Fig. 12.3 we compare our LO RG-resummed predictions for $\tilde{f}^{\gamma(P^2)}(x, Q^2)$ with the naive non-resummed universal (process independent) box expressions [cf. Sec. 9.3.4]

$$q_{\text{box}}^{\gamma(P^2)}(x, Q^2) = \bar{q}_{\text{box}}^{\gamma(P^2)}(x, Q^2) = 3e_q^2 \frac{\alpha}{2\pi} [x^2 + (1-x)^2] \ln \frac{Q^2}{P^2}. \quad (12.3)$$

Although the fully QCD-resummed results are sizeable and somewhat larger in the small P^2 region than the universal box expectations, present H1 data [161] at $Q^2 \equiv (p_T^{\text{jet}})^2 = 85 \text{ GeV}^2$ cannot definitely distinguish between these predictions. It should be furthermore noted that the QCD gluon contribution $g^{\gamma(P^2)}(x, Q^2)$ is suppressed at the large values of x shown in Fig. 12.3. Therefore present data [161] cannot discriminate between the finite QCD resummed component $g^{\gamma(P^2)}(x, Q^2)$ and the non-resummed $g_{\text{box}}^{\gamma(P^2)}(x, Q^2) = 0$.

It is obvious that these two results shown in Fig. 12.3 are only appropriate for virtualities $P^2 \ll Q^2$, typically $P^2 = 10$ to 20 GeV^2 at $Q^2 = 85 \text{ GeV}^2$, since $\mathcal{O}(P^2/Q^2)$ contributions are neglected in RG-resummations as well as in the definition (12.3). In order to demonstrate the importance of $\mathcal{O}(P^2/Q^2)$ power corrections in the large P^2 region let us define, generalizing the definition (9.34), some effective (anti)quark distributions as common via

$$\frac{1}{x} F_{2,\text{box}}^\ell(x, Q^2) \equiv \sum_{q=u,d,s} e_q^2 \left[q_{\text{eff}}^{\gamma(P^2)}(x, Q^2) + \bar{q}_{\text{eff}}^{\gamma(P^2)}(x, Q^2) \right] \quad (12.4)$$

where, of course, $q_{\text{eff}}^{\gamma(P^2)} = \bar{q}_{\text{eff}}^{\gamma(P^2)}$ and the full box expression for $F_{2,\text{box}}^\ell(x, Q^2)$ can be obtained from the general definition in Eq. (7.25) and the full box results in Eq. (8.11) utilizing $m \equiv m_q = 0$, i.e. $\lambda = 0$ and summing over the light quarks. The full box expressions imply again $g_{\text{eff}}^{\gamma(P^2)}(x, Q^2) = 0$ in contrast to the QCD resummed gluon distribution. The $q_{\text{eff}}^{\gamma(P^2)}$ introduced in (12.4) is, in contrast to (12.3), of course non-universal. The ‘effective’ results shown in Fig. 12.3 clearly demonstrate the importance of the $\mathcal{O}(P^2/Q^2)$ terms at larger values of $P^2 \lesssim Q^2$ which are not taken into account by the QCD resummations and by the universal box expressions in (12.3) also shown in Fig. 12.3. It is interesting that the non-universal $q_{\text{eff}}^{\gamma(P^2)}$ defined via F_2 in (12.4) describes the H1-data at large values of P^2 in Fig. 12.3 remarkably well. This may be accidental and it remains to be seen whether future LO analyses will indicate the general relevance of $q_{\text{eff}}^{\gamma(P^2)}(x, Q^2)$ in the large P^2 region.

As we have seen, present DIS dijet data cannot discriminate between the universal naive box and QCD-resummed expectations in the theoretically relevant region $P^2 \ll Q^2$,

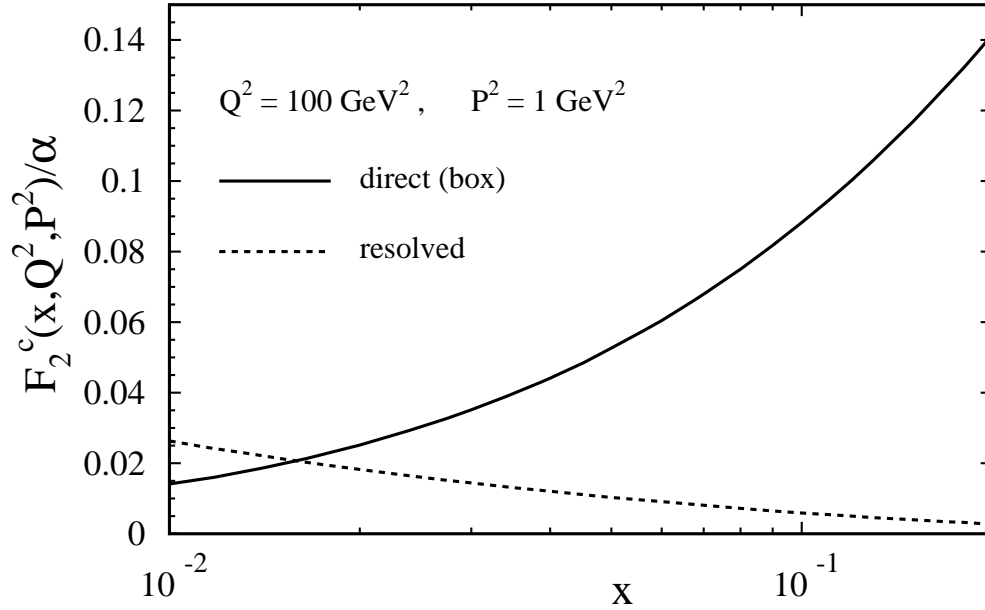


Figure 12.4: Expected charm contributions to F_2 . The naive ‘direct (box)’ result refers to (9.13) [or (C.12)] and the LO–QCD ‘resolved’ prediction is given in (9.14) with $g^{\gamma(P^2)}(x, 4m_c^2)$ taken from GRSc [6]. This latter ‘resolved’ contribution is absent in the naive box (QPM) approach.

mainly because these data are insensitive to the gluon content in $\gamma(P^2)$ generated by QCD–evolutions which is absent within the naive box approach. Therefore we finally turn to a brief discussion where such typical QCD effects may be observed and delineated by future experiments.

12.4 Possible Signatures for the QCD Parton Content of Virtual Photons

Since e^+e^- and DIS ep dijet data cannot, at present, delineate the QCD–resummed parton content of a virtual photon, in particular not its gluon content, we shall now propose and discuss a few cases where such typical QCD effects may be observed and possibly confirmed by future experiments.

Charm production in $e^+e^- \rightarrow e^+e^- c\bar{c}X$ would be a classical possibility to delineate such effects due to a nonvanishing $g^{\gamma(P^2)}(x, Q^2)$. In Fig. 12.4 we compare the usual (fixed

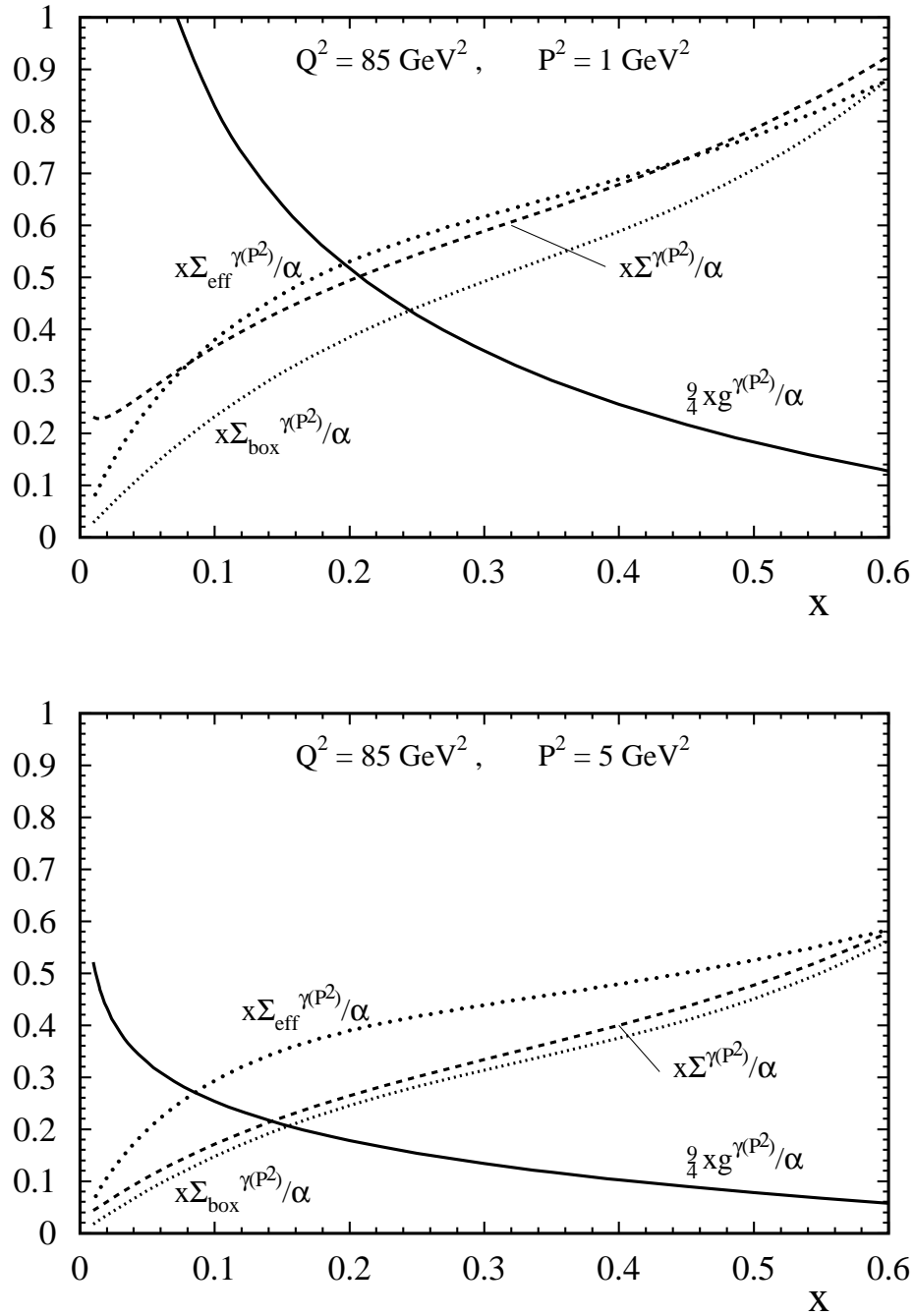


Figure 12.5: Predictions for the total light quark $\Sigma^{\gamma(P^2)} \equiv 2\Sigma_{q=u,d,s} q^{\gamma(P^2)}$ and gluon contributions to the effective parton density in (12.2) at a fixed scale $Q^2 = 85 \text{ GeV}^2$ and two fixed virtualities $P^2 = 1$ and 5 GeV^2 . The naive box results refer to the universal $q_{\text{box}}^{\gamma(P^2)}$ defined in (12.3) and to $q_{\text{eff}}^{\gamma(P^2)}$ defined in (12.4). The LO-QCD RG-resummed predictions are denoted by $\Sigma^{\gamma(P^2)}$ and $g^{\gamma(P^2)}$ according to GRSc [6]. The latter gluon contribution is absent in the naive box (QPM) approach.

order) ‘direct’ box contribution to F_2^c with the ‘resolved’ gluon-initiated one as given by (9.14). The ‘direct’ box contribution entirely dominates in the large- x region, $x \gtrsim 0.05$, accessible by present experiments (cf. Figs. 12.1 and 12.2), whereas the typical QCD-resummed ‘resolved’ contribution becomes comparable to the ‘direct’ one and eventually dominates in the small- x region, $x < 0.05$. Thus a careful measurement of the charm contribution to F_2 at $x \lesssim 0.05$ would shed some light on the QCD parton (gluon) content of virtual photons, since such a ‘resolved’ contribution in Fig. 12.4 would be absent within the naive box approach.

The effective parton distribution $\tilde{f}^{\gamma(P^2)}(x, Q^2)$ in (12.2) at not too large values of x and P^2 , as may be extracted in LO from DIS ep dijet data, would be another possibility to observe QCD-resummation effects due to a nonvanishing gluon component $g^{\gamma(P^2)}(x, Q^2)$. In Fig. 12.5 we show the quark and gluon contributions to $\tilde{f}^{\gamma(P^2)}$ in (12.2) separately. The box (anti-)quark contributions, which are similar to the QCD-resummed ones, entirely dominate over the QCD-resummed gluon contribution in the large- x region, $x \gtrsim 0.4$, accessible to present experiments (cf. Fig. 12.3). Only *below* $x \simeq 0.3$ does the QCD gluon contribution become comparable to the (anti-)quark components and dominates, as usual, for $x \lesssim 0.1$. It should be remembered that $g_{\text{box}}^{\gamma(P^2)}(x, Q^2) = 0$. Furthermore, the increase of the RG-resummed $q^{\gamma(P^2)}(x, Q^2)$ at small x in Fig. 12.5 is induced by the vector-meson-dominance-like input for the Q^2 -evolution of the ‘hadronic’ component of the photon’s parton distribution [6, 97] and is disregarded in our naive box (QPM) analysis.

Thus a measurement of dijets produced in DIS ep reactions in the not too large x region, $x \lesssim 0.3$, would probe the QCD parton content of virtual photons, in particular their gluon content which is absent in the naive QPM box approach. In this region, and at not too large photon virtualities $P^2 \lesssim 5 \text{ GeV}^2$ shown in Fig. 12.5, the ‘resolved’ gluon-dominated contribution of the virtual photon to high E_T jet production at scales $Q \equiv E_T \simeq 5 - 10 \text{ GeV}$ exceeds by far the ‘direct’ box-like contribution of a pointlike virtual photon [162]. The production of prompt photons at HERA via a tagged DIS process $ep \rightarrow e\gamma X$ may offer additional probes of the gluonic content of virtual photons [184].

12.5 Summary and Conclusions

Virtual photons $\gamma(P^2)$, probed at a large scale $Q^2 \gg P^2$, may be described either by fixed order perturbation theory, which in lowest order of QCD yield the quarks and anti-quarks generated by the universal part of the ‘box’ diagram, or alternatively by their renormalization group (RG) improved counterparts including particularly the gluon distribution $g^{\gamma(P^2)}(x, Q^2)$.

The results in Sections 12.2 and 12.3 demonstrate that all presently available e^+e^- and DIS ep dijet data can be fully accounted for by the standard doubly virtual QED box diagram and are not yet sensitive to RG resummation effects which are manifest only in the presently unexplored low- x region of the parton distributions in $\gamma(P^2)$. In fact, as shown in Section 12.4, these resummation effects start to dominate only at $x < 0.3$ and may be observed by future measurements at $P^2 = \mathcal{O}(1 \text{ GeV}^2)$ of $\sigma(ep \rightarrow e jjX)$ or $\sigma(e^+e^- \rightarrow e^+e^- c\bar{c}X)$ at high energy collisions. These measurements could finally discriminate between the fixed order and RG-improved parton distributions of the virtual photon.

Chapter 13

Summary

It was the main theme of Part II of this thesis to analyze the parton content of pions and real and virtual photons in leading order (LO) and next-to-leading order (NLO) of QCD within the framework of the recently updated [26] radiative parton model [26, 41, 57, 92, 93].

We started with a detailed consideration of the $ee \rightarrow eeX$ scattering process being presently the main source of information on the structure of real and virtual photons. We defined structure functions for virtual photons in a model independent way and related them to the photon-photon scattering cross sections. These structure functions can be measured in deep inelastic electron-photon scattering ($\text{DIS}_{e\gamma}$) and we demonstrated the factorization of the cross section for the process $ee \rightarrow eeX$ into a flux of photons (produced by bremsstrahlung off the incident lepton) times the $\text{DIS}_{e\gamma}$ cross section for the general $P^2 \neq 0$ case in the Bjorken limit $P^2 \ll Q^2$. However, we found that the neglected terms are of the order $\mathcal{O}(\sqrt{xP^2/Q^2})$ only and not of the order $\mathcal{O}(xP^2/Q^2)$ as might have been naively expected. Clearly, a numerical comparison of the factorization formula with the exact $ee \rightarrow eeX$ cross section would be interesting in order to clarify when xP^2/Q^2 is small enough such that the factorization formula is a good approximation.

From these general kinematical considerations we turned to a calculation of the photon-photon cross sections σ_{ab} according to the doubly virtual box $\gamma^*(Q^2)\gamma^*(P^2) \rightarrow q\bar{q}$ in lowest order perturbation theory. We utilized these results in order to compute the effective structure function $F_{\text{eff}}(x, Q^2, P^2)$ in fixed order perturbation theory (FOPT) which we compared with all present e^+e^- virtual photon data [105, 106]. It came out that the LO-box predictions for F_{eff} are in agreement with the present low statistics data even in

the case of the PLUTO data [106] with $P^2 = 0.35 \text{ GeV}^2$ which is just in the transition region from deeply virtual ($P^2 \gg \Lambda^2$) to real ($P^2 \simeq 0$) photons where non-perturbative effects are expected to become increasingly important, especially in the small- x region. More precise data for F_{eff} in this 'transition region' with intermediate target virtualities would be highly desirable in order to observe the onset of such non-perturbative effects. On the other hand, NLO corrections to the doubly virtual box [108] offer the possibility to investigate the perturbative stability of the fixed order results and to see if the description of the data further improves in NLO accuracy.

After presenting the complete theoretical framework we started our phenomenological studies of radiatively generated parton distributions with an analysis of the parton content of the pion in LO and NLO QCD. Since only the pionic valence density $v^\pi(x, Q^2)$ is experimentally rather well known at present, we utilized a constituent quark model [94, 95] in order to unambiguously relate the pionic light sea $\bar{q}^\pi(x, Q^2)$ and gluon $g^\pi(x, Q^2)$ to the much better known (recently updated) parton distributions of the proton [26] and the pionic valence density $v^\pi(x, Q^2)$.

Next we formulated a consistent set of boundary conditions which allowed for a perturbatively stable LO and NLO calculation of the photonic parton distributions $f^{\gamma(P^2)}(x, Q^2)$ as well as for a smooth transition to the parton densities of a real ($P^2 = 0$) photon. Employing the above summarized pionic distributions $f^\pi(x, Q^2)$, required for describing –via vector meson dominance (VMD)– the nonpointlike hadronic components of a photon, we arrived at essentially parameter-free predictions for $f^{\gamma(P^2)}(x, Q^2)$ which turned out to be in good agreement with all present measurements of the structure function $F_2^\gamma(x, Q^2)$ of real photons $\gamma \equiv \gamma(P^2 = 0)$. More specifically, we implemented these hadronic components by using a VMD ansatz for a coherent superposition of vector mesons which maximally enhances the contributions of the up-quarks to $F_2^\gamma(x, Q^2)$ as favored by all present data. Since these hadronic contributions are generated from the valence-like input parton distributions at the universal target-mass independent low resolution scale $Q_0^2 = \mu^2 \simeq 0.3 \text{ GeV}^2$, we arrived, at least for real ($P^2 = 0$) photons, at unique small- x predictions for $x \lesssim 10^{-2}$ at $Q^2 > \mu^2$ which are of purely dynamical origin, as in the case of hadrons. A comparison with most recent small- x measurements of the photon structure function $F_2^\gamma(x, Q^2)$ [98] showed that these small- x predictions are in perfect agreement with the data at all presently accessible values of Q^2 . The agreement with the data on $F_2^\gamma(x, Q^2)$ confirms our radiatively generated quark distributions $q^\gamma(x, Q^2) = \bar{q}^\gamma(x, Q^2)$

while the gluon is probed only indirectly at small- x due to the evolution. It would be also interesting and important to extend present measurements [89, 90, 180, 181] of the gluon distribution of the photon, $g^\gamma(x, Q^2)$, below the presently measured region $0.1 \lesssim x < 1$ where $g^\gamma(x < 0.1, Q^2)$ is expected to be somewhat flatter in the small- x region than previously anticipated [96]. Our expectations for the parton content of virtual ($P^2 \neq 0$) photons are clearly more speculative, depending on how one models the hadronic component (input) of a virtual photon. We assumed the latter to be similar to the VMD input for a real photon times a dipole suppression factor which derives from an effective vector-meson P^2 -propagator representing somehow the simplest choice. We formulated similar boundary conditions in LO and NLO which gave rise to perturbatively stable parton distributions and cross sections (i.e. also structure functions of virtual photons) as long as they are probed at scales $Q^2 \gg P^2$ where Q^2 is a hard scale of the process under consideration. We showed that effective parton distributions of virtual photons extracted recently from DIS ep dijet data are in good agreement with our (parameter-free) predictions.

Finally, we turned to more detailed tests of our model for the parton content of virtual photons and we compared these QCD-resummed expectations with the above summarized fixed order box expressions. Our results demonstrated that all presently available e^+e^- and DIS ep dijet data can be fully accounted for by the standard doubly virtual QED box diagram and are not yet sensitive to RG resummation effects which are manifest only in the presently unexplored low- x region of the parton distributions in $\gamma(P^2)$. It turned out that these resummation effects start to dominate only at $x \lesssim 0.3$ (the larger P^2 the smaller x) and may be observed by future measurements at $P^2 = \mathcal{O}(1 \text{ GeV}^2)$ of $\sigma(ep \rightarrow e jjX)$ or $\sigma(e^+e^- \rightarrow e^+e^- c\bar{c}X)$ at high energy collisions. These measurements could finally discriminate between the fixed order and RG-improved parton distributions of the virtual photon.

FORTTRAN packages containing simple analytic parametrizations of our most recent parton distributions of the pion and the (real and virtual) photon are available upon request by electronic mail from schien@zylon.physik.uni-dortmund.de.

Appendix A

Deep Inelastic Scattering on Massive Quarks at $\mathcal{O}(\alpha_s^1)$

A.1 Real Gluon Emission

We define a partonic tensor

$$\hat{\omega}^{\mu\nu} \equiv \sum_{\text{color}} \sum_{\text{spin}} \langle Q_2(p_2), g(k) | \bar{Q}_2 \gamma^\mu (V - A\gamma_5) Q_1 | Q_1(p_1) \rangle \times \langle \mu \rightarrow \nu \rangle^* \quad (\text{A.1})$$

which can be decomposed into its different tensor components as usual

$$\hat{\omega}^{\mu\nu} = -\hat{\omega}_1^Q g^{\mu\nu} + \hat{\omega}_2^Q p_1^\mu p_1^\nu + i\hat{\omega}_3^Q \varepsilon^{\mu\nu} p_1^\alpha q^\beta + \hat{\omega}_4^Q q^\mu q^\nu + \hat{\omega}_5^Q (q^\mu p_1^\nu + q^\nu p_1^\mu) \quad . \quad (\text{A.2})$$

$\hat{\omega}_{\mu\nu}$ can be easily calculated from the general Feynman rules for invariant matrix elements which are customarily expressed as functions of the Mandelstam variables $\hat{s} \equiv (p_1 + q)^2$ and $\hat{t} \equiv (p_1 - k)^2$ to which we will refer in the following. Projection onto the individual $\hat{\omega}_{i=1,2,3}^Q$ in Eq. (A.2) is performed for nonzero masses and in $n = 4 + 2\varepsilon$ dimensions with the following operators

$$\begin{aligned} P_1^{\mu\nu} &= \frac{-1}{2(1+\varepsilon)} \left\{ g^{\mu\nu} + [m_1^2 q^\mu q^\nu - Q^2 p_1^\mu p_1^\nu - (p_1 \cdot q)(q^\mu p_1^\nu + p_1^\mu q^\nu)] \right. \\ &\quad \times \left. 4\Delta^{-2}[m_1^2, \hat{s}, -Q^2] \right\} \\ P_2^{\mu\nu} &= 2 \left[-g^{\mu\nu} Q^2 + 4 q^\mu q^\nu \frac{2(1+\varepsilon)(p_1 \cdot q)^2 - m_1^2 Q^2}{\Delta^2[m_1^2, \hat{s}, -Q^2]} \right. \\ &\quad \left. + 4(3+2\varepsilon)Q^2 \frac{Q^2 p_1^\mu p_1^\nu + (p_1 \cdot q)(q^\mu p_1^\nu + p_1^\mu q^\nu)}{\Delta^2[m_1^2, \hat{s}, -Q^2]} \right] \left\{ (1+\varepsilon)\Delta^2[m_1^2, \hat{s}, -Q^2] \right\}^{-1} \\ P_3^{\mu\nu} &= \frac{-2i}{\Delta^2[m_1^2, \hat{s}, -Q^2]} \varepsilon^{\mu\nu}{}_{\lambda\kappa} p_1^\lambda q^\kappa \end{aligned} \quad (\text{A.3})$$

such that $P_i \cdot \hat{\omega} = \hat{\omega}_i^Q$. The normalization in Eqs. (A.1), (A.2) is such that real gluon emission contributes F_i^R to the hadronic structure functions via

$$\begin{aligned} F_1^R &= \frac{1}{8\pi} \int_{\chi}^1 \frac{d\xi}{\xi} Q_1(\xi) \int d\widehat{\text{PS}} \hat{\omega}_1^Q \\ F_2^R &= \frac{2x}{16\pi} \int_{\chi}^1 \frac{d\xi}{\xi} \frac{\Delta^2[m_1^2, \hat{s}, -Q^2]}{2Q^2} Q_1(\xi) \int d\widehat{\text{PS}} \hat{\omega}_2^Q \\ F_3^R &= \frac{1}{8\pi} \int_{\chi}^1 \frac{d\xi}{\xi} \Delta[m_1^2, \hat{s}, -Q^2] Q_1(\xi) \int d\widehat{\text{PS}} \hat{\omega}_3^Q \end{aligned} \quad (\text{A.4})$$

where [185]

$$\int d\widehat{\text{PS}} = \frac{1}{8\pi} \frac{\hat{s} - m_2^2}{\hat{s}} \frac{1}{\Gamma(1+\varepsilon)} \left[\frac{(\hat{s} - m_2^2)^2}{4\pi\hat{s}} \right]^\varepsilon \int_0^1 [y(1-y)]^\varepsilon dy \quad (\text{A.5})$$

is the partonic phase space. In Eq. (A.5) y is related to the partonic center of mass scattering angle θ^* and the partonic Mandelstam variable \hat{t} via

$$\begin{aligned} y &\equiv \frac{1}{2} (1 + \cos \theta^*) \\ &= \frac{1}{2\Delta[m_1^2, \hat{s}, -Q^2]} \left[Q^2 + m_1^2 + \hat{s} + \Delta[m_1^2, \hat{s}, -Q^2] + \frac{2\hat{s}(\hat{t} - m_1^2)}{\hat{s} - m_2^2} \right] \quad . \end{aligned} \quad (\text{A.6})$$

We have chosen dimensional regularization for the soft gluon poles stemming from $\hat{s} \rightarrow m_2^2$ which arise from propagators in the $\hat{\omega}_i$ times phase space factors in $d\widehat{\text{PS}}$. In Eq. (A.4) we use [48]

$$(\hat{s} - m_2^2)^{2\varepsilon-1} \sim \left(1 - \frac{\chi}{\xi} \right)^{2\varepsilon-1} = \frac{1}{2\varepsilon} \delta(1 - \chi/\xi) + \frac{1}{(1 - \chi/\xi)_+} + \mathcal{O}(\varepsilon) \quad (\text{A.7})$$

which separates hard gluon emission ($\sim \hat{f}_i^Q$) from soft gluon (S_i) contributions in Eq. (3.10). Note that in Eqs. (3.9), (3.10) the integration variable ξ , which is implicitly defined in Eq. (3.2), has been changed to $\xi' \equiv \chi/\xi$ for an easier handling of the distributions. For the relation between \hat{s} and ξ' see Eq. (A.39) below.

Since all quark masses are kept nonzero, no poles in y (collinear singularities) are contained in the integration volume. The \hat{f}_i^Q which occur in Eq. (3.10) and which are given below in Eq. (A.40) are therefore straightforward integrals of the $\hat{\omega}_i^Q$

$$\hat{f}_i^Q = (g_s^2 C_F)^{-1} \int_0^1 dy \hat{\omega}_i^Q \quad (\text{A.8})$$

and the S_i in Eqs. (3.10), (A.37) pick up the pole in Eq. (A.7)

$$S_i \sim \frac{1}{\varepsilon} \int_0^1 dy [y(1-y)]^\varepsilon \left[\hat{\omega}_i^Q (\hat{s} - m_2^2)^2 \right] \Big|_{\xi=\chi} , \quad (\text{A.9})$$

where the proportionality is given by kinematical and phase space factors which must be kept up to $\mathcal{O}(\varepsilon)$.

The normalization of our hadronic structure functions in Eq. (A.4) can be clearly inferred from the corresponding LO results in Eq. (3.3). Nevertheless, for definiteness we also give the hadronic differential cross section to which it corresponds

$$\begin{aligned} \frac{d^2 \sigma^{l,\bar{l}}}{dx dy} &= \frac{1}{n_l} \frac{(G_l^{B,B'})^2 (G_q^{B,B'})^2 2M_N E_l}{2\pi} \\ &\times \left[S_{l,+} (1-y) F_2 + S_{l,+} y^2 x F_1 \pm R_{l,+} 2y(1 - \frac{y}{2}) x F_3 \right] , \end{aligned} \quad (\text{A.10})$$

where $(G_{l,q}^{B,B'})^2 = [g_{l,q}^B]^2 / (Q^2 + M_B^2) [g_{l,q}^{B'}]^2 / (Q^2 + M_{B'}^2)]^{1/2}$ is the effective squared gauge coupling –including the gauge boson propagator– of the $\gamma_\mu(V - A\gamma_5)$ lepton and quark current, respectively, and n_l counts the spin degrees of freedom of the lepton, e.g. $n_l = 1, 2$ for $l = \nu, e^-$. The leptonic couplings $S_{l,+}, R_{l,+}$ are defined analogous to the quark couplings in Eq. (3.6). As noted below Eq. (3.6), $B = B'$ for non-interference (pure B scattering).

A.2 Vertex Correction

A.2.1 Results

We have calculated the vertex correction in $n = 4 + 2\varepsilon$ dimensions at $\mathcal{O}(\alpha_s^1)$ for general masses and couplings using the Feynman gauge. The unrenormalized vertex Λ_0^μ [Fig. 3.1(c.1)] has the structure

$$\begin{aligned} \Lambda_0^\mu &= C_F \frac{\alpha_s}{4\pi} \Gamma(1-\varepsilon) \left(\frac{Q^2}{4\pi\mu^2} \right)^\varepsilon \left\{ C_{0,-} \gamma^\mu L_5 + C_+ \gamma^\mu R_5 \right. \\ &\quad \left. + C_{1,-} m_2 p_1^\mu L_5 + C_{1,+} m_1 p_1^\mu R_5 + C_{q,-} m_2 q^\mu L_5 + C_{q,+} m_1 q^\mu R_5 \right\} \end{aligned} \quad (\text{A.11})$$

with $L_5 = (V - A \gamma_5)$, $R_5 = (V + A \gamma_5)$. The coefficients read

$$C_{0,-} = \frac{1}{\varepsilon} (-1 - \Sigma_{++} I_1) + \left[\frac{\Delta^2}{2Q^2} + \Sigma_{++} \left(1 + \ln \left(\frac{Q^2}{\Delta} \right) \right) \right] I_1$$

$$\begin{aligned}
& + \frac{1}{2} \ln \left(\frac{Q^2}{m_1^2} \right) + \frac{1}{2} \ln \left(\frac{Q^2}{m_2^2} \right) + \frac{m_2^2 - m_1^2}{2Q^2} \ln \left(\frac{m_1^2}{m_2^2} \right) + \frac{\Sigma_{++}}{\Delta} \\
& \times \left\{ \frac{1}{2} \ln^2 \left| \frac{\Delta - \Sigma_{+-}}{2Q^2} \right| + \frac{1}{2} \ln^2 \left| \frac{\Delta - \Sigma_{-+}}{2Q^2} \right| - \frac{1}{2} \ln^2 \left| \frac{\Delta + \Sigma_{+-}}{2Q^2} \right| - \frac{1}{2} \ln^2 \left| \frac{\Delta + \Sigma_{-+}}{2Q^2} \right| \right. \\
& \left. - \text{Li}_2 \left(\frac{\Delta - \Sigma_{+-}}{2\Delta} \right) - \text{Li}_2 \left(\frac{\Delta - \Sigma_{-+}}{2\Delta} \right) + \text{Li}_2 \left(\frac{\Delta + \Sigma_{+-}}{2\Delta} \right) + \text{Li}_2 \left(\frac{\Delta + \Sigma_{-+}}{2\Delta} \right) \right\}
\end{aligned} \tag{A.12}$$

$$\begin{aligned}
C_+ &= 2m_1 m_2 I_1 \\
C_{1,-} &= \frac{-1}{Q^2} \left[\Sigma_{+-} I_1 + \ln \left(\frac{m_1^2}{m_2^2} \right) \right] \\
C_{1,+} &= \frac{-1}{Q^2} \left[\Sigma_{-+} I_1 - \ln \left(\frac{m_1^2}{m_2^2} \right) \right] \\
C_{q,-} &= \frac{1}{Q^4} \left[(\Delta^2 - 2m_1^2 Q^2) I_1 - 2Q^2 + \Sigma_{+-} \ln \left(\frac{m_1^2}{m_2^2} \right) \right] \\
C_{q,+} &= \frac{1}{Q^4} \left[(-\Delta^2 + 2m_2^2 Q^2 - \Sigma_{-+} Q^2) I_1 + 2Q^2 + (\Sigma_{-+} + Q^2) \ln \left(\frac{m_1^2}{m_2^2} \right) \right]
\end{aligned} \tag{A.13}$$

with

$$I_1 = \frac{1}{\Delta} \ln \left[\frac{\Sigma_{++} + \Delta}{\Sigma_{++} - \Delta} \right] \tag{A.14}$$

$$\begin{aligned}
I_2 &= I_1 \ln \Delta - \frac{1}{\Delta} \\
& \times \left\{ \frac{1}{2} \ln^2 \left| \frac{\Delta - \Sigma_{+-}}{2Q^2} \right| + \frac{1}{2} \ln^2 \left| \frac{\Delta - \Sigma_{-+}}{2Q^2} \right| - \frac{1}{2} \ln^2 \left| \frac{\Delta + \Sigma_{+-}}{2Q^2} \right| - \frac{1}{2} \ln^2 \left| \frac{\Delta + \Sigma_{-+}}{2Q^2} \right| \right. \\
& \left. - \text{Li}_2 \left(\frac{\Delta - \Sigma_{+-}}{2\Delta} \right) - \text{Li}_2 \left(\frac{\Delta - \Sigma_{-+}}{2\Delta} \right) + \text{Li}_2 \left(\frac{\Delta + \Sigma_{+-}}{2\Delta} \right) + \text{Li}_2 \left(\frac{\Delta + \Sigma_{-+}}{2\Delta} \right) \right\}.
\end{aligned} \tag{A.15}$$

The renormalized vertex [Fig. 3.1 (c.1)–(c.3)] is obtained by wave function renormalization:

$$\Lambda_R^\mu = \gamma^\mu L_5 (Z_1 - 1) + \Lambda_0^\mu + \mathcal{O}(\alpha_s^2) \tag{A.16}$$

where $Z_1 = \sqrt{Z_2(p_1)Z_2(p_2)}$. The fermion wave function renormalization constants are defined on mass shell:

$$Z_2(m_i) = 1 + C_F \frac{\alpha_s}{4\pi} \Gamma(1 - \varepsilon) \left(\frac{m_i^2}{4\pi\mu^2} \right)^\varepsilon \frac{1}{\varepsilon} [3 - 4\varepsilon + \mathcal{O}(\varepsilon^2)] \tag{A.17}$$

such that

$$Z_1 = 1 + C_F \frac{\alpha_s}{4\pi} \Gamma(1 - \varepsilon) \left(\frac{Q^2}{4\pi\mu^2} \right)^\varepsilon \left[\frac{3}{\varepsilon} - \frac{3}{2} \ln \left(\frac{Q^2}{m_1^2} \right) - \frac{3}{2} \ln \left(\frac{Q^2}{m_2^2} \right) - 4 \right] . \tag{A.18}$$

The final result for the renormalized vertex Λ_R^μ reads

$$\begin{aligned} \Lambda_R^\mu = & C_F \frac{\alpha_s}{4\pi} \Gamma(1-\varepsilon) \left(\frac{Q^2}{4\pi\mu^2} \right)^\varepsilon \left\{ C_{R,-} \gamma^\mu L_5 + C_{+,} \gamma^\mu R_5 \right. \\ & + C_{1,-} m_2 p_1^\mu L_5 + C_{1,+} m_1 p_1^\mu R_5 + C_{q,-} m_2 q^\mu L_5 + C_{q,+} m_1 q^\mu R_5 \left. \right\} \end{aligned} \quad (\text{A.19})$$

with $C_{+,}$, $C_{1,\pm}$, $C_{q,\pm}$ as given above and

$$\begin{aligned} C_{R,-} = & \frac{1}{\varepsilon} (2 - \Sigma_{++} I_1) + \left[\frac{\Delta^2}{2Q^2} + \Sigma_{++} \left(1 + \ln \left(\frac{Q^2}{\Delta} \right) \right) \right] I_1 \\ & + \frac{m_2^2 - m_1^2}{2Q^2} \ln \left(\frac{m_1^2}{m_2^2} \right) - \ln \left(\frac{Q^2}{m_1^2} \right) - \ln \left(\frac{Q^2}{m_2^2} \right) - 4 + \frac{\Sigma_{++}}{\Delta} \\ & \times \left\{ \frac{1}{2} \ln^2 \left| \frac{\Delta - \Sigma_{+-}}{2Q^2} \right| + \frac{1}{2} \ln^2 \left| \frac{\Delta - \Sigma_{-+}}{2Q^2} \right| - \frac{1}{2} \ln^2 \left| \frac{\Delta + \Sigma_{+-}}{2Q^2} \right| - \frac{1}{2} \ln^2 \left| \frac{\Delta + \Sigma_{-+}}{2Q^2} \right| \right. \\ & \left. - \text{Li}_2 \left(\frac{\Delta - \Sigma_{+-}}{2\Delta} \right) - \text{Li}_2 \left(\frac{\Delta - \Sigma_{-+}}{2\Delta} \right) + \text{Li}_2 \left(\frac{\Delta + \Sigma_{+-}}{2\Delta} \right) + \text{Li}_2 \left(\frac{\Delta + \Sigma_{-+}}{2\Delta} \right) \right\}. \end{aligned} \quad (\text{A.20})$$

A.2.2 Calculation

Basic ingredient in the calculation of one-loop virtual corrections are one-loop integrals classified according to the number N of propagator factors in the denominator and the number P of integration momenta in the numerator. Integrals with $N = 1, 2, 3, 4$ are usually called one-, two-, three- and four-point functions (1PF...4PF). For $P+4-2N \geq 0$ these integrals are UV-divergent. In dimensional regularization these divergences are regulated by evaluating the integrals in general dimensions $n \neq 4$ and the divergences become manifest as poles in the limit $n \rightarrow 4$.

We define the following one-loop tensor integrals¹ (see for example [186, 187]):

$$T_{\mu_1 \dots \mu_P}^N(p_1, \dots, p_{N-1}, m_0, \dots, m_{N-1}) \equiv \frac{(2\pi\mu)^{4-n}}{i\pi^2} \int d^n l \frac{l_{\mu_1} \dots l_{\mu_P}}{D_0 D_1 \dots D_{N-1}} \quad (\text{A.21})$$

where all the external momenta p_i are defined to be incoming and the denominators stemming from the propagators in the Feynman diagram are given by

$$D_i = (l + \bar{p}_i)^2 - m_i^2 + i\varepsilon, \quad \text{with} \quad \bar{p}_i \equiv \sum_{j=1}^i p_j, \quad (i = 0, \dots, N-1). \quad (\text{A.22})$$

¹Note that this definition is related to Eq. (4.1) in [186] as follows:

$T_{\mu_1 \dots \mu_P}^N(p_1, \dots, p_{N-1}, m_0, \dots, m_{N-1}) = T_{\mu_1 \dots \mu_P}^{N, \text{Denner}}(\bar{p}_1, \dots, \bar{p}_{N-1}, m_0, \dots, m_{N-1}).$

To achieve a cyclic symmetry we furthermore identify the 0–th with the N –th propagator: $D_N \equiv D_0$, $m_N \equiv m_0$ and $\bar{p}_N = \bar{p}_0 = 0$. Furthermore it is convenient to define

$$p_{i0} = \bar{p}_i, \quad p_{ij} = \bar{p}_i - \bar{p}_j. \quad (\text{A.23})$$

The $+i\varepsilon$ part in the denominators with an infinitesimal $\varepsilon > 0$ is needed to regulate singularities of the integrand and its specific choice ensures causality. After integration it determines the correct imaginary parts of the logarithms and dilogarithms. The arbitrary mass scale μ has been introduced such that the integrals have an integer mass dimension. Conventionally T^N is denoted by the N –th character of the alphabet, i.e. $T^1 \equiv A$, $T^2 \equiv B$, \dots , and the scalar integrals carry an index 0.

The tensor integrals in (A.21) can be related to the scalar integrals A_0 , B_0 , C_0 and D_0 by a Passarino–Veltman decomposition [188] which will be described in the following. Due to Lorentz covariance the tensor integrals (A.21) can be decomposed into tensors constructed from the external momenta p_i and the metric tensor $g_{\mu\nu}$. The choice of the tensor basis is not unique and we will stick to the following form [187, 189]:

$$\begin{aligned} B^\mu &= p_1^\mu B_1 \\ B^{\mu\nu} &= p_1^\mu p_1^\nu B_{21} + g^{\mu\nu} B_{22} \\ \\ C^\mu &= p_1^\mu C_{11} + p_2^\mu C_{12} \\ C^{\mu\nu} &= p_1^\mu p_1^\nu C_{21} + p_2^\mu p_2^\nu C_{22} + \{p_1 p_2\}^{\mu\nu} C_{23} + g^{\mu\nu} C_{24} \\ C^{\mu\nu\rho} &= p_1^\mu p_1^\nu p_1^\rho C_{31} + p_2^\mu p_2^\nu p_2^\rho C_{32} + \{p_1 p_1 p_2\}^{\mu\nu\rho} C_{33} + \{p_1 p_2 p_2\}^{\mu\nu\rho} C_{34} \\ &\quad + \{p_1 g\}^{\mu\nu\rho} C_{35} + \{p_2 g\}^{\mu\nu\rho} C_{36} \\ \\ D^\mu &= p_1^\mu D_{11} + p_2^\mu D_{12} + p_3^\mu D_{13} \\ D^{\mu\nu} &= p_1^\mu p_1^\nu D_{21} + p_2^\mu p_2^\nu D_{22} + p_3^\mu p_3^\nu D_{23} + \{p_1 p_2\}^{\mu\nu} D_{24} + \{p_1 p_3\}^{\mu\nu} D_{25} \\ &\quad + \{p_2 p_3\}^{\mu\nu} D_{26} + g^{\mu\nu} D_{27} \\ D^{\mu\nu\rho} &= p_1^\mu p_1^\nu p_1^\rho D_{31} + p_2^\mu p_2^\nu p_2^\rho D_{32} + p_3^\mu p_3^\nu p_3^\rho D_{33} + \{p_1 p_1 p_2\}^{\mu\nu\rho} D_{34} + \{p_1 p_1 p_3\}^{\mu\nu\rho} D_{35} \\ &\quad + \{p_1 p_2 p_2\}^{\mu\nu\rho} D_{36} + \{p_1 p_3 p_3\}^{\mu\nu\rho} D_{37} + \{p_2 p_2 p_3\}^{\mu\nu\rho} D_{38} + \{p_2 p_3 p_3\}^{\mu\nu\rho} D_{39} \\ &\quad + \{p_1 p_2 p_3\}^{\mu\nu\rho} D_{310} + \{p_1 g\}^{\mu\nu\rho} D_{311} + \{p_2 g\}^{\mu\nu\rho} D_{312} + \{p_3 g\}^{\mu\nu\rho} D_{313} \end{aligned} \quad (\text{A.24})$$

where we have used the shorthand notations

$$\{p_i p_j p_k\}_{\mu\nu\rho} \equiv \sum_{\sigma(i,j,k)} p_{\sigma(i)\mu} p_{\sigma(j)\nu} p_{\sigma(k)\rho}$$

with $\sigma(i, j, k)$ denoting all *different* permutations of (i, j, k) and

$$\{p_i g\}_{\mu\nu\rho} \equiv p_{i\mu} g_{\nu\rho} + p_{i\nu} g_{\mu\rho} + p_{i\rho} g_{\mu\nu} .$$

For example $\{p_1 p_1 p_2\}^{\mu\nu\rho} = p_1^\mu p_1^\nu p_2^\rho + p_1^\nu p_1^\rho p_2^\mu + p_1^\rho p_1^\mu p_2^\nu$ and $\{p_1 g\}^{\mu\nu\rho} = p_1^\mu g^{\nu\rho} + p_1^\nu g^{\rho\mu} + p_1^\rho g^{\mu\nu}$. The scalar coefficients $B_{j(k)}$, C_{jk} and $D_{jk(l)}$ can depend on all possible invariants (built from the leg momenta) and the masses m_i .

Using the Lorentz decomposition (A.24) of the tensor integrals all scalar coefficients can be iteratively reduced to scalar integrals (with equal or less propagator factors) [187, 189], see [186] for a general treatment. With other words, all one-loop tensor integrals can be expressed in terms of scalar integrals (with equal or less propagator factors). In simple cases the reduction can be done by hand, however, in general the reduction algorithm has to be automatized on a computer.²

We now present some details of the derivation of the unrenormalized vertex in Eq. (A.11). In Feynman gauge the vertex correction diagram in [Fig. 3.1(c.1)] is given in n dimensions by

$$\Lambda_0^\mu = C_F \frac{\alpha_s (2\pi\mu)^{4-n}}{4\pi i\pi^2} \int d^n k \gamma^\rho \frac{\not{k} + \not{p}_2 + m_2}{(k + p_2)^2 - m_2^2} \frac{\gamma^\mu L_5}{k^2} \frac{\not{k} + \not{p}_1 + m_1}{(k + p_1)^2 - m_1^2} \gamma_\rho \quad (\text{A.25})$$

where $L_5 = (V - A\gamma_5)$, $C_F = 4/3$ and the scale μ has been introduced in order to maintain the coupling g_s dimensionless (see above).

In the following we consider on-shell fermions, i.e. $p_1^2 = m_1^2$ and $p_2^2 = m_2^2$, and a spacelike gauge boson with 4-momentum $q = p_2 - p_1$, $q^2 < 0$. Furthermore, since Λ_0^μ will be eventually sandwiched between external spinors $\bar{u}(p_2)\Lambda_0^\mu u(p_1)$ we apply the Dirac equations $\bar{u}(p_2)\not{p}_2 = m_2\bar{u}(p_2)$ and $\not{p}_1 u(p_1) = m_1 u(p_1)$ whenever possible which will be indicated by a ' $\hat{=}$ ' instead of a '='. Utilizing an anti-commuting γ_5 , $\{\gamma_\mu, \gamma_5\} = 0$ [190], the numerator (under the integral) in Eq.(A.25) can be written as

$$\begin{aligned} \text{Num} \hat{=} & \left\{ \gamma^\mu [(n-6)k^2 + 2[(k+p_1)^2 - m_1^2] + 2[(k+p_2)^2 - m_2^2] + 4p_1 \cdot p_2] \right. \\ & \left. + 2m_2 \gamma^\mu \not{k} - 2\not{k} [2q^\mu + (n-2)k^\mu + 4p_1^\mu] \right\} L_5 - 2m_1 \gamma^\mu \not{k} R_5 + 4m_1 k^\mu R_5 \end{aligned} \quad (\text{A.26})$$

²We are grateful to Dr. I. Bojak for providing us his **Mathematica** package for the reduction of the tensor integrals. This package is described in [189].

with $R_5 = (V + A\gamma_5)$.

Inserting the numerator into Eq. (A.25) and utilizing the Passarino–Veltman–decomposition (A.24) of the encountered tensor integrals (and again exploiting the Dirac equation in order to eliminate \not{p}_1 and \not{p}_2) there remain only Dirac structures as given in Eq. (A.11). Comparing the corresponding coefficients we obtain

$$\begin{aligned}
C_{0,-} &\hat{=} \left[\Gamma\left(\frac{6-n}{2}\right) \left(\frac{Q^2}{4\pi\mu^2}\right)^{(n-4)/2} \right]^{-1} \left[(n-6)B_0(q, m_1, m_2) + 2B_0(p_1, 0, m_1) \right. \\
&\quad \left. + 2B_0(p_1 + q, 0, m_2) + 4(m_1^2 + p_1 \cdot q)C_0 \right. \\
&\quad \left. - 2m_1^2 C_{11} + 2(m_1^2 - m_2^2)C_{12} - 2(n-2)C_{24} \right] \\
C_+ &\hat{=} 2m_1 m_2 C_{11} \\
C_{1,-} &\hat{=} -4C_{12} - 2(n-2)C_{23} \\
C_{1,+} &\hat{=} -4C_{11} + 4C_{12} - 2(n-2)(C_{21} - C_{23}) \\
C_{q,-} &\hat{=} -2(n-2)C_{22} \\
C_{q,+} &\hat{=} -4C_{11} + 4C_{12} + 2(n-2)(C_{22} - C_{23})
\end{aligned} \tag{A.27}$$

with $C_{ij,0} = C_{ij,0}(p_1, q, 0, m_1, m_2)$.

As described above the coefficients of the Passarino–Veltman–decomposition can be expressed in terms of the scalar integrals

$$\begin{aligned}
D C_{11} &= \frac{q \cdot p_2}{2} [B_0(p_2, 0, m_2) - B_0(q, m_1, m_2)] - \frac{q \cdot p_1}{2} [B_0(p_1, 0, m_1) - B_0(q, m_1, m_2)] \\
D C_{12} &= -\frac{p_1 \cdot p_2}{2} [B_0(p_2, 0, m_2) - B_0(q, m_1, m_2)] + \frac{m_1^2}{2} [B_0(p_1, 0, m_1) - B_0(q, m_1, m_2)] \\
D C_{21} &= A_0(m_1) \frac{p_1 \cdot q}{4m_1^2} - A_0(m_2) \frac{p_1 \cdot q + q^2}{4m_2^2} + B_0(q, m_1, m_2) q^2 \frac{n-3}{2(n-2)} \\
D C_{22} &= (A_0(m_1) - A_0(m_2)) \frac{p_1 \cdot q}{4q^2} + A_0(m_2) \frac{p_1 \cdot q + m_1^2}{4m_2^2} \\
&\quad + B_0(q, m_1, m_2) \left(\frac{m_1^2}{2(n-2)} - \frac{p_1 \cdot q}{4} + \frac{(m_2^2 - m_1^2)p_1 \cdot q}{4q^2} \right) \\
D C_{23} &= A_0(m_1) \frac{-1}{4} + A_0(m_2) \frac{p_1 \cdot q + m_1^2}{4m_2^2} - B_0(q, m_1, m_2) p_1 \cdot q \frac{n-3}{2(n-2)} \\
C_{24} &= B_0(q, m_1, m_2) \frac{1}{2(n-2)}
\end{aligned}$$

with $D = m_1^2 q^2 - (p_1 \cdot q)^2$. It is easy to convince oneself that the coefficients C_{11}, \dots, C_{23} are finite, whereas C_{24} is UV-divergent. Furthermore, $C_0(p_1, q, 0, m_1, m_2)$ is IR-divergent.

At this place the problem has reduced to the calculation of the scalar integrals A_0 , B_0 and C_0 . Introducing Feynman parameters and performing a Wick rotation the N -point scalar integral can be brought into the following form:

$$\begin{aligned} T_0^N &\equiv T_0^N(p_1, \dots, p_{N-1}, m_0, \dots, m_{N-1}) = \frac{(2\pi\mu)^{4-n}}{i\pi^2} \int d^n l \prod_{i=1}^N \frac{1}{D_i} \\ &= (-1)^N \Gamma(N - n/2) (4\pi\mu^2)^{\frac{4-n}{2}} \int_0^1 [d\alpha]_N (M^2)^{n/2-N} \end{aligned} \quad (\text{A.28})$$

with

$$\begin{aligned} [d\alpha]_N &= d\alpha_1 \cdot \dots \cdot d\alpha_N \delta \left(1 - \sum_{i=1}^N \alpha_i \right) \\ M^2 &= - \sum_{N \geq i > j \geq 1} \alpha_i \alpha_j p_{ij}^2 + \sum_{i=1}^N \alpha_i m_i^2 - i\varepsilon \end{aligned} \quad (\text{A.29})$$

where p_{ij} has been introduced in Eq. (A.23).

The calculation of the scalar one-point function $A_0(m)$ is trivial:

$$A_0(m) = -m^2 \left(\frac{m^2}{4\pi\mu^2} \right)^{\frac{n-4}{2}} \Gamma \left(1 - \frac{n}{2} \right) = m^2 \left(\Delta_{\text{UV}} - \ln \frac{m^2}{\mu^2} + 1 \right) + \mathcal{O}(n-4) \quad (\text{A.30})$$

with the UV-divergence contained in

$$\Delta_{\text{UV}} = \frac{-2}{n-4} - \gamma_E + \ln 4\pi \quad (\text{A.31})$$

and γ_E is Euler's constant. Note that Eq. (A.30) implies $A_0(0) = 0$. The terms of order $\mathcal{O}(n-4)$ are only relevant for two- or higher-loop calculations.

The evaluation of the needed two-point functions is still easy

$$\begin{aligned} B_0(q, m_1, m_2)|_{q^2 < 0} &= \Delta_{\text{UV}} + 2 - \ln \frac{m_1 m_2}{\mu^2} + \frac{m_1^2 - m_2^2}{q^2} \ln \frac{m_2}{m_1} \\ &+ \beta \left(1 - \frac{(m_1 - m_2)^2}{q^2} \right) \ln \left(-\frac{1 - \beta}{1 + \beta} \right) \end{aligned} \quad (\text{A.32})$$

with

$$\beta^2 = \frac{(m_1 + m_2)^2 - q^2}{(m_1 - m_2)^2 - q^2}$$

and

$$B_0(p, 0, m)|_{p^2 = m^2} = \Delta_{\text{UV}} - \ln \frac{m^2}{\mu^2} + 2. \quad (\text{A.33})$$

Finally the required three-point function is given in $n = 4 + 2\varepsilon$ dimensions by ($M^2 = m_1^2 x + m_2^2(1-x) - q^2 x(1-x) - i\varepsilon$)

$$C_0(p_1, q, 0, m_1, m_2)|_{p_1^2=m_1^2, (p_1+q)^2=m_2^2, q^2<0} = (4\pi\mu^2)^{-\varepsilon} \Gamma(1-\varepsilon) \frac{1}{2\varepsilon} I \quad (\text{A.34})$$

with

$$I = \int_0^1 dx [m_1^2 x + m_2^2(1-x) - q^2 x(1-x)]^{-1+\varepsilon}. \quad (\text{A.35})$$

The Feynman parameter integral I is finite at $\varepsilon = 0$ since $\mathcal{X} \equiv M^2 \equiv m_1^2 x + m_2^2(1-x) - q^2 x(1-x) > 0$ for $x \in [0, 1]$ as long as $m_1^2 > 0$ and $m_2^2 > 0$. Therefore we can expand I in ε up to negligible terms of the order $\mathcal{O}(\varepsilon^2)$

$$I = \int_0^1 dx \mathcal{X}^{-1+\varepsilon} = \int_0^1 dx \frac{1 + \varepsilon \ln \mathcal{X}}{\mathcal{X}} + \mathcal{O}(\varepsilon^2) = I_1 + \varepsilon I_2 + \mathcal{O}(\varepsilon^2). \quad (\text{A.36})$$

The integral $I_1 = \int_0^1 dx \frac{1}{\mathcal{X}}$ is elementary and can be found in Eq. (A.14). $I_2 = \int_0^1 dx \frac{\ln \mathcal{X}}{\mathcal{X}}$ can be calculated by writing \mathcal{X} in linear factors and by partial fractioning the denominator. After some algebra one finds the result given in Eq. (A.15).

A.3 Real and Virtual Contributions to Structure Functions

The soft real contributions S_i to the coefficient functions in Eq. (3.10) are given by

$$\begin{aligned} S_1 &= \frac{1}{\varepsilon}(-2 + \Sigma_{++} I_1) + 2 + \frac{\Sigma_{++}}{\Delta} \left[\Delta I_1 + \text{Li}_2 \left(\frac{2\Delta}{\Delta - \Sigma_{++}} \right) - \text{Li}_2 \left(\frac{2\Delta}{\Delta + \Sigma_{++}} \right) \right] \\ &\quad + \ln \frac{\Delta^2}{m_2^2 Q^2} (-2 + \Sigma_{++} I_1) \\ S_{2,3} &= S_1 \end{aligned} \quad (\text{A.37})$$

with I_1 given in Appendix A.2 and where χ is given in Eq. (3.7). The virtual contributions are derived from the renormalized vertex in Eq. (A.19) by using the projectors in Eq. (A.3):

$$\begin{aligned} V_1 &= C_{R,-} + \frac{S_- \Sigma_{++} - 2S_+ m_1 m_2}{S_+ \Sigma_{++} - 2S_- m_1 m_2} C_+ \\ V_2 &= C_{R,-} + \frac{1}{2} (m_1^2 C_{1,+} + m_2^2 C_{1,-}) + \frac{S_-}{S_+} \left[C_+ + \frac{m_1 m_2}{2} (C_{1,+} + C_{1,-}) \right] \\ V_3 &= C_{R,-} + \frac{R_-}{R_+} C_+ \end{aligned} \quad (\text{A.38})$$

where the C s are given in Appendix A.2. Note that the soft poles ($1/\varepsilon$) of S_i , V_i cancel in the sum $S_i + V_i$ in Eq. (3.10) as must be.

The massive matrix elements $\hat{f}_i^Q(\xi')$ are most conveniently given as functions of the Mandelstam variable $\hat{s}_1(\xi') \equiv (p_1 + q)^2 - m_2^2$, i.e. $\hat{f}_i^Q(\xi') \equiv \hat{f}_i^Q[\hat{s}_1(\xi')]$ with

$$\hat{s}_1(\xi') \equiv \hat{s} - m_2^2 = \frac{1 - \xi'}{2\xi'} [(\Delta - \Sigma_{+-})\xi' + \Delta + \Sigma_{+-}] \quad . \quad (\text{A.39})$$

From the real graphs of Fig. 3.1 (b) one obtains

$$\begin{aligned} \hat{f}_1^Q(\hat{s}_1) &= \frac{8}{\Delta'^2} \left\{ -\Delta^2(S_+\Sigma_{++} - 2m_1m_2S_-)I_{\xi'} + 2m_1m_2S_- \left(\frac{1}{\hat{s}_1} [\Delta'^2 + 4m_2^2\Sigma_{+-}] \right. \right. \\ &\quad + 2\Sigma_{+-} - \Sigma_{-+} + \frac{\Sigma_{++} + \hat{s}_1}{2} + \frac{\hat{s}_1 + m_2^2}{\Delta'\hat{s}_1} \left[\Delta'^2 + 2\Sigma_{+-}\Sigma_{++} + (m_2^2 + Q^2)\hat{s}_1 \right] L_{\xi'} \Bigg) \\ &\quad + S_+ \left(\frac{-m_2^2\Sigma_{++}}{(\hat{s}_1 + m_2^2)\hat{s}_1} (\Delta^2 + 4m_2^2\Sigma_{+-}) - \frac{1}{4(\hat{s}_1 + m_2^2)} \left[3\Sigma_{++}^2\Sigma_{-+} + 4m_2^2(10\Sigma_{++}\Sigma_{+-} \right. \right. \\ &\quad - \Sigma_{+-}\Sigma_{-+} - m_1^2\Sigma_{++}) + \hat{s}_1[-7\Sigma_{++}\Sigma_{-+} + 18\Delta^2 - 4m_1^2(7Q^2 - 4m_2^2 + 7m_1^2)] \\ &\quad + 3\hat{s}_1^2[\Sigma_{+-} - 2m_1^2] - \hat{s}_1^3] + \frac{\hat{s}_1 + m_2^2}{2\Delta'} \left[\frac{-2}{\hat{s}_1} \Sigma_{++} (\Delta^2 + 2\Sigma_{+-}\Sigma_{++}) \right. \\ &\quad + (4m_1^2m_2^2 - 7\Sigma_{+-}\Sigma_{++}) - 4\Sigma_{+-}\hat{s}_1 - \hat{s}_1^2] L_{\xi'} \Bigg) \Bigg\} \\ \hat{f}_2^Q(\hat{s}_1) &= \frac{16}{\Delta'^4} \left\{ -2\Delta^4S_+I_{\xi'} + 2m_1m_2S_- \left(\frac{\hat{s}_1 + m_2^2}{\Delta'} (\Delta'^2 - 6m_1^2Q^2) L_{\xi'} \right. \right. \\ &\quad - \frac{\Delta'^2(\hat{s}_1 + \Sigma_{++})}{2(\hat{s}_1 + m_2^2)} + \left(2\Delta'^2 - 3Q^2(\hat{s}_1 + \Sigma_{++}) \right) \Bigg) + S_+ \left(-2(\Delta^2 - 6m_1^2Q^2)(\hat{s}_1 + m_2^2) \right. \\ &\quad - 2(m_1^2 + m_2^2)\hat{s}_1^2 - 9m_2^2\Sigma_{+-}^2 + \Delta^2(2\Sigma_{++} - m_2^2) + 2\hat{s}_1(2\Delta^2 + (m_1^2 - 5m_2^2)\Sigma_{+-}) \\ &\quad + \frac{(\Delta'^2 - 6Q^2(m_2^2 + \hat{s}_1))\Sigma_{++}(\hat{s}_1 + \Sigma_{++})}{2(\hat{s}_1 + m_2^2)} - \frac{2\Delta^2}{\hat{s}_1} (\Delta^2 + 2(2m_2^2 + \hat{s}_1)\Sigma_{+-}) \\ &\quad + \frac{(\hat{s}_1 + m_2^2)}{\Delta'} \left[\frac{-2}{\hat{s}_1} \Delta^2(\Delta^2 + 2\Sigma_{+-}\Sigma_{++}) - 2\hat{s}_1(\Delta^2 - 6m_1^2Q^2) \right. \\ &\quad - (\Delta'^2 - 18m_1^2Q^2)\Sigma_{++} - 2\Delta^2(\Sigma_{++} + 2\Sigma_{+-})] L_{\xi'} \Bigg) \Bigg\} \\ \hat{f}_3^Q(\hat{s}_1) &= \frac{16}{\Delta'^2} \left\{ -2\Delta^2R_+I_{\xi'} + 2m_1m_2R_- \left(1 - \frac{\Sigma_{-+}}{\hat{s}_1} + \frac{(\hat{s}_1 + m_2^2)(\hat{s}_1 + \Sigma_{+-})}{\Delta'\hat{s}_1} L_{\xi'} \right) \right. \\ &\quad + R_+ \left(\Sigma_{-+} - 3\Sigma_{+-} - \frac{2}{\hat{s}_1} (\Delta^2 + 2m_2^2\Sigma_{+-}) - \frac{(\hat{s}_1 - \Sigma_{-+})(\hat{s}_1 + \Sigma_{++})}{2(\hat{s}_1 + m_2^2)} \right. \\ &\quad + \frac{\hat{s}_1 + m_2^2}{\Delta'\hat{s}_1} [-\hat{s}_1^2 + 4(m_1^2\Sigma_{-+} - \Delta^2) - 3\hat{s}_1\Sigma_{+-}] L_{\xi'} \Bigg) \Bigg\} \quad (\text{A.40}) \end{aligned}$$

with

$$L_{\xi'} \equiv \ln \left(\frac{\Sigma_{++} + \hat{s}_1 - \Delta'}{\Sigma_{++} + \hat{s}_1 + \Delta'} \right)$$

and

$$I_{\xi'} = \left(\frac{\hat{s}_1 + 2m_2^2}{\hat{s}_1^2} + \frac{\hat{s}_1 + m_2^2}{\Delta' \hat{s}_1^2} \Sigma_{++} L_{\xi'} \right) .$$

Δ is given below Eq. (3.4) and $\Delta' \equiv \Delta[m_1^2, \hat{s}, -Q^2]$.

Finally, the normalization factors in Eq. (3.10) are

$$N_1 = \frac{S_+ \Sigma_{++} - 2m_1 m_2 S_-}{2\Delta}, \quad N_2 = \frac{2S_+ \Delta}{(\Delta')^2}, \quad N_3 = \frac{2R_+}{\Delta'} . \quad (\text{A.41})$$

A.4 Comparison with E. Hoffmann and R. Moore, Z. Phys. **C20**, 71 (1983): Detailed List

HM: Refers to E. Hoffmann and R. Moore, Z. Phys. **C20**, 71 (1983)

KS: Refers to S. Kretzer and I. Schienbein, Phys. Rev. **D58**, 094035 (1998), as documented in this thesis in Chapter 3 and the above Appendices A.1–A.3.

Replacements:

$$m_{1,2}(\text{KS}) \rightarrow m$$

$$V, A(\text{KS}) \rightarrow 1, 0$$

As in HM: $\lambda \equiv m^2/Q^2$.

The bracketed numbers refer to the equations in the Hoffmann & Moore article and in this Thesis, respectively.

Vertex Correction

$$\left. \begin{aligned} \Lambda_R^\mu &= \Gamma^\mu \\ (\text{A.19})_{\text{KS}} &= (31)_{\text{HM}} \end{aligned} \right\} \text{up to a Gordon decomposition}$$

Virtual Contributions

$$\left. \begin{aligned} \frac{\alpha_s}{2\pi} C_F \Gamma(1-\varepsilon) \left(\frac{Q^2}{4\pi\mu^2} \right)^\varepsilon V_2 \delta(1-\xi') &= \sqrt{1+4\lambda} \sigma_{1V}^{(2)} \\ \frac{\alpha_s}{2\pi} C_F \Gamma(1-\varepsilon) \left(\frac{Q^2}{4\pi\mu^2} \right)^\varepsilon (\text{A.38})_{\text{KS}} \delta(1-\xi') &= \sqrt{1+4\lambda} (38)_{\text{HM}} \\ \frac{\alpha_s}{2\pi} C_F (V_2 - V_1) \delta(1-\xi') &= -2 \sqrt{1+4\lambda} \sigma_{1V}^{(L)} \\ \frac{\alpha_s}{2\pi} C_F [\Delta(\text{A.38})]_{\text{KS}} \delta(1-\xi') &= -2 \sqrt{1+4\lambda} (39)_{\text{HM}} \end{aligned} \right\} \begin{aligned} &\delta(1-\xi') \\ &= \\ &\sqrt{1+4\lambda} \delta(1-z) \end{aligned}$$

Soft Real Contributions

$$\begin{aligned} \frac{\alpha_s}{2\pi} C_F \Gamma(1-\varepsilon) \left(\frac{Q^2}{4\pi\mu^2} \right)^\varepsilon S_2 \delta(1-\xi') &= \sqrt{1+4\lambda} \left[\sigma_{1B}^{(2)} \Big|_{\sim\delta(1-z)} + f(\lambda) \right] \delta(1-z) \\ \frac{\alpha_s}{2\pi} C_F \Gamma(1-\varepsilon) \left(\frac{Q^2}{4\pi\mu^2} \right)^\varepsilon (\text{A.37})_{\text{KS}} \delta(1-\xi') &= \sqrt{1+4\lambda} \left[(48)_{\text{HM}} \Big|_{\sim\delta(1-z)} + f(\lambda) \right] \delta(1-z) \end{aligned}$$

where the discrepancy $f(\lambda)$

$$f(\lambda) = \frac{\alpha_s}{2\pi} C_F 2 \ln(1+4\lambda) \left(-1 - \frac{1+2\lambda}{\sqrt{1+4\lambda}} \ln \frac{\sqrt{1+4\lambda}-1}{\sqrt{1+4\lambda}+1} \right) \rightarrow 0; \quad \lambda \rightarrow 0$$

arises from the different choice of the convolution variables and is exactly cancelled if the identity

$$\frac{1}{(1-z)_+} = \frac{1}{(1-\xi')_+} \left(\frac{1-\xi'}{1-z} \right) + \ln \sqrt{1+4\lambda} \delta(1-z)$$

is used in Eq. (48)_{HM} or in Eq. (3.10)_{KS}.

Hard Real Contributions

$$\begin{aligned} \frac{\alpha_s}{2\pi} \hat{H}_2^q \Big|_{\xi' \neq 1} &= \frac{1+4\lambda z^2}{\sqrt{1+4\lambda}} \sigma_1^{(2)} \Big|_{z \neq 1} \\ \frac{\alpha_s}{2\pi} (3.10)_{\text{KS}} \Big|_{\xi' \neq 1} &= \frac{1+4\lambda z^2}{\sqrt{1+4\lambda}} (51)_{\text{HM}} \Big|_{z \neq 1} \\ \frac{\alpha_s}{2\pi} \hat{H}_1^q \Big|_{\xi' \neq 1} &= \sqrt{1+4\lambda} (-2 \sigma_1^{(L)} + \sigma_1^{(2)}) \Big|_{z \neq 1} \\ \frac{\alpha_s}{2\pi} (3.10)_{\text{KS}} \Big|_{\xi' \neq 1} &= \sqrt{1+4\lambda} [-2 (52)_{\text{HM}} + (51)_{\text{HM}}] \Big|_{z \neq 1}, \end{aligned}$$

where (52)_{HM} should be multiplied by an obvious factor z .

Summary

We (KS) agree with HM up to:

- The sign of the virtual contribution to the longitudinal structure function (which is irrelevant for F_2^c)
- The overall normalization of F_1^c . According to the above equations our (KS) normalization differs from HM by a factor $\sqrt{1+4\lambda}$. This does not really mean a discrepancy but stems from the choice of normalizing the $\mathcal{O}(\alpha_s^1)$ coefficient function relative to a Born term contribution of $\delta(1-z)$ (HM) or $\delta(1-\xi')$ (KS), corresponding to $(37)_{\text{HM}}$ or $(3.8)_{\text{KS}}$. However, we regard our normalization as preferable since it corresponds according to $(3.2)_{\text{KS}}$ directly to the notion of $c(\xi)$ carrying a light cone fraction ξ of the nucleon's momentum and is therefore directly related to
 - the original derivation of the conventionally used intrinsic charm component in Phys. Rev. **D23**, 2745 (1981) (*Intrinsic heavy-quark states*)
 - the all-order proof of *Hard-scattering factorization with heavy quarks* in Phys. Rev. **D58**, 094002 (1998)
- The normalization of F_2^c , which is –besides the $\sqrt{1+4\lambda}$ normalization ambiguity– wrong by a factor $(1+4\lambda z^2)/(1+4\lambda)$ in HM. The HM expression corresponds to the partonic structure function multiplying the $\sim p_c^\mu p_c^\nu 2z^2/Q^2$ partonic tensor. This normalization is only correct in the massless case and neglects finite mass terms which arise when contracting with the leptonic tensor and extracting the F_2^c structure function as the properly normalized coefficient of the $\sim (1-y)$ term.

Appendix B

Matrix Elements for Real Gluon Emission off Massive Quarks

The projections \hat{f}_i^Q of the partonic Matrix Element onto the structure functions are most conveniently given in the Mandelstam variables \hat{s}_1 and \hat{t}_1 which are defined below Eq. (4.6):

$$\begin{aligned}
\hat{f}_1^Q(\hat{s}_1, \hat{t}_1) &= \frac{8}{\Delta'^2} \left\{ -\Delta^2(S_+\Sigma_{++} - 2m_1m_2S_-) \left(\frac{m_2^2}{\hat{s}_1^2} + \frac{m_1^2}{\hat{t}_1^2} + \frac{\Sigma_{++}}{\hat{s}_1\hat{t}_1} \right) \right. \\
&+ 2m_1m_2S_- \left(\frac{m_1^2\hat{s}_1(\hat{s}_1 + 2\Sigma_{+-})}{\hat{t}_1^2} + \frac{\Delta'^2 + (m_2^2 + Q^2)\hat{s}_1 + 2\Sigma_{+-}\Sigma_{++}}{\hat{t}_1} \right. \\
&+ \left. \frac{\Delta'^2 - \hat{s}_1(m_1^2 + Q^2 + \hat{s}_1) + 2m_2^2\Sigma_{+-}}{\hat{s}_1} - \hat{t}_1 \frac{(m_2^2 + \hat{s}_1)}{\hat{s}_1} \right) \\
&+ S_+ \left(-\frac{m_1^2\hat{s}_1\Sigma_{+-}(\hat{s}_1 + 2\Sigma_{++})}{\hat{t}_1^2} + \frac{-\hat{s}_1^3 - 4\hat{s}_1^2\Sigma_{+-} + \hat{s}_1(4m_1^2m_2^2 - 7\Sigma_{+-}\Sigma_{++})}{2\hat{t}_1} \right. \\
&+ \frac{2\Sigma_{++}(-\Delta^2 - 2\Sigma_{+-}\Sigma_{++})}{2\hat{t}_1} + \left[4m_1^4 + 2m_1^2\hat{s}_1 - \Sigma_{+-}(m_2^2 + \Sigma_{+-}) \right. \\
&- \left. \left. \frac{(\Delta^2 + 2m_2^2\Sigma_{+-})\Sigma_{++}}{\hat{s}_1} \right] - \hat{t}_1 \frac{\Delta'^2 - 2(m_2^2 + \hat{s}_1)\Sigma_{++}}{2\hat{s}_1} \right) \Big\} \\
\hat{f}_2^Q(\hat{s}_1, \hat{t}_1) &= \frac{16}{\Delta'^4} \left\{ -2\Delta^4 S_+ \left(\frac{m_2^2}{\hat{s}_1^2} + \frac{m_1^2}{\hat{t}_1^2} + \frac{\Sigma_{++}}{\hat{s}_1\hat{t}_1} \right) + 2m_1m_2S_- \left(\frac{(\Delta'^2 - 6m_1^2Q^2)\hat{s}_1}{\hat{t}_1} \right. \right. \\
&+ \left. \left. \left[2(\Delta'^2 - 3Q^2(\hat{s}_1 + \Sigma_{++})) \right] + \hat{t}_1 \frac{\Delta'^2 - 6Q^2(m_2^2 + \hat{s}_1)}{\hat{s}_1} \right) \right\}
\end{aligned}$$

$$\begin{aligned}
& + S_+ \left(\frac{-2m_1^2 \hat{s}_1 [(\Delta^2 - 6m_1^2 Q^2) \hat{s}_1 + 2\Delta^2 \Sigma_{+-}]}{\hat{t}_1^2} + \frac{-2\Delta^2 (\Delta^2 + 2\Sigma_{+-} \Sigma_{++})}{\hat{t}_1} \right. \\
& + \frac{-\hat{s}_1 [2(\Delta^2 - 6m_1^2 Q^2) \hat{s}_1 + (\Delta'^2 - 18m_1^2 Q^2) \Sigma_{++} + 2\Delta^2 (3\Sigma_{++} - 4m_1^2)]}{\hat{t}_1} \\
& + \left[-2(m_1^2 + m_2^2) \hat{s}_1^2 - 9m_2^2 \Sigma_{+-}^2 - \frac{2\Delta^2 (\Delta^2 + 2m_2^2 \Sigma_{+-})}{\hat{s}_1} + 2\hat{s}_1 [2\Delta^2 \right. \\
& + (m_1^2 - 5m_2^2) \Sigma_{+-}] + \Delta^2 (2\Sigma_{++} - m_2^2) \left. \right] - \hat{t}_1 \frac{[\Delta'^2 - 6Q^2 (m_2^2 + \hat{s}_1)] \Sigma_{++}}{\hat{s}_1} \left. \right) \Bigg\} \\
\hat{f}_3^Q(\hat{s}_1, \hat{t}_1) &= \frac{16}{\Delta'^2} \left\{ -2\Delta^2 R_+ \left(\frac{m_2^2}{\hat{s}_1^2} + \frac{m_1^2}{\hat{t}_1^2} + \frac{\Sigma_{++}}{\hat{s}_1 \hat{t}_1} \right) + 2m_1 m_2 R_- \left(\frac{\hat{s}_1 + \Sigma_{+-}}{\hat{t}_1} + \frac{\hat{s}_1 - \Sigma_{-+}}{\hat{s}_1} \right) \right. \\
& + R_+ \left(\frac{-2m_1^2 \hat{s}_1 \Sigma_{+-}}{\hat{t}_1^2} + \frac{-\hat{s}_1^2 - 4(\Delta^2 - m_1^2 \Sigma_{-+}) - 3\hat{s}_1 \Sigma_{+-}}{\hat{t}_1} \right. \\
& + \left. \left[2(m_1^2 - m_2^2) - \frac{2(\Delta^2 + m_2^2 \Sigma_{+-})}{\hat{s}_1} \right] + \hat{t}_1 \frac{\hat{s}_1 - \Sigma_{-+}}{\hat{s}_1} \right) \left. \right\} \quad (B.1)
\end{aligned}$$

where we conveniently use the shorthands $\Delta \equiv \Delta[m_1^2, m_2^2, -Q^2]$ and $\Delta' \equiv \Delta[m_1^2, \hat{s}, -Q^2]$. In order to obtain the inclusive results $\hat{f}_i^Q(\hat{s}_1)$ in Appendix A the $\hat{f}_i^Q(\hat{s}_1, \hat{t}_1)$ have to be integrated over $0 \leq y \leq 1$, i.e.

$$\hat{f}_i^Q(\hat{s}_1) = \int_0^1 dy \hat{f}_i^Q(\hat{s}_1, \hat{t}_1) \quad , \quad (B.2)$$

where y is defined via the partonic center of mass scattering angle θ^* and related to \hat{t}_1 through

$$\begin{aligned}
y &\equiv \frac{1}{2} (1 + \cos \theta^*) \\
\hat{t}_1 &= \frac{\hat{s}_1}{\hat{s}_1 + m_2^2} \Delta' (y - y_0) \quad , \quad (B.3)
\end{aligned}$$

with $y_0 = [1 + (\Sigma_{++} + \hat{s}_1)/\Delta']/2$ being the would-be collinear pole of the \hat{t} -channel propagator.

Appendix C

Limits of the Doubly Virtual Box

Due to the particular choice of variables, the results in Eq. (8.11) are especially well suited for deriving various important limits wide-spread over the literature which are relevant for some of the chapters in this thesis:

- Most important for our purposes is the Bjorken limit ($Q^2 \rightarrow \infty, \nu \rightarrow \infty, x = \text{const}$) in which we can study structure functions of the real and virtual photon as has already been discussed in Chapter 7.
- Also needed is the real photon $P^2 = 0$ ($\delta = 0$) case in which the general virtual box results in (8.11) reduce to the standard box-diagram $\gamma^*(Q^2)\gamma \rightarrow q\bar{q}$ expressions for a *real* photon $\gamma \equiv \gamma(P^2 = 0)$. Keeping the full mass dependence in (8.11) we obtain expressions relevant for the heavy quark contribution to the photon structure functions.
- Finally, the general light quark mass limit (for arbitrary P^2, Q^2) can be easily obtained from (8.11) by setting $m = 0$ ($\lambda = 0, \beta = 1$) and needs no separate discussion.

In the following, our main concern will lie on the Bjorken limit. Practically this limit means that Q^2 is much larger than the other scales m^2 and P^2 . Beside the general case $m^2, P^2 \ll Q^2$ which will be studied in Section C.1 additional orderings $m^2 = 0, P^2 \ll Q^2$ (Section C.2) and $P^2 = 0, m^2 \ll Q^2$ (Section C.3) are of interest and the expressions further simplify under these circumstances. One must be careful in handling these limits because for some of the box cross sections the result depends on which of the two limits

$m \rightarrow 0$ and $P^2 \rightarrow 0$ is taken first. For example, below we will find the following asymptotic expressions for σ_{TL} derived from (8.11):

$$0 = \lim_{m^2 \rightarrow 0} \lim_{P^2 \rightarrow 0} \sigma_{\text{TL}} \neq \lim_{P^2 \rightarrow 0} \lim_{m^2 \rightarrow 0} \sigma_{\text{TL}} = N_c e_q^4 \frac{4\pi\alpha^2}{Q^2} 4x^2(1-x)$$

Mathematically, the origin of such a behavior is easily identified. Terms like $\frac{4x\delta}{4x\delta + \lambda\bar{\beta}^2}$ occurring in (8.11) (not only as the argument of the logarithm) require a careful treatment. In general they are *not* negligible even for small m^2 and P^2 and, viewed as a function of m^2 and P^2 , they are discontinuous at $(m^2, P^2) = (0, 0)$. Finally, in Section C.3 we also derive expressions for the heavy quark contributions to the photon structure functions in the real photon limit by setting $P^2 = 0$ ($\delta = 0$) but keeping the full mass dependence in (8.11).

All results for the photon-photon cross sections will be given for a single quark with charge e_q and mass m . The photon structure functions F_i , ($i = 1, 2, \text{L}$) can be obtained from these expressions with help of the relations in Section 7.2 which simplify in the Bjorken limit ($P^2 \ll Q^2 \Rightarrow \bar{\beta} \simeq 1$):

$$\begin{aligned} F_2^{\gamma\text{T}} &= \frac{Q^2}{4\pi^2\alpha} \sigma_{2\text{T}}, & F_{\text{L}}^{\gamma\text{T}} &= \frac{Q^2}{4\pi^2\alpha} \sigma_{\text{LT}} \\ F_2^{\gamma\text{L}} &= \frac{Q^2}{4\pi^2\alpha} \sigma_{2\text{L}}, & F_{\text{L}}^{\gamma\text{L}} &= \frac{Q^2}{4\pi^2\alpha} \sigma_{\text{LL}} \end{aligned} \quad (\text{C.1})$$

with $\sigma_{2\text{T}} = \sigma_{\text{TT}} + \sigma_{\text{LT}}$, $\sigma_{2\text{L}} = \sigma_{\text{TL}} + \sigma_{\text{LL}}$. The commonly utilized expressions for a spin-averaged target photon are given by

$$F_i^{<\gamma>} = F_i^{\gamma\text{T}} - \frac{1}{2} F_i^{\gamma\text{L}}, \quad (i = 1, 2, \text{L}). \quad (\text{C.2})$$

Finally, the structure function F_1 can be deduced from $F_{\text{L}} = F_2 - 2xF_1$. Since the structure functions are (apart from the normalization factor $Q^2/4\pi^2\alpha$) simple linear combinations of the photon-photon cross sections they will only be written out in those cases where they are needed explicitly in the thesis.

C.1 General Bjorken Limit: $m^2, P^2 \ll Q^2$

In the general Bjorken limit the normalization factor N given in Eq. (8.10) and the logarithm L from Eq. (8.9) are given by

$$\begin{aligned} N &= 4\pi N_c e_q^4 \frac{4\pi\alpha^2}{Q^2} x (1 + \mathcal{O}(\delta)) \\ L &= \ln \frac{4}{4x\delta + \lambda} + \mathcal{O}(\delta, \lambda) . \end{aligned} \quad (\text{C.3})$$

Keeping this in mind and using $\beta = 1 + \mathcal{O}(\lambda)$, $\bar{\beta} = 1 + \mathcal{O}(\delta)$ the following results can be easily deduced from Eq. (8.11):

$$\begin{aligned} \sigma_{\text{TT}} &= N_c e_q^4 \frac{4\pi\alpha^2}{Q^2} x \left\{ \left[x^2 + (1-x)^2 \right] L + 4x(1-x) - 1 - \frac{4x\delta}{4x\delta + \lambda} + \mathcal{O}(\delta, \lambda) \right\} \\ \sigma_{\text{LT}} &= N_c e_q^4 \frac{4\pi\alpha^2}{Q^2} x \left\{ 4x(1-x) + \mathcal{O}(\delta, \lambda) \right\} \\ \sigma_{\text{TL}} &= N_c e_q^4 \frac{4\pi\alpha^2}{Q^2} x \left\{ 4x(1-x) \frac{4x\delta}{4x\delta + \lambda} + \mathcal{O}(\delta, \lambda) \right\} \\ \tau_{\text{TT}} &= N_c e_q^4 \frac{4\pi\alpha^2}{Q^2} x \left\{ -2x^2 + \mathcal{O}(\delta, \lambda) \right\} \\ \tau_{\text{TT}}^{\text{a}} &= N_c e_q^4 \frac{4\pi\alpha^2}{Q^2} x \left\{ (2x-1)L + 3 - 4x - \frac{4x\delta}{4x\delta + \lambda} + \mathcal{O}(\delta, \lambda) \right\} . \end{aligned} \quad (\text{C.4})$$

The remaining expressions are suppressed by powers of $\delta = xP^2/Q^2$ (see Eq. (8.11)).

At the price of a slightly worse approximation (at larger x) one can further use

$$\begin{aligned} \frac{4x\delta}{4x\delta + \lambda} &= \frac{P^2 x(1-x)}{P^2 x(1-x) + m^2} + \mathcal{O}\left(\frac{P^2}{W^2}, \lambda\right), \\ L &= \ln \frac{Q^2(1-x)}{x[P^2 x(1-x) + m^2]} + \mathcal{O}\left(\frac{P^2}{W^2}, \lambda\right). \end{aligned} \quad (\text{C.5})$$

For example we can write:

$$\begin{aligned} \sigma_{\text{TT}} &= N_c e_q^4 \frac{4\pi\alpha^2}{Q^2} x \left\{ \left[1 - 2x(1-x) \right] \ln \frac{Q^2(1-x)}{x[P^2 x(1-x) + m^2]} + 4x(1-x) - 1 \right. \\ &\quad \left. - \frac{P^2 x(1-x)}{P^2 x(1-x) + m^2} + \mathcal{O}\left(\frac{P^2}{W^2}, \lambda\right) \right\} . \end{aligned} \quad (\text{C.6})$$

C.2 $m^2 = 0, P^2 \ll Q^2$

In this section we consider the asymptotic virtual ($P^2 \neq 0$) box expressions for light quarks in the Bjorken limit for which the expressions in Eq. (C.4) further reduce. Noticing that

the logarithm L is given by $L = \ln \frac{Q^2}{P^2 x^2}$ we can write in this case (neglecting terms of the order $\mathcal{O}(\delta)$):

$$\begin{aligned}\sigma_{\text{TT}} &\simeq N_c e_q^4 \frac{4\pi\alpha^2}{Q^2} x \left\{ [x^2 + (1-x)^2] \ln \frac{Q^2}{P^2 x^2} + 4x(1-x) - 2 \right\} \\ \sigma_{\text{TL}} &\simeq \sigma_{\text{LT}} \simeq N_c e_q^4 \frac{4\pi\alpha^2}{Q^2} x [4x(1-x)] \\ \tau_{\text{TT}} &\simeq N_c e_q^4 \frac{4\pi\alpha^2}{Q^2} x [-2x^2] \\ \tau_{\text{TT}}^{\text{a}} &\simeq N_c e_q^4 \frac{4\pi\alpha^2}{Q^2} x \left\{ (2x-1) \ln \frac{Q^2}{P^2 x^2} + 2 - 4x \right\} .\end{aligned}\quad (\text{C.7})$$

Summing over $q = u, d, s$ and utilizing Eqs. (C.1) and (C.2) we recover the well known asymptotic results for the virtual ($P^2 \neq 0$) box structure functions for the light $q = u, d, s$ quarks in the Bjorken limit $P^2/Q^2 \ll 1$:

$$F_{2,\text{box}}^{\gamma\text{T},\ell}(x, Q^2, P^2) \simeq N_c \sum e_q^4 \frac{\alpha}{\pi} x \left\{ [x^2 + (1-x)^2] \ln \frac{Q^2}{P^2 x^2} + 8x(1-x) - 2 \right\} \quad (\text{C.8})$$

$$F_{2,\text{box}}^{\gamma\text{L},\ell}(x, Q^2, P^2) \simeq N_c \sum e_q^4 \frac{\alpha}{\pi} x \{4x(1-x)\} \quad (\text{C.9})$$

$$F_{2,\text{box}}^{<\gamma>,\ell}(x, Q^2, P^2) \simeq N_c \sum e_q^4 \frac{\alpha}{\pi} x \left\{ [x^2 + (1-x)^2] \ln \frac{Q^2}{P^2 x^2} + 6x(1-x) - 2 \right\} . \quad (\text{C.10})$$

C.3 Real Photon Limit: $P^2 = 0$

For $P^2 = 0$ the virtual box results in (8.11) reduce to the standard box-diagram $\gamma^*(Q^2)\gamma \rightarrow q\bar{q}$ expressions for a *real* photon $\gamma \equiv \gamma(P^2 = 0)$.

The heavy quark contribution becomes, utilizing $\delta = 0$, $\bar{\beta} = 1$ and $\lambda = \frac{4m_h^2 x}{Q^2(1-x)}$,

$$\begin{aligned}\sigma_{\text{TT}} &= N_c e_h^4 \frac{4\pi\alpha^2}{Q^2} x \Theta(\beta^2) \left\{ \left[x^2 + (1-x)^2 + x(1-x) \frac{4m_h^2}{Q^2} - x^2 \frac{8m_h^4}{Q^4} \right] \ln \frac{1+\beta}{1-\beta} \right. \\ &\quad \left. + \beta \left[4x(1-x) - 1 - x(1-x) \frac{4m_h^2}{Q^2} \right] \right\} \\ \sigma_{\text{LT}} &= N_c e_h^4 \frac{4\pi\alpha^2}{Q^2} x \Theta(\beta^2) \left\{ -x^2 \frac{8m_h^2}{Q^2} \ln \frac{1+\beta}{1-\beta} + \beta 4x(1-x) \right\} \\ \tau_{\text{TT}} &= N_c e_h^4 \frac{4\pi\alpha^2}{Q^2} x \Theta(\beta^2) \left\{ \left[-x^2 \frac{8m_h^2}{Q^2} - x^2 \frac{8m_h^4}{Q^4} \right] \ln \frac{1+\beta}{1-\beta} - \beta \left[2x^2 + x(1-x) \frac{4m_h^2}{Q^2} \right] \right\} \\ \tau_{\text{TT}}^{\text{a}} &= N_c e_h^4 \frac{4\pi\alpha^2}{Q^2} x \Theta(\beta^2) \left\{ (2x-1) \ln \frac{1+\beta}{1-\beta} + \beta(3-4x) \right\} .\end{aligned}\quad (\text{C.11})$$

i.e., according to (C.2) (or (C.1))

$$\begin{aligned}
F_{2,\text{box}}^{\gamma,h}(x, Q^2) &= 3 e_h^4 \frac{\alpha}{\pi} x \Theta(\beta^2) \left\{ \left[x^2 + (1-x)^2 + x(1-3x) \frac{4m_h^2}{Q^2} - x^2 \frac{8m_h^4}{Q^4} \right] \ln \frac{1+\beta}{1-\beta} \right. \\
&\quad \left. + \beta \left[8x(1-x) - 1 - x(1-x) \frac{4m_h^2}{Q^2} \right] \right\} \\
F_{L,\text{box}}^{\gamma,h}(x, Q^2) &= 3 e_h^4 \frac{\alpha}{\pi} x \Theta(\beta^2) \left\{ -x^2 \frac{8m_h^2}{Q^2} \ln \frac{1+\beta}{1-\beta} + \beta 4x(1-x) \right\} \quad (\text{C.12})
\end{aligned}$$

which are the familiar massive Bethe–Heitler expressions [117] relevant for the heavy quark contributions to the structure functions of real photons (cf. [6], for example).

In the light quark sector where $\lambda \ll 1$, i.e. $m^2 \equiv m_q^2 \ll Q^2$, the logarithm can be written as

$$L = \ln \frac{1+\beta}{1-\beta} = \ln \frac{Q^2(1-x)}{m_q^2 x} + \mathcal{O}(\lambda) .$$

and we obtain from (C.4) or (C.11) the following results (neglecting terms of the order $\mathcal{O}(\lambda)$):

$$\begin{aligned}
\sigma_{\text{TT}} &\simeq N_c e_q^4 \frac{4\pi\alpha^2}{Q^2} x \left\{ [x^2 + (1-x)^2] \ln \frac{Q^2(1-x)}{m_q^2 x} + 4x(1-x) - 1 \right\} \\
\sigma_{\text{LT}} &\simeq N_c e_q^4 \frac{4\pi\alpha^2}{Q^2} x [4x(1-x)] \\
\tau_{\text{TT}} &\simeq N_c e_q^4 \frac{4\pi\alpha^2}{Q^2} x [-2x^2] \\
\tau_{\text{TT}}^{\text{a}} &\simeq N_c e_q^4 \frac{4\pi\alpha^2}{Q^2} x \left\{ (2x-1) \ln \frac{Q^2(1-x)}{m_q^2 x} + 3 - 4x \right\} , \quad (\text{C.13})
\end{aligned}$$

i.e., according to (C.2) (or (C.1))

$$F_{2,\text{box}}^{\gamma,\ell}(x, Q^2) \simeq N_c \sum e_q^4 \frac{\alpha}{\pi} x \left\{ [x^2 + (1-x)^2] \ln \frac{Q^2(1-x)}{m_q^2 x} + 8x(1-x) - 1 \right\} . \quad (\text{C.14})$$

Note also that σ_{TL} vanishes like $\sigma_{\text{TL}} \propto P^2/m_q^2$.

Appendix D

Parametrizations

D.1 Pion Distributions

D.1.1 Parametrization of LO Parton Distributions

Defining [26]

$$s \equiv \ln \frac{\ln[Q^2/(0.204 \text{ GeV})^2]}{\ln[\mu_{\text{LO}}^2/(0.204 \text{ GeV})^2]} \quad (\text{D.1})$$

to be evaluated for $\mu_{\text{LO}}^2 = 0.26 \text{ GeV}^2$, all our resulting pionic parton distributions can be expressed by the following simple parametrizations, valid for $0.5 \lesssim Q^2 \lesssim 10^5 \text{ GeV}^2$ (i.e. $0.31 \leq s \lesssim 2.2$) and $10^{-5} \lesssim x < 1$. For the valence distribution we take

$$x v^\pi(x, Q^2) = N x^a (1 + A\sqrt{x} + Bx)(1 - x)^D \quad (\text{D.2})$$

with

$$\begin{aligned} N &= 1.212 + 0.498 s + 0.009 s^2 \\ a &= 0.517 - 0.020 s \\ A &= -0.037 - 0.578 s \\ B &= 0.241 + 0.251 s \\ D &= 0.383 + 0.624 s. \end{aligned} \quad (\text{D.3})$$

The gluon and light sea-quark distributions are parametrized as

$$x w^\pi(x, Q^2) = \left[x^a (A + B\sqrt{x} + Cx) \left(\ln \frac{1}{x} \right)^b + s^\alpha \exp \left(-E + \sqrt{E' s^\beta \ln \frac{1}{x}} \right) \right] (1-x)^D. \quad (\text{D.4})$$

For $w = g$

$$\begin{aligned} \alpha &= 0.504, & \beta &= 0.226, \\ a &= 2.251 - 1.339 \sqrt{s}, & b &= 0, \\ A &= 2.668 - 1.265 s + 0.156 s^2, & B &= -1.839 + 0.386 s, \\ C &= -1.014 + 0.920 s - 0.101 s^2, & D &= -0.077 + 1.466 s, \\ E &= 1.245 + 1.833 s, & E' &= 0.510 + 3.844 s, \end{aligned} \quad (\text{D.5})$$

and for the light sea $w = \bar{q}$

$$\begin{aligned} \alpha &= 1.147, & \beta &= 1.241, \\ a &= 0.309 - 0.134 \sqrt{s}, & b &= 0.893 - 0.264 \sqrt{s}, \\ A &= 0.219 - 0.054 s, & B &= -0.593 + 0.240 s, \\ C &= 1.100 - 0.452 s, & D &= 3.526 + 0.491 s, \\ E &= 4.521 + 1.583 s, & E' &= 3.102. \end{aligned} \quad (\text{D.6})$$

The strange sea distribution $s^\pi = \bar{s}^\pi$ is parametrized as

$$x \bar{s}^\pi(x, Q^2) = \frac{s^\alpha}{(\ln \frac{1}{x})^a} (1 + A\sqrt{x} + Bx) (1-x)^D \exp \left(-E + \sqrt{E' s^\beta \ln \frac{1}{x}} \right) \quad (\text{D.7})$$

with

$$\begin{aligned} \alpha &= 0.823, & \beta &= 0.650, \\ a &= 1.036 - 0.709 s, & A &= -1.245 + 0.713 s, \\ B &= 5.580 - 1.281 s, & D &= 2.746 - 0.191 s, \\ E &= 5.101 + 1.294 s, & E' &= 4.854 - 0.437 s. \end{aligned} \quad (\text{D.8})$$

D.1.2 Parametrization of NLO($\overline{\text{MS}}$) Parton Distributions

Defining [26]

$$s \equiv \ln \frac{\ln[Q^2/(0.299 \text{ GeV})^2]}{\ln[\mu_{\text{NLO}}^2/(0.299 \text{ GeV})^2]} \quad (\text{D.9})$$

to be evaluated for $\mu_{\text{NLO}}^2 = 0.40 \text{ GeV}^2$, our NLO predictions can be parametrized as the LO ones and are similarly valid for $0.5 \lesssim Q^2 \lesssim 10^5 \text{ GeV}^2$ (i.e. $0.14 \lesssim s \lesssim 2.38$) and $10^{-5} \lesssim x < 1$. The valence distribution is given by (D.2) with

$$\begin{aligned} N &= 1.500 + 0.525 s - 0.050 s^2 \\ a &= 0.560 - 0.034 s \\ A &= -0.357 - 0.458 s \\ B &= 0.427 + 0.220 s \\ D &= 0.475 + 0.550 s. \end{aligned} \quad (\text{D.10})$$

The gluon and light sea distributions are parametrized as in (D.4) where for $w = g$

$$\begin{aligned} \alpha &= 0.793, & \beta &= 1.722, \\ a &= 1.418 - 0.215\sqrt{s}, & b &= 0, \\ A &= 5.392 + 0.553 s - 0.385 s^2, & B &= -11.928 + 1.844 s, \\ C &= 11.548 - 4.316 s + 0.382 s^2, & D &= 1.347 + 1.135 s, \\ E &= 0.104 + 1.980 s, & E' &= 2.375 - 0.188 s, \end{aligned} \quad (\text{D.11})$$

and for the light sea $w = \bar{q}$

$$\begin{aligned} \alpha &= 1.118, & \beta &= 0.457, \\ a &= 0.111 - 0.326\sqrt{s}, & b &= -0.978 - 0.488\sqrt{s}, \\ A &= 1.035 - 0.295 s, & B &= -3.008 + 1.165 s, \\ C &= 4.111 - 1.575 s, & D &= 6.192 + 0.705 s, \\ E &= 5.035 + 0.997 s, & E' &= 1.486 + 1.288 s. \end{aligned} \quad (\text{D.12})$$

The strange sea distribution is parametrized as in (D.7) with

$$\begin{aligned} \alpha &= 0.908, & \beta &= 0.812, \\ a &= -0.567 - 0.466 s, & A &= -2.348 + 1.433 s, \\ B &= 4.403, & D &= 2.061, \\ E &= 3.796 + 1.618 s, & E' &= 0.309 + 0.355 s. \end{aligned} \quad (\text{D.13})$$

Let us recall that in the light quark sector $u_v^{\pi^+} = \bar{d}_v^{\pi^+} = \bar{u}_v^{\pi^-} = d_v^{\pi^-}$, $\bar{u}^{\pi^+} = d^{\pi^+} = u^{\pi^-} = \bar{d}^{\pi^-}$ and $f^{\pi^0} = (f^{\pi^+} + f^{\pi^-})/2$.

D.2 Photon Distributions

Simple analytic parametrizations in LO and NLO of the ‘hadronic’ piece of the real and virtual photonic parton distributions, being proportional to $f^\pi(x, Q^2)$ in Eqs. (11.5) and (11.13), respectively, are already known according to the parametrizations for $f^\pi(x, Q^2)$ in Appendix D.1. Therefore we only need to parametrize the remaining ‘pointlike’ components in Eqs. (11.5) and (11.13).

D.2.1 Parametrization of LO ‘pointlike’ Photonic Parton Distributions

In LO the Q^2 dependence of the ‘pointlike’ $f_{\text{pl}}^\gamma(x, Q^2)$ term in (11.5) enters, apart from an overall $1/\alpha_s(Q^2)$ factor, merely via the combination $L \equiv \alpha_s(Q^2)/\alpha_s(\mu_{\text{LO}}^2)$ as is evident, for example, from Eq. (2.12) in Ref. [112]. Therefore, we prefer to parametrize the quantity $f_{\text{pl}}^\gamma(x, Q^2)$ in terms of

$$s \equiv \ln \frac{\ln [Q^2/(0.204 \text{ GeV})^2]}{\ln [\mu_{\text{LO}}^2/(0.204 \text{ GeV})^2]} \quad (\text{D.14})$$

where [26] $\mu_{\text{LO}}^2 = 0.26 \text{ GeV}^2$, which will later provide us a parametrization also for the virtual ‘pointlike’ component in (11.13). Our resulting ‘pointlike’ distributions in Eq. (11.5) can be expressed by the following simple parametrizations, valid for $0.5 \lesssim Q^2 \lesssim 10^5 \text{ GeV}^2$ (i.e. $0.31 \lesssim s \lesssim 2.2$) and $10^{-5} \lesssim x < 1$:

$$\begin{aligned} \frac{1}{\alpha} x f_{\text{pl}}^\gamma(x, Q^2) &= \frac{9}{4\pi} \ln \frac{Q^2}{(0.204 \text{ GeV})^2} \left[s^\alpha x^a (A + B\sqrt{x} + C x^b) \right. \\ &\quad \left. + s^{\alpha'} \exp \left(-E + \sqrt{E' s^\beta \ln \frac{1}{x}} \right) \right] (1-x)^D \end{aligned} \quad (\text{D.15})$$

where for $f_{\text{pl}}^\gamma = u_{\text{pl}}^\gamma = \bar{u}_{\text{pl}}^\gamma$

$$\begin{aligned}
\alpha &= 0.897, & \alpha' &= 2.626, \\
\beta &= 0.413, \\
a &= 2.137 - 0.310 \sqrt{s}, & b &= -1.049 + 0.113 s, \\
A &= -0.785 + 0.270 \sqrt{s}, & B &= 0.650 - 0.146 s, \\
C &= 0.252 - 0.065 \sqrt{s}, & D &= -0.116 + 0.403 s - 0.117 s^2, \\
E &= 6.749 + 2.452 s - 0.226 s^2, & E' &= 1.994 s - 0.216 s^2,
\end{aligned} \tag{D.16}$$

for $f_{\text{pl}}^\gamma = d_{\text{pl}}^\gamma = \bar{d}_{\text{pl}}^\gamma = s_{\text{pl}}^\gamma = \bar{s}_{\text{pl}}^\gamma$

$$\begin{aligned}
\alpha &= 1.084, & \alpha' &= 2.811, \\
\beta &= 0.960, \\
a &= 0.914, & b &= 3.723 - 0.968 s, \\
A &= 0.081 - 0.028 \sqrt{s}, & B &= -0.048, \\
C &= 0.094 - 0.043 \sqrt{s}, & D &= 0.059 + 0.263 s - 0.085 s^2, \\
E &= 6.808 + 2.239 s - 0.108 s^2, & E' &= 1.225 + 0.594 s - 0.073 s^2,
\end{aligned} \tag{D.17}$$

and for $f_{\text{pl}}^\gamma = g_{\text{pl}}^\gamma$

$$\begin{aligned}
\alpha &= 1.262, & \alpha' &= 2.024, \\
\beta &= 0.770, \\
a &= 0.081, & b &= 0.848, \\
A &= 0.012 + 0.039 \sqrt{s}, & B &= -0.056 - 0.044 s, \\
C &= 0.043 + 0.031 s, & D &= 0.925 + 0.316 s, \\
E &= 3.129 + 2.434 s - 0.115 s^2, & E' &= 1.364 + 1.227 s - 0.128 s^2.
\end{aligned} \tag{D.18}$$

With these parametrizations at hand in terms of s in (D.14), the appropriate ones for the ‘pointlike’ distributions $f_{\text{pl}}^{\gamma(P^2)}(x, Q^2)$ of a virtual photon appearing in Eq. (11.13) are simply given by the same expressions above where in (D.14) μ_{LO}^2 has to be replaced by $\tilde{P}^2 = \max(P^2, \mu_{\text{LO}}^2)$. As discussed in Sec. 11.4, these parametrizations can, within sufficient accuracy, also be used for the parton distribution of virtual photons in NLO.

D.2.2 Parametrization of NLO ‘pointlike’ Photonic Parton Distributions

In NLO the Q^2 dependence of the ‘pointlike’ distributions of real photons in (11.5), $f_{\text{pl}}^\gamma(x, Q^2)$, can be easily described in terms of the following ‘effective’ logarithmic ratio

$$s \equiv \ln \frac{\ln [Q^2/(0.299 \text{ GeV})^2]}{\ln [\mu_{\text{NLO}}^2/(0.299 \text{ GeV})^2]} \quad (\text{D.19})$$

to be evaluated for $\mu_{\text{NLO}}^2 = 0.40 \text{ GeV}^2$. Our NLO(DIS $_\gamma$) predictions can now be parametrized as the LO ones and are similarly valid for $0.5 \lesssim Q^2 \lesssim 10^5 \text{ GeV}^2$ (i.e. $0.14 \lesssim s \lesssim 2.38$) and $10^{-5} \lesssim x < 1$. For convenience we include now the NLO α_s in the r.h.s. of (D.15), i.e.

$$\begin{aligned} \frac{1}{\alpha} x f_{\text{pl}}^\gamma(x, Q^2) = & \left[s^\alpha x^a (A + B\sqrt{x} + Cx^b) \right. \\ & \left. + s^{\alpha'} \exp \left(-E + \sqrt{E' s^\beta \ln \frac{1}{x}} \right) \right] (1-x)^D \end{aligned} \quad (\text{D.20})$$

where for $f_{\text{pl}}^\gamma = u_{\text{pl}}^\gamma = \bar{u}_{\text{pl}}^\gamma$

$$\begin{aligned} \alpha &= 1.051, & \alpha' &= 2.107, \\ \beta &= 0.970, \\ a &= 0.412 - 0.115 \sqrt{s}, & b &= 4.544 - 0.563 s, \\ A &= -0.028 \sqrt{s} + 0.019 s^2, & B &= 0.263 + 0.137 s, \\ C &= 6.726 - 3.264 \sqrt{s} - 0.166 s^2, & D &= 1.145 - 0.131 s^2, \\ E &= 4.122 + 3.170 s - 0.598 s^2, & E' &= 1.615 s - 0.321 s^2, \end{aligned} \quad (\text{D.21})$$

for $f_{\text{pl}}^\gamma = d_{\text{pl}}^\gamma = \bar{d}_{\text{pl}}^\gamma = s_{\text{pl}}^\gamma = \bar{s}_{\text{pl}}^\gamma$

$$\begin{aligned} \alpha &= 1.043, & \alpha' &= 1.812, \\ \beta &= 0.457, \\ a &= 0.416 - 0.173 \sqrt{s}, & b &= 4.489 - 0.827 s, \\ A &= -0.010 \sqrt{s} + 0.006 s^2, & B &= 0.064 + 0.020 s, \\ C &= 1.577 - 0.916 \sqrt{s}, & D &= 1.122 - 0.093 s - 0.100 s^2, \\ E &= 5.240 + 1.666 s - 0.234 s^2, & E' &= 1.284 s, \end{aligned} \quad (\text{D.22})$$

and for $f_{\text{pl}}^\gamma = g_{\text{pl}}^\gamma$

$$\begin{aligned}
\alpha &= 0.901, & \alpha' &= 1.773, \\
\beta &= 1.666, \\
a &= 0.844 - 0.820 \sqrt{s}, & b &= 2.302 - 0.474 s, \\
A &= 0.194, & B &= -0.324 + 0.143 s, \\
C &= 0.330 - 0.177 s, & D &= 0.778 + 0.502 s - 0.154 s^2, \\
E &= 2.895 + 1.823 s - 0.441 s^2, & E' &= 2.344 - 0.584 s.
\end{aligned} \tag{D.23}$$

Bibliography

- [1] I. Schienbein, *Strahlungskorrekturen und schwere Quarkproduktion in tief-inelastischen neutralen und geladenen Streuprozessen*, Diplomarbeit, Universität Dortmund, Germany, 1997.
- [2] S. Kretzer and I. Schienbein, Phys. Rev. **D56**, 1804 (1997).
- [3] S. Kretzer and I. Schienbein, Phys. Rev. **D58**, 094035 (1998).
- [4] S. Kretzer and I. Schienbein, Phys. Rev. **D59**, 054004 (1999).
- [5] M. Glück, E. Reya, and I. Schienbein, Eur. Phys. J. **C10**, 313 (1999).
- [6] M. Glück, E. Reya, and I. Schienbein, Phys. Rev. **D60**, 054019 (1999), Erratum: **D62** (2000) 019902.
- [7] M. Glück, E. Reya, and I. Schienbein, Phys. Rev. **D64**, 017501 (2001).
- [8] M. Glück, E. Reya, and I. Schienbein, Phys. Rev. **D63**, 074008 (2001).
- [9] I. Schienbein, Nucl. Phys. Proc. Suppl. **82**, 14 (2000).
- [10] I. Schienbein, talk given at 8th International Workshop on Deep Inelastic Scattering and QCD (DIS 2000), Liverpool, England, 25–30 Apr 2000, hep-ph/0006218.
- [11] C. Adloff *et al.*, H1 Collaboration, Z. Phys. **C72**, 593 (1996).
- [12] J. Breitweg *et al.*, ZEUS Collaboration, Phys. Lett. **B407**, 402 (1997).
- [13] J. Breitweg *et al.*, ZEUS Collaboration, Eur. Phys. J. **C12**, 35 (2000).
- [14] A. Vogt, in *Proceedings of the Durham Workshop on HERA Physics: Proton, Photon and Pomeron Structure*, 17–23 Sep 1995, Durham, England (1996), pp. 254–258, hep-ph/9601352.

- [15] C. Adloff *et al.*, H1 Collaboration, Nucl. Phys. **B545**, 21 (1999).
- [16] S. A. Rabinowitz *et al.*, CCFR Collaboration, Phys. Rev. Lett. **70**, 134 (1993).
- [17] A. O. Bazarko *et al.*, CCFR Collaboration, Z. Phys. **C65**, 189 (1995).
A. O. Bazarko, *Determination of the strange quark distribution from a next-to-leading order QCD analysis of neutrino and anti-neutrino production of charm*, Ph.D. thesis, Columbia University (1994), NEVIS-285.
- [18] M. Glück, E. Reya, and M. Stratmann, Nucl. Phys. **B422**, 37 (1994).
- [19] M. A. G. Aivazis, F. I. Olness, and W.-K. Tung, Phys. Rev. **D50**, 3085 (1994).
- [20] M. A. G. Aivazis, J. C. Collins, F. I. Olness, and W.-K. Tung, Phys. Rev. **D50**, 3102 (1994).
- [21] J. C. Collins, Phys. Rev. **D58**, 094002 (1998).
- [22] R. S. Thorne and R. G. Roberts, Phys. Rev. **D57**, 6871 (1998).
R. S. Thorne and R. G. Roberts, Phys. Lett. **B421**, 303 (1998).
- [23] M. Buza, Y. Matiounine, J. Smith, and W. L. van Neerven, Eur. Phys. J. **C1**, 301 (1998).
- [24] A. D. Martin, R. G. Roberts, M. G. Ryskin, and W. J. Stirling, Eur. Phys. J. **C2**, 287 (1998).
- [25] M. Kramer, F. I. Olness, and D. E. Soper, Phys. Rev. **D62**, 096007 (2000).
- [26] M. Glück, E. Reya, and A. Vogt, Eur. Phys. J. **C5**, 461 (1998).
- [27] A. D. Martin, R. G. Roberts, W. J. Stirling, and R. S. Thorne, Eur. Phys. J. **C4**, 463 (1998).
- [28] H. L. Lai *et al.*, CTEQ Collaboration, Eur. Phys. J. **C12**, 375 (2000).
- [29] G. Altarelli, R. K. Ellis, G. Martinelli, and S.-Y. Pi, Nucl. Phys. **B160**, 301 (1979).
- [30] W. Furmanski and R. Petronzio, Z. Phys. **C11**, 293 (1982).

- [31] M. Glück, S. Kretzer, and E. Reya, Phys. Lett. **B398**, 381 (1997), Erratum: **B405** (1997) 392.
- [32] J. P. Leveille and T. Weiler, Nucl. Phys. **B147**, 147 (1979).
- [33] M. Glück, R. M. Godbole, and E. Reya, Z. Phys. **C38**, 441 (1988), Erratum: **C39** (1988) 590.
- [34] G. A. Schuler, Nucl. Phys. **B299**, 21 (1988).
- [35] U. Baur and J. J. van der Bij, Nucl. Phys. **B304**, 451 (1988).
- [36] I. Schienbein, Phys. Rev. **D59**, 013001 (1999).
- [37] C. Peterson, D. Schlatter, I. Schmitt, and P. Zerwas, Phys. Rev. **D27**, 105 (1983).
- [38] J. Chrin, Z. Phys. **C36**, 163 (1987).
- [39] S. Bethke, Z. Phys. **C29**, 175 (1985).
- [40] J. J. Hernández *et al.*, Phys. Lett. **B239**, 1 (1990).
- [41] M. Glück, E. Reya, and A. Vogt, Z. Phys. **C67**, 433 (1995).
- [42] H. L. Lai *et al.*, CTEQ Collaboration, Phys. Rev. **D55**, 1280 (1997).
- [43] W. G. Seligman *et al.*, CCFR Collaboration, Phys. Rev. Lett. **79**, 1213 (1997).
W. G. Seligman, *A next-to-leading order QCD analysis of neutrino-iron structure functions at the Tevatron*, Ph.D. thesis, Columbia University (1997), NEVIS-292.
- [44] J. Blümlein, S. Riemersma, and A. Vogt, in *Proceedings of the International Workshop on Deep Inelastic Scattering and Related Phenomena (DIS 96), Rome, Italy, 15-19 Apr 1996*. (1996), pp. 572–576, hep-ph/9607329.
- [45] H. Abramowicz *et al.*, CDHSW Collaboration, Z. Phys. **C15**, 19 (1982).
- [46] P. Vilain *et al.*, CHARM II Collaboration, Eur. Phys. J. **C11**, 19 (1999).
- [47] J. C. Collins and W.-K. Tung, Nucl. Phys. **B278**, 934 (1986).
S. Qian, *A New Renormalization Prescription (CWZ Subtraction Scheme) for QCD and its Application to DIS*, Rep. ANL-HEP-PR-84-72, Argonne National Laboratory (1984).

- [48] G. Altarelli, R. K. Ellis, and G. Martinelli, Nucl. Phys. **B157**, 461 (1979).
- [49] M. Glück, S. Kretzer, and E. Reya, Phys. Lett. **B380**, 171 (1996), Erratum: **B405** (1997) 391.
- [50] S. Kretzer, *Heavy Quark Production and Fragmentation Processes in Next-to-Leading Order QCD*, Ph.D. thesis, Dortmund University (1999), DO-TH 99/12.
- [51] B. Mele and P. Nason, Nucl. Phys. **B361**, 626 (1991).
- [52] J. J. van der Bij and G. J. van Oldenborgh, Z. Phys. **C51**, 477 (1991).
- [53] E. Hoffmann and R. Moore, Z. Phys. **C20**, 71 (1983).
E. Hoffmann, *QCD-Strahlungskorrekturen Höherer Ordnung und Higher-Twist-Beiträge zur Tiefinelastischen Lepton-Nukleon-Streuung*, Ph.D. thesis, Universität Dortmund (1983), (in German).
- [54] W. A. Bardeen, A. J. Buras, D. W. Duke, and T. Muta, Phys. Rev. **D18**, 3998 (1978).
- [55] S. J. Brodsky, P. Hoyer, C. Peterson, and N. Sakai, Phys. Lett. **B93**, 451 (1980).
S. J. Brodsky, C. Peterson, and N. Sakai, Phys. Rev. **D23**, 2745 (1981).
- [56] B. W. Harris, J. Smith, and R. Vogt, Nucl. Phys. **B461**, 181 (1996).
J. F. Gunion and R. Vogt, UCD-97-14, LBNL-40399, hep-ph/9706252.
- [57] M. Glück, E. Reya, and A. Vogt, Z. Phys. **C53**, 127 (1992).
- [58] M. A. G. Aivazis, F. I. Olness, and W.-K. Tung, Phys. Rev. Lett. **65**, 2339 (1990).
- [59] J. C. Collins, in *Proceedings of the XXVth Rencontre de Moriond: High Energy Hadronic Interactions*, edited by J. Tran Thanh Van (Editions Frontieres, 1990), p. 123.
- [60] C. R. Schmidt, in *Proceedings of the 5th International Workshop on Deep Inelastic Scattering and QCD (DIS 97), Chicago, IL, USA, April 1997*, hep-ph/9706496.
- [61] U. D'Alesio, *Produzione di charm nella diffusione profondamente anelastica mediata da correnti elettrodeboli: studio teorico e fenomenologico*, Ph.D. thesis, Turin University (1996), (in Italian).

- [62] P. Nason and B. R. Webber, Nucl. Phys. **B421**, 473 (1994).
- [63] M. Cacciari and M. Greco, Phys. Rev. **D55**, 7134 (1997).
- [64] J. Breitweg *et al.*, ZEUS Collaboration, Eur. Phys. J. **C6**, 67 (1999).
- [65] S. Kretzer, Phys. Lett. **B471**, 227 (1999).
- [66] K. G. Chetyrkin, B. A. Kniehl, and M. Steinhauser, Phys. Rev. Lett. **79**, 2184 (1997).
W. Wetzel, Nucl. Phys. **B196**, 259 (1982).
W. Bernreuther and W. Wetzel, Nucl. Phys. **B197**, 228 (1982), Erratum: **B513** (1998) 758.
W. Bernreuther, Ann. Phys. **151**, 127 (1983).
W. Bernreuther, Z. Phys. **C20**, 331 (1983).
S. A. Larin, T. van Ritbergen, and J. A. M. Vermaseren, Nucl. Phys. **B438**, 278 (1995).
- [67] K. Kleinknecht and B. Renk, Z. Phys. **C17**, 325 (1983).
- [68] J. C. Collins, D. E. Soper, and G. Sterman, in *Perturbative Quantum Chromodynamics*, edited by A. H. Mueller (World Scientific, 1989).
- [69] P. D. B. Collins and T. P. Spiller, J. Phys. **G11**, 1289 (1985).
- [70] J. Binnewies, B. A. Kniehl, and G. Kramer, Z. Phys. **C76**, 677 (1997).
- [71] J. Binnewies, B. A. Kniehl, and G. Kramer, Phys. Rev. **D58**, 014014 (1998).
- [72] T. Adams, talk at the 'HQ98' workshop, Fermilab, Oct. 1998, AIP Conference Proceedings 459, H. W. K. Cheung and J.N. Butler (eds.).
- [73] J. Yu, CCFR / NuTeV Collaboration, talk given at 33rd Rencontres de Moriond: QCD and High Energy Hadronic Interactions, Les Arcs, France, 21-28 Mar 1998, hep-ex/9806030.
J. Yu, NuTeV Collaboration, talk given at 6th International Workshop on Deep Inelastic Scattering and QCD (DIS 98), Brussels, Belgium, 4-8 Apr 1998, hep-ex/9806032.

- [74] K. Zuber, private communication.
- [75] H. Albrecht *et al.*, ARGUS Collaboration, Z. Phys. **C52**, 353 (1991).
- [76] D. Bortoletto *et al.*, CLEO Collaboration, Phys. Rev. **D37**, 1719 (1988), Erratum: **D39** (1989) 1471.
- [77] R. M. Barnett *et al.*, Phys. Rev. **D54**, 1 (1996).
- [78] F. I. Olness and S. T. Riemersma, Phys. Rev. **D51**, 4746 (1995).
H. L. Lai and W.-K. Tung, Z. Phys. **C74**, 463 (1997).
K. Daum, S. Riemersma, B. W. Harris, E. Laenen, and J. Smith, in *Future Physics at HERA*, edited by G. Ingelman, A. De Roeck, and R. Klanner, Proceedings of the 1995/96 Workshop “*Future Physics at HERA*”, Hamburg, Germany (DESY, 1996), vol. 1, p. 89.
- [79] K. Daum, private communication.
- [80] B. W. Harris and J. Smith, Nucl. Phys. **B452**, 109 (1995).
- [81] E. Tzamariudaki, H1 Collaboration, talk given at the 29th International Conference on High-Energy Physics (ICHEP 98), Vancouver, British Columbia, Canada, 23-29 July 1998.
- [82] V. M. Budnev, I. F. Ginzburg, G. V. Meledin, and V. G. Serbo, Phys. Rep. **15**, 181 (1975).
- [83] T. H. Bauer, R. D. Spital, D. R. Yennie, and F. M. Pipkin, Rev. Mod. Phys. **50**, 261 (1978), Erratum: *ibid* **51** (1979) 407.
- [84] H. Kolanoski, Springer Tracts in Mod. Phys. **105**, 187 (1984).
- [85] C. Berger and W. Wagner, Phys. Rep. **146**, 1 (1987).
- [86] H. Abramowicz, M. Krawczyk, K. Charchula, A. Levy, and U. Maor, Int. J. Mod. Phys. **A8**, 1005 (1993).
- [87] M. Drees and R. M. Godbole, Pramana **41**, 83 (1993).
M. Drees and R. M. Godbole, J. Phys. **G21**, 1559 (1995).

- [88] S. J. Brodsky and P. M. Zerwas, Nucl. Instrum. Meth. **A355**, 19 (1995).
- [89] M. Erdmann, *The Partonic Structure of the Photon*, Springer Tracts in Modern Physics Vol. **138** (Springer–Verlag, Berlin, 1997).
- [90] R. Nisius, Phys. Rept. **332**, 165 (2000).
- [91] M. Krawczyk, A. Zembruski, and M. Staszal, Phys. Rept. **345**, 265 (2001).
- [92] M. Glück, E. Reya, and A. Vogt, Z. Phys. **C48**, 471 (1990).
- [93] M. Glück, E. Reya, and A. Vogt, Phys. Lett. **B306**, 391 (1993).
- [94] G. Altarelli, N. Cabibbo, L. Maiani, and R. Petronzio, Nucl. Phys. **B69**, 531 (1974).
- [95] R. C. Hwa, Phys. Rev. **D22**, 1593 (1980).
- [96] M. Glück, E. Reya, and A. Vogt, Phys. Rev. **D46**, 1973 (1992).
- [97] G. A. Schuler and T. Sjöstrand, Z. Phys. **C68**, 607 (1995).
- [98] G. Abbiendi *et al.*, OPAL Collaboration, Eur. Phys. J. **C18**, 15 (2000).
- [99] R. W. Brown and I. J. Muzinich, Phys. Rev. **D4**, 1496 (1971).
- [100] C. E. Carlson and W.-K. Tung, Phys. Rev. **D4**, 2873 (1971).
- [101] S. Wolfram, *Mathematica — Ver. 3 or higher*, Wolfram Research (1997).
- [102] M. Jamin and M. E. Lautenbacher, Comput. Phys. Commun. **74**, 265 (1993).
- [103] R. Nisius and M. H. Seymour, Phys. Lett. **B452**, 409 (1999).
- [104] G. Rossi, *Virtual Photon Structure Functions in Quantum Chromodynamics*, Ph.D. thesis, UC San Diego (1983), UC San Diego report UCSD–10P10-227 (unpublished).
- [105] M. Acciarri *et al.*, L3 Collaboration, Phys. Lett. **B483**, 373 (2000).
- [106] C. Berger *et al.*, PLUTO Collaboration, Phys. Lett. **B142**, 119 (1984).
- [107] M. Cacciari, V. D. Duca, S. Frixione, and Z. Trocsanyi, JHEP **02**, 029 (2001).
S. Frixione, Nucl. Phys. Proc. Suppl. **96**, 109 (2001), hep-ph/0010044.

- [108] S. Kretzer and I. Schienbein, work in progress.
- [109] J. C. Collins and D. E. Soper, *Ann. Rev. Nucl. Part. Sci.* **37**, 383 (1987).
- [110] W. A. Bardeen and A. J. Buras, *Phys. Rev.* **D20**, 166 (1979), Erratum: **D21** (1980) 2041.
- [111] M. Glück, E. Reya, and M. Stratmann, *Phys. Rev.* **D51**, 3220 (1995).
- [112] M. Glück, E. Reya, and A. Vogt, *Phys. Rev.* **D45**, 3986 (1992).
- [113] P. Aurenche, M. Fontannaz, and J.-P. Guillet, *Z. Phys.* **C64**, 621 (1994).
- [114] A. Vogt, in *Photon '97 Workshop, Egmond aan Zee, The Netherlands, May 1997*, edited by A. Buijs and F. C. Ern  (World Scientific, 1998), p. 3, hep-ph/9709345.
- [115] M. Glück, E. Reya, and A. Vogt, *Phys. Rev.* **D48**, 116 (1993).
- [116] M. Glück, E. Reya, and M. Stratmann, *Eur. Phys. J.* **C2**, 159 (1998).
- [117] E. Witten, *Nucl. Phys.* **B104**, 445 (1976).
M. Glück and E. Reya, *Phys. Lett.* **83B**, 98 (1979).
- [118] M. Stratmann, *Leading and Next-to-Leading Order QCD Analyses of the Parton Content of Unpolarized and Polarized Nucleons and Photons*, Ph.D. thesis, University of Dortmund (1996), Univ. Dortmund Report No. DO-TH 96/24 (unpublished).
- [119] E. Laenen, S. Riemersma, J. Smith, and W. L. van Neerven, *Phys. Rev.* **D49**, 5753 (1994).
E. Laenen and S. Riemersma, proceedings of the Photon '95 Conference, Sheffield, April 1995, p. 117, hep-ph/9505230.
E. Laenen and S. Riemersma, *Phys. Lett.* **B376**, 169 (1996).
- [120] R. J. DeWitt, L. M. Jones, J. D. Sullivan, D. E. Willen, and H. W. Wyld Jr., *Phys. Rev.* **D19**, 2046 (1979), Erratum: **D20** (1979) 1751.
- [121] G. Curci, W. Furmanski, and R. Petronzio, *Nucl. Phys.* **B175**, 27 (1980).
W. Furmanski and R. Petronzio, *Phys. Lett.* **B97**, 437 (1980).
E. G. Floratos, C. Kounnas, and R. Lacaze, *Nucl. Phys.* **B192**, 417 (1981).

-
- [122] M. Fontannaz and E. Pilon, Phys. Rev. **D45**, 382 (1992).
- [123] A. Vogt, *The Partonic Structure of Hadrons and Photons*, Ph.D. thesis, University of Dortmund (1992), Univ. Dortmund Report No. DO-TH 92/15 (unpublished).
- [124] M. Glück, E. Reya, and C. Sieg, Eur. Phys. J. **C20**, 271 (2001).
- [125] T. Uematsu and T. F. Walsh, Phys. Lett. **B101**, 263 (1981).
- [126] T. Uematsu and T. F. Walsh, Nucl. Phys. **B199**, 93 (1982).
- [127] G. Rossi, Phys. Rev. **D29**, 852 (1984).
- [128] L. L. Frankfurt and E. G. Gurvich, *Momentum Sum Rules in QCD for a Photon Target*, hep-ph/9505406.
L. L. Frankfurt and E. G. Gurvich, Phys. Lett. **B386**, 379 (1996).
L. L. Frankfurt and E. G. Gurvich, J. Phys. **G22**, 903 (1996).
G. A. Schuler and T. Sjostrand, Phys. Lett. **B376**, 193 (1996).
- [129] M. Glück and E. Reya, Phys. Lett. **B443**, 298 (1998).
- [130] J. Chyla and M. Tasevsky, Eur. Phys. J. **C16**, 471 (2000).
- [131] J. Chyla and M. Tasevsky, Eur. Phys. J. **C18**, 723 (2001).
- [132] J. Chyla, Phys. Lett. **B488**, 289 (2000).
- [133] K. Freudenreich, Int. J. Mod. Phys. **A5**, 3643 (1990).
- [134] B. Betev *et al.*, NA10 Collaboration, Z. Phys. **C28**, 9 (1985).
- [135] B. Bordalo *et al.*, NA10 Collaboration, Phys. Lett. **B193**, 368 (1987).
- [136] J. S. Conway *et al.*, E615 Collaboration, Phys. Rev. **D39**, 92 (1989).
- [137] P. J. Sutton, A. D. Martin, W. J. Stirling, and R. G. Roberts, Phys. Rev. **D45**, 2349 (1992).
- [138] C. de Marzo *et al.*, NA24 Collaboration, Phys. Rev. **D36**, 8 (1987).
- [139] M. Bonesini *et al.*, WA70 Collaboration, Z. Phys. **C37**, 535 (1988).

- [140] L. Apanasevich *et al.*, E706 Collaboration, Phys. Rev. Lett. **81**, 2642 (1998).
- [141] M. Glück, E. Reya, and A. Vogt, Z. Phys. **C53**, 651 (1992).
- [142] G. Altarelli, S. Petrarca, and F. Rapuano, Phys. Lett. **B373**, 200 (1996).
- [143] S. Aid *et al.*, H1 Collaboration, Nucl. Phys. **B470**, 3 (1996).
- [144] C. Adloff *et al.*, H1 Collaboration, Nucl. Phys. **B497**, 3 (1997).
- [145] C. Adloff *et al.*, H1 Collaboration, Papers 260 and 275, submitted to the Int. Europhysics Conf. on HEP, Jerusalem, August 1997.
- [146] M. Derrick *et al.*, ZEUS Collaboration, Z. Phys. **C69**, 607 (1996).
- [147] M. Derrick *et al.*, ZEUS Collaboration, Z. Phys. **C72**, 399 (1996).
- [148] M. Derrick *et al.*, ZEUS Collaboration, Papers N-646 and N-647, submitted to the Int. Europhysics Conf. on HEP, Jerusalem, August 1997.
- [149] L. E. Gordon and J. K. Storrow, Z. Phys. **C56**, 307 (1992).
L. E. Gordon and J. K. Storrow, Nucl. Phys. **B489**, 405 (1997).
- [150] C. Adloff *et al.*, H1 Collaboration, Eur. Phys. J. **C6**, 587 (1999).
- [151] K. Hagiwara, M. Tanaka, I. Watanabe, and T. Izubuchi, Phys. Rev. **D51**, 3197 (1995).
- [152] Recent experimental results can be found in *Proceedings of the Photon '97 Conference* [114].
- [153] W. Ibes and T. F. Walsh, Phys. Lett. **B251**, 450 (1990).
- [154] F. M. Borzumati and G. A. Schuler, Z. Phys. **C58**, 139 (1993).
- [155] M. Drees and R. M. Godbole, Phys. Rev. **D50**, 3124 (1994).
- [156] M. Stratmann, talk presented at the Workshop on Photon Interactions and the Photon Structure, Lund, 1998, University of Durham Report No. DTP/98/80, hep-ph/9811260.

- [157] M. L. Utle, ZEUS Collaboration, in *Proceedings of the International Europhysics Conference on HEP '95*, Brussels, 1995, edited by J. Lemonne *et al.* (World Scientific, Singapore, 1996), p. 570, hep-ex/9508016.
- [158] C. Adloff *et al.*, H1 Collaboration, Phys. Lett. **B415**, 418 (1997).
- [159] C. Adloff *et al.*, H1 Collaboration, Eur. Phys. J. **C13**, 415 (2000).
- [160] C. Adloff *et al.*, H1 Collaboration, Paper 544, submitted to the 29th International Conference on HEP ICHEP98, Vancouver, 1998.
- [161] C. Adloff *et al.*, H1 Collaboration, Eur. Phys. J. **C13**, 397 (2000).
- [162] M. Glück, E. Reya, and M. Stratmann, Phys. Rev. **D54**, 5515 (1996).
- [163] D. de Florian, C. G. Canal, and R. Sassot, Z. Phys. **C75**, 265 (1997).
J. Chýla and J. Cvach, in *Future Physics at HERA*, edited by G. Ingelman, A. De Roeck, and R. Klanner, Proceedings of the 1995/96 Workshop “*Future Physics at HERA*”, Hamburg, Germany (DESY, 1996), vol. 1, p. 545.
- [164] M. Klasen, G. Kramer, and B. Pötter, Eur. Phys. J. **C1**, 261 (1998).
G. Kramer and B. Pötter, Eur. Phys. J. **C5**, 665 (1998).
B. Pötter, Comput. Phys. Commun. **119**, 45 (1999).
- [165] H. Jung, Comp. Phys. Commun. **86**, 147 (1995).
- [166] C. Caso *et al.*, Eur. Phys. J. **C3**, 1 (1998).
- [167] Y. M. Antipov *et al.*, Z. Phys. **C42**, 185 (1989).
- [168] H. Kolanoski and P. Zerwas, in *High Energy Electron–Positron Physics*, edited by A. Ali and P. Söding (World Scientific, 1988), pp. 695–784, DESY-87-175.
- [169] B. L. Ioffe, V. A. Khoze, and L. N. Lipatov, *Hard Processes*, (North-holland, Amsterdam, 1984).
- [170] C. Berger *et al.*, PLUTO Collaboration, Phys. Lett. **B142**, 111 (1984).
C. Berger *et al.*, PLUTO Collaboration, Nucl. Phys. **B281**, 365 (1987).
- [171] W. Bartel *et al.*, JADE Collaboration, Z. Phys. **C24**, 231 (1984).

- [172] M. Althoff *et al.*, TASSO Collaboration, Z. Phys. **C31**, 527 (1986).
- [173] S. K. Sahu *et al.*, AMY Collaboration, Phys. Lett. **B346**, 208 (1995).
- [174] T. Kojima *et al.*, AMY Collaboration, Phys. Lett. **B400**, 395 (1997).
- [175] K. Muramatsu *et al.*, TOPAZ Collaboration, Phys. Lett. **B332**, 477 (1994).
- [176] K. Ackerstaff *et al.*, OPAL Collaboration, Z. Phys. **C74**, 33 (1997).
K. Ackerstaff *et al.*, OPAL Collaboration, Phys. Lett. **B411**, 387 (1997).
K. Ackerstaff *et al.*, OPAL Collaboration, Phys. Lett. **B412**, 225 (1997).
- [177] P. Abreu *et al.*, DELPHI Collaboration, Z. Phys. **C69**, 223 (1996).
F. Kapusta *et al.*, DELPHI Collaboration, HEP '97 Conference, Jerusalem, August 1997, contribution 416.
- [178] A. Finch *et al.*, ALEPH Collaboration, HEP '97 Conference, Jerusalem, August 1997, contribution 607.
A. Finch *et al.*, ALEPH Collaboration, in *Photon '97 Workshop, Egmond aan Zee, The Netherlands, May 1997*, edited by A. Buijs and F. C. Ern  (World Scientific, 1998).
A. Finch *et al.*, ALEPH Collaboration, ICHEP '98 Conference, Vancouver, July 1998, Abstract No. 898.
- [179] M. Acciarri *et al.*, L3 Collaboration, Phys. Lett. **B436**, 403 (1998).
- [180] T. Ahmed *et al.*, H1 Collaboration, Nucl. Phys. **B445**, 195 (1995).
- [181] C. Adloff *et al.*, H1 Collaboration, Eur. Phys. J. **C10**, 363 (1999).
- [182] H. Burkhardt and B. Pietrzyk, Phys. Lett. **B356**, 398 (1995).
- [183] B. L. Combridge and C. J. Maxwell, Nucl. Phys. **B239**, 429 (1984).
B. P tter, Eur. Phys. J. direct **C5**, 1 (1999).
- [184] M. Krawczyk and A. Zembrzuski, Nucl. Phys. B (Proc. Suppl.) **82**, 167 (2000).
- [185] T. Gottschalk, Phys. Rev. **D23**, 56 (1981).

-
- [186] A. Denner, Fortschr. Phys. **41**, 307 (1993).
 - [187] W. J. P. Beenakker, *Electroweak Corrections: Techniques and Applications*, Ph.D. thesis, University of Leiden (1989).
 - [188] G. Passarino and M. Veltman, Nucl. Phys. **B160**, 151 (1979).
 - [189] I. Bojak, *NLO QCD Corrections to the Polarized Photo- and Hadroproduction of Heavy Quarks*, Ph.D. thesis, University of Dortmund (2000), hep-ph/0005120.
 - [190] F. Jegerlehner, Eur. Phys. J. **C18**, 673 (2001).

Acknowledgements

It is a pleasure to thank Prof. Dr. M. Glück and Prof. Dr. E. Reya for their instructive scientific guidance and for a fruitful collaboration. I have benefitted from their continuous advice on all topics covered in this thesis.

I am by no means less grateful to Dr. Stefan Kretzer for a collaboration on the ACOT calculations and for being a pleasant office-mate over the 3 1/2 years in which we shared the same office. Furthermore, I wish to thank Christoph Sieg for an enjoyable collaboration on issues about the photon tensor and the QED-factorization. I am thankful to the last two persons and Dr. Werner Vogelsang for critically reading parts of the manuscript.

I would like to express my gratitude to Jens Noritzsch for generously taking over part of my teaching load in this semester and for help concerning computer and L^AT_EX questions.

Thanks to Dr. Ingo Bojak for numerous enjoying (physics) discussions and for providing his **Mathematica** implementation of the Passarino-Veltman-decomposition.

Finally, my thanks go to all other members of our working group TIV and to THH and to our secretary Susanne Laurent for a pleasant working atmosphere.